Lawrence Berkeley National Laboratory
Recent Work

Title

SURFACE SCIENCE AND CATALYTIC STUDIES OF HYDROCARBON SKELETAL REARRANGEMENTS: THE PLATINUM AND THEBIMETALLIC PLATINUM-RHENIUM SINGLE CRYSTAL SYSTEMS

Permalink

https://escholarship.org/uc/item/8xq6n7qt

Author

Godbey, D.J.

Publication Date

1987-10-01

eScholarship.org Powered by the California Digital Library
University of California

LBL-24404
c.2

Lawrence Berkeley Laboratory
UNIVERSITY OF CALIFORNIA

Materials & Chemical Sciences Division

RECEIVED
LAWRENCE
BERKELEY LABORATORY
FEB 19 1988
LIBRARY AND
DOCUMENTS SECTION

Surface Science and Catalytic Studies of Hydrocarbon Skeletal Rearrangements: The Platinum and the Bimetallic Platinum-Rhenium Single Crystal Systems

D.J. Godbey
(Ph.D. Thesis)

October 1987

TWO-WEEK LOAN COPY

This is a Library Circulating Copy which may be borrowed for two weeks.

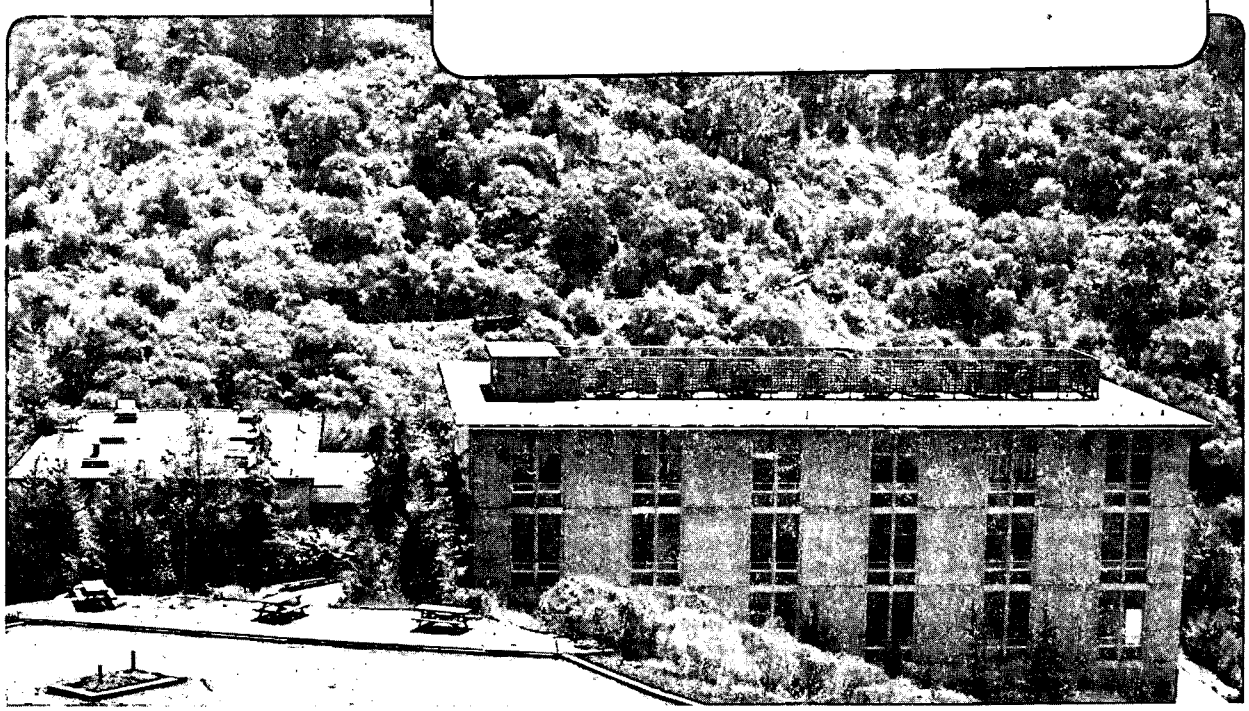

Prepared for the U.S. Department of Energy under Contract DE-AC03-76SF00098

LBL-24404
c.2

DISCLAIMER

This document was prepared as an account of work sponsored by the United States Government. While this document is believed to contain correct information, neither the United States Government nor any agency thereof, nor the Regents of the University of California, nor any of their employees, makes any warranty, express or implied, or assumes any legal responsibility for the accuracy, completeness, or usefulness of any information, apparatus, product, or process disclosed, or represents that its use would not infringe privately owned rights. Reference herein to any specific commercial product, process, or service by its trade name, trademark, manufacturer, or otherwise, does not necessarily constitute or imply its endorsement, recommendation, or favoring by the United States Government or any agency thereof, or the Regents of the University of California. The views and opinions of authors expressed herein do not necessarily state or reflect those of the United States Government or any agency thereof or the Regents of the University of California.

LBL-24404

Surface Science and Catalytic Studies of Hydrocarbon Skeletal Rearrangements: The Platinum and the Bimetallic Platinum-Rhenium Single Crystal Systems

David john Godbey
Ph.D. Thesis

Lawrence Berkeley Laboratory
University of California
Berkeley, California 94720

October, 1987

This work was supported by the Office of Energy Research, Office of Basic Energy Sciences, and the Material Science Division of the U. S. Department of Energy under contract number DE-AC03-76SF00098.

Surface Science and Catalytic Studies of Hydrocarbon Skeletal Rearrangements: The Platinum and the Bimetallic Platinum–Rhenium Single Crystal Systems

David John Godbey

Department of Chemistry

University of California

and

Materials and Chemical Sciences Division

Lawrence Berkeley Laboratory

Berkeley, California 94720

Abstract

Bimetallic surfaces were prepared by vapor deposition of rhenium onto Pt(111) and Pt(100), and of platinum onto Re(0001) and polycrystalline rhenium foils. The physical and chemical properties of the prepared surfaces were characterized using Auger electron spectroscopy, low energy electron diffraction, X–ray photoelectron spectroscopy (XPS), temperature programmed desorption, and hydrocarbon rearrangement (reforming) reactions. Rhenium was found to grow layer by layer on both Pt(111) and Pt(100); it formed a hexagonal close-packed (hcp) film on Pt(111) and a face-centered cubic film on Pt(100). Platinum was found to grow layer by layer on Re(0001) with the formation of an hcp film. Evidence for an electronic interaction between the two metals was shown by XPS because the $4f_{7/2}$ peaks shifted to higher binding energies for both metals when rhenium was

deposited on platinum.

The addition of rhenium metal to Pt(111) caused a 4–8 kJ/mole decrease of the metal-hydrogen bond strength. Surfaces composed of between 0.2–0.35 monolayers of rhenium on Pt(111) displayed maximum low pressure adsorption capacities for hydrogen and carbon monoxide. Maximum rates of hydrogenolysis for reactions near atmospheric pressure were observed from all hydrocarbons studied and were obtained over bimetallic surfaces composed of rhenium and platinum in an atomic ratio of 2:1. Compared to a monometallic Pt(111) surface, 0.3 monolayers of rhenium on Pt(111) gave a surface that was as active as a clean Re(0001) surface for ethane hydrogenolysis, yet the hydrogen partial pressure dependence observed was closest to that obtained for Pt(111). An enhancement in the production rate of aromatics from n–hexane and cyclohexane indicates that platinum atoms with rhenium ligands are more active than monometallic platinum for this class of reactions. The isomerization rate of n–hexane was smaller in the presence of rhenium than on clean platinum due to a decrease in the desorption of ring opening products from cyclic intermediates on the bimetallic surface. However, cyclization activity was not strongly effected by the addition of rhenium to platinum. The presence of rhenium on platinum resulted in a surface more resistant towards the accumulation of carbonaceous deposits under some conditions.

To my parents,

Jim and Jo

Contents

Acknowledgments

As my graduate career nears a close here at Berkeley, I find myself contemplating the last four years and reflecting on the high points and the low points of life as a graduate student. One important and sobering point is that the execution of such a research project and the preparation of this thesis could not have been accomplished without the help of many people. To them I owe a great deal. My advisor, Professor Gabor Somorjai, gave me a lot of freedom to explore, yet was always ready to offer help and keep my research on a steady course. I am deeply grateful to my parents, Jim and Jo, who have offered me their unwavering support for all my endeavors no matter how crazy, for all these years. I am also thankful to the rest of my family for their love and support.

A number of past and present Somorjai group members deserve special thanks, particularly Francisco Zaera for his help and patience while I learned to do Surface Science during my rookie year. I am especially grateful to Françoise Garin who contributed significantly to this project over the last six months. Eddie Tysoe, Andy Gellman, and Mark Logan were always available for stimulating scientific discussions but were also intent on demonstrating that serious fun and hard work are not incompatible. Learning quantum mechanics would not have been fun at all without the companionship of Rob Continetti, Jeff Owrutsky, Steve Wolk, and the "Upstairs Center."

I also extend my appreciation to the highly skilled technical staff at MCSD, in particular: Dan Colomb, Keith Franck, Weyland Wong, and Chip Flor in the machine shop; Jim Severns and Hank Brendel in the electronics shop; and Sandy Stewart in administration. Basketball was brought to building 62 at LBL with the help of Don Krieger and Conway Petersen, and late afternoon hoop was enjoyable

with the participation of Gil (Gilford) Vandentop, Kevin (Cal) Williams, and Dan (Tuna) Strongin. I will certainly miss softball and all of my comrades from the Dawgs, the Hurtin' Puppies, the Summer Guys, the Express, and What It Is. It was most enjoyable having championship seasons with the 1984 Dawgs and the 1987 What It Is teams.

I am especially appreciative of Tuna, José (Magic) Carrazza, and Tom (Buck) Rucker for their friendship over the past years. Bless the Celtics for making the finals four times and winning two NBA titles during the last four years! Thanks to Ellice Luh, François Garin, Greg Blackman, Kevin Williams, Gerard Vurens, and Chi -Tzu Kao for proofreading the manuscript. Finally, my deepest appreciation is reserved for the very talented Ellice Luh. Not only did her flying fingers type most of this manuscript at breathtaking speed, but her friendship and support have helped me keep things in perspective during these last hectic months.

Last but not least, this work was supported by the Office of Energy Research, Office of Basic Energy Sciences, and the Material Science Division of the U.S. Department of Energy under contract number DE-AC03-76SF00098.

List of Figures

List of Tables

Chapter 1

Introduction

1.1 Preface

Heterogeneous catalysis is an area in chemistry of great economical importance. One of the major uses of heterogeneous catalysis is to provide the means of converting crude oil pumped out of the earth into refined and useful products. Not only does petroleum provide products for transportation and electrical power generation, *e.g.* fuels and lubricating oils, but it also provides raw materials for the petrochemical industry which manufactures products including waxes, polymers, rubber, plastics, asphalt, and others. The work described in this thesis is a study of hydrocarbon rearrangement reactions, or commonly known as catalytic reforming, using unsupported platinum–rhenium catalysts. Reforming is just one of many processes used in the petroleum industry; its utility is in the conversion to higher octane of liquid hydrocarbon fuels and in the generation of important raw materials such as aromatic molecules used in the petrochemical industry.

1.2 Crude Oil Conversion

1.2.1 Production of gasoline

Motor gasoline is produced from the hydrocarbon distillate obtained in the normal boiling range of 30–205 °C, which includes hydrocarbons containing between 4 and 12 carbon atoms [1]. When crude oil is removed from the ground, it is an enormously complex mixture of hydrocarbons consisting of small hydrocarbons such as gases (CH_4, C_2H_6, C_3H_8), up to very large hydrocarbon molecules containing in excess of 50 carbon atoms. In addition to organic matter, crude oil contains other elements such as sulfur, nitrogen, oxygen, and metals including magnesium, nickel, and vanadium. The first step in refining the crude oil is distillation where hydrocarbons are separated according to molecular weight, or more precisely, according to boiling point. The fractions obtained are then sent to different parts of the refinery appropriate to processing that fraction. Table 1.1 shows the fractions obtained during the distillation process. The gasoline fraction obtained is sent for further processing, first to remove inorganic impurities through hydrotreating such as sulphur, nitrogen, and oxygen. Finally, to minimize knocking in the modern automobile engine, the gasoline fraction has its octane rating improved through the process of *catalytic reforming*–the subject of most of this thesis.

1.2.2 Engine knocking

The engineering of an automobile and its fuel requirements are intimately related. The theoretical fuel efficiency increases with increasing compression ratio. However, the tendency for engine knocking also increases with increasing compression ratio.

The conversion of chemical energy stored in fuel to mechanical energy required

Table 1.1: Distillate fractions from crude oil.

Fraction	Boiling Range °C
Gases C_1–C_3	<25
Gasoline	30-190
Kerosine	150-230
Diesel Fuel	230-340
Lubricating Oils	340-400
Asphalt	remaining residues

for moving an automobile is achieved by burning the fuel in air to obtain hot expanding gases, which do work against the piston. To accomplish this, a mixture of fuel and air is vaporized and introduced into the engine cylinder. Following compression of the mixture by the piston, a spark plug discharges igniting the fuel/air mixture. The fuel should burn in a well controlled manner, and not explode. The less controlled the fuel burns, the greater the tendency towards knocking will be.

Knocking can be described as follows. As the flame front initiated by the discharging spark plug propagates through the cylinder, burned or exhaust gases are found on one side, and the remaining unburned fuel–air mixture are on the other side of the flame front. The pressure and temperature increases on the unburned fuel side of the front as the expanding burning gases compress the remaining unburned gases, sometimes to the point of spontaneous combustion. When spontaneous combustion occurs, you get knocking which decreases the fuel efficiency

and may damage the engine. The higher the octane rating of a fuel, the smaller the tendency for spontaneous combustion; hence the susceptibility to knocking is lessened. The modern automobile is engineered with a high compression ratio for greater fuel efficiency, and thus puts greater demands on the octane rating of the fuel.

1.2.3 What is octane?

The octane number can be thought of as a measure of the tendency of a fuel to resist knocking in an internal combustion engine, as discussed in the previous section. The scale of octane numbers is defined as follows: n-heptane is assigned an octane number of zero, and isooctane (2,2,4-trimethylpentane) is assigned an octane number of 100. A mixture of these two components has an octane number equal to the percentage of isooctane in the mixture. The octane rating of a fuel is measured using a "knockmeter," which is a specially designed combustion engine where the number of vibrations or "knocks" caused by the fuel are counted electronically. The octane number assigned to the fuel is the same as the octane number of an n–heptane/isooctane standard that gives the same "knockmeter" reading.

The knocking characteristics of a fuel also depend on driving conditions, resulting in a need for several knock-rating methods. The research octane number (RON) relates to mild driving conditions such as cruising and low speed driving; whereas the motor method octane number relates to driving under more severe conditions such as during acceleration (high load) or at high speeds. Many of the nations gasoline stations display octane ratings obtained by the (R + M)/2 method, which is the average of the research and motor octane numbers. Octane numbers for many pure liquid compounds found in gasoline have been measured.

Table 1.2: Octane numbers of selected hydrocarbons.

Hydrocarbon	Octane Number	
	Research	Motor
n-pentane	62	62
2-methylbutane	92	90
cyclopentane	–	85
n-hexane	25	26
2-methylpentane	73	73
cyclohexane	83	77
methylcyclopentane	91	80
benzene	>100	>100
n-heptane	0	0
2,2,4-trimethylpentane	100	100
ethanol	–	99

A condensed list of the octane numbers for some of the compounds used as reactants or products produced during catalytic experiments reported in this thesis is compiled in Table 1.2.

The easiest way to boost the octane rating of a fuel is through the addition of additives. The most widely used additives for enhancement of the octane rating of a fuel prior to the introduction of the catalytic converter were based on lead compounds (*e.g.* tetraethyl lead, $Pb(C_2H_5)_4$). Others include the family $Pb(CH_3)_x(C_2H_5)_{4-x}$ for $0 \leq x \leq 4$. Today, it is possible to find "gasohol" at some service stations, where ethanol is used as an additive to enhance octane of the fuel.

1.2.4 Improving octane in the 1980's

The high temperatures produced during the combustion of fuels in automobile engines leads to the formation of NO_x compounds which is one cause of photochemical smog. Smog has become a major problem in many metropolitan areas, particularly in the Los Angeles area. Carbon monoxide and unburned hydro-

carbons also contribute to the air pollution problem. A partial solution to the pollution problem was the introduction of the catalytic converter in 1978. The catalytic converter is a platinum-based catalyst that oxidizes CO and unburned hydrocarbons to CO_2, and converts NO_x species to harmless N_2 and O_2. Unfortunately, lead poisons the catalytic converter and is being phased out of use. Eventually as the older automobiles are removed from the nations roads, all lead additives will be phased out of gasoline sold in the United States. By 1990, less than 0.1 grams of lead per gallon on average will be added to gasoline. Lead concentration in gasoline was as high as 4 grams per gallon prior to the introduction of the catalytic converter. Other problems associated with lead gasoline additives are that lead is toxic and that lead emissions are found to contribute to the formation of particulate matter in the atmosphere. For these reasons, lead additives are being phased out of use in gasoline. However, the phasing out of lead additives in gasoline places greater demands on the reforming process to boost the octane of gasoline [1,2].

An increased emphasis on the production of aromatics is now required of reforming catalysts since these compounds have the highest octane rating for a series of hydrocarbon molecules with a given number of carbon atoms (see Figure 1.1). A number of bimetallic reforming catalysts have been studied or are in use today (Pt–Au, Pt–Ir, Pt–Sn, Pt–Re), but none display selectivities towards aromatics production as high as the platinum–rhenium catalyst.

1.3 The Platinum–Rhenium Catalyst

It was shown in the previous section how the development of high compression combustion engines led to the need of higher octane fuels and how environmental concerns requiring the removal of lead from gasoline have put greater demands on

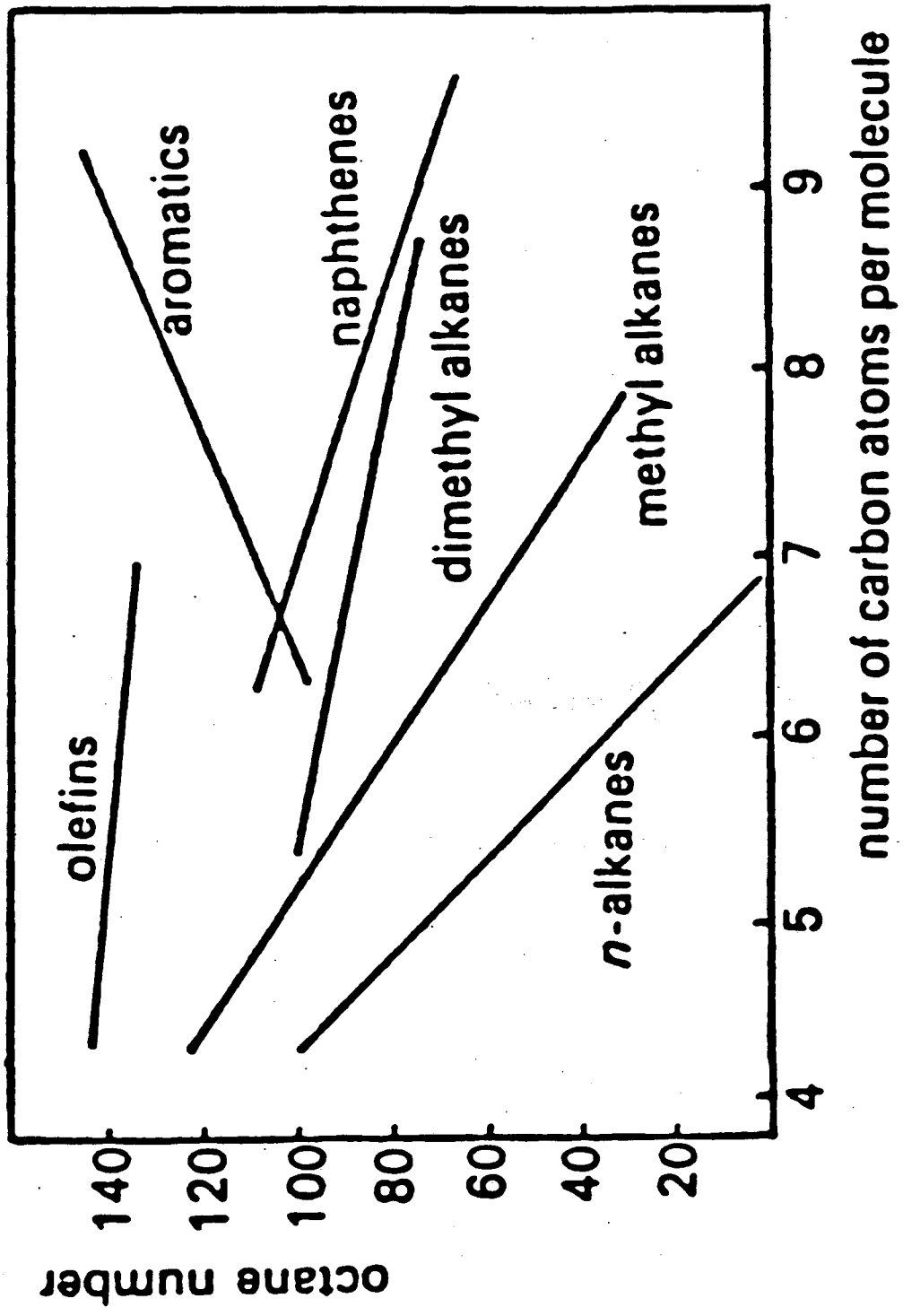

Figure 1.1: Octane number vs. hydrocarbon length for several classes of hydrocarbons.

the reforming catalyst. The introduction of the platinum–rhenium catalyst in 1968 has been of great economic importance to the petroleum industry. In this section the reforming process will be discussed in greater detail as well as some of the unanswered questions remaining regarding why the bimetallic platinum–rhenium catalyst is superior to the monometallic platinum catalyst.

1.3.1 Development of the reforming catalyst

Between the time the internal combustion engine was developed and prior to World War II, the octane of a fuel did not need to be increased much beyond what the gasoline fraction of the petroleum distillate already had. When needed, the octane was improved by the cracking of paraffins to higher octane olefins. During World War II a need for high octane aviation fuel led to the development of the Hydroforming process by Standard Oil, which used an alumina supported molybdena catalyst. In 1949, Universal Oil Products announced the development of the noble metal based catalyst. Their process was called Platforming and it employed platinum supported on alumina [3]. Later in 1968, Chevron introduced the Rheniforming catalyst, which is composed roughly of an equimolar loading of platinum and rhenium supported on alumina [4]. This catalyst remains in use today as its performance has been substantially improved and continues to be improved.

Figure 1.2 demonstrates that the Pt–Re/Al_2O_3 catalyst displays an increased activity maintenance compared to the monometallic Pt/Al_2O_3 catalyst. The change in temperature vs. time on stream required to maintain a constant octane number of the effluent is a measure of the deactivation of the catalyst. Figure 1.2 shows that the rate of deactivation of the bimetallic Pt–Re catalyst is much lower than that of the monometallic platinum catalyst. Another advantage offered by

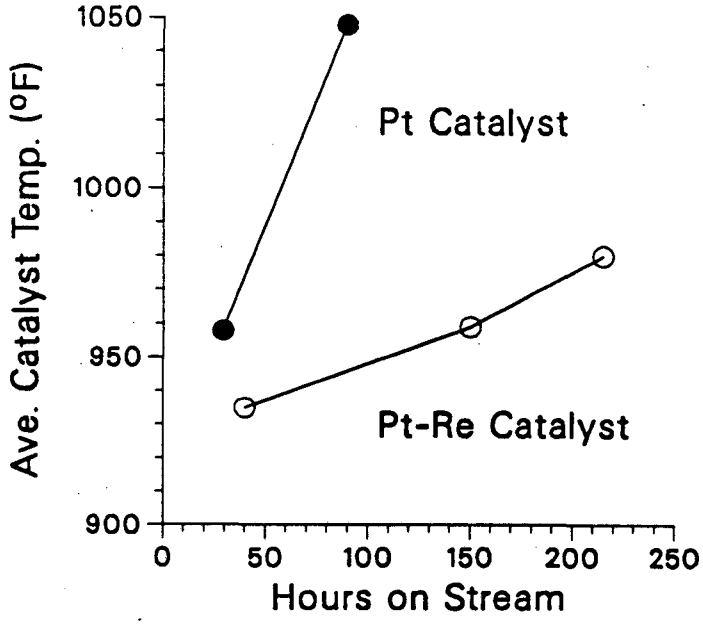

Figure 1.2: The deactivation of Pt/Al_2O_3 and $Pt–Re/Al_2O_3$ reforming catalysts taken from reference [4]. The average catalyst temperature is the temperature required to maintain 100 octane of the effluent.

the Pt–Re catalyst is an enhanced selectivity towards aromatics production. Not only is the reforming process a major producer of aromatics for use by the chemical industry, it is estimated that the aromatics content of unleaded gasoline ranges from 15% to near 50% for premium fuel [2].

1.3.2 Reforming

The improvement in octane of hydrocarbon molecules as obtained through catalytic reforming is done by rearranging the hydrocarbon backbone without the loss of carbon number or carbon atoms. Although smaller paraffins have higher octane ratings than larger paraffins as shown in Figure 1.1, they are too volatile to be useful in a combustion engine. The desired process then is to "reform" a paraffin. Consider the reforming of n-hexane. The octane of the parent molecule

is less than the reformed products that can be obtained through isomerization, cyclization (or dehydrocyclization), and aromatization. The major reforming reactions of n–hexane are summarized below.

Reactions of n–hexane

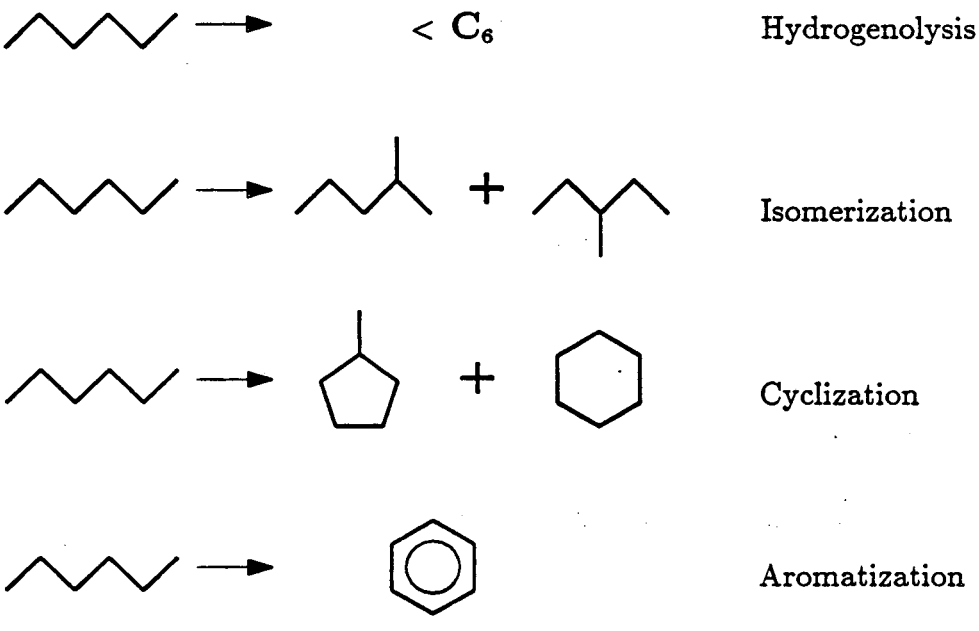

The products increase in octane number from top (isomerization) to bottom (aromatization) as can be seen in Table 1.2. Cracking reactions also occur during reforming and are shown below.

$$C_6H_{14} + H_2 \rightarrow CH_4 + C_5H_{12}$$

$$C_6H_{14} + H_2 \rightarrow C_2H_6 + C_4H_{10}$$

$$C_6H_{14} + H_2 \rightarrow 2C_3H_8$$

However, these reactions are undesirable during reforming; therefore efforts must be made to minimize them.

Catalytic reforming has been studied extensively, and many review articles

exist discussing reforming over platinum-based and other type catalysts [5,6,7,8]. In addition, much work has been done on well characterized metal surfaces such as metal foils and single crystals [9,10,11], and has been reviewed recently by Davis and Somorjai [12].

Reforming on bimetallic catalysts has also been studied over many systems including Pt–Rh [13], Pt–Ni [14], Ir–Co [15], Pt–Co [16], Ir–Au [17,18], Pt–Sn [19], Ru–Cu [20], Pt–Au [21,22,23], and Pt–Cu [24], to name a few. The Pt–Re catalyst is the most important catalyst economically and has probably received the most attention in the literature.

There have been many ideas presented on the mode of operation of the platinum–rhenium catalyst, some of them conflicting. One way that the addition of a refractory metal, such as rhenium, might help is by reducing the sintering rate of the metal particles. Results obtained by Eskinazi suggest that this may be so [25]. However, two of the hotly debated issues in the literature today are, what is the degree of alloying between the two metal components of the catalyst, and what is the oxidation state of rhenium in the active catalyst. In the following discussion these and other issues regarding the behavior of the bimetallic catalyst are reviewed.

Do the two metallic components need to be in intimate contact for the catalyst to show enhanced activity maintenance, or is it sufficient for the two metals to be in close proximity (*e.g.* a physical mixture composed of Pt/Al_2O_3 mixed with Re/Al_2O_3) but not in intimate contact? In a frequently cited paper, Bertolacinni and Pellet reported that a physical mixture can show good activity maintenance, while no mixing of the metals had occurred [26]. However, using reduction techniques, such as temperature programmed reduction, several investigators have demonstrated that platinum catalyzes the reduction of rhenium [27,28,29].

Mieville even found that reductive interactions can occur in physical mixtures if the catalyst was not thoroughly dried, perhaps through vapor transport to platinum reduction centers of volatile Re_2O_7. In Chapter 6 it will be shown that small amounts of the second metal on the substrate, even below the detection limit of Auger spectroscopy, changes the cracking activity of the catalyst dramatically. Since there is some water present under reforming conditions (20–50 ppm), the possibility exists that some vapor transport can occur. Perhaps undetected rhenium transport was responsible for the high activity maintenance observed by Bertolacinni and Pellet for physical mixtures of platinum and rhenium. Using spectroscopic techniques, some investigators have concluded that no significant interaction exists between platinum and rhenium [30,31,32] while others have concluded that indeed significant interaction does occur [33,34,35].

Another point of debate part of this question is the oxidation state of rhenium. Considering alumina-supported platinum and rhenium,Johnson and Leroy found that only Re^{4+} exists after reduction [36]. However, several investigators have reported that rhenium exists in the metallic form on alumina supported rhenium [37,38,39,40]. Johnson later reported that rhenium exists in both Re^{4+} and Re^0 oxidation states when larger metallic loadings are used. When in contact with the alumina support, rhenium is apparently stabilized in the 4+ oxidation state; while in three dimensional Re or Pt–Re particles, rhenium is reduced to metal. This view is supported by a recent paper published by Nacheff *et al.* [35].

There is a growing body of evidence that the behavior of the bimetallic towards hydrogen is modified compared to monometallic platinum. Barbier *et al.* and Margitfalvi *et al.* have reported that the presence of rhenium enables the catalyst to bind more hydrogen than the monometallic platinum counterpart [41,42]. However, Carter *et al.* supplied evidence that the converse is true: the bimetallic

catalyst can bind less hydrogen than the platinum alone catalyst [43]. Fouling studies seem to show that alloying is important [44,45,46]. Pacheco and Petersen found that the hydrogen pressure dependence of catalyst fouling from methylcyclohexane was different for the monometallic platinum and the bimetallic Pt–Re catalysts [47,48]. However, Burch and Mitchell support Bertolacinni and Pellet in their belief that rhenium alone can remove coking precursors without alloying [19,26].

Finally, there are many studies reported focusing on the chemistry of the bimetallic surface. It seems fairly certain that when intimate contact does occur, the catalytic behavior cannot be explained as a linear combination of the two metallic components and that synergistic effects do occur [49,50,51,52,53].

1.4 Well Characterized Pt–Re Surfaces

1.4.1 Single crystal surface alloys vs. supported bimetallic alloys

The primary advantage of using a well characterized single crystal or a foil bimetallic surface is the ability to utilize surface science techniques that can be used to characterize the composition and crystallographic orientation of a surface. This is advantageous because on practical catalysts, the structure of a supported small metal particle is not well understood. Adding a second metal to the catalyst further complicates matters because the metallic composition of the surface cannot be accurately determined on the supported catalyst. Using surface science techniques, surfaces of known composition can be prepared and their properties studied. With low pressure–high pressure techniques, the state of a surface following an atmospheric reaction can also be examined. In this way the quantity and nature of the carbon deposit on a catalyst can be localized on the metal surface.

Carbon deposited on a supported catalyst cannot be localized quite as easily.

The disadvantage of using unsupported catalysts is that the system is somewhat removed from reality. However, much evidence gathered over the years suggests that single crystal catalysts can be compared to supported catalysts, especially to catalysts of low dispersion [12].

1.4.2 Objective and overview

The object of these studies is to determine why the bimetallic Pt–Re catalyst is a better catalyst than the monometallic Pt catalyst. Are there electronic or geometric factors operating, and how can they be distinguished? Does the character of a particular reaction change as a function of surface composition, and what is the site responsible for the change? Does the perturbation of one metal on the other result in the formation of new crystallographic structures? How does the chemisorption behavior change as a function of surface composition for different molecules?

Chapter 2 outlines the experimental approach, the apparatus, and the techniques used. Chapter 3 discusses the role of carbonaceous overlayers on platinum surfaces for some important hydrogenation reactions. Chapter 4 describes the preparation and characterization of bimetallic surfaces for both rhenium deposited on platinum, and for platinum deposited on rhenium. Characterization is performed using Auger electron spectroscopy, low energy electron diffraction, and photoelectron spectroscopy. The adsorption and desorption behavior of several small molecules on the bimetallic surfaces is described in Chapter 5. Finally, Chapter 6 discusses the reforming chemistry of several hydrocarbons near atmospheric pressure.

1.4.3 The properties of platinum and rhenium

Some selected properties of platinum and rhenium are shown in Table 1.3. Although the difference in the nearest neighbor distances between Pt and Re is less than 1%, their melting points are quite different, and they crystallize in different structures. The Pt–Re phase diagram is shown in Figure 1.3. The bimetallic alloy forms a face-centered cubic (fcc) solid solution in the platinum-rich region, and a hexagonal close-packed (hcp) solid solution in the rhenium-rich region, with a two phase region existing between 40-60% rhenium. A schematic representation of the crystallographic faces studied in this thesis are shown in Figure 1.4.

Table 1.3: Selected properties of platinum and rhenium.

Property	Pt	Re
Atomic Number	78	75
Atomic Weight	195	186
Melting Point °C	1772	3180
Crystal Structure	fcc	hcp
Nearest Neighbor Distance Å	2.77	2.74
Metallic density of basal plane, Pt(111) & Re(0001) ($\times 10^{-15}$ atoms/cm^2)	1.503	1.514

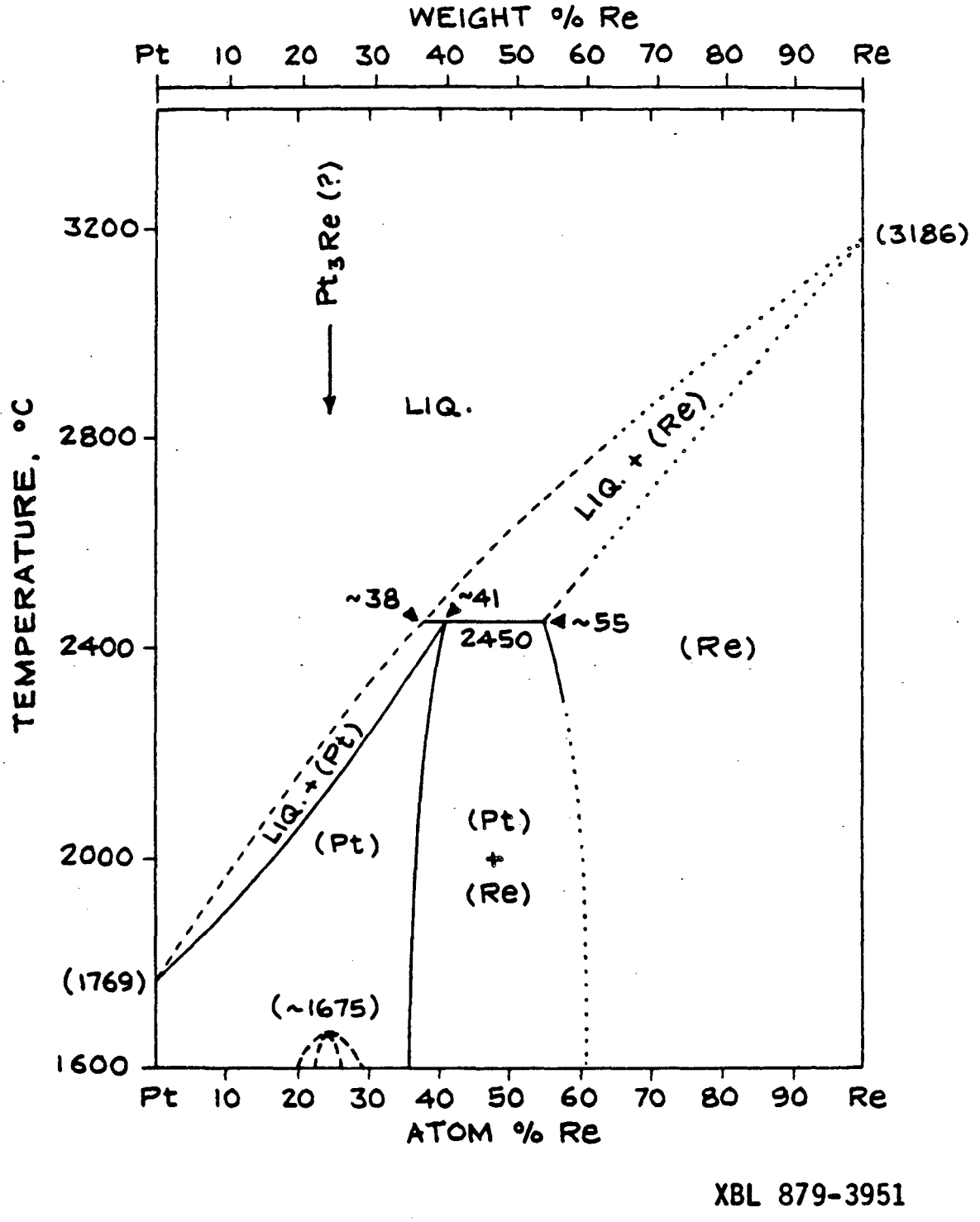

Figure 1.3: Phase diagram of the binary platinum–rhenium alloy. From Moffatt [54].

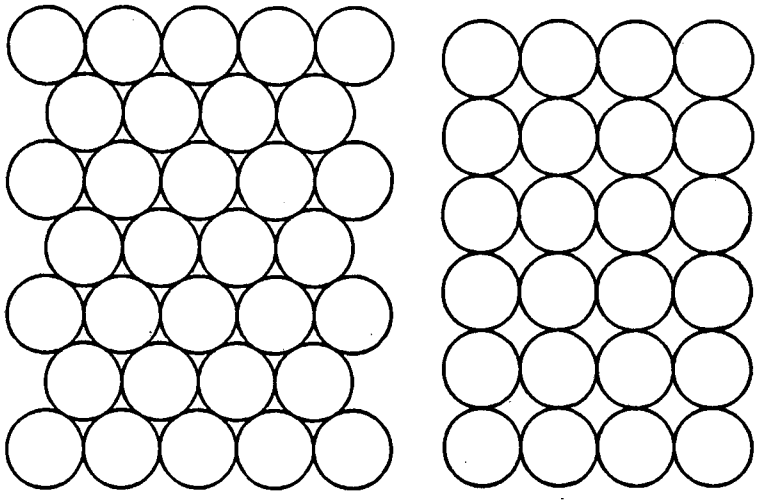

Figure 1.4: The crystallographic surfaces used in this study. The Re(0001) surface has an identical configuration to the Pt(111) surface for two atomic layers.

References

[1] G.D. Hobson and W. Rohl, editors. *Modern Petroleum Technology.* Halstead Press, John Wiley, New York, 1973.

[2] Robert F. Gould, editor. *Origin and Refining of Petroleum.* American Chemical Society, Washington, D.C., 1971.

[3] V. Haensel. *U. S. Patent 2,479,109* (1949) .

[4] H. E. Kluksdahl. *U. S. Patent 3,415,737* (1968) .

[5] G.L.C. Maire and F.G. Garin. *Catalysis Science and Technology*, page 161. Volume 6, Springer-Verlag, Berlin, 1984.

[6] V. Ponec. *Advances in Catalysis* **32** (1983) 149.

[7] F. Gault. *Advances in Catalysis* **30** (1981) 1.

[8] J.R. Anderson. *Advances in Catalysis* **23** (1973) 1.

[9] F. Zaera. PhD thesis, University of California, Berkeley, CA 94720, 1984.

[10] W.D. Gillespie. PhD thesis, University of California, Berkeley, CA 94720, 1980.

[11] S.M. Davis. PhD thesis, University of California, Berkeley, CA 94720, 1981.

[12] S.M. Davis and G.A. Somorjai. *The Chemical Physics of Solid Surfaces and Heterogeneous Catalysis*, page 217. Volume 4, Elsevier Science Publishers, Amsterdam, The Netherlands, 1982.

[13] T.C. Wong, L.C. Chang, G.L. Haller, J.A. Oliver, N.R. Scaife, and C. Kemball. *J. Catalysis* **87** (1984) 389.

[14] J. Assardier and J.C. Bertolini. *J. Catalysis* **90** (1984) 358.

[15] P.E. Puges, F. Garin, G. Maire, F. Weisang, P. Bernhardt, P. Girard, L. Guczi, and Z. Schay. *J. Catalysis* (1987) To be published.

[16] S. Zyade, F. Garin, and G. Maire. *Nouv. J. de Chimie* **11** (1987) 429.

[17] K. Foger and J.R. Anderson. *J. Catalysis* **64** (1980) 448.

[18] T.J. Plunkett and J.K.A. Clarke. *J. Catalysis* **35** (1974) 330.

[19] R. Burch and A.J. Mitchell. *Applied Catalysis* **6** (1983) 121.

[20] C.H.F. Peden and D.W. Goodman. *J. Catalysis* **100** (1986) 520.

[21] J.W.A. Sachtler and G.A. Somorjai. *J. Catalysis* **89** (1984) 35.

[22] J.W.A. Sachtler and G.H. Somorjai. *J. Catalysis* **81** (1983) 77.

[23] R.C. Yeates and G.A. Somorjai. *J. Catalysis* **103** (1987) 208.

[24] R.C. Yeates and G.H. Somorjai. *Surface Sci.* **34** (1983) 729.

[25] V. Eskinazi. *Applied Catalysis* **4** (1982) 37.

[26] R.J. Bertolacinni and R.J. Pellet. *Catalyst Deactivation*, pages 73–77. Elsevier, Amsterdam, The Netherlands, 1980.

[27] C. Bolivar, H. Charcosset, R. Fretty, M. Primet, L.Tournayan, C. Betizeau, G. Leclercq, and R. Maurel. *J. Catalysis* **39** (1975) 249.

[28] B.H. Isaacs and E.E. Petersen. *J. Catalysis* **77** (1982) 43.

[29] R.L. Mieville. *J. Catalysis* **87** (1984) 437.

[30] J.H. Onuferko, D.R. Short, and M.J. Kelley. *Appl. of Surface Sci.* **19** (1984) 227.

[31] D.R. Short, S.M. Khalid, J.R.Katzer, and M.J. Kelley. *J. Catalysis* **72** (1981) 288.

[32] J.B. Peri. *J. Catalysis* **52** (1978) 144.

[33] C. Bolivar, H. Charcosset, R. Fretty, M. Primet, L.Tournayan, C. Betizeau, G. Leclercq, and R. Maurel. *J. Catalysis* **45** (1976) 163.

[34] P. Biloen, J.N. Helle, H. Verbeek, F.M. Dautzenberg, and W.M.H. Sachtler. *J. Catalysis* **63** (1980) 112.

[35] M.S. Nacheff, L.S. Kraus, M. Ichikawa, B.M. Hoffman, J.B. Butt, and W.M.H. Sachtler. *J. Catalysis* **106** (1987) 263.

[36] M. F. L. Johnson and V. M. LeRoy. *J. Catalysis* **35** (1974) 434.

[37] A. N. Webb. *J. Catalysis* **39** (1975) 485.

[38] H.C. Yao and M. Shelef. *J. Catalysis* **44** (1976) 392.

[39] E.S. Shapiro, V.I. Avaev, G.V. Autoshin, M.A. Ryashentseva, and K.M. Minachev. *J. Catalysis* **55** (1978) 402.

[40] L. Wang and W.K. Hall. *J. Catalysis* **82** (1983) 177.

[41] J. Barbier, H. Charcosset, G. dePeriera, and J. Riviere. *Applied Catalysis* **1** (1981) 71.

[42] J. Margitfalvi, S. Gőbölös, E. Kwayzer, M. Hegedüs, F. Nagy, and L. Koltai. *React. Kinet. Catal. Lett.* **24** (1984) 315.

[43] J.L. Carter, G.B. Vicker, W. Weissman, W.S. Kmak, and J.H. Sinfelt. *Applied Catalysis* **3** (1982) 327.

[44] R.W. Coughlin, K. Kawakami, and A. Hasan. *J. Catalysis* **88** (1984) 150.

[45] R.W. Coughlin, A. Hasan, and K. Kawakami. *J. Catalysis* **88** (1984) 163.

[46] J.M. Parera, C.A. Querini J.N. Beltramini, E.E. Martinelli, E.J. Churin, P.E. Aloe, and N.S. Figoli. *J. Catalysis* **99** (1986) 39.

[47] M.A. Pacheco and E.E. Petersen. *J. Catalysis* **96** (1985) 499.

[48] M.A. Pacheco and E.E. Petersen. *J. Catalysis* **96** (1985) 507.

[49] C. Betizeau, G. Leclercq, R. Maurel, C. Bolivar, H. Charcosset, R. Fretty, and L. Tourayan. *J. Catalysis* **45** (1976) 179.

[50] H. Charcosett, R. Frety, G Leclercq, E. Mendes, M. Primet, and L. Tournayan. *J. Catalysis* **56** (1979) 468.

[51] C.R. Apestequía and J. Barbier. *J. Catalysis* **78** (1982) 352.

[52] M. Alnot, A. Cassuto, R. Ducros, J.J.Ehrhardt, and B. Weber. *Surface Sci.* **114** (1982) L48.

[53] V.K. Shum, J.B. Butt, and W.M.H. Sachtler. *J. Catalysis* **96** (1985) 371.

[54] William G. Moffatt, editor. *Binary Phase Diagram Handbook.* Volume 4, General Electric Company, Schenectady, N.Y., 1976.

Chapter 2

Experimental

2.1 Equipment

2.1.1 Ultra–high vacuum apparatus

Surface science and catalytic studies reported in this thesis were performed in two different ultra-high vacuum systems. One of the systems combined an internal isolation cell (high pressure or HP cell) that provided an environment to perform hydrocarbon or other reactions at atmospheric pressures, while the second chamber was equipped to perform X-ray and ultraviolet photoelectron spectroscopies (XPS and UPS).

The first chamber (UHV/High pressure or UHV/HP) consisted of a cylindrically shaped stainless steel bell jar with a volume of about 50 liters and has been described in detail elsewhere [1,2]. The system is pumped with a liquid nitrogen trapped six inch diffusion pump (Varian VHS-6), and following bakeout could attain a pressure of better than 1×10^{-9} Torr. The system was baked internally using a 12 inch long tungsten halogen lamp (GE quartzline Q1500T3/CL). Internal bakeout offers the advantage of effectively heating the internal isolation cell.

The chamber was equipped with a number of ports that housed the various techniques which will be described later in this Chapter (Figures 2.1 and 2.2).

Precision calibrated leak valves provide a means of introducing gases to clean the metallic surfaces studied or to dose the surfaces with desired adsorbate gases (Figure 2.1).

The second chamber (UHV only) lacked an internal isolation cell and utilized external heating for bakeout. Except for the lack of a high pressure cell and the inclusion of XPS and UPS techniques, the general configuration and pumping on this chamber is almost identical to the UHV/HP system shown in Figure 2.1. The chambers were also equipped with the following:

- An ion gun for argon ion sputtering (Phi 4-161) was used for crystal cleaning.
- A quadrupole mass spectrometer (UTI–100C) was used for residual gas analysis and temperature programmed desorption studies.
- A nude ion gauge (Varian 971-5008) monitored the chamber pressure.
- An electron gun (LBL built) provided a source of thermal electrons used in Auger excitation.
- Four grid electron optics was employed as a retarding field analyzer (RFA: Varian 981-0127) used for Auger electron spectroscopy and low energy electron diffraction.
- An off-axis electron gun was located in the middle of the RFA (Varian 981-2125) and was used for low energy electron diffraction experiments. The collector of the RFA was covered with a phosphor which glowed when excited by incident electrons.
- Three precision calibrated leak valves (Varian 951-5106) provided measured dosing of metallic surfaces with various gases.

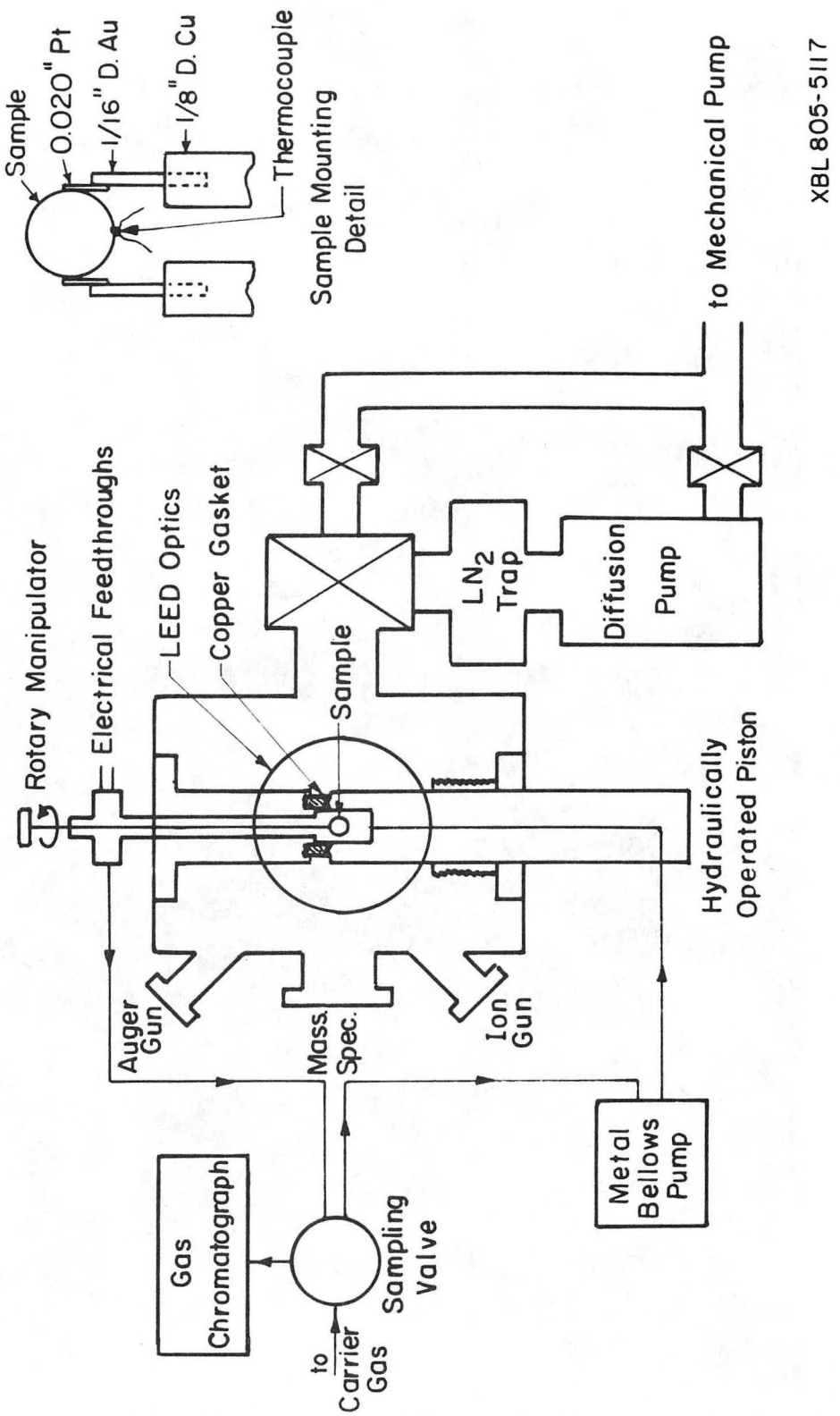

Figure 2.1: Schematic diagram of ultra–high vacuum/high pressure apparatus used for combined surface science and catalytic studies.

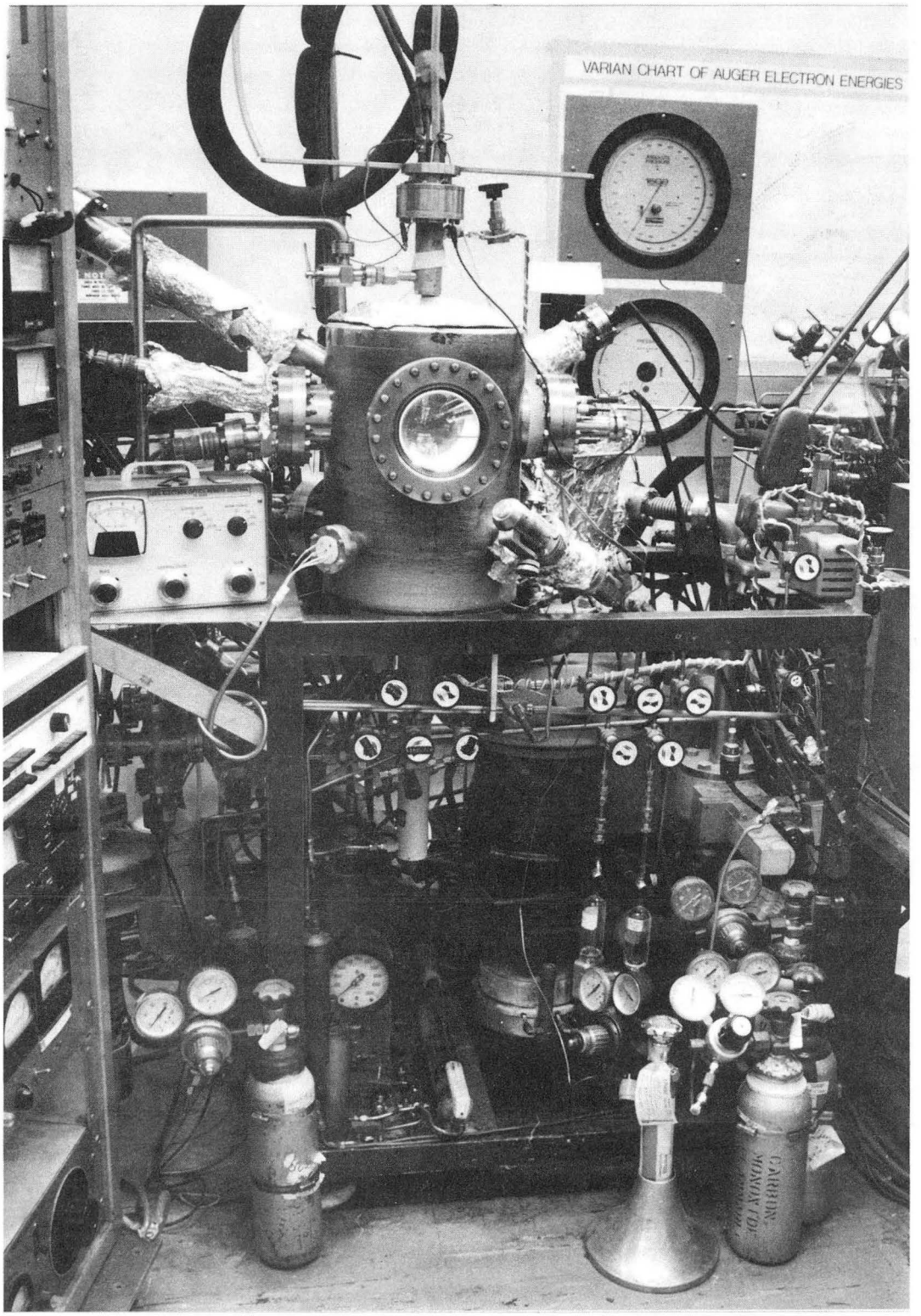

Figure 2.2: Photograph of the UHV chamber depicted in Figure 2.1.
XBB 870-8403

The UHV only chamber was equipped with the following additional equipment:

- A cylindrical mirror analyzer (CMA: Phi 15-25G) was employed as a detector for AES, XPS, and UPS. The CMA was also equipped with an internal electron gun and that was used for AES.
- An X–ray source (Phi 04-151) provided a high intensity source of X–rays from a Mg K_α target.
- An ultraviolet light source (GCA/McPherson model 630) provides UV light from a helium plasma source.

2.1.2 Metal samples and sample mounting

Single crystal and foil catalysts were mounted on a rotaTable manipulator in the UHV/HP chamber. The mounting is shown schematically in Figure 2.1 and has been discussed in detail previously [2,3]. Single crystal catalysts (Pt and Re) were spot welded to platinum wires (0.020 in) which were spot welded to gold support rods (0.062 in). Both gold rods passed through a copper block at the bottom of the manipulator and were mechanically clamped to copper heating rods mounted on ceramic feedthroughs. One of the gold rods was electrically isolated from the copper block using a ceramic sleeve. The other gold rod was placed in thermal contact with the copper block. The copper block was welded onto stainless steel tubes (1/8 inch) that were connected to feedthroughs and could be cooled by passing air or liquid nitrogen through. Samples mounted on this manipulator could be heated to over 2000 K without significant heating of the rest of the manipulator and chamber. The cooling provided at the copper block enabled the sample to return to room temperature within 5 minutes of high temperature treatments. The sample could also be cooled to 150 K when precooling the coolant

gases through a coiled copper tube immersed in liquid nitrogen. When mounting rhenium foils on this manipulator, the gold rods were replaced by tantalum rods (0.062 in) and the foil spot welded directly to the Ta rods.

The UHV only chamber was equipped with a manipulator (Varian 981-2523) which has X, Y, Z, tilt and rotational motion. Experiments done on this chamber were performed using Pt(111) crystals only. Mounting and heating was provided by spot welding the crystal between two parallel platinum wires (0.020 in) that were connected to tantalum heating leads on the manipulator.

In all cases resistive heating was used. Thermocouple wire pairs (0.005 in.) were spot welded to the edge of the crystal or to one face of the rhenium foil. Chromel vs. alumel thermocouple was preferred due to the temperature calibration that exists between liquid nitrogen temperatures and 1700° C, and to the comparatively large millivolt intervals with the temperature scale (*e.g.* 25 K/millivolt). Chromel/alumel was used whenever platinum was employed. Rhenium can be heated to much higher temperatures, but practical limitations (due to the large currents necessary) prevented heating rhenium crystals above 1600 K. In this case Pt vs. Pt–(10%)Rh thermocouple pairs were used. No problem existed in heating rhenium foils to above 2000 K, and for this case tungsten-5% rhenium vs. tungsten-26% rhenium thermocouple pairs were used.

2.1.3 The high pressure cell

The goal of this research was to study the catalytic behavior of bimetallic platinum-rhenium catalysts towards hydrocarbons. When hydrocarbon reactions were performed near atmospheric pressures, the internal isolation cell or high pressure cell (HP cell) was employed. Its position in the UHV chamber can be seen in Figure 2.1.

The high pressure cell is basically a stainless steel tube approximately one inch I.D. and one foot long. The inner wall of the HP cell is gold plated to help minimize the strong adsorption of gases. It is mounted on a hydraulically operated piston with a welded bellows allowing movement of the HP cell while providing a seal between the UHV environment and the atmosphere. A knife edge was machined onto the top of the HP cell, and this knife edge provides a seal between the pressurized reaction loop and the UHV environment when it is closed against a copper gasket situated at the bottom of the upper part of the HP cell.

2.1.4 High pressure loop and manifold system

Into the upper and lower parts of the HP cell, external to the UHV chamber, are located the input and output of the HP cell into the reaction loop (Figure 2.3). The HP cell is isolated from the loop by the use of Nu-Pro valves. The reaction loop is composed of 1/4 inch stainless steel tubing, and along the loop are located: a bellows pump (Metal Bellows Corp., MB-21) that provides gas circulation in the pressure range of 100 Torr to 1.5 atmospheres, two pressure gauges (Wallace & Tiernan models 61A-1A-0500 and FA 145-JJ15319), an eight port valve with two 0.5 cm^3 sample loops located inside a gas chromatograph, and a port giving access to the gas manifold. A bypass is provided across the GC sample valve for ease of gas mixing. The gas volume of the HP cell plus the reaction loop is $\sim$200 cm^3.

The reaction loop is pumped separately from the main chamber at two locations: by a mechanical pump connected to the reaction loop near the Wallace & Tiernan pressure gauges, and through the gas manifold. The loop can be pumped to 50 millitorr through these two pumping locations.

The gas manifold is pumped by a 2-inch liquid nitrogen trapped diffusion pump (Varian VHS-2). Rough pumping is provided by a rotary mechanical pump that

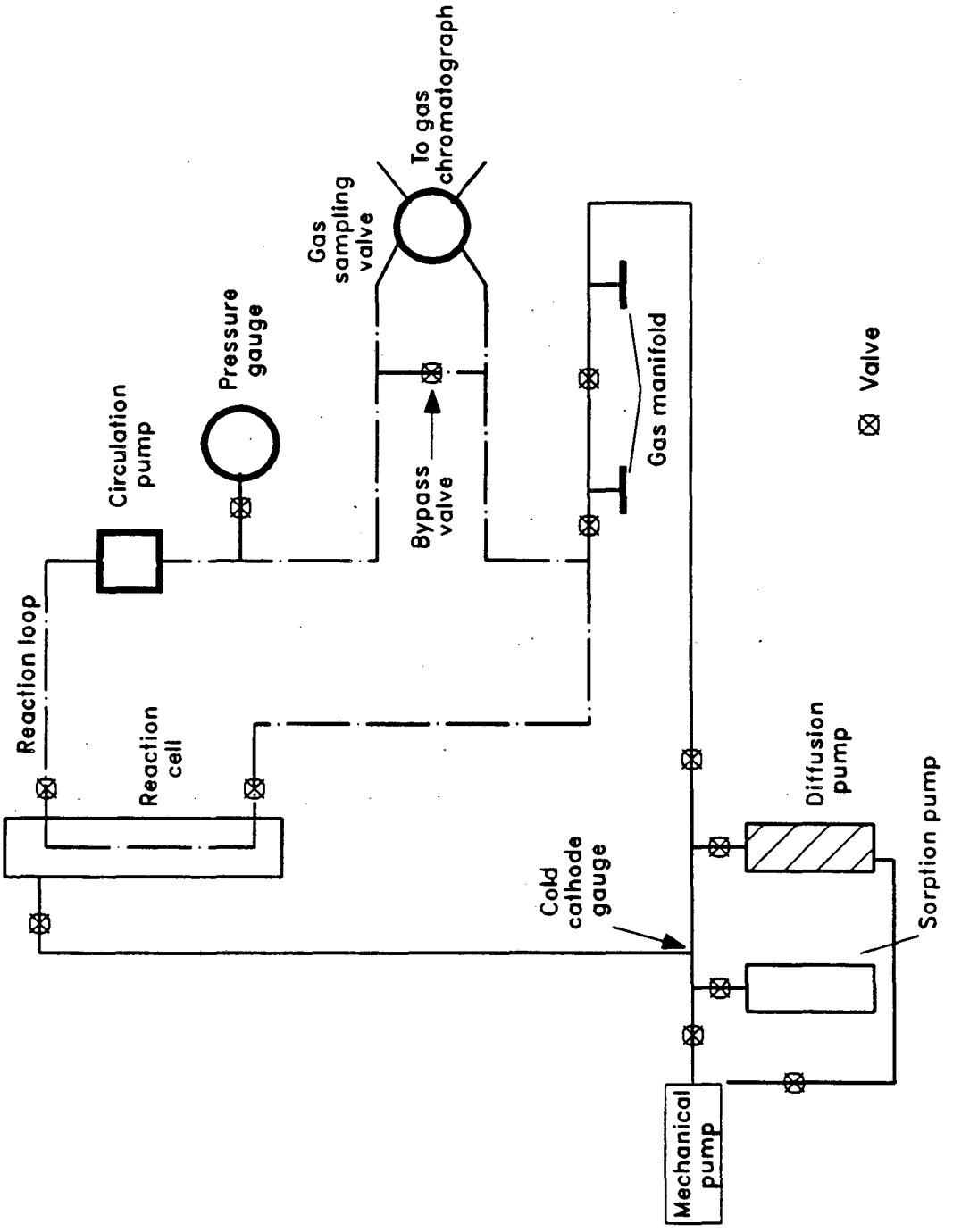

Figure 2.3: Schematic representation of the reaction loop with high pressure (reaction) cell.

Table 2.1: Gas chromatographic supports used and the separations obtained.

Support	Separation
Poropak N	CH_4, C_2H_4, C_2H_6
0.19% Picric acid on Chromosorb	C1-C6 hydrocarbons excluding benzene
5% TCEP on Chromosorb G	Benzene from other hydrocarbons

also serves as a backing pump for the diffusion pump. Alternately, the manifold can be pumped by a liquid nitrogen cooled sorption pumps. Ten 1/4 inch conduits, each valved with Nu Pro valves, are connected to the manifold so that gases (H_2, O_2, N_2, Ar, CO, and hydrocarbons) can be introduced to the reaction loop, or to the three leak valves. The manifold was isolated from the reaction loop by a Nu–Pro valve, and a needle valve provides control of the input rate of gases into the reaction loop.

2.1.5 Hydrocarbon separation and detection

Product accumulation during atmospheric reactions was monitored using a gas chromatograph (Hewlett-Packard 5830A). This GC is microprocessor controlled (Hewlett-Packard 18850A) and can accommodate two columns simultaneously. Temperature ramps as well as isothermal operation is also possible with this unit.

The separations required were achieved with three basic supports: Poropak N, 0.19% Picric acid on Chromosorb, and 5% TCEP on 60/80 Chromosorb G. The function of these columns is shown in Table 2.1.

The reaction mixture was sampled automatically by the gas chromatograph. With the bypass valve in the closed position (Figure 2.3), the reaction mixture

passes through the primary gas sampling valve. Larger hydrocarbons such as n-hexane give a complex reaction mixture including benzene. Two columns were necessary to separate these mixtures in a reasonable period of time; for this purpose a 0.19% picric acid on Chromosorb and a 5% TCEP on Chromosorb G were used. Two columns can be used during a single run to get complete separation of the reaction mixture using the sampling valve configuration shown in Figure 2.4.

The separated hydrocarbons are detected with a flame ionization detector. Integration of the peaks is done automatically by the integrator/microprocessor interfaced with the gas chromatograph and reported at the end of the chromatogram. Calibration of the GC was made with a gas mixture of 100 ppm methane in nitrogen. Other hydrocarbon products were calibrated against methane using published data for the flame ionization detector [4].

2.1.6 Metal deposition source

Many of the experiments reported in this thesis are concerned with the properties and catalytic behavior of bimetallic surfaces. Bimetallic surfaces were prepared by depositing one metal onto a monometallic single crystal or foil substrate. The metal deposition source consists of two 1/4 inch copper feedthroughs mounted on a six inch flange on one chamber port and is shown in Figure 2.5. The metal filaments are attached to the ends of the feedthroughs inside the vacuum system at 1.5 inches from the substrate surface. Both rhenium and platinum metals were deposited from the same source. A tantalum shield was fixed to the source to minimize the evaporation of metal onto other parts of the chamber.

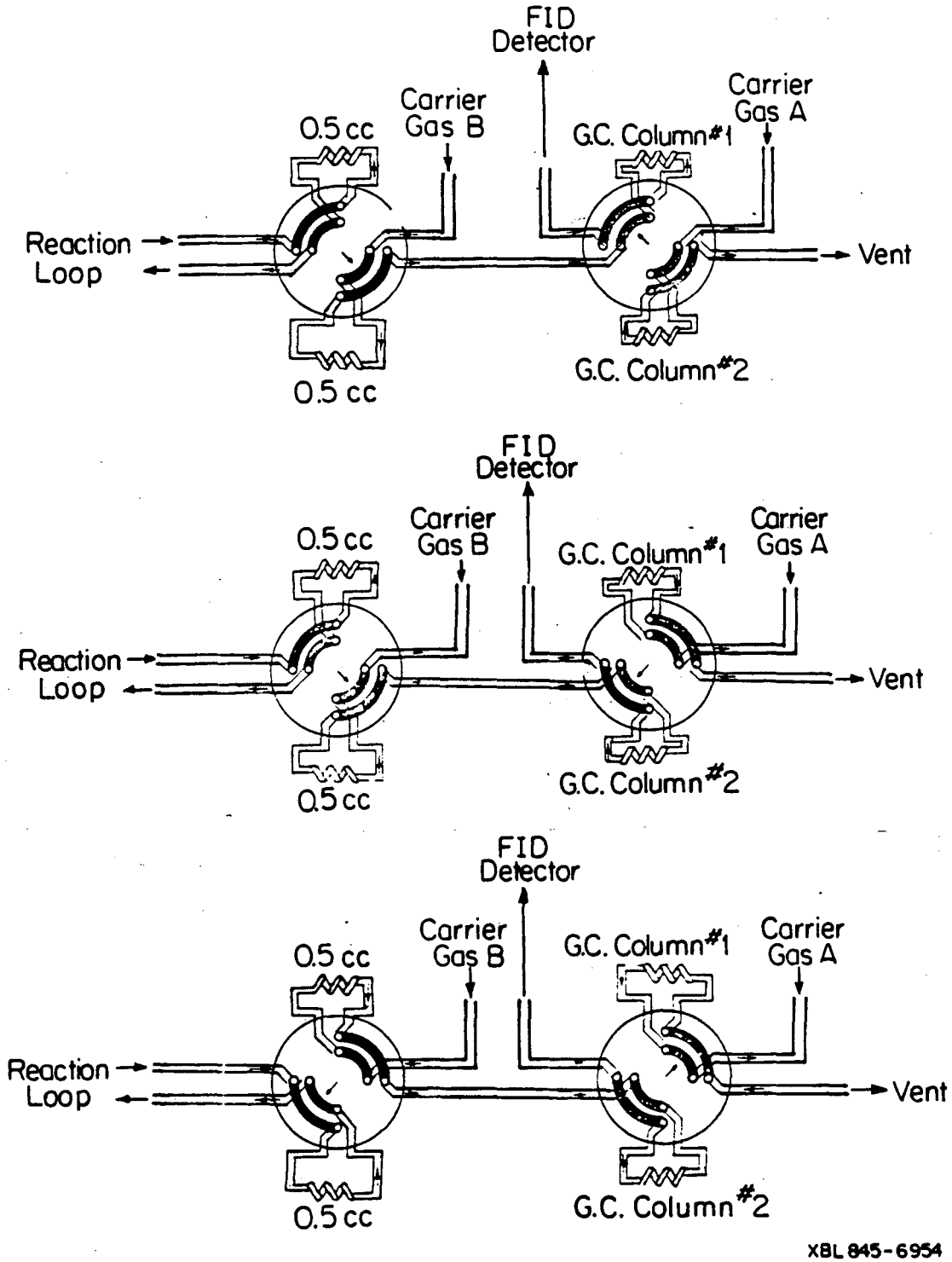

Figure 2.4: Schematic for the two sampling valve configuration used during online gas chromatographic analysis shows how two columns can be employed in parallel. Notice how a 1/4 turn of either valve activates a new flow pattern.

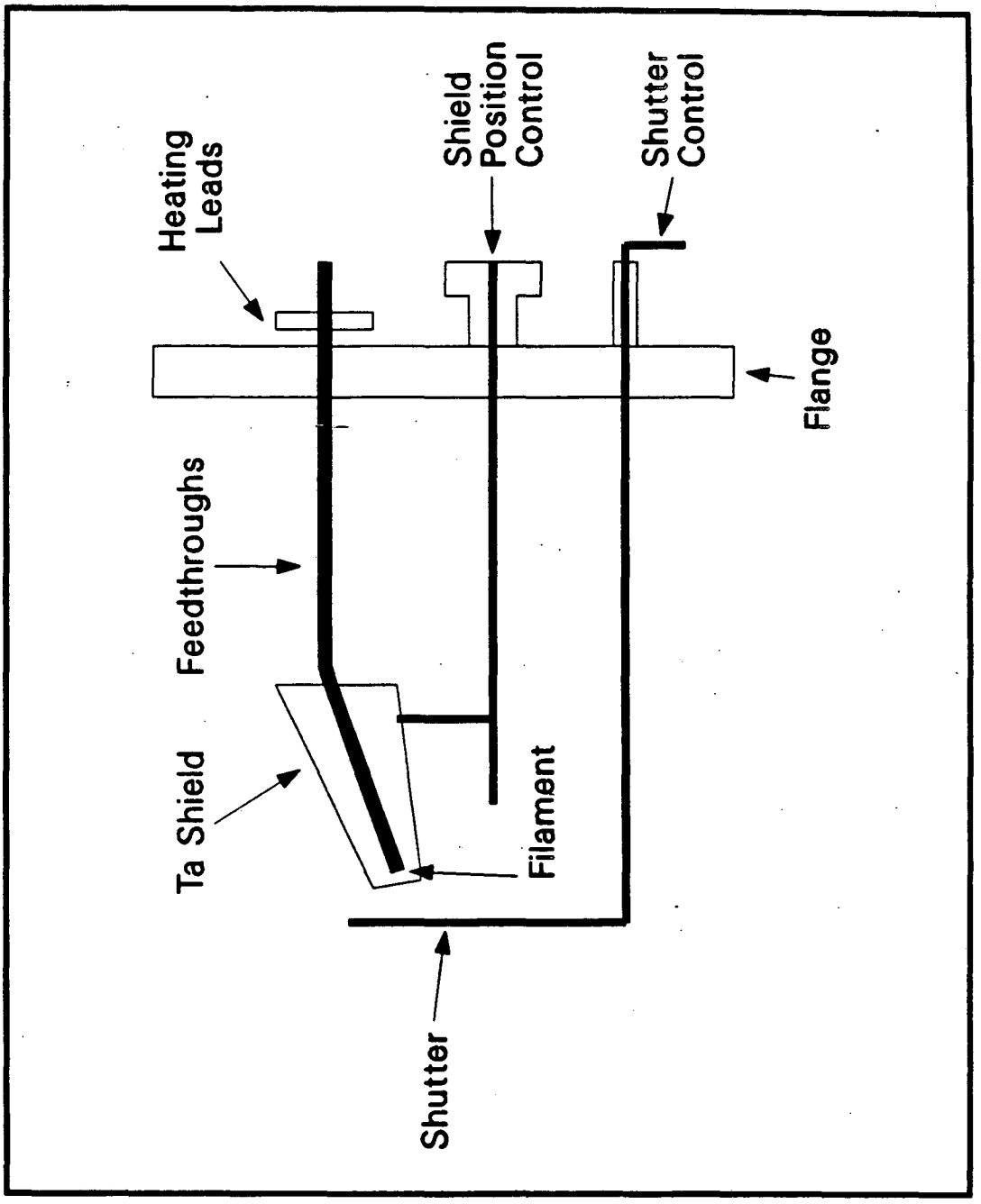

Figure 2.5: Schematic representation of the metal deposition source used for both platinum and rhenium deposition.

2.2 Surface Analysis Methods

2.2.1 Auger electron spectroscopy

Auger electron spectroscopy (AES) was used routinely to monitor the state of the substrate surface. The cleanliness of the surface achieved during cleaning procedures was one important use of AES. The accumulation of carbon and other impurities following chemisorption, temperature programmed desorption, and atmospheric pressure hydrocarbon studies was also determined using AES. When performing experiments on bimetallic surfaces, Auger electron spectroscopy was the primary tool used for the determination of the metallic composition of the surface.

The low penetration depth that slow electrons have in solids makes AES surface sensitive and such a useful technique in surface science studies. The so-called universal curve relating the mean free path of electrons to their kinetic energy is shown in Figure 2.6.

The surface sensitivity is further enhanced by using an incident electron beam at a grazing angle relative to the surface. Auger electron spectra were obtained by operating the electron gun at an energy of 1–2 KeV and at a 90° angle with respect to the RFA axis. The crystal was tilted 20° off normal with respect to the RFA axis. The minimum in the curve is obtained near the region of interest for Auger electrons (50 – 300 eV). This surface sensitivity coupled to the characteristic Auger spectrum or "fingerprint" generated by each element makes this technique an extremely useful one.

The Auger process can be described as follows: primary ionization involves a core level electron that is removed from an atom (these studies were always concerned with solid surfaces) by bombardment with 1–2 KeV electrons. Two

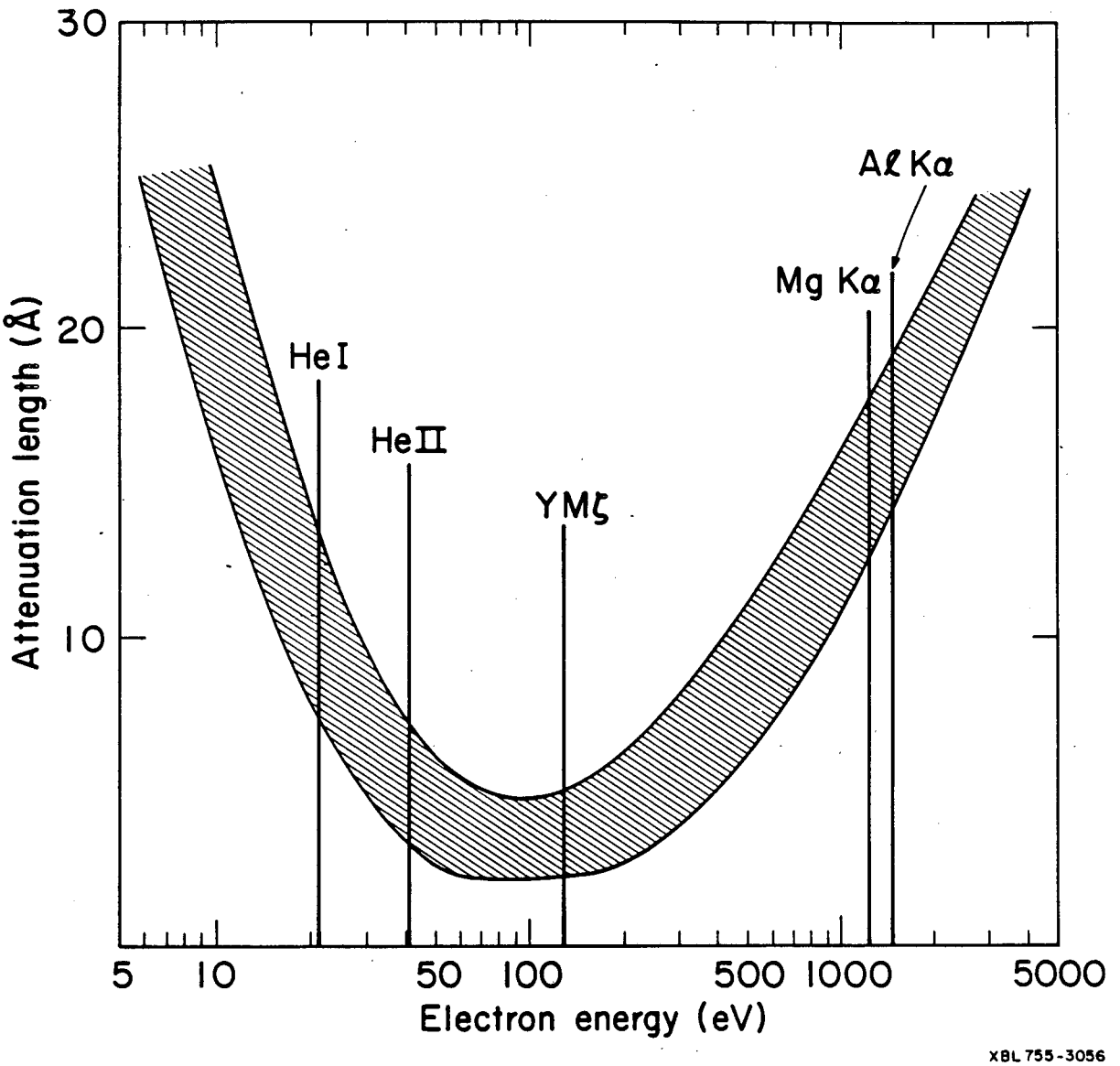

Figure 2.6: Universal curve for condensed phases showing the attenuation length or inelastic mean free path dependence on the electron kinetic energy.

competing relaxation processes follow, X-ray fluorescence and Auger emission. Both processes involve the transition of an electron in a higher energy orbital to the core level orbital vacated during primary ionization. This electron loses energy in the process, and in the case of X-ray fluorescence, the energy is emitted as an X-ray photon. In the Auger process, a third electron in an autoionization process carries the energy away in the form of kinetic energy. The measured kinetic energy of the emitted Auger electron is

$$E_{Auger}^{KE} = E_1 - E_2 - E_3^* - e \cdot \phi_{sp} \tag{2.1}$$

where E_1 is the binding energy of the core level electron, E_2 is the binding energy of the electron which fills the core level from a higher energy level, E_3^* is the binding energy of the ejected Auger electron moving in a field of increased charge, and ϕ_{sp} is the work function of the spectrometer. A schematic representation of the Auger and X-ray deexcitation processes are shown in Figure 2.7.

The kinetic energy of the Auger electrons were determined using a four-grid retarding field analyzer (RFA). For the Auger mode, the first and fourth grids were grounded, and the retarding field was applied to the second and third grids. Electrons with kinetic energies exceeding that of the retarding potential (V_r) were accelerated to a collector with a +900 volt applied potential. The diagram in Figure 2.8 shows how the Auger signal is measured. In a typical Auger experiment, a negative potential was scanned from 20 to 550 volts on the second and third grids of the RFA, and electrons with enough energy to reach the collector were measured. The measured current is a function of the retarding potential (V_r), and all electrons with a kinetic energy exceeding that of V_r are collected. The current is given by

$$I(V_r) \propto \int_{E=eV_r}^{\infty} N(E)dE \tag{2.2}$$

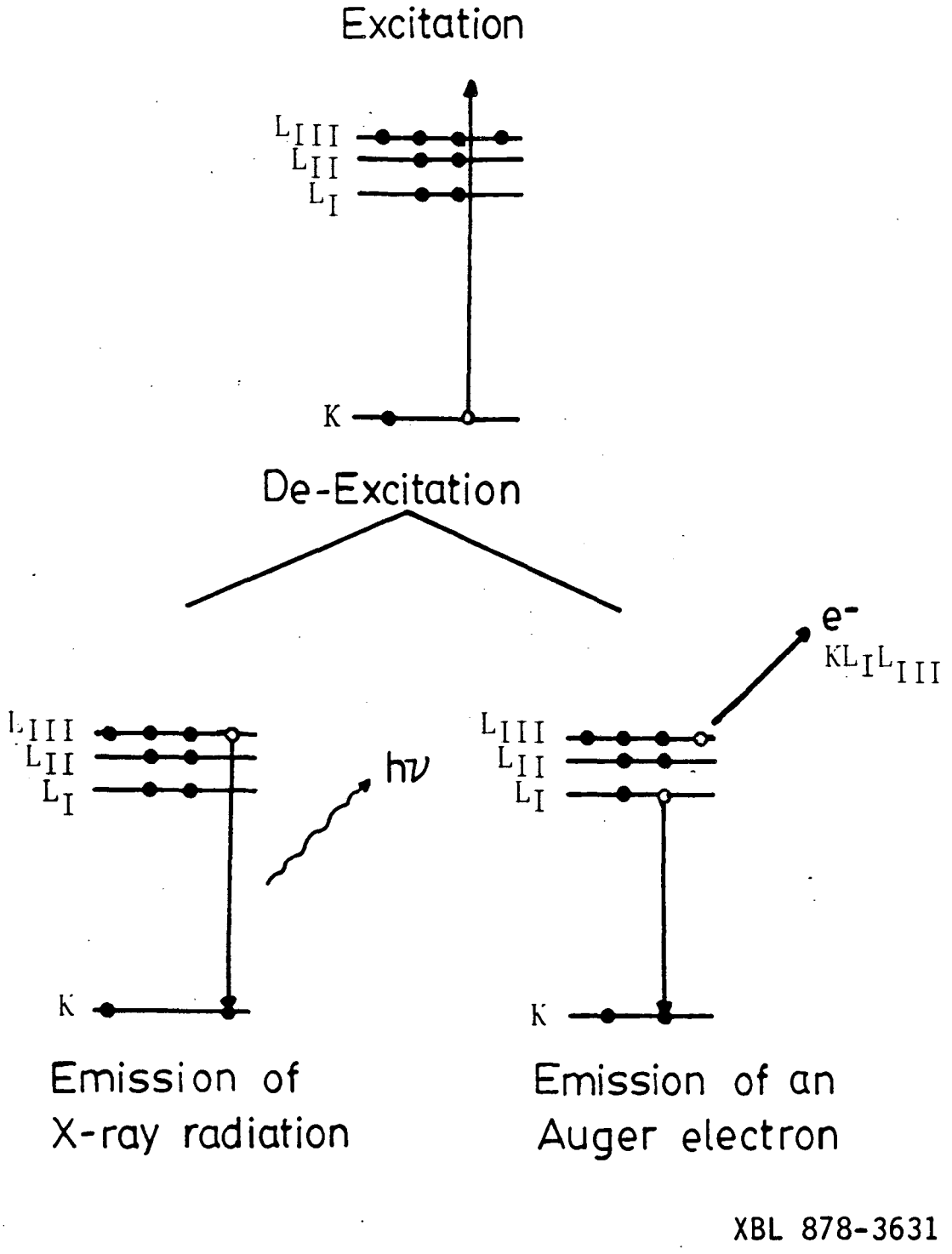

Figure 2.7: Electron energy level representation of the excitation and deexcitation of an atom during X–ray fluoresence and Auger emission.

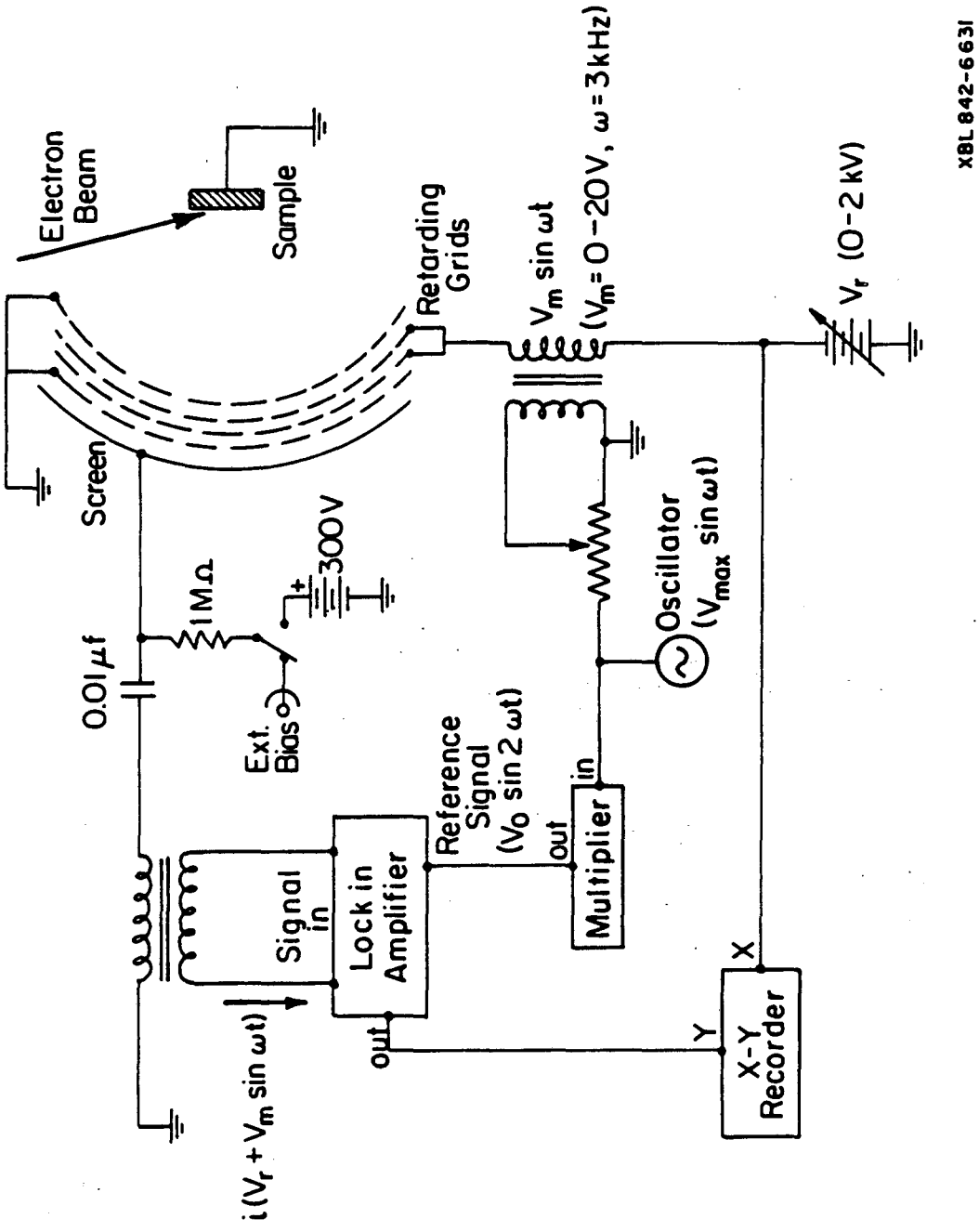

Figure 2.8: Schematic of the electron collection and analysis system used for Auger electron spectroscopy and low energy electron diffraction.

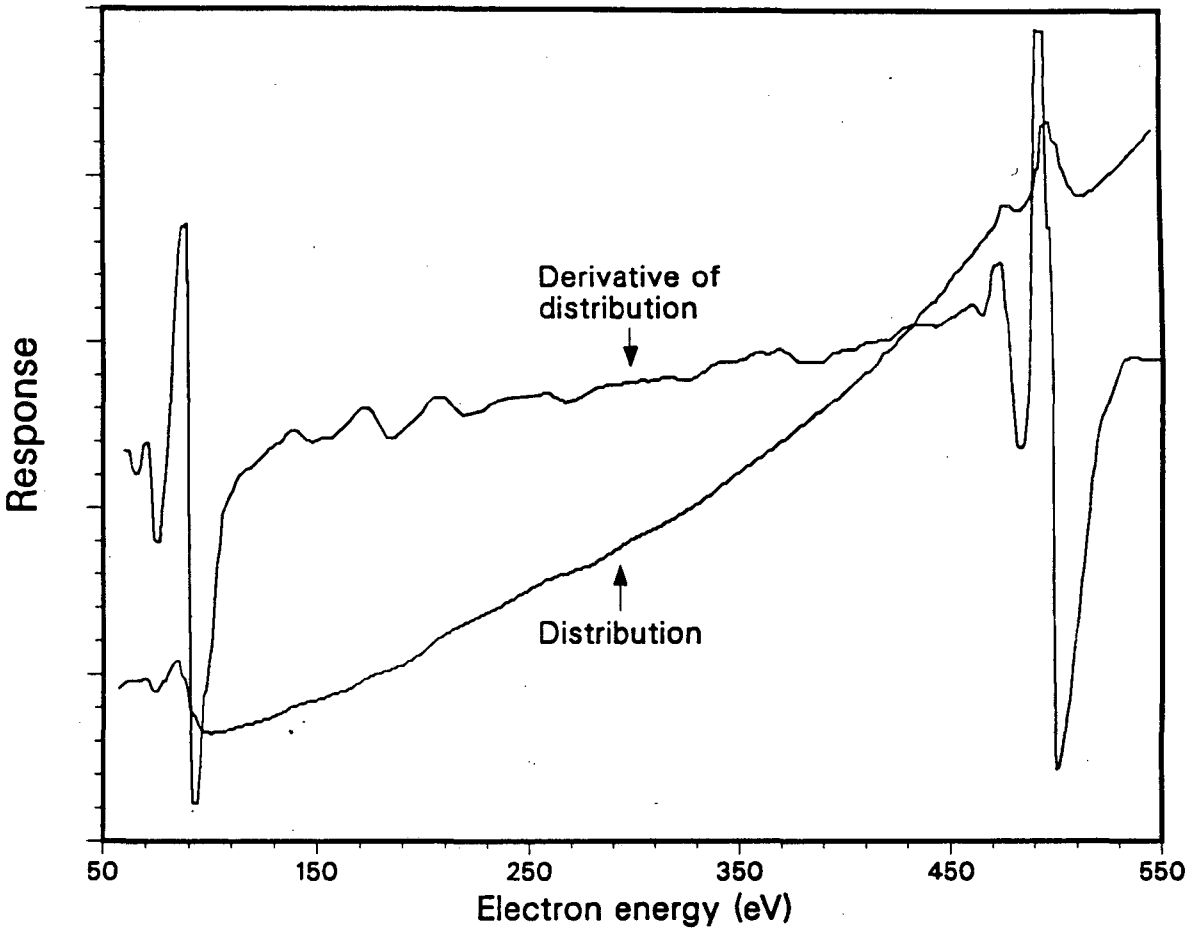

Figure 2.9: Energy distribution of secondary electrons ejected from a solid surface. Both N(E) and dN(E)/dE vs. E are shown for beryllium (from [5]).

where $N(E)$ is the number of electrons with the kinetic energy E. The secondary electron distribution versus electron energy is shown in Figure 2.9. However, there exists a background of secondary electrons ejected by other processes which complicates the discrimination and measurement of Auger electrons. For this reason, electronic differentiation techniques are applied to discriminate the Auger electrons from the secondary electron background.

A small modulation voltage is added to the retarding potential V_r of the form $V_m \sin \omega t$. The magnitude of V_m used was 1–10 volts peak to peak and the modulation frequency used was between 2–3 KHz. Now the current collected can

be represented by a Taylor series

$$I(V_r + V_m \sin\omega t) = I(V_r) + I'(V_r)V_m \sin\omega t + \frac{1}{2}I''(V_r)V_m^2 \sin^2\omega t + ... \quad (2.3)$$

Now

$$\sin^2\omega t = \frac{1}{2}[1 - \cos 2\omega t] \quad (2.4)$$

and

$$\frac{dN(E)}{dE} \propto I''(V_r) \quad (2.5)$$

The signal measured with a lock-in amplifier tuned to 2ω is proportional to dN(E)/dE (the Auger signal) and is recorded as a function of V_r. In this way the Auger spectrum is recorded, and the dN(E)/dE signal is compared to the N(E) distribution in Figure 2.9. Ertl and Kuppers give a more detailed treatment of the Auger process and should be consulted for further information [5].

Auger electron spectroscopy can also be utilized to distinguish thin film growth mechanisms. Commonly observed thin film growth mechanisms are: 1) Frank-van der Merwe or a layer by layer growth mechanism; 2) Stranski-Krastanov or three dimensional crystallites growing on one or more completed monolayers; and 3) Volmer-Weber or three dimensional crystallites growth [6]. Carefully controlling the adsorbate dosing so that a constant flux is obtained while monitoring the uptake using AES will result in curves for the three different mechanisms as shown in Figure 2.10.

The growth mechanism which is probably the most important mechanism for metal on metal growth is the layer by layer mechanism. A very simple model was proposed by Gallon [7] to describe this mechanism. The important assumption is that a monolayer fills in completely before the next layer begins to grow. For a given number of complete monolayers n of an adsorbate on a different substrate,

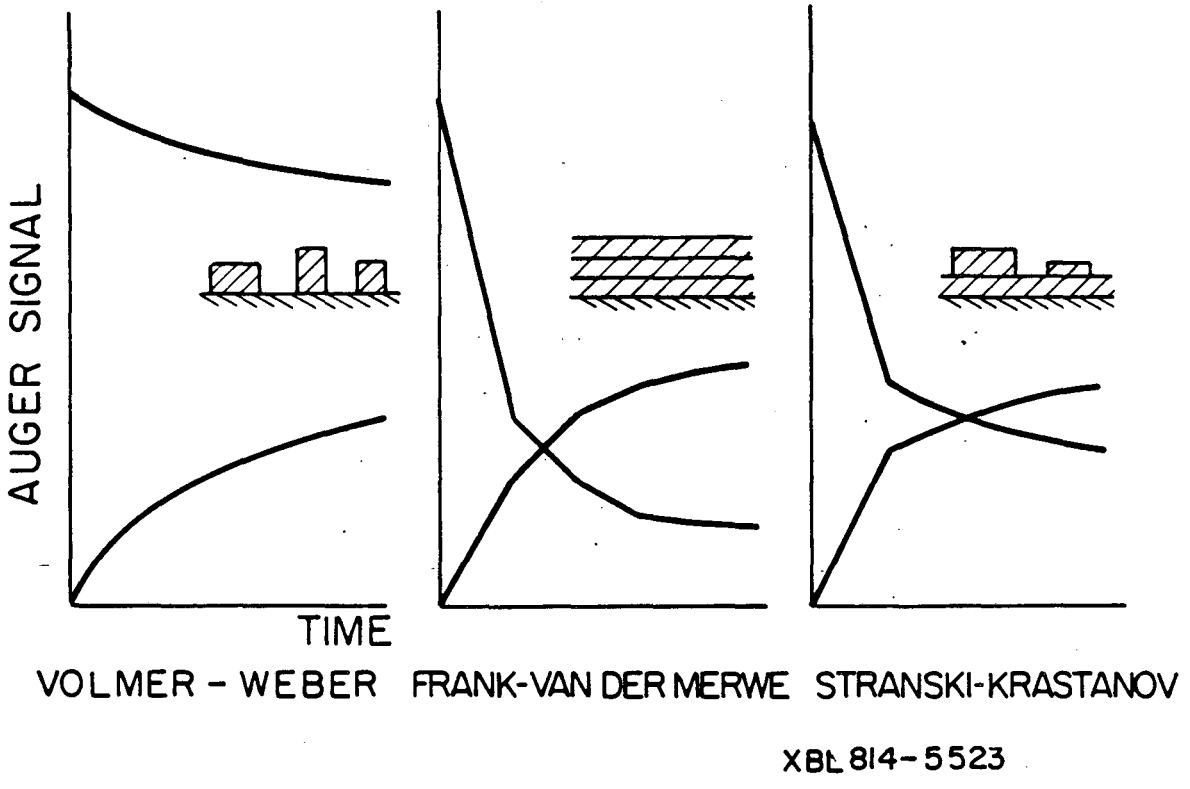

Figure 2.10: Thin film growth mechanisms obtained from solid surfaces are shown by the characteristic variation of the Auger signal vs. the time of deposition.

the attenuation of the substrate signal is given by

$$I_s^{(n)} = \alpha^n \tag{2.6}$$

where $I_s^{(n)}$ is the signal from the substrate covered with n complete layers of adsorbate. α is defined by

$$\alpha = \frac{I_s^{(1)}}{I_s^{\circ}} \tag{2.7}$$

where I_s° is the intensity of the clean substrate peak uncovered and $I_s^{(1)}$ is the intensity of the same peak covered with one monolayer of adsorbate. The adsorbate signal increases according to

$$I_a^{(n)} = I_a^{(\infty)} \left[1 - (1 - \frac{I_a^{(1)}}{I_a^{(\infty)}})^n \right] \tag{2.8}$$

where $I_a^{(n)}$ is the intensity of the Auger signal for n complete layers of adsorbate and $I_a^{(\infty)}$ is the intensity of bulk adsorbate. For an incomplete layer $n-1 < \theta_a < n$ where θ is coverage in monolayers, the Auger signals for the substrate and the adsorbate is assumed to be a linear combination of the above expressions (Equations 2.6 and 2.8) for $n-1$ and n monolayers. A general expression can be derived for the substrate signal using Equation 2.6 obtaining

$$I_s = I^{\circ}[\alpha^{n-1}(n-(n-1)\alpha) - \alpha^{n-1}(1-\alpha)\theta_a] \tag{2.9}$$

for the intensity of the substrate Auger peak I_s covered with θ_a monolayers of adsorbate where $n-1 \leq \theta_a \leq n$. When a system follows the Frank-van der Merwe growth mechanism, clear breaks are usually observed for both the substrate and the adsorbate Auger uptake curves, as will be seen later for the platinum on rhenium and the rhenium on platinum systems.

2.2.2 Low energy electron diffraction

Low energy electron diffraction (LEED) yields information on the surface structure if two dimensional order exists. LEED is the two dimensional analog of X-ray

diffraction and is surface sensitive because electrons interact strongly with matter. An inspection of the universal curve shown in Figure 2.6 reveals that LEED electrons (50–200 eV) sample only the top few monolayers of a surface.

The wavelength associated with a beam of electrons was first postulated by deBroglie

$$\lambda = \sqrt{\frac{150}{E}} \tag{2.10}$$

where λ is given in Å and E in eV. When a monoenergetic beam of electrons impinges on an ordered surface, diffraction occurs and results in constructive and destructive interference in preferred directions. The diffraction angle ϕ can be calculated from the Bragg condition for an electron beam striking the surface by

$$\sin\phi = \frac{n\lambda}{d_{h,k}} = \frac{n}{d_{h,k}}\sqrt{\frac{150}{E}} \tag{2.11}$$

where n is the order of diffraction, and $d_{h,k}$ is the distance between parallel rows of scatterers in the [h,k] direction. Please consult the following references for more information on LEED [5,8].

Using this technique, information can be obtained about the size and symmetry of a unit cell including the ordering of adsorbates. In principle, information regarding bond angles and distances in the z direction for the uppermost layers including adsorbates can also be obtained if one painstakingly collects intensity vs. electron energy data (*e.g.* I(V) curve). No I(V) curves are reported in this thesis, and only information about the unit cell is included.

A schematic representation of the LEED experiment is shown in Figure 2.11. The retarding field analyzer is used for LEED as well as for AES. In the low energy electron diffraction mode, grids 2 and 3 are negatively charged and are used as a suppressor to repel inelastic electrons since the imaging of only elastically scattered electrons is desired for LEED. The elastically scattered electrons that overcome

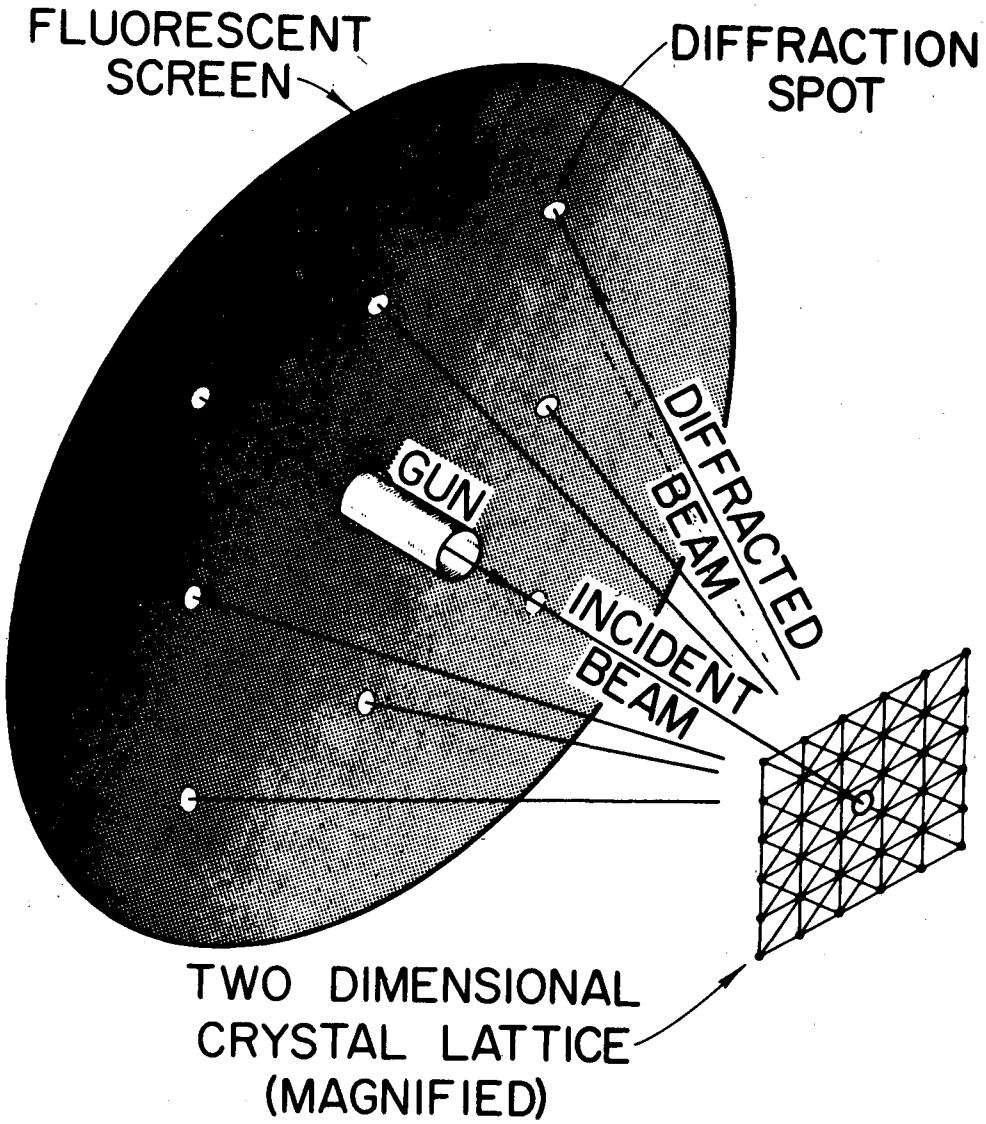

Figure 2.11: A schematic representation of the low energy electron diffraction (LEED) experiment. XBB 708-3583

the suppressor voltage are accelerated by a 4–6 kilovolt potential at the phosphor covered collector or screen as shown in Figure 2.8. A LEED pattern is recorded by taking a photograph in a darkened room.

2.2.3 X-ray photoelectron spectroscopy

X-ray photoelectron spectroscopy (XPS) gives information on the chemical state of a material. When a high intensity source of X-rays is focused on a sample, electrons are emitted from the sample that are characteristic of the material and its chemical state. For example, a simplistic view is that when a material is oxidized, electronic charge is shifted away from an atom towards the oxidizing or more electronegative species. The result is that the shielding experienced by the remaining electrons around the nucleus from the nuclear charge is decreased, so the electrostatic potential experienced by these electrons is increased and an increased binding energy is measured for the electrons emitted. For further information on this technique, consult references [5,9].

Experiments were performed in the UHV only chamber using a double pass cylindrical mirror analyzer [5,10]. X-rays were generated using a Mg Kα source (1253.6 eV). Since electrons with high kinetic energies ($\sim$1000 eV) are less surface sensitive than the 100 eV electrons used for AES (Figure 2.6), it was desirable to enhance the substrate surface X-ray photoelectron signal by tilting the Pt(111) crystal 50° off normal with respect to the CMA axis. The binding energy of the photoelectron is related to the measured kinetic energy through the following relation:

$$1253.6eV = E_{kinetic} + E_{binding} + e \cdot \phi_{sp} \tag{2.12}$$

where the third term is a correction taking into account the work function of the spectrometer. Since the magnitude of the spectrometer work function is unknown,

the binding energies were referenced either to the platinum $4f_{7/2}$ line with a binding energy of 70.9 eV or the gold $4f_{7/2}$ line at 83.8 eV [11].

XPS experiments were performed on Pt(111) crystals that were dosed with rhenium. Oxidative and reductive treatments were also applied to these surfaces followed by analyses using XPS. When rhenium covered the platinum crystal, a gold foil that was mounted on the back side of the manipulator was used as a reference. The spectrometer and data acquisition was controlled by a Commodore Pet computer, and the software used has been described in detail elsewhere [12].

2.2.4 Temperature programmed desorption

Temperature programmed desorption (TPD) yields information on chemisorption and bonding energetics of adsorbates. It is also useful in studying surface reactions. Once a surface is prepared and dosed with the desired adsorbate, a linear heating ramp is applied between 10–50 K/sec, and the desorption of different chemical species are monitored using the mass spectrometer. The data is recorded by tracing the partial pressure vs. substrate temperature, or in some cases vs. time. Under the conditions of high pumping speeds and a linear heating ramp, the change in partial pressure of a chemical species is proportional to the desorption rate [13]. Redhead showed that for a first order desorption, the activation energy of desorption can be calculated using

$$\frac{E_a}{RT_{max}} = \ln\left(\frac{\nu_1 T_{max}}{\beta}\right) - 3.64. \qquad (2.13)$$

Here E_a is the activation energy of desorption, T_{max} is the temperature where the maximum rate of desorption occurs, ν_1 is the first order preexponential factor, and β is the heating rate. For a Redhead analysis, a preexponential factor of 10^{13} sec^{-1} is often assumed. In order to obtain the preexponential factor using this

method, a series of TPD experiments must be performed varying the heating rate preferably over 2 orders of magnitude. Soler and García have shown that one can expect an activation energy calculation that varies only by about 15% when ν_1 is varied over 7 orders of magnitude [14].

The calculation of E_a of desorption for a second order process is complicated by the dependence of T_{max} on coverage, which means that the coverage must also be determined. The coverage of hydrogen was estimated by assuming that at saturation, one hydrogen atom per platinum atom was adsorbed on the clean Pt(111) surface. With high pumping speeds and a linear heating rate, the area under a desorption peak is proportional to the surface coverage before desorption. To estimate the initial hydrogen coverage n_o, the desorption area was compared to the area obtained at saturation on clean Pt(111). This area was assumed to correspond to $n_{sat} = 1.5\times10^{15}$ hydrogen atoms/cm^2. Now the activation energy of desorption is calculated using the relation from reference [13].

$$\frac{E_a}{RT_{max}^2} = \frac{n_o\nu_2}{\beta}\exp(-E_a/RT_{max}) \tag{2.14}$$

Rearrangement yields

$$\ln(n_oT_{max}^2) = \frac{E_a}{RT_{max}} + \ln\left(\frac{E_a}{R}\right) - \ln\left(\frac{\nu_2}{\beta}\right) \tag{2.15}$$

Plotting $\ln(n_oT_{max}^2)$ versus $1/T_{max}$ for a series of TPD experiments yields a line with a slope of E_a/R [15].

Alternative methods for calculating activation energies of desorption were taken from Chan *et.al.* [16]. For a first order desorption, the activation energy of desorption is given by

$$E_a = RT_{max}\left[-1 + \frac{Y_{1/2}^2 + 5.832)^{1/2}}{Y_{1/2}}\right] \tag{2.16}$$

Table 2.2: Mass spectrum cracking intensities of ethanes, $C_2H_{6-n}D_n$. Signal intensity is relative to the parent peak.

amu	d_0	d_1	d_2	d_3	d_4	d_5	d_6
26	23	14	10	3	3	2	3
27	33.3	24	23	13	12	8	0.2
28	100	48	37	16	22	23	21
29	20.2	100	78	20	22	18	0.7
30	26.2	22	100	100	68	27	27
31	0.6	31	24	21	100	100	1
32	–	–	38	15	51	89	100
33	–	–	–	29	17	27	2
34	–	–	–	–	44	7	15
35	–	–	–	–	–	47	0.8
36	–	–	–	–	–	–	19

where

$$Y_{1/2} = \frac{\Delta T_{max}}{T_{max}} \tag{2.17}$$

and ΔT_{max} is the full width at half maximum of the desorption peak.

Ethylene deuteration experiments were performed using TPD, and the deuterated ethanes formed, D_0–D_6, were estimated by deconvoluting TPD data. Cracking patterns for hydrocarbons are complex as shown in Figure 2.12. When a mixture of deuterated ethanes was obtained, the following recursive formula was used to estimate the relative contribution of each deuterated ethane [10].

$$D_n = \left[\frac{1}{\alpha^n_{30+n}} (M_{30+n} - \sum_{i=n+1}^{6} D_i \cdot \alpha^i_{30+n}) \right] \tag{2.18}$$

where α^n_{30+n} is the signal intensity of D_n at $30+n$ amu (from Table 2.2) and M_{30+n} is the signal of the mixture spectrum at $30+n$ amu. D_n is proportional to the amount of desorbing ethane, $C_2H_{6-n}D_n$.

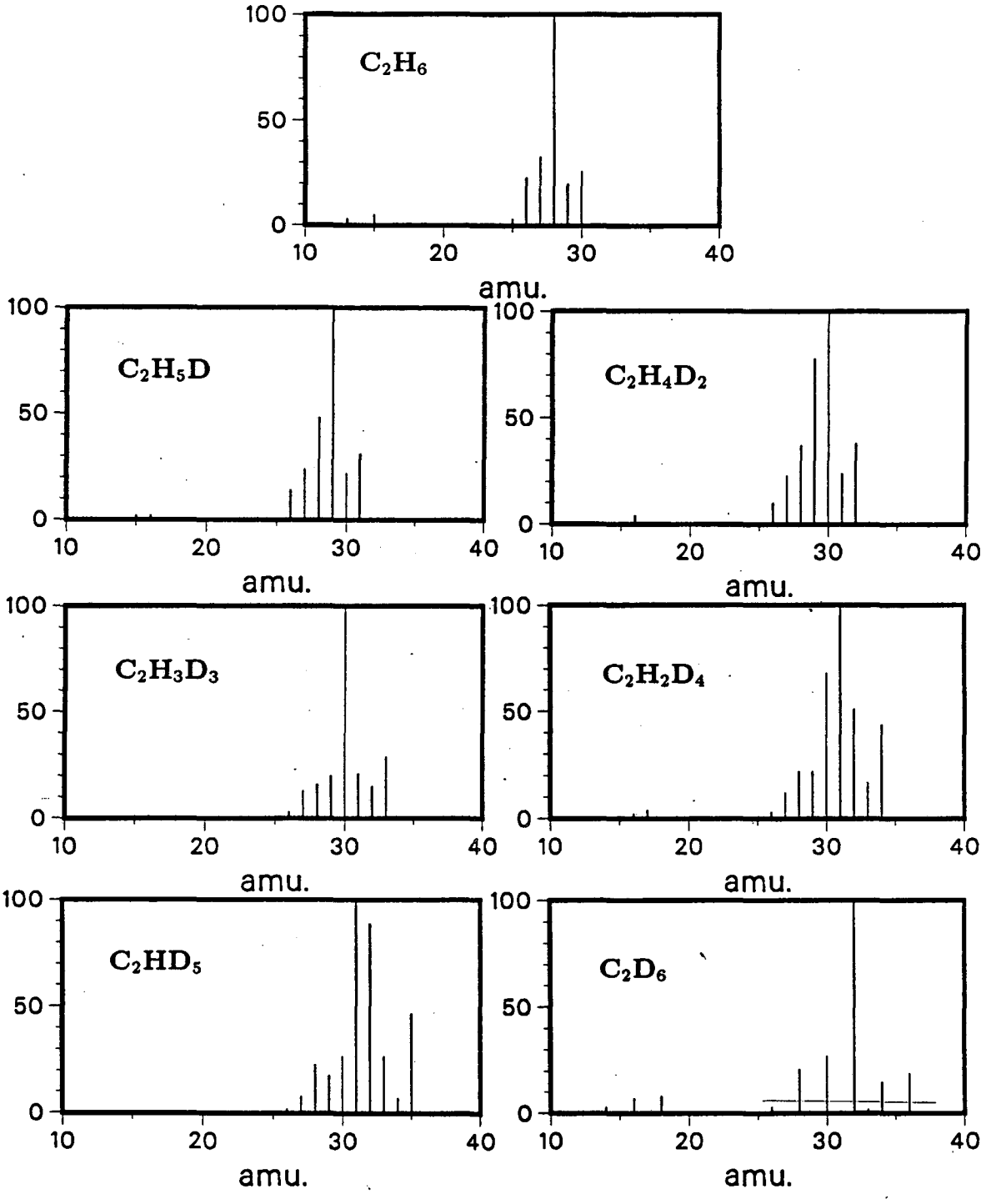

Figure 2.12: The mass spectrum of D_0–D_6 ethanes ($C_2H_{6-n}D_n$) demonstrates the complexity of hydrocarbon cracking patterns (from reference [17]).

2.3 Materials

2.3.1 Catalyst samples

The catalyst samples used in this study were platinum single crystals having a (111) or (100) orientation, rhenium single crystals with a (0001) orientation, and polycrystalline rhenium foils.

The platinum and rhenium single crystals were cut by spark erosion and polished using diamond paste and 0.25 μm alumina slurry on both sides at LBL so that the crystal face exposed was cut to within 1° of the desired orientation. All crystals used have an area of approximately 1 cm^2 and a thickness $\leq$ 0.5 mm. Laue X-ray back diffraction was utilized to ensure that the proper orientations were obtained, and the photos obtained from these crystals are shown in Figure 2.13.

The platinum crystals were cut from a rod obtained from the Materials Research Corporation and was claimed to be 99.996% pure by the manufacturer. The rhenium crystal was cut from a single crystal boule that existed in the group before 1983. The source is unknown, but the the purity is probably near 99.99%. Rhenium foil used was 0.025 mm thick and was obtained from Alfa Products at 99.99% purity.

Rhenium wire was obtained from Gallard-Schlesinger. It was 99.99% pure and had a diameter of 0.5 mm. Platinum wire was 0.020 inches in diameter and was obtained through Lawrence Livermore stock. Its purity was also 99.99%.

2.3.2 Reagents

Hydrocarbons obtained were the purest available, and were purchased when possible from Matheson or Phillips. Gases such as CO, H_2, O_2, and D_2 were purchased

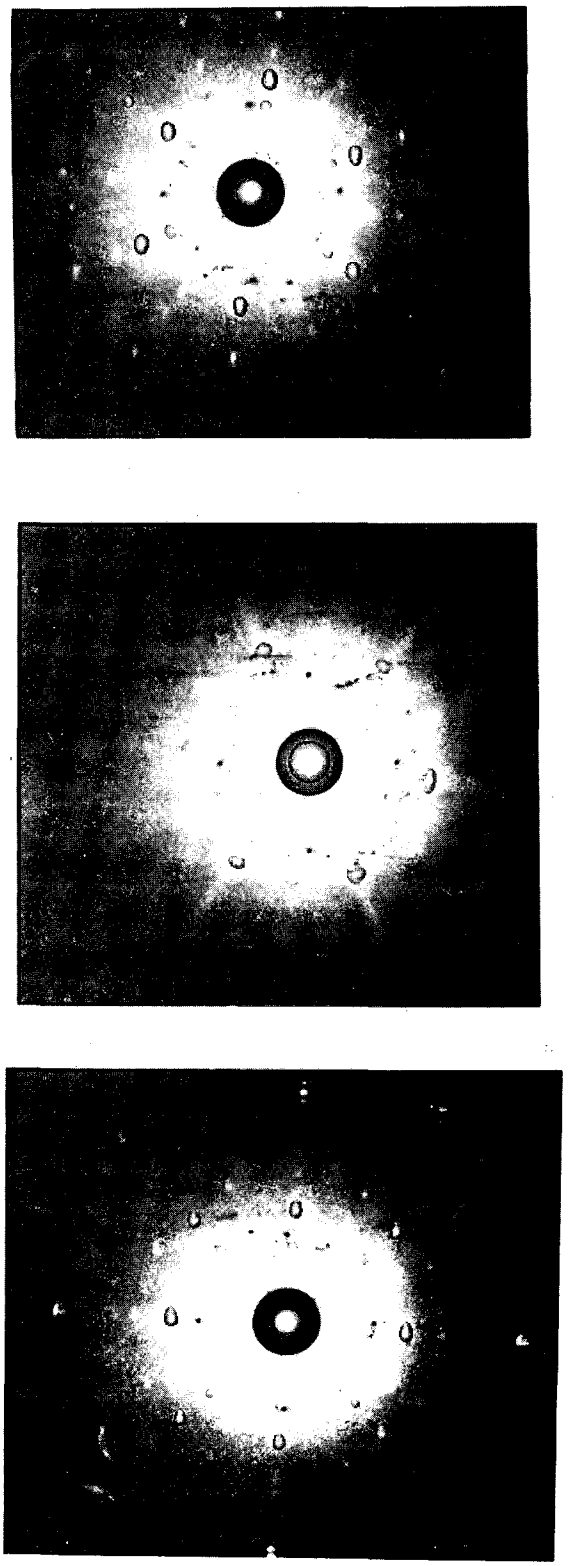

Figure 2.13: Laue X–ray back diffraction photos obtained for a) Pt(111), b) Re(0001), c) and Pt(100). XBB 878-6968

Table 2.3: Reagents and gases used: their sources and purities.

Reagent	Source	Purity
oxygen	Matheson-LBL	>99.9
hydrogen	Matheson-LBL	>99.9
deuterium	Matheson-LBL	>99.5 D_2
		>99.95 D_2 + HD + H_2
carbon monoxide	Matheson-LBL	>99.5
ethylene	Matheson	>99.99
ethane	Matheson	>99.99
n-butane	Matheson	>99.99
n-hexane	Phillips	>99.9
methylcyclopentane	Phillips	>99.9
cyclohexane	Phillips	>99.9

from Matheson-LBL. Table 2.3 lists the reagents used and their sources.

2.4 Procedures

2.4.1 Sample cleaning

Platinum and rhenium single crystals were cleaned by cycles of heating in oxygen ($\sim 3\times10^{-7}$ Torr) and argon ion sputtering (1×10^{-4} Torr Ar) at 1000 K with a 1 KeV argon ion beam energy, and annealing at 1300 K for platinum and 1600 K for rhenium until no impurities (mainly S, Ca, C, O) could be detected by AES or XPS. Rhenium foils were easily cleaned by heating to 1900–2200 K. Rhenium was removed from platinum, and platinum removed from rhenium by prolonged argon ion sputtering (about 2 hours) at room temperature and 2 KeV primary beam energy after carbon had been removed in 3×10^{-7} Torr oxygen at 900 K. Following crystal cleaning, it was verified that sharp LEED patterns were obtained corresponding to a (1×1) for Pt(111) and Re(0001), and a (5×20) for the Pt(100) [18].

2.4.2 Rhenium and platinum deposition

Rhenium metal was deposited from a 0.5 mm diameter filament resistively heated to 1800–2100 K. Platinum metal was deposited by heating to 1400–1700 K a 0.5 mm. diameter filament that was coiled about ten turns (the coil diameter was about 2 mm.). The condition of the filaments was monitored by checking the current required to just reach the visual threshold in a darkened room, about 785 K. As the filament deteriorated over a period weeks, the amount of current needed to reach this visual threshold decreased, hence the current needed to deposit metal at a given rate also decreased.

Deposition rates obtained were in the range of 2–8 minutes per monolayer (min/ML). The base pressure increased about fourfold, or to 4×10^{-9} Torr, after about one minute of operation of the rhenium source at 5 min/ML. A fresh rhenium filament required about 24 amps to operate at this deposition rate. The increase in pressure observed was due to CO and CO_2 generated from the heating leads and tantalum shield of the source as it heated up. The rhenium source was allowed to cool after each minute of operation for about 30 seconds, and the platinum crystal was usually flashed to 700 K to remove any adsorbed CO or CO_2. When the deposition source was operated with platinum, only about 9 amps of current was required to operate at 5 min/ML, and no significant increase in temperature of the deposition source or in base pressure was observed. The platinum source has been operated for periods of over 30 minutes without requiring cool down.

2.4.3 Dosing of adsorbates

Adsorbates were introduced into the chamber using the precision calibrated leak valves described previously. Gases introduced into the chamber were in the range of 10^{-9} Torr to as high as 10^{-4} Torr. Pressures reported are not adjusted for ion

Table 2.4: Ion gauge correction factors for selected gases.

Gas	Correction C_f
ethane	2.63
ethylene	2.30
hydrogen	0.428

gauge sensitivity unless otherwise specified. When quantitative data was reduced from TPD experiments reported in Chapter 3, it was necessary to adjust exposures for ion gauge sensitivity. The ion gauge was calibrated for nitrogen, and correction factors were taken from reference [19] and are included in Table 2.4. The true pressure of the gas is calculated according to

$$P = \frac{P_{IG}}{C_f} \tag{2.19}$$

where P is the true partial pressure, P_{IG} is the observed ion gauge pressure, and C_f is the correction factor from Table 2.4.

2.4.4 Hydrocarbon reactions at atmospheric pressure

The reactions employed in this study utilized a hydrocarbon pressure of between 5 and 50 Torr. The hydrogen pressures employed were between 10 Torr and 1000 Torr, and the hydrogen to hydrocarbon ratios of interest were from 2 to 200. Typical conditions were 20 Torr of hydrocarbon and 200 Torr of hydrogen. Temperatures of interest were between 20–400° C.

Gases were introduced sequentially (usually hydrocarbon followed by hydrogen) to the reaction loop after the catalyst surface returned to room temperature following cleaning procedures and the HP cell closed. Room temperature was usually attained before the characterization by AES and LEED was complete (5 minutes or less).

Reactions were performed from one to two hours typically, but occasionally were performed overnight to check longterm stability of catalyst surfaces. Following a high pressure reaction, the catalyst was cooled to room temperature in the reaction mixture, and the high pressure cell was evacuated and pumped using either a sorption pump or a liquid nitrogen trapped diffusion pump for up to two hours before exposing the sample to UHV. Following the opening of the high pressure cell, the background pressure was found to increase to 5×10^{-8} Torr when heavier hydrocarbons such as n–hexane were used. Lighter hydrocarbons such as ethane or butane caused an increase only up to 5×10^{-9} Torr following high pressure reactions.

Characterization of the post reaction surface was obtained, and usually started with an Auger measurement. An H_2 TPD gave an estimation of the amount of hydrogen bound to the surface carbonaceous deposit [20], and then the surface was titrated with carbon monoxide. The purpose of the CO titration was to quantify the number of bare metal sites remaining after high pressure reactions [21].

Restart reactions were employed to test the deactivation characteristics of the surfaces. For these restart experiments, the original reaction mixture was removed after the crystal cooled to room temperature, a fresh reaction mixture was introduced, and the surface brought to the desired reaction temperature after a background gas chromatograph was obtained.

References

[1] D.W. Blakely, E. Kozak, B.A. Sexton, and G.A. Somorjai. *J. Vac. Sci. Technol.* **13** (1976) 1091.

[2] W.D. Gillespie. PhD thesis, University of California, Berkeley, CA 94720, 1980.

[3] R.K. Herz, W.D. Gillespie, E.E. Petersen, and G.A. Somorjai. *J. Catalysis*

67 (1981) 371.

[4] W.A. Dietz. *J. Gas Chromatography* **5** (1967) 68.

[5] G. Ertl and J. Küppers. *Low Energy Electrons and Surface Chemistry.* Verlag–Chemie, Weinheim, Germany, 1974.

[6] F.C.M.J.M. van Delft, A.D. van Langeveld, and B.E. Nieuwenhuys. *Thin Solid Films* **123** (1985) 333.

[7] T.E. Gallon. *Surface Sci.* **17** (1969) 486.

[8] L.J. Clarke. *Surface Crystallography: An Introduction to Low Energy Electron Diffraction.* John Wiley and Sons, Chichester, England, 1985.

[9] D. Briggs and M.P. Seah. *Practical Surface Analysis by Auger and X–ray Photoelectron Spectroscopy.* John Wiley and Sons, Chichester, England, 1983.

[10] F. Zaera. PhD thesis, University of California, Berkeley, CA 94720, 1984.

[11] C.D. Wagner, W.M. Riggs, L.E. Davis, J.F. Moulder, and G.E. Muilenberg (editor). *Handbook of X-Ray Photoelectron Spectroscopy.* Perkin-Elmer Corporation, 1979.

[12] E.L. Garfunkel. PhD thesis, University of California, Berkeley, CA 94720, 1983.

[13] P.A. Redhead. *Vacuum* **12** (1962) 203.

[14] J.M. Soler and N. García. *Surface Sci.* **124** (1983) 563.

[15] K. Christmann, G. Ertl, and T. Pignet. *Surface Sci.* **54** (1976) 365.

[16] C.-M. Chan, R. Aris, and W.H. Weinberg. *Appl. Surface Sci.* **1** (1978) 360–387.

[17] E. Stenhagen, S. Abrahmsson, and F.W. McLafferty, editors. *Registry of Mass Spectral Data.* Volume 1, John Wiley & Sons, New York, 1974.

[18] J.W.A. Sachtler, M.A. Van Hove, J.P. Biberian, and G.A. Somorjai. *Surface Sci.* **110** (1981) 19.

[19] R. Holanda. *J. Vac. Sci. Technol.* **10** (1973) 1133.

[20] F. Zaera, D. Godbey, and G.A. Somorjai. *J. Catalysis* **101** (1986) 73.

[21] S.M. Davis, F. Zaera, and G.A. Somorjai. *J. Catalysis* **77** (1982) 439.

Chapter 3

Hydrogenation of Ethylene and Adsorption of Ethylene and Propylene on Pt(111) and Pt(100)

3.1 Preface

The adsorption of ethylene on Pt(111) has been extensively studied from 77 K to above 500 K [1,2,3,4,5,6]. Using temperature programmed desorption (TPD) and high resolution electron energy loss spectroscopy (HREELS), different adsorbed species have been identified in different temperature regions [1,2,3]. Below 290 K ethylene chemisorbs molecularly to Pt(111) and lies parallel to the surface with a carbon-carbon bond length of 1.49 Å [4,5]. Around room temperature a hydrogen atom is lost to the surface with a subsequent C–H bond shift so that the remaining hydrogen atoms are all bonded to one of the carbon atoms. The resulting ethylidyne species (CCH_3), as identified through LEED I–V structural analysis for the (2×2) overlayer [6], stands perpendicular to the surface in a three fold hollow, the α carbon atom being bonded to three platinum atoms with a carbon-carbon bond length of 1.50 Å. Above 450 K further decomposition occurs with additional loss

of hydrogen, forming first hydrocarbon fragments of the stoichiometry C_xH where x is between 1 and 2, followed by total dehydrogenation and the formation of a graphitic overlayer at higher temperatures.

The adsorbed state of ethylene on platinum (and other metals) at room temperature is particularly important because of the role it plays during the catalytic hydrogenation of ethylene. It has been proposed recently [7] that the steady state catalytic hydrogenation of ethylene over Pt(111) at atmospheric pressures and at 300 K occurs not on the bare metal surface, but on top of a tenaciously adsorbed ethylidyne layer. This model is supported by the following results: i) the hydrogenation rate of ethylidyne is much slower than that of ethylene near room temperature [8]; ii) a Pt(111) surface saturated with ethylidyne yields the same reactivity and kinetic parameters for this reaction as does a clean surface; iii) ethylidyne is also present at the completion of a high pressure ($\sim$ atmospheric) reaction when the crystal is returned to ultra-vacuum (UHV). However, the state of the surface during the high pressure hydrogenation is not known.

Since it is difficult to probe the surface at pressures larger than 10^{-5} Torr using most surface science techniques, these studies were undertaken to gather information relating to the hydrogenation of adsorbed ethylene over Pt(111) using temperature programmed desorption (TPD) under UHV. Coadsorption of ethylidyne and hydrogen under different hydrogen pressures, and coadsorption of ethylene and CO were also examined. It was anticipated that further support of the model previously proposed where the steady state catalytic hydrogenation of ethylene occurs on top of an ethylidyne/ethylidene overlayer and not over the bare metal surface might be found [7,8,9,10]. Is the apparent role played by ethylidyne in the catalytic hydrogenation of ethylene over Pt(111) also assumed during hydrogenation over Pt(100)? Catalytic hydrogenation studies of ethylene were extended to

include the Pt(100) surface to help answer this question. Finally, the decomposition of propylidyne in the presence of hydrogen was examined in an effort to explore the role of hydrogen in hydrocarbon decomposition on metallic surfaces.

3.2 Hydrogenation of Chemisorbed Ethylene on Clean and Hydrogen Covered Platinum (111) Crystal Surfaces

3.2.1 Self-hydrogenation of Ethylene on Pt(111)

Ethylene adsorbs molecularly on platinum at 150 K [1,2,3], and during TPD the desorption of H_2, C_2H_4, and C_2H_6 were observed (Figure 3.1). The mole ratio of desorbing C_2H_6, H_2, and C_2H_4 was 1:20:50 when the surface was saturated with ethylene. The formation of methane and C_4 products was not detected.

Ethane was produced from ethylene on Pt(111) in a self-hydrogenation process. To prove that background hydrogen was not participating in the hydrogenation, TPD experiments were carried out using an ethylene saturated surface while keeping a background pressure of 10^{-6} Torr deuterium. The intensity and temperature of the desorption maximum of the 30 amu. peak was the same whether or not D_2 was present, and no deuterated ethanes (31 and 32 amu.) were observed.

The temperature of the desorption maximum (T_{max}) of ethane for the self-hydrogenation process was found to be 302 K and independent of the initial ethylene coverage indicating first order kinetics. Following an induction period below 0.4 Langmuirs (L, 1 L = 10^{-6} Torr-sec) of ethylene, the ethane yield increased almost linearly with respect to ethylene exposure until at 1.2 L where saturation of the surface occurred (Figure 3.2).

Desorption activation energies were calculated from TPD using the method

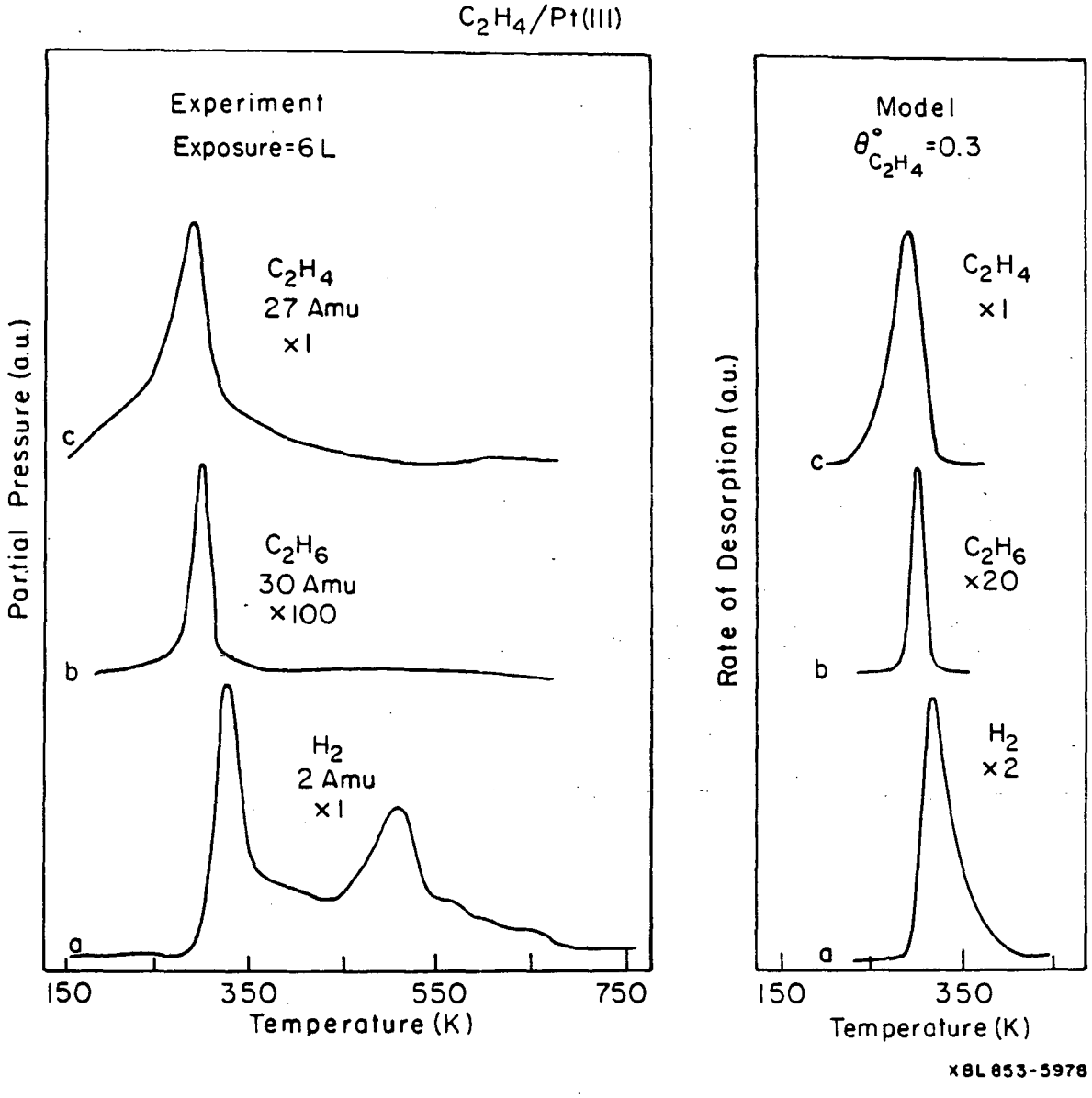

Figure 3.1: TPD products of ethylene on Pt(111), heating rate: β =30 K/sec. Left panel from experiment: T_{ads} = 150 K, exposure = 6 L (saturation). Right panel from model (see text): T_{init} = 150 K, $\theta^{\circ}_{C_2H_4}$ = 0.3 ML. a) H_2, 2 amu. TPD. b) C_2H_6, 30 amu. TPD. c) C_2H_4, 27 amu. TPD.

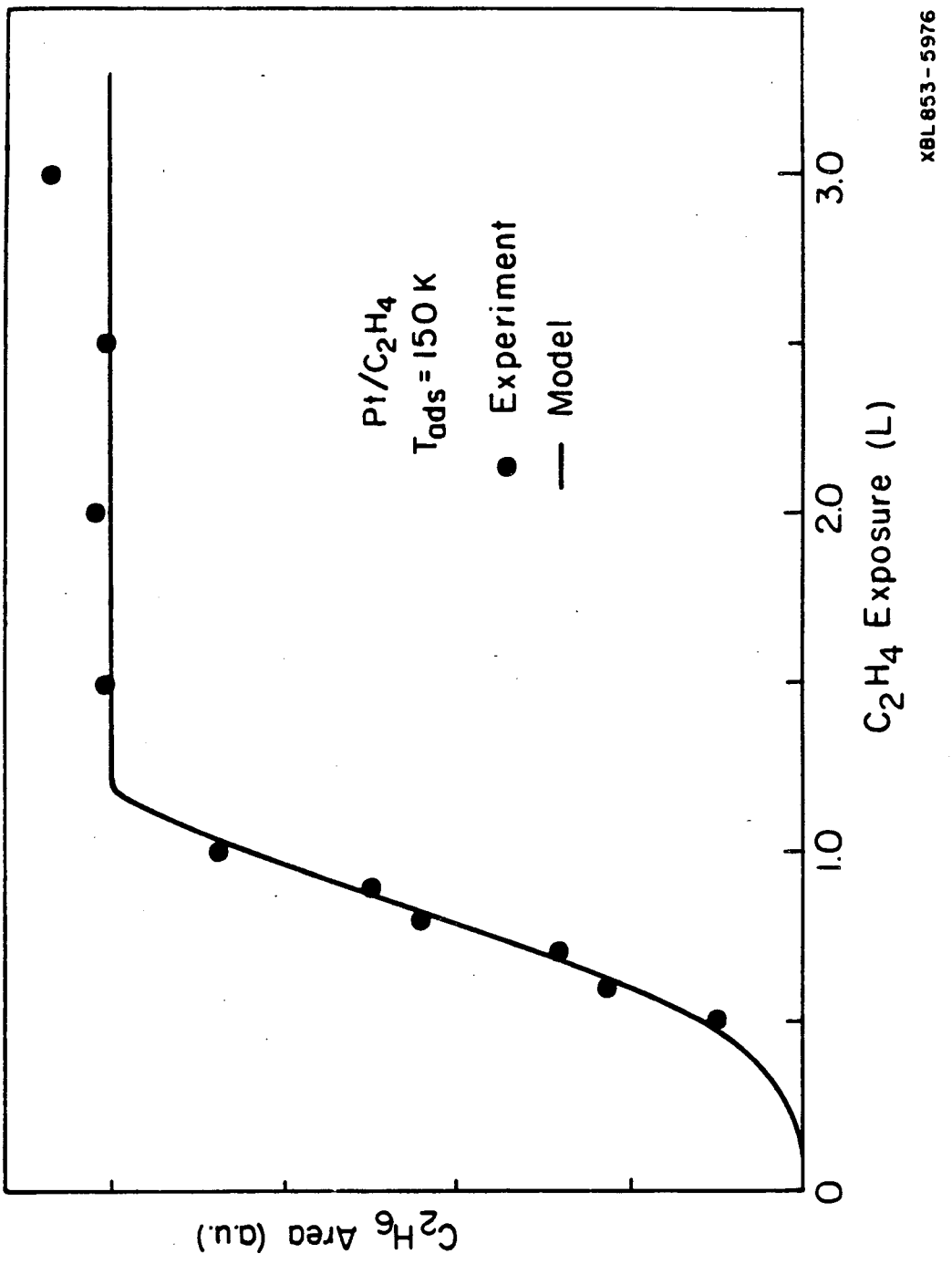

Figure 3.2: Ethane production yield for self-hydrogenation as a function of ethylene exposure over Pt(111). The experimental points fall on the curve generated by the computer model (see text for details).

Table 3.1: Kinetic Parameters From TPD on Pt(111): $\beta \sim 30$ K/sec.

Process	T_{max} (K)	E_a (Kcal/mole)
C_2H_4 molecular desorption	291	9±2
C_2H_6 formation with desorption	302	18±4
H_2 evolution from $C_2H_4 \rightarrow CCH_3 + \frac{1}{2}H_2$	320	17±3
C_2H_6 formation when H preadsorbed	252	6±1

of Chan *et al.* [11]. The desorption of H_2, C_2H_4, and C_2H_6 were all found to be first order in ethylene coverage, and the values obtained in units of Kcal/mole were: 17±3 for the first H_2 evolution peak, 9±2 for ethylene molecular desorption, and 18±4 for ethane formation (Table 3.1). The values obtained for hydrogen and ethylene desorption are in agreement with those obtained by Salmerón and Somorjai [2].

3.2.2 Hydrogenation of ethylene over the hydrogen predosed Pt(111) surface

The presence of ethylene on the platinum surface inhibited the coadsorption of hydrogen. However, when the surface was predosed with hydrogen or deuterium, ethylene coadsorption did take place and ethane formation was enhanced. TPD taken after predosing the surface with 25 L (near saturation) of hydrogen followed by 0.4 L of ethylene gave an ethane peak centered at 252 K and much broader than in the self-hydrogenation case (Table 3.1 and Figure 3.3). The mole

ratio of desorbing ethylene to ethane decreased with increasing coverage of preadsorbed hydrogen from 50 for self-hydrogenation to near unity with 25 L of predosed hydrogen. This was qualitatively in agreement with results recently reported by Berlowitz *et al.* [12]. When the surface was predosed with deuterium all deuterated ethanes, including d_6 ethane, were detected indicating that considerable exchange occurred on the ethane precursors. The distribution of deuterated ethanes was determined by fitting the experimental data using Equation 2.18 from Chapter 2. A rigorous calculation of the ethane product distribution was complicated by the simultaneous exchange occurring on ethylene. The TPD data recorded in the 30-36 amu. range were deconvoluted (Figure 3.4), but precise values for ethanes below d_2 were not possible to obtain and only upper limits are reported.

The coverage dependence for ethane production on hydrogen and ethylene was examined. Predosing the surface with varying exposures of hydrogen followed by an ethylene exposure of 0.4 L gave an increase in ethane production and a decrease in T_{max} with increasing hydrogen exposure (Figures 3.3, 3.5). Exposing the surface to 30 L of hydrogen followed by varying exposures of ethylene also gave an increase in ethane production and a decreasing T_{max} with increasing ethylene exposure (Figure 3.6). Interestingly, the temperature of the desorption maximum reached a minimum of $\sim$ 250 K near a 1 L exposure of ethylene and remained near 250 K while the C_2H_6 desorption area continued to increase even at ethylene exposures of 20 L.

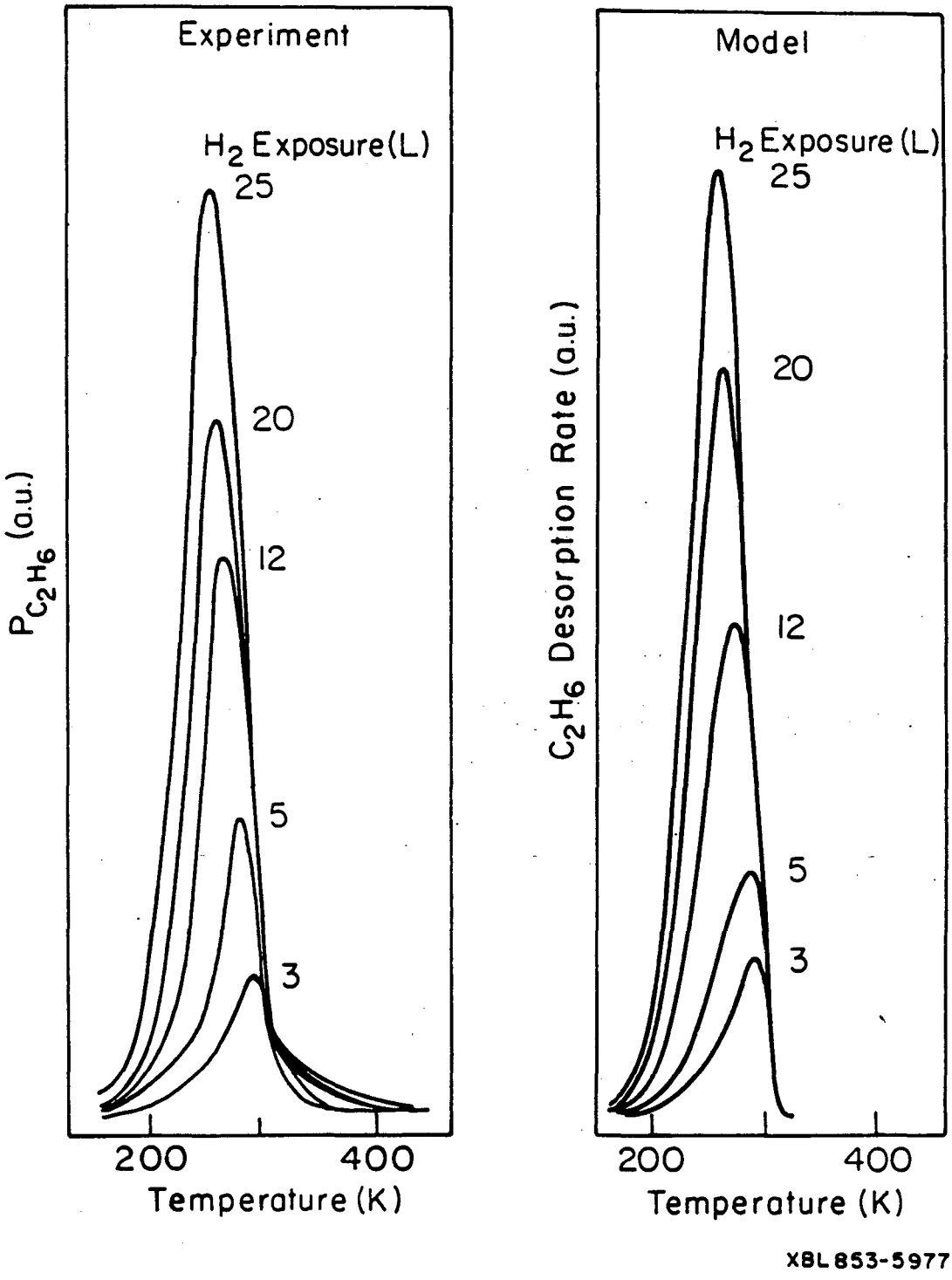

Figure 3.3: Ethane TPD as a function of hydrogen exposure for H_2 + C_2H_4 on Pt(111). Heating rate: β = 30 K/sec. Variable hydrogen dose was followed by 0.4 L of ethylene. Left panel, experimental C_2H_6 TPD: T_{ads} = 150 K. Right panel, computer generated TPD: T_{init} = 150 K

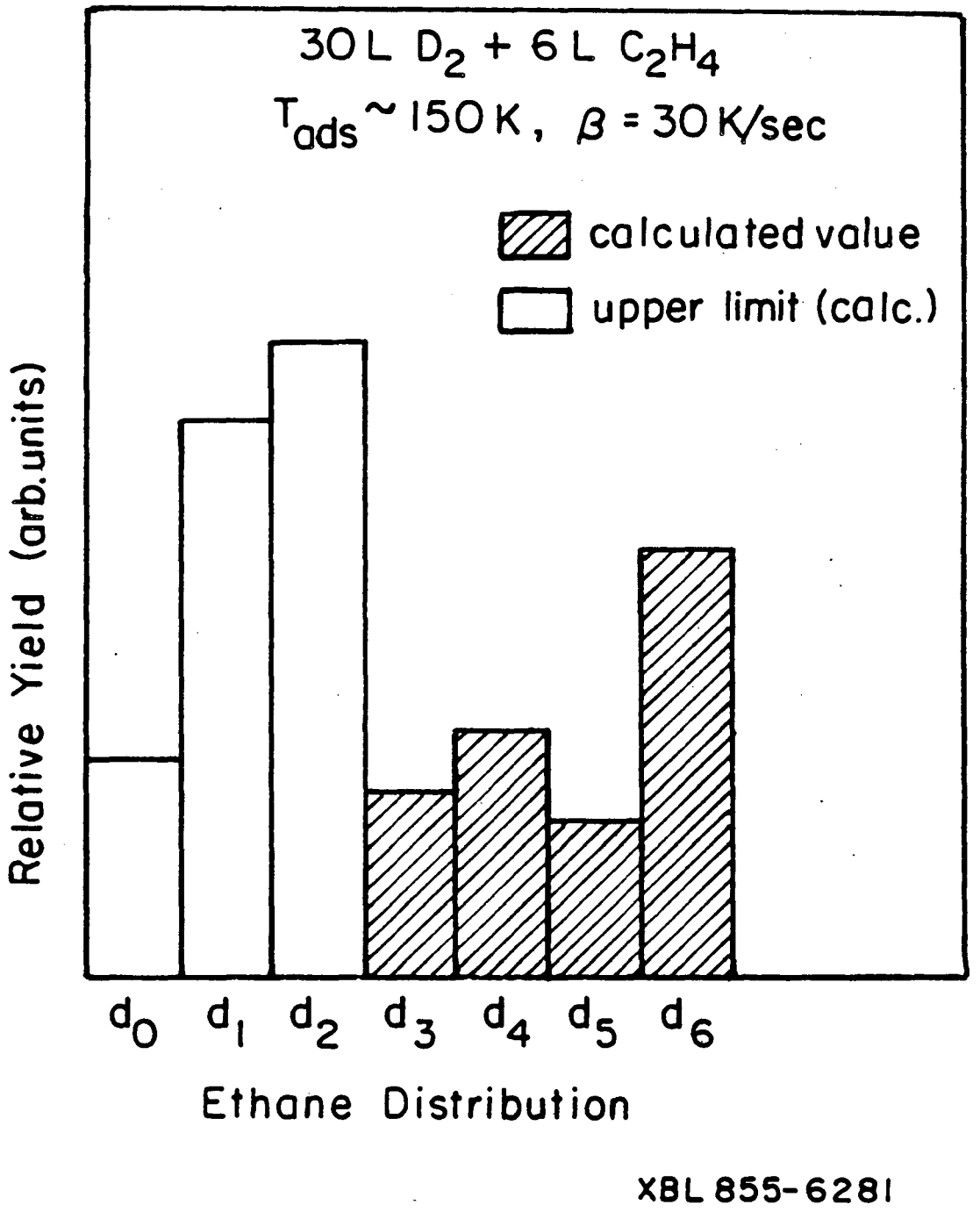

Figure 3.4: Deuterium distribution in ethane produced during temperature programmed desorption when a Pt(111) surface was dosed with 30 L deuterium followed by 6 L C_2H_4. The distribution was determined by deconvoluting the data; however only upper limits were estimated for $d_o - d_2$ ethanes due to simultaneous exchange and desorption of ethylene.

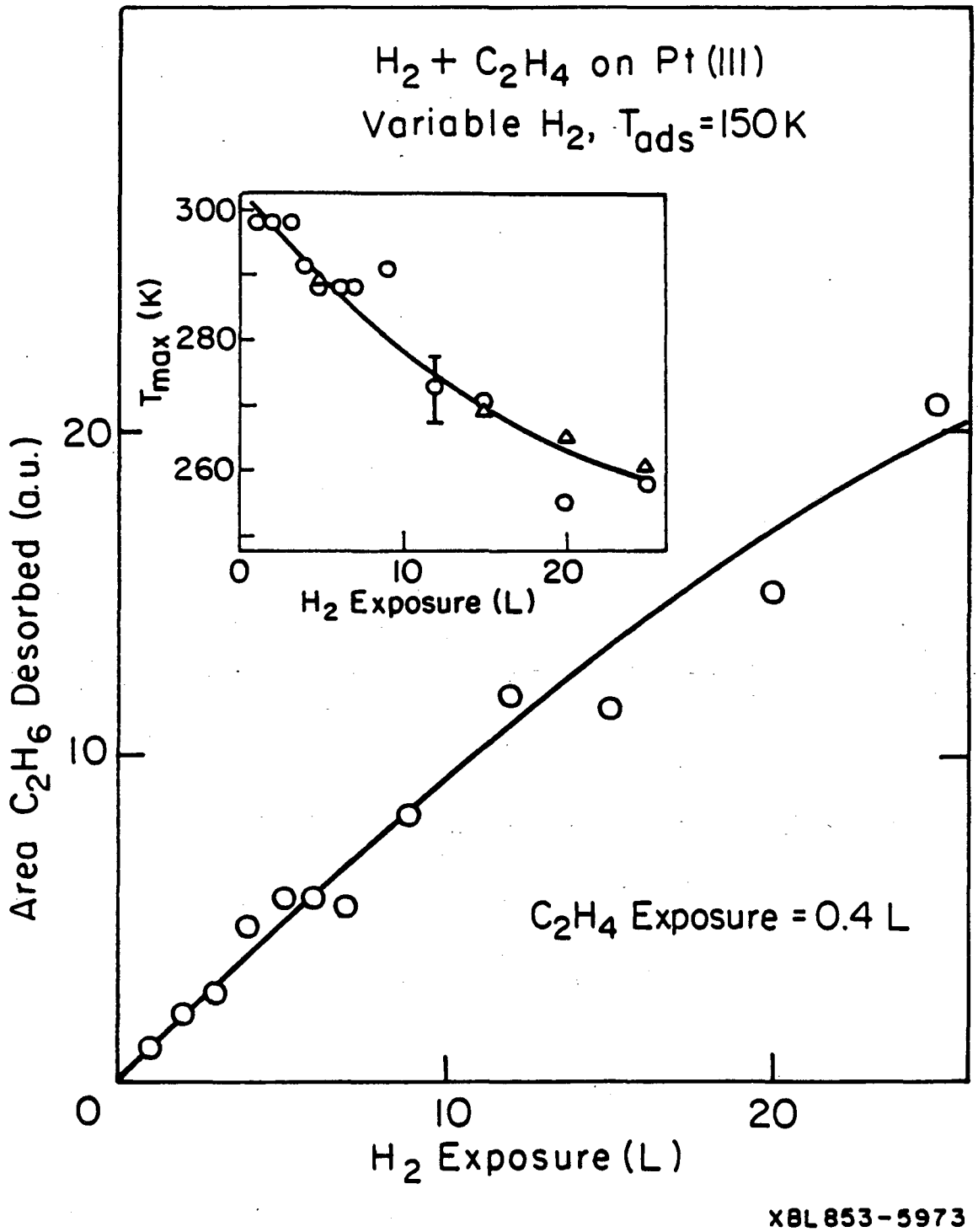

Figure 3.5: Ethane TPD area as a function of hydrogen exposure for H_2 + C_2H_4 on Pt(111). Variable hydrogen dose was followed by 0.4 L C_2H_4. T_{ads} = 150 K. The solid line was generated by the model. Inset: Position of the temperature maximum. ○ Experimental. △ Model.

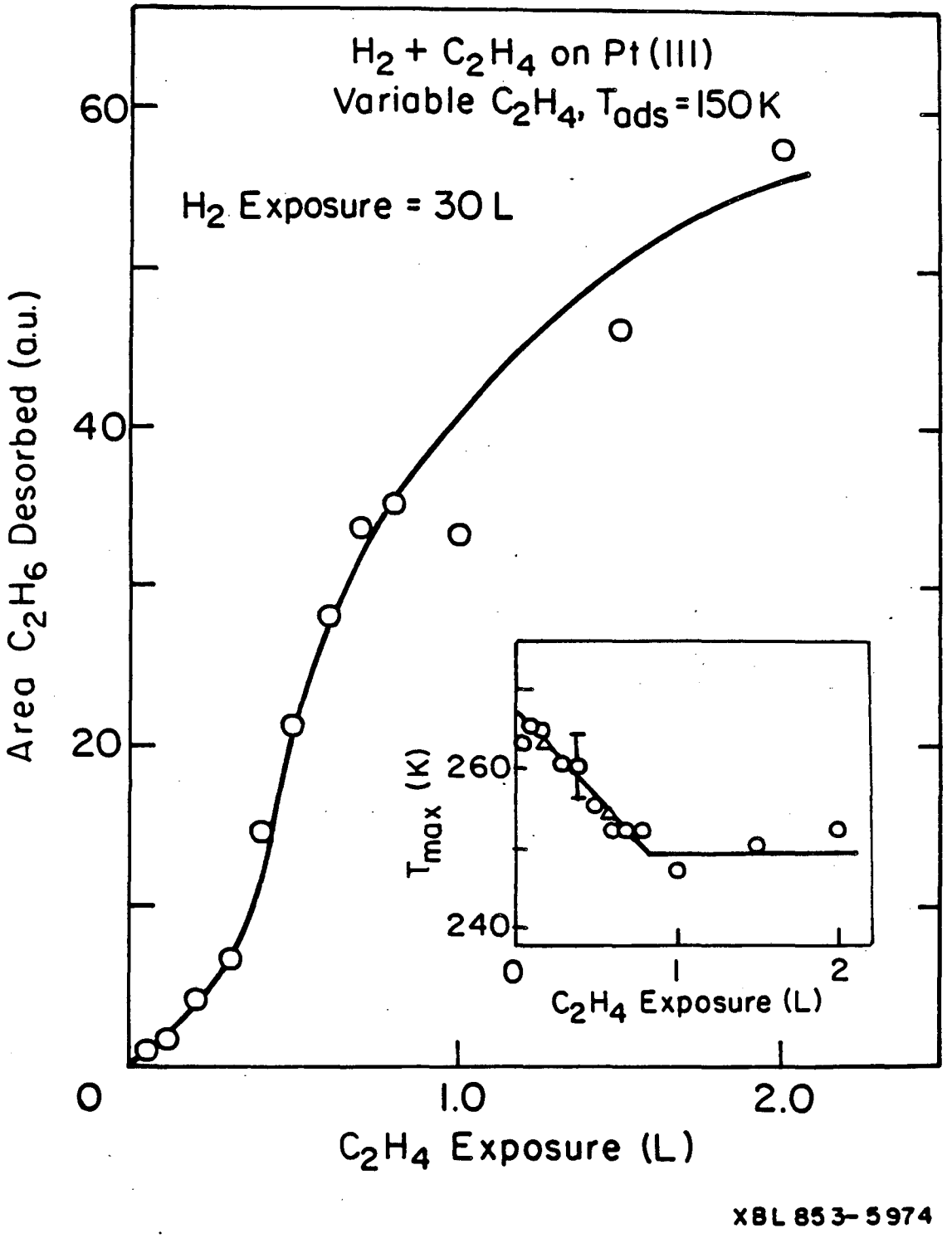

Figure 3.6: Ethane TPD area as a function of ethylene exposure. 30 L hydrogen exposure followed by variable ethylene dosing. $T_{ads} = 150$ K. The solid line was generated by the model. Inset: Position of the temperature maximum. ○ Experimental. △ Model.

3.3 Adsorption of Small Molecules on Ethylidyne Covered Pt(111)

3.3.1 Ethylene adsorption on ethylidyne saturated Pt(111)

Ethylene chemisorption on Pt(111) at room temperature forms surface ethylidyne [6]. Once the surface is saturated with ethylidyne, no further ethylene will adsorb either under UHV or high pressure conditions. TPD experiments following exposures of ethylidyne saturated platinum to $1\text{-}10^8$ L of ethylene from 150 to 320 K resulted in no production of ethane or molecular desorption of ethylene.

3.3.2 Hydrogen adsorption in the presence of ethylidyne on Pt(111)

The ability of the Pt(111) surface to adsorb hydrogen in the presence of ethylidyne was also examined. The H_2 TPD of an ethylidyne saturated surface is shown in Figure 3.7a. The same spectrum was obtained when hydrogen coadsorption was attempted at 150 K under UHV, suggesting that no hydrogen adsorption takes place under these conditions. However, hydrogen could be coadsorbed at 5×10^{-7} Torr when a sub-saturation coverage of ethylidyne was present on the platinum surface (Figures 3.7b and 3.7c). An H_2 TPD from clean platinum is shown for reference (Figure 3.7d). Saturation of the surface with respect to ethylidyne occurred at ethylene exposures near 1.6 L (Figure 3.8).

Hydrogen could be adsorbed on an ethylidyne saturated surface when higher hydrogen pressures were used. For example, when an ethylidyne saturated surface was exposed to one atmosphere of hydrogen for one minute ($\sim 10^{10}$ L), the H_2 TPD displayed an additional low temperature peak near 270 K (Figure 3.9d). This peak was most likely due to hydrogen desorbing directly from the platinum surface. Experiments performed with deuterium indicated that no deuterium exchange

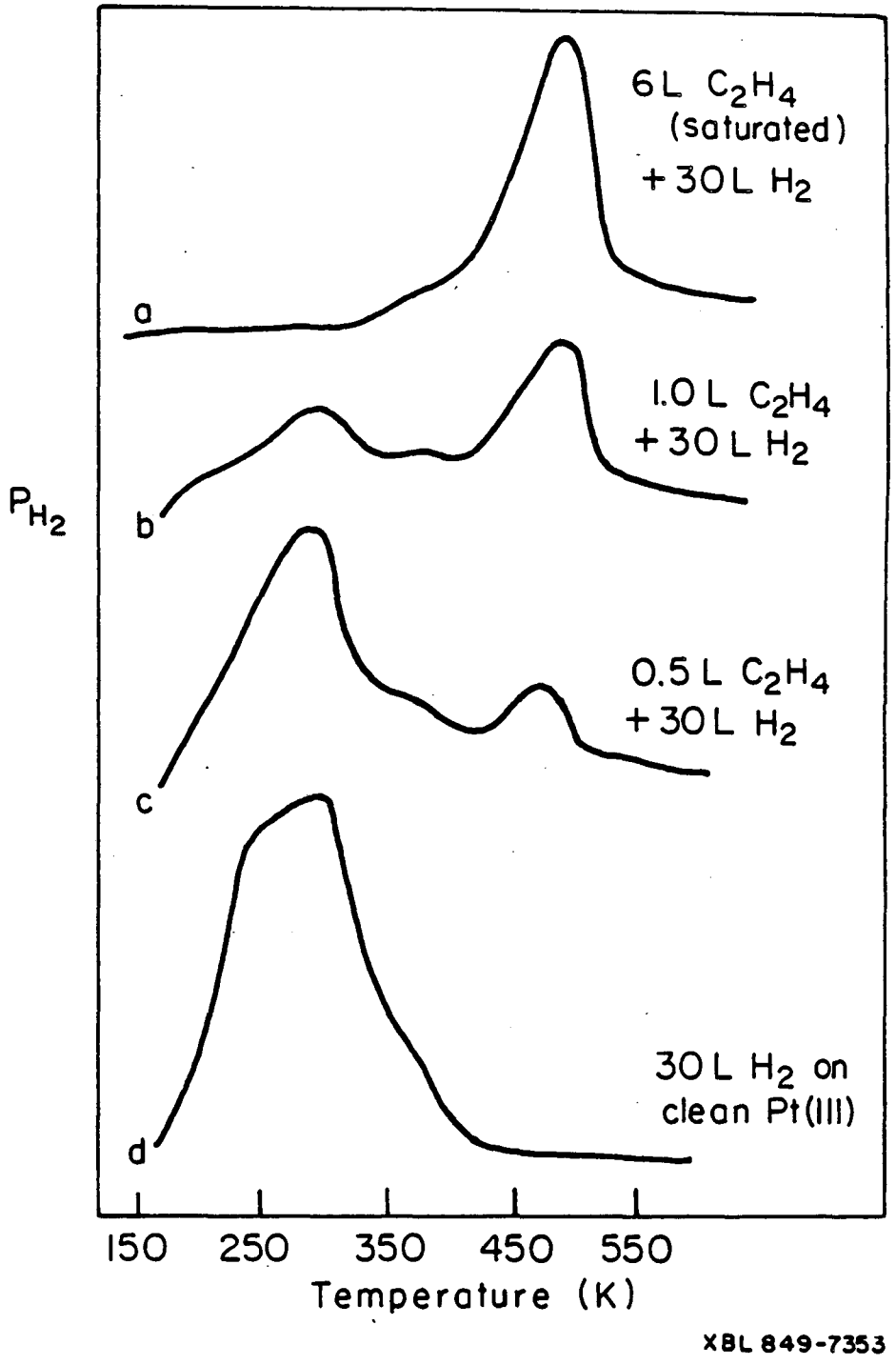

Figure 3.7: H_2 TPD following ethylidyne + H_2 exposure on Pt(111). Ethylidyne was deposited by dosing the surface with 10^{-8} Torr C_2H_4 at 320 K. H_2 was introduced at 5×10^{-7} Torr after crystal cooled to 150 K. a) Ethylidyne saturated surface followed by 30 L H_2 exposure. b) Ethylidyne from 1.0 L C_2H_4 followed by 30 L H_2. c) Ethylidyne from 0.5 L C_2H_4 followed by 30 L H_2. d) 30 L hydrogen adsorbed on a clean platinum surface.

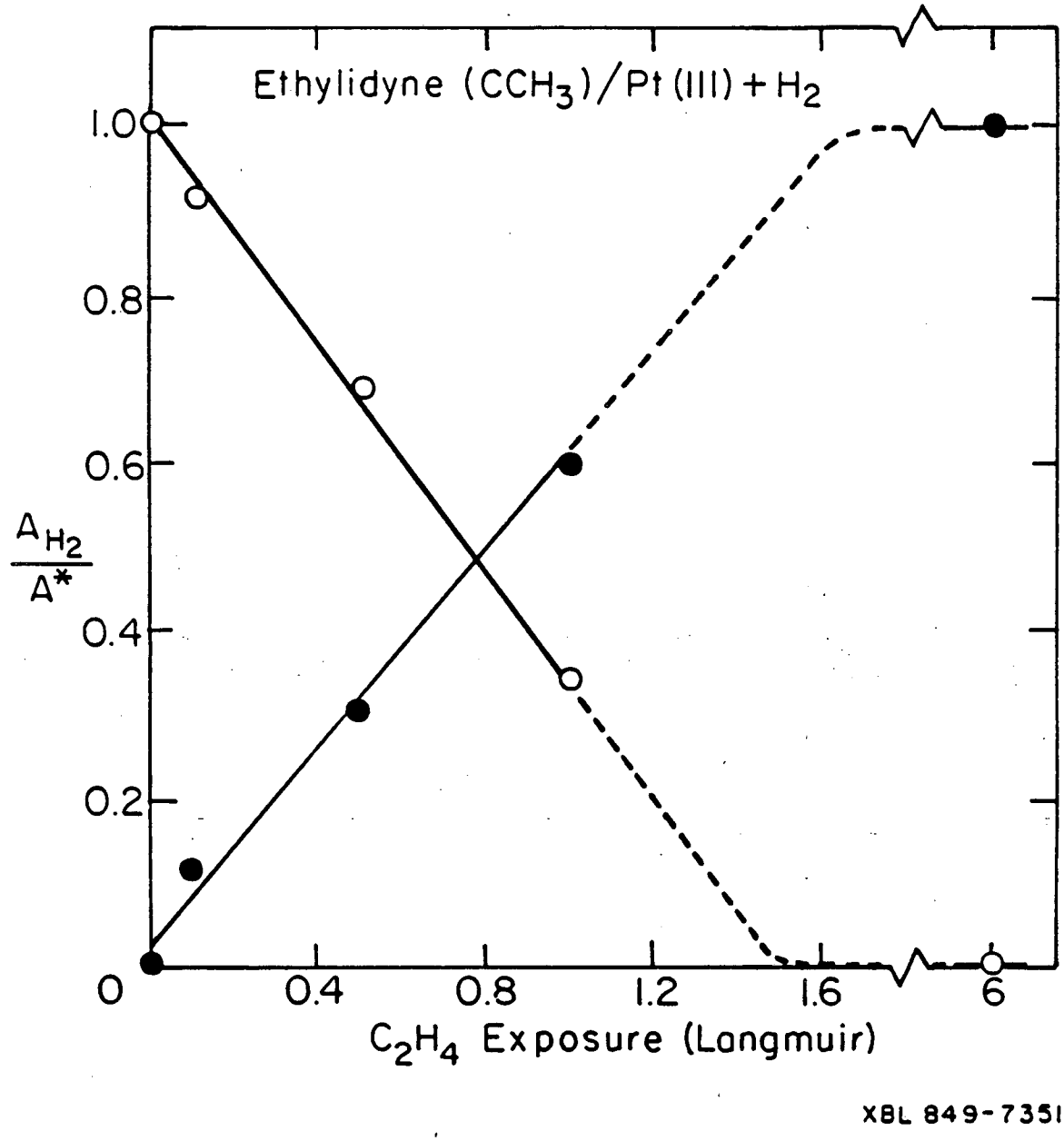

Figure 3.8: Hydrogen yield from the prepared surfaces of Figure 3.7. Ethylidyne + H_2 on Pt(111). o The H_2 TPD area as evolved from uncovered Pt (low temperature peak) was normalized to the TPD area of H_2 desorbing from clean Pt (Figure 3.7d). • The H_2 TPD area evolved from ethylidyne decomposition (high temperature peak) normalized to the TPD area of H_2 produced from an ethylidyne saturated surface (Figure 3.7a).

occurred on the methyl group, and only the low temperature peak was seen in the deuterium TPD (Figure 3.9e). Ethylidyne hydrogenation is very slow at these temperatures [8], and was not observed during these experiments.

It was also found that hydrogen could be coadsorbed on an ethylidyne saturated surface at pressures as low as 10^{-5} Torr. The hydrogen adsorption state observed depended on the temperature of coadsorption (Figures 3.9b and 3.9c). When hydrogen was dosed at 150 K, H_2 desorption peaks were observed at 219 and 298 K corresponding to desorption from uncovered platinum metal (Figure 3.9b). When hydrogen was dosed at 320 K followed by immediate cooling of the crystal to 150 K, an H_2 desorption peak was observed at 385 K (Figure 3.9c). The hydrogen adsorption state corresponding to the 385 K desorption peak was found to decay rapidly at 320 K, and significant decay was observed even at 150 K after 10 minutes. The proportion of hydrogen desorbing in the 385 K desorption peak was estimated to be around 25%. Pressures significantly lower than 10^{-5} Torr (*ie.* 10^{-6} Torr) were ineffective in producing the above hydrogen adsorption states on ethylidyne saturated platinum.

3.3.3 Adsorption of carbon monoxide on ethylidyne saturated Pt(111)

Unlike hydrogen adsorption on ethylidyne saturated Pt(111), CO could be coadsorbed with ethylidyne on Pt(111) when adsorption was performed at room temperature. Figure 3.10 shows CO TPD spectra after exposure to saturation doses of CO on clean Pt(111), ethylidyne saturated Pt(111), and the saturated surface following thermal decomposition of ethylidyne. Quantitative results from these experiments are shown in Table 3.2.

An inspection of Table 3.2 reveals that the position of T_{max} of CO desorption

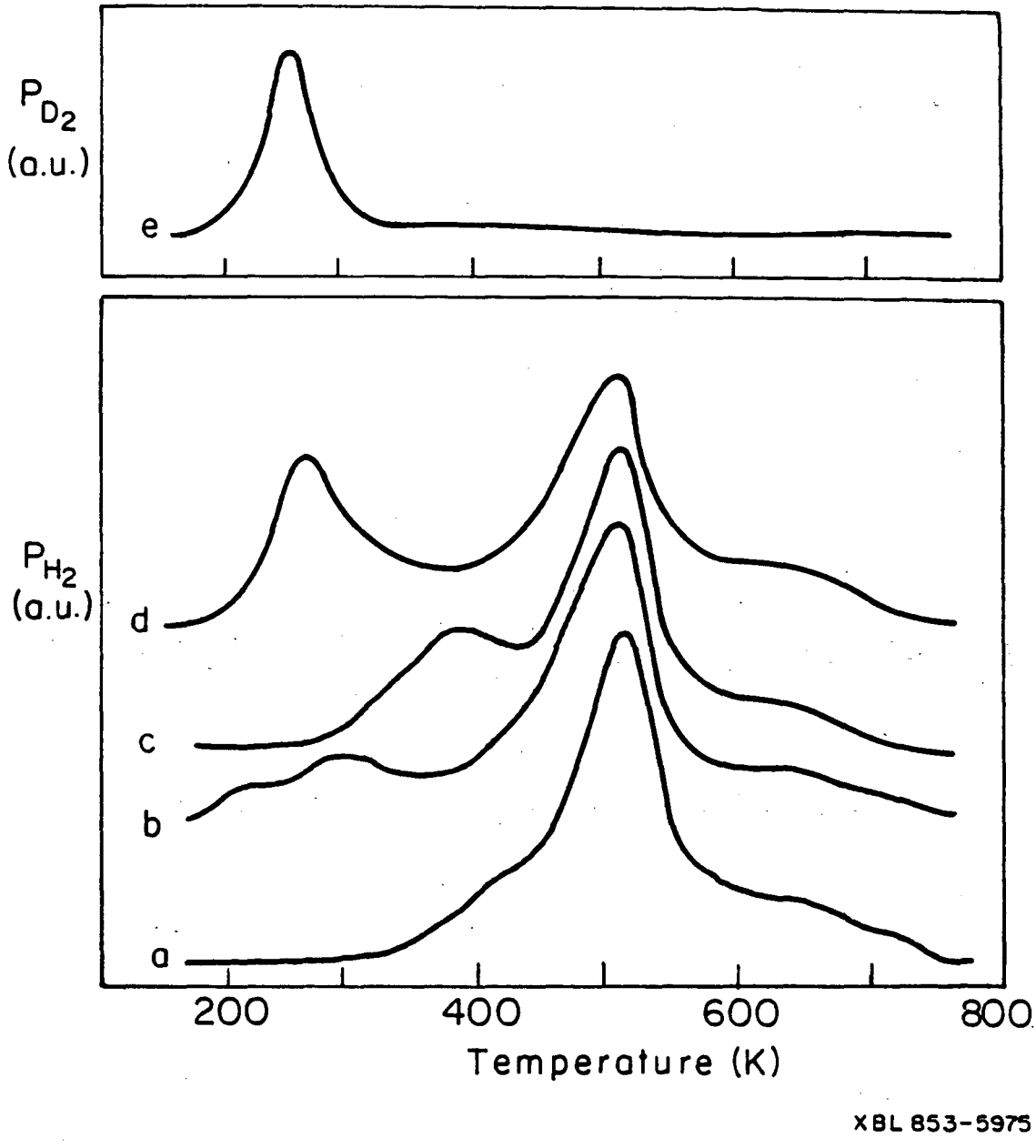

Figure 3.9: H_2 or D_2 TPD from Pt(111) for: a) 6 L C_2H_4 dosed at 320 K (saturated ethylidyne) and followed by: b) 1200 L H_2, 10^{-5} Torr at 150 K. c) 1200 L H_2, 10^{-5} Torr at 320 K, then cooled immediately to 150 K. d) $\sim 10^{10}$ L H_2, 1 atmosphere at 250 K. e) $\sim 10^{10}$ L D_2, 1 atmosphere at 250 K, 4 amu. TPD.

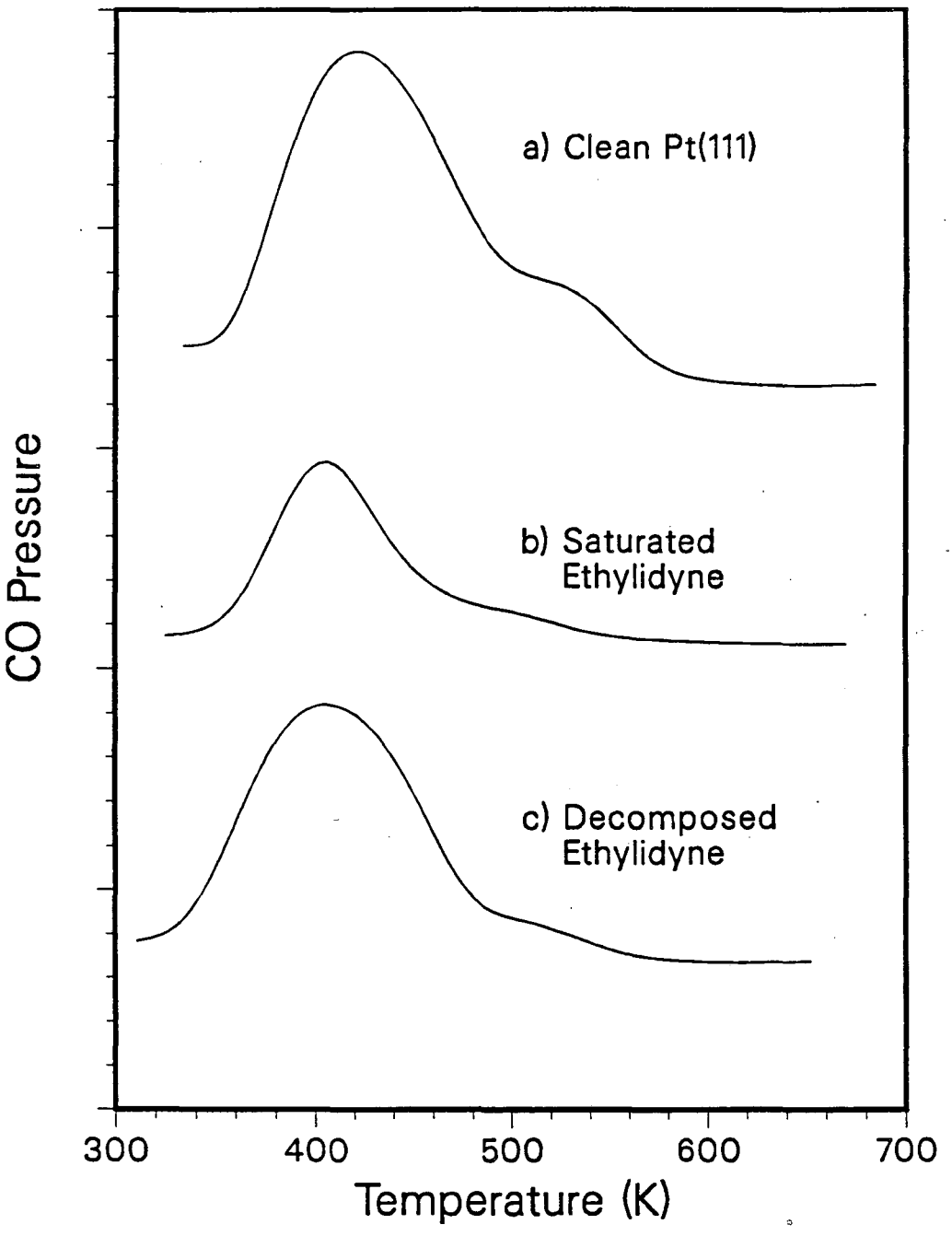

Figure 3.10: Adsorption and TPD of CO on: a) Clean Pt(111). b) Ethylidyne saturated Pt(111). c) Surface from b after ethylidyne decomposition.

Table 3.2: CO desorption from surfaces derived from ethylidyne saturated Pt(111). All TPD areas are compared to the CO desorption areas from the clean Pt(111) surface.

Surface	Relative CO Desorption Area	T_{max} (K)
Clean	1	420
C_2H_3	0.35	400
Decomposed C_2H_3	0.7	410

shifted when carbonaceous residues derived from ethylidyne were on the surface compared to CO desorption from a CO only covered surface. T_{max} shifted to about 20 degrees lower in temperature in the presence of ethylidyne, and 10 degrees lower in the presence of its decomposition products. The ethylidyne saturated surface adsorbed about 65% less CO than could be adsorbed by a clean Pt(111) surface. After the TPD shown in Figure 3.10b was performed, the resulting carbon coverage following ethylidyne decomposition was the same as the surface carbon coverage of undecomposed ethylidyne. Pt(111) is ineffective at dissociating CO, so no accumulation of carbon from CO decomposition was observed, nor was carbon derived from ethylidyne observed to leave the surface. However, the bare platinum area apparently increased to about 70% of the clean platinum area after TPD as shown in Figure 3.10 and Table 3.2, and this indicates a rearrangement of carbonaceous deposits following ethylidyne decomposition in such a way as to accommodate the adsorption of twice as much CO compared to the undecomposed ethylidyne covered surface.

3.4 Propylene Decomposition on Pt(111)

The decomposition of propylene on Pt(111) is shown in Figure 3.11a. It can be seen that total dehydrogenation has occurred under UHV by 470 K (Figure 3.11 a & e). However, when the surface was flashed to 470, 480, and 490 K in the presence of 1×10^{-4} Torr of H_2 (Figure 3.11b, c, & d) and allowed to cool back to 150 K, subsequent TPD spectra obtained reveal that decomposition was inhibited by the presence of hydrogen. One of the decomposition products could be ethylidyne as shown by the shoulder near 510 K in Figure 3.11b, c, & d. The ethylene decomposition spectrum is shown in Figure 3.11f for comparison; the second peak is due to the decomposition of ethylidyne.

3.5 Hydrogenation of Ethylene on Pt(100) Near Atmospheric Pressures

The hydrogenation of ethylene was performed on the Pt(100) surface and comparisons were made with the hydrogenation over the Pt(111) surface as previously reported by Zaera and Somorjai [7]. The conditions under which ethylene hydrogenation reactions were executed were 10 Torr C_2H_4, 20 Torr H_2, 80 Torr N_2, and the temperature range was between 300–375 K. The initial rates obtained vs. reciprocal temperature are shown in Figure 3.12. The rates obtained on the Pt(100) surface were about 60% higher than the rates obtained on the Pt(111) surface. The activation energy obtained was 11±1 Kcal/mole and identical to the activation energy obtained by Zaera and Somorjai on the Pt(111) within experimental error [7].

The role of ethylidyne has previously been implicated as an indirect interme-

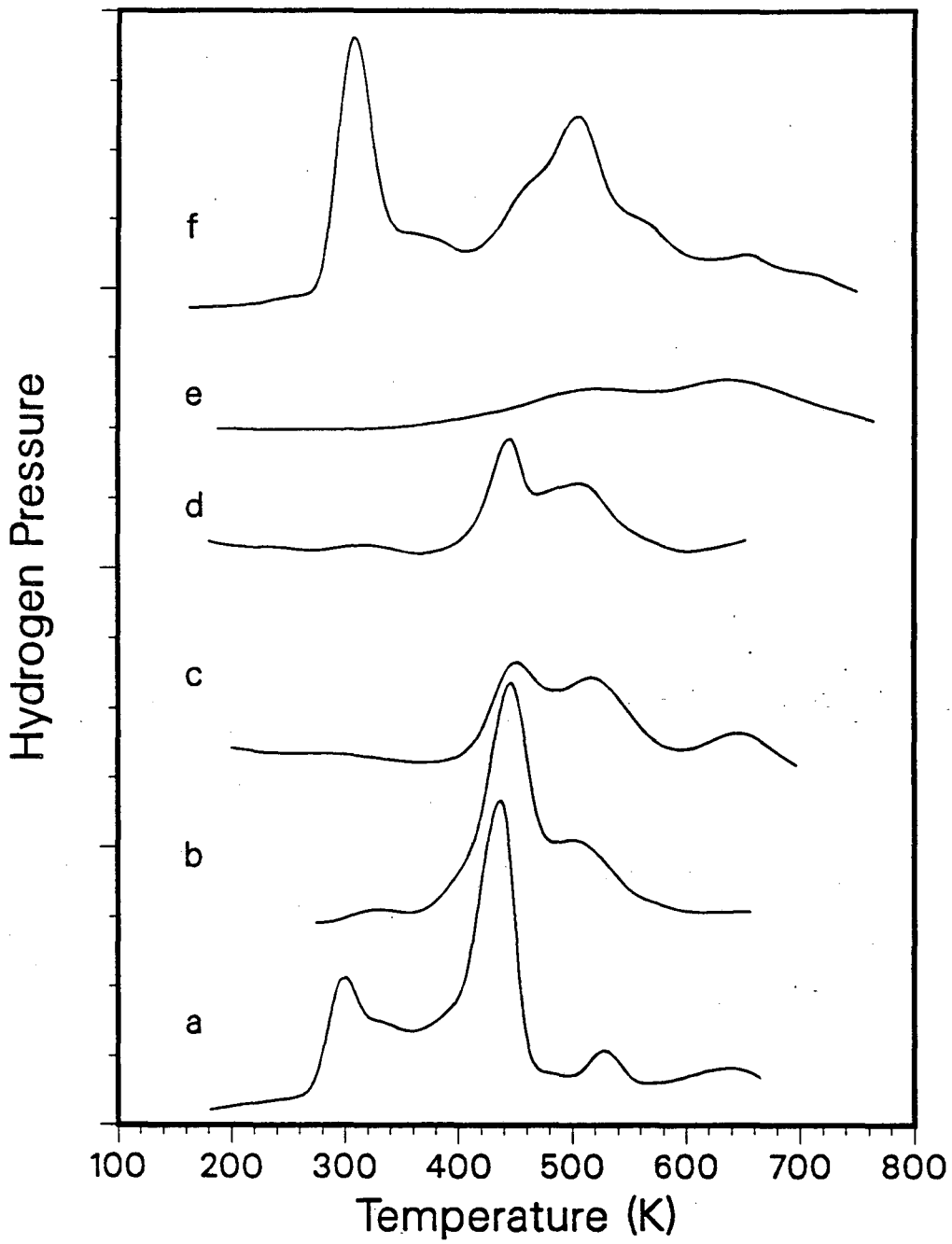

Figure 3.11: H_2 TPD from propylene and propylidyne decomposition on Pt(111): a) Propylene decomposition spectrum. After propylene was adsorbed at 300 K to form propylidyne, decomposition spectra were obtained after first flashing the surface in the presence of 1×10^{-4} Torr H_2 to: b) 470 K. c) 480 K. d) 490 K. e) 470 K without H_2. f) Ethylene decomposition spectrum.

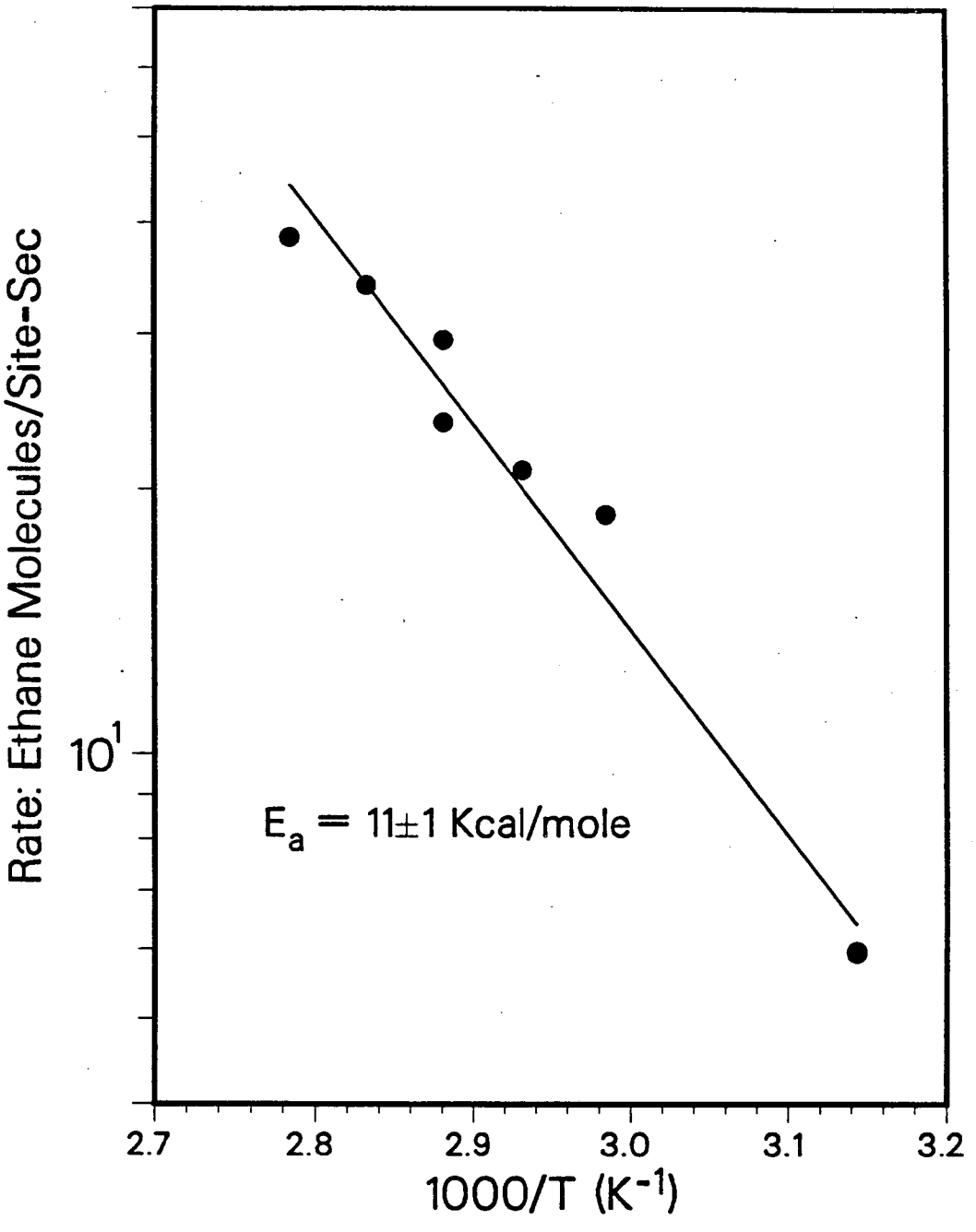

Figure 3.12: Activation energy plot for C_2H_4 hydrogenation on Pt(100). Conditions: $P_{C_2H_4}$ = 10 Torr, P_{H_2} = 20 Torr, P_{N_2} = 80 Torr.

diate in the catalytic hydrogenation of ethylene over Pt(111) [7]. Since ethylidyne has also been shown to form on Pt(100) [13], experiments were performed to determine whether or not ethylidyne plays a similar role on Pt(100). Ethylene gives a similar TPD spectrum from clean Pt(100) compared to clean Pt(111), as shown in Figure 3.13. The main difference observed between the two surfaces is that the Pt(100) has a higher proportion of its hydrogen desorbing into the lower temperature (325 K) peak. After a high pressure ethylene hydrogenation reaction on Pt(111) was performed, the hydrogen TPD taken was very similar to a hydrogen TPD taken after adsorption of ethylene on clean Pt(111) at room temperature and under UHV where ethylidyne is formed [7]. Furthermore, θ_C on Pt(111) after a high pressure hydrogenation reaction was near 0.5 ML, which is consistent with the existence of ethylidyne following a high pressure reaction. Saturated ethylidyne on Pt(111) also gives a carbon coverage of $\theta_C \sim 0.5$ ML, so during catalytic hydrogenation of ethylene very little additional carbon accumulates on the Pt(111) surface beyond the initial formation of ethylidyne. The Pt(100) surface behaves differently, however. The TPD peak obtained after a high pressure reaction is much broader than the peak obtained from ethylidyne decomposition after ethylene adsorption on clean Pt(100) under UHV. The peak is centered near 480 K which is consistent with the presence of ethylidyne, but the peak broadness clearly indicates the presence of other fragments (Figure 3.13). The amount of carbon left on the Pt(100) surface after a high pressure reaction was about 3 times higher, $\theta_C \sim 1.5$ ML, and consequently more hydrogen was found to desorb from the carbidic overlayer after returning the surface to UHV following reaction.

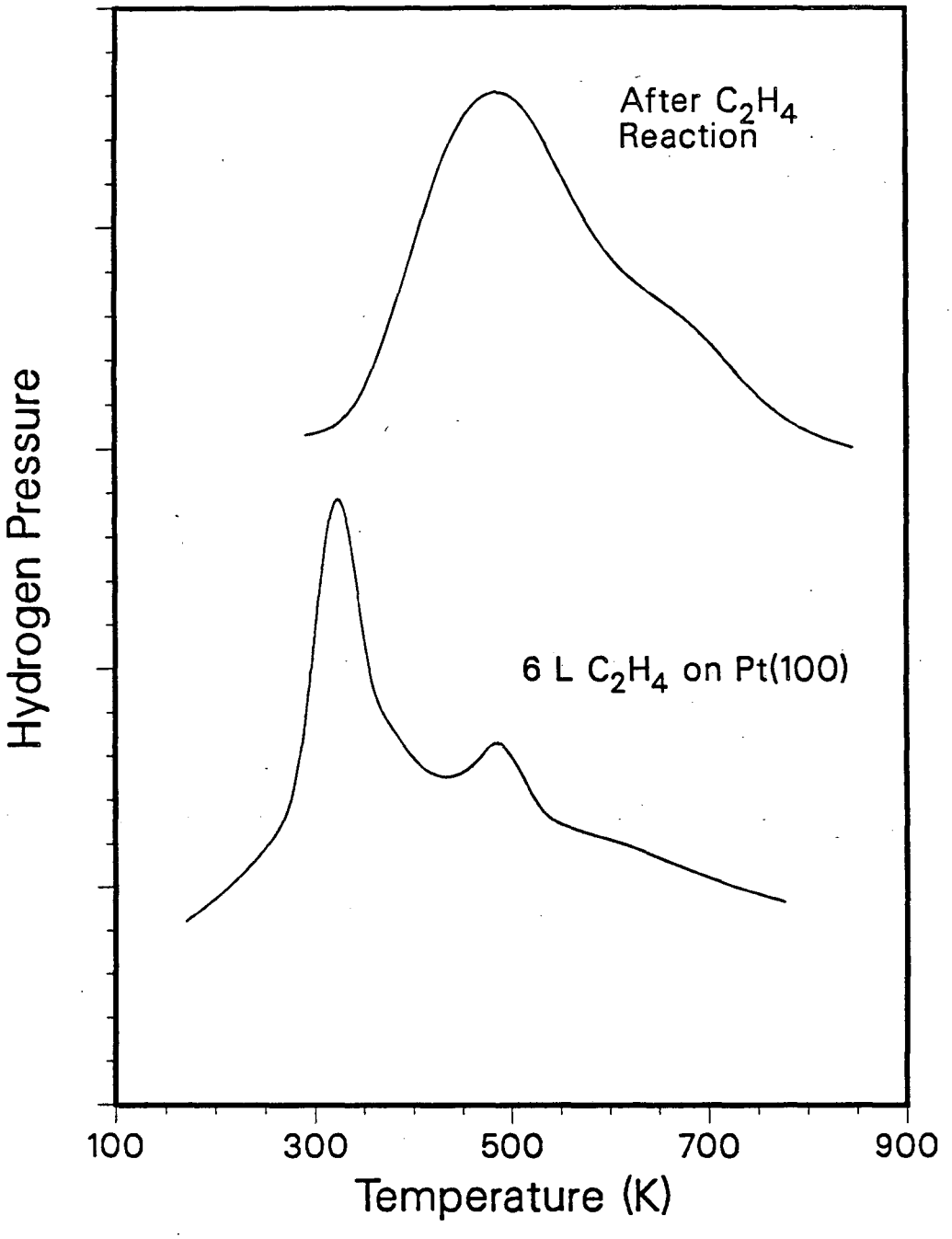

Figure 3.13: H_2 TPD from the decomposition of C_2H_4 on clean Pt(100) and after a high pressure C_2H_4 hydrogenation over Pt(100).

3.6 Discussion

3.6.1 Model for the UHV hydrogenation of chemisorbed ethylene on clean and hydrogen predosed platinum

Ethylene decomposition on Pt(111) surfaces have been previously studied [1,2]. The peaks at 320 and 530 K in the H_2 TPD of ethylene are known to correspond to the conversion of adsorbed C_2H_4 to ethylidyne and to the decomposition of ethylidyne respectively. Ethane is among the thermal desorption products of ethylene, a product of self-hydrogenation. Self-hydrogenation of ethylene has been observed previously on Pt, Rh, Ir, Ni, Pd, and W [14,15,16,17,18,19]. During the decomposition of adsorbed ethylene to ethylidyne on platinum, hydrogen atoms are spilled onto the surface. These hydrogen atoms are then able to hydrogenate other adsorbed ethylene molecules to ethane which then desorb. The rate determining step (RDS) for this process is the breaking of a C-H bond, which is responsible for the first order dependence on ethylene coverage for ethane formation at 302 K, and H_2 desorption at 320 K. Additionally, activation energies calculated for both processes were equivalent within experimental error (18±4 Kcal/mole for C_2H_6 formation and 17±3 Kcal/mole for H_2 evolution). When hydrogen is coadsorbed with ethylene (as was the case for the predosing experiments), the hydrogenation proceeds directly without involving any C-H bond breaking. This is why the ethane peak became broader and shifted from 300 K for very low hydrogen exposures to 250 K for larger exposures. Based on these observations, the following mechanism for the self-hydrogenation is proposed:

Table 3.3: Model for the Hydrogenation of Chemisorbed Ethylene on Pt(111)

Step	Rate Expression	E_a (kcal/mole)	ν	ref.
(1)	$\theta_{C_2H_4}\nu\exp(-E/RT)$	17	4×10^{13}	a
(2)	$\theta_H^2\nu\exp(-E/RT)$	9	0.075	b
(3)	$K_{eq} = k_3/k_{-3} = \nu\exp(E/RT)$	2	0.03	c
(4)	$\theta_{C_2H_5}\theta_H\nu\exp(-E/RT)$	6	1.47×10^{-3}	c
(5)	$\theta_{C_2H_4}\nu\exp(-E/RT)$	9	9.2×10^{6}	a

a) This work and ref. [2].
b) Ref. [20].
c) This work and parameters adjusted to fit the self-hydrogenation process.

$$
\begin{aligned}
&(1) && C_2H_{4\ (ads)} \rightarrow C_2H_{3\ (ads)} + H_{(ads)} && \text{(RDS)}\\
&(2) && 2H_{(ads)} \rightarrow H_{2\ (g)} &&\\
&(3) && C_2H_{4\ (ads)} + H_{(ads)} \rightleftharpoons C_2H_{5\ (ads)} &&\\
&(4) && C_2H_{5\ (ads)} + H_{(ads)} \rightarrow C_2H_{6\ (g)} &&\\
&(5) && C_2H_{4\ (ads)} \rightarrow C_2H_{4\ (g)} &&
\end{aligned}
$$

A computer simulation of the preceeding model was developed using the kinetic parameters determined from this work and elsewhere (Table 3.3). The kinetic parameters for step (1) were extracted from the first hydrogen desorption peak that was due to the decomposition of ethylene to ethylidyne. This is so because once hydrogen is formed on the surface due to the breaking of C–H bonds, the temperature is high enough so that the recombination and desorption of H_2 is fast. The parameters used were: E_a = 17 Kcal/mole and $\nu = 4\times10^{13}$ sec^{-1}. The activation energy was taken from this work and the preexponential factor was taken from the paper by Salmerón and Somorjai [2].

The desorption parameters of step (2) (H_2 desorption from Pt(111)) were taken from the work of Christmann *et al.* [20]. The parameters used were E_a = 9 Kcal/mole and ν = 0.075 for the second order process. Molecular desorption of ethylene was

observed and the kinetic parameters used for step (5) were taken from Salmerón and Somorjai [2]. They were: $E_a = 9$ Kcal/mole and $\nu = 9.2\times10^6$.

The kinetic parameters for steps (3) and (4) were not as easily accessible. If the hydrogenation were to take place in a concerted way, the overall rate expression for the two hydrogenation steps combined would be:

$$rate = \theta_H^2 \theta_{C_2H_4} \nu \exp(-E_a/RT)$$

This expression is third order overall, second order in hydrogen and first order in ethylene. However, it is likely that the hydrogenation occurs in two successive steps, one of which is rate determining, and each of which is first order in hydrogen and second order overall. The coverages of hydrogen and ethylene for step (3) and the coverages of hydrogen and the surface ethyl radical for step (4) change with time (and temperature) in an undetermined way. For this reason it may not be possible to use the well established methods of determining kinetic parameters from the TPD for the hydrogen predosed system (Figure 3.3). This leaves four undetermined parameters to be fixed in order to get good agreement with the experimental data.

A considerable amount of C_2D_6 desorbed during TPD when D_2 and C_2H_4 were coadsorbed on the Pt(111) surface (Figure 3.4). This can be explained if a fast equilibrium is attained between adsorbed ethylene and the surface ethyl radical, and if the second hydrogenation step is rate limiting for the formation of ethane. The method of Chan *et al.* [11] for a second order desorption was used as a first approximation, and an activation energy of 6±1 Kcal/mole was calculated for the thermal desorption processes shown in Figure 3.3. This activation energy was assigned to step (4), the second and rate limiting hydrogenation step.

The first hydrogenation step and its reverse were assumed to be faster than

the second hydrogenation step. This leads to deuterium exchange:

$$C_2H_{4\ (ads)} + D_{(ads)} \overset{K_{eq}}{\rightleftharpoons} C_2H_3D_{\ (ads)} + H_{(ads)}$$

Furthermore, adsorbed C_2H_4 and C_2H_5 are proposed to be in dynamic equilibrium, then:

$$K_{eq} = \theta_{C_2H_5}/\theta_{C_2H_4}\theta_H = k_3/k_{-3} = (\nu_3/\nu_{-3})\exp[(E_{-3} - E_3)/RT]$$

The following three parameters were selected for use in the model:

$$(\nu_3/\nu_{-3}) = 0.03;\ (E_{-3} - E_3) = 2\ Kcal/mole;\ \nu_4 = 1.47 \times 10^{-3}$$

The surface hydrogenation model is summarized in Table 3.3, and computer generated results accompany the experimental results in Figures 3.1, 3.2, 3.3, 3.5, and 3.6. They were in excellent agreement with experiment for both the self-hydrogenation and hydrogen coverage dependence for the hydrogen preadsorbed system.

Additional calculations were performed in order to justify the selection of the kinetic parameters for the hydrogenation steps. Keeping all other parameters the same, the activation energy for step (4), the final hydrogenation step, was adjusted with its corresponding preexponential factor so that the ethane yield during self-hydrogenation of ethylene remained unchanged. The position of T_{max} and the full width at half maximum (FWHM) for ethane desorption were computed as a function of the activation energy (E_4) for ethylene hydrogenation when a large coverage of preadsorbed hydrogen was present. Experimentally, T_{max} was 250 K and the FWHM was 65 K under these conditions (30 L H_2 predose). The model gave the best agreement with experiment (T_{max} and FWHM) when E_4 was 6 kcal/mole. As E_4 was increased, T_{max} increased and the FWHM decreased. At

E_4 = 9 Kcal/mole, T_{max} was 265 K and the FWHM was too narrow at 45 K. On the other hand, as E_4 was decreased, T_{max} decreased rapidly and was 200 K at E_4 = 3 Kcal/mole.

3.6.2 Availability of platinum surface sites in the presence of ethylidyne

Attempts have been made to determine the amount of open surface available when the Pt(111) surface is saturated with ethylidyne [21]. It was found that the ethylidyne saturated Pt(111) surface adsorbed 0.25 ML of hydrogen only when hydrogen dosing was performed at atmospheric pressures. Hydrogen is known to adsorb on clean Pt(111) at room temperature [22], so the ethylidyne either occupies all the hydrogen adsorption sites, or increases the activation energy of hydrogen adsorption either by altering the electronic state of the surface or by breaking up large platinum ensembles that dissociate hydrogen most easily. The latter explanation is perhaps the most satisfactory, and the H_2 desorption peak in Figure 3.9d shows that the position of T_{max} was not significantly different than for H_2 desorbing off clean Pt(111) (Figure 3.7d). The adsorption of CO on ethylidyne saturated Pt(111) also supports this explanation since CO does not dissociate on platinum and therefore requires a smaller ensemble for adsorption.

An ethylidyne saturated surface was found to adsorb CO quite readily as shown in Figure 3.10, despite the fact that CO is a larger molecule than H_2. The results obtained indicate that the saturation coverage of CO (θ_{CO} is defined by $\theta_{sat} = 1$ on a clean Pt(111) surface) on ethylidyne saturated Pt(111) is around $\theta_{CO} \sim 0.35$ ML (Table 3.2). It is known from LEED experiments that ethylidyne forms a (2×2) overlayer on Pt(111), due either to 3 superimposed (2×1) domains resulting in an ethylidyne coverage of 0.5 ML [21], or to a single (2×2) domain resulting in an

ethylidyne coverage of 0.25 ML. The results obtained indicate that the presence of ethylidyne on the Pt(111) surface block CO adsorption sites, perhaps due to steric hindrance. If it is assumed that a single platinum atom can bind either to a CO molecule or to an ethylidyne species, then θ_{CO} should be 0.25 ML for θ_{CCH_3} = 0.25 ML since each ethylidyne species bonds to three platinum atoms, or 0 for θ_{CCH_3} = 0.5 ML. The results obtained here indicate that θ_{CCH_3} is closest to 0.25 ML. The shift in T_{max} observed for CO to 20 degrees lower temperature when the Pt(111) surface was saturated with ethylidyne compared to clean Pt(111) indicates that a repulsion exists between CO and ethylidyne.

The increase in CO desorption area observed after ethylidyne was thermally decomposed indicates that the carbonaceous residues left on the surface have reorganized to occupy less surface area through polymerization or condensation; and possibly by forming 3 dimensional deposits.

3.6.3 The role of hydrogen in propylidyne decomposition

The decomposition of propylene has been studied previously [2,23], and the H_2 TPD spectrum is shown in Figure 3.11. The first H_2 desorption peak is obtained near 400 K and is due to the formation of propylidyne, analogous to the formation of ethylidyne from ethylene [2]. The decomposition of the propylidyne species is completed by 470 K, as shown in Figure 3.11a, and particularly by Figure 3.11e.

The decomposition of the propylidyne species is inhibited by surface hydrogen. In fact most of the propylidyne remained undecomposed when heated to 470 K with 1×10^{-4} Torr hydrogen (Figure 3.11b), and the shoulder near 510 K suggests that some of the decomposing species formed ethylidyne. Propylidyne is known to form ethylidyne upon decomposition on Rh(111) in UHV, and perhaps the ability of rhodium to bind hydrogen tightly is the reason this occurs [23]. It therefore

follows that if hydrogen is forced to occupy platinum sites at the decomposition temperature of propylidyne by using higher H_2 pressures, then this metal may decompose propylidyne through a similar reaction pathway as rhodium. Substantial propylidyne was observed to remain undecomposed even after flashing up to 490 K in the presence of hydrogen. During catalytic conversion of hydrocarbons as discussed in Chapter 6, high pressures of hydrogen are needed to keep the catalytic surfaces free from deactivation due to the buildup of coke, even for dehydrogenation reactions. The results obtained from propylidyne decomposition are clear proof that the presence of surface hydrogen passivates the surface against decomposition of surface carbonaceous residues.

3.6.4 The behavior of hydrogen on ethylidyne saturated Pt(111)

Zaera and Somorjai [7] have recently reported that a saturation layer of ethylidyne was formed immediately and irreversibly on the Pt(111) surface during the high pressure ($\sim$ 200 Torr) steady state catalytic hydrogenation of ethylene. Ethylidyne is stable under atmospheric pressures of hydrogen and at room temperature since the hydrogenation, and exchange of deuterium for hydrogen on the methyl group, are much slower ($\sim 10^{-3}$ times slower) than the catalytic hydrogenation of ethylene [8,9,10]. Ethylidyne was always found on the Pt(111) crystal upon return to UHV conditions following a hydrogenation reaction. Also, restart reactions on ethylidyne covered platinum gave the same rates of reaction as for clean surfaces. All of the above suggest direct participation of the carbonaceous overlayer during the steady state hydrogenation of ethylene at atmospheric pressure and near room temperature. It was proposed that after dihydrogen dissociates on the platinum surface, the hydrogen atoms are transferred indirectly from the platinum surface to

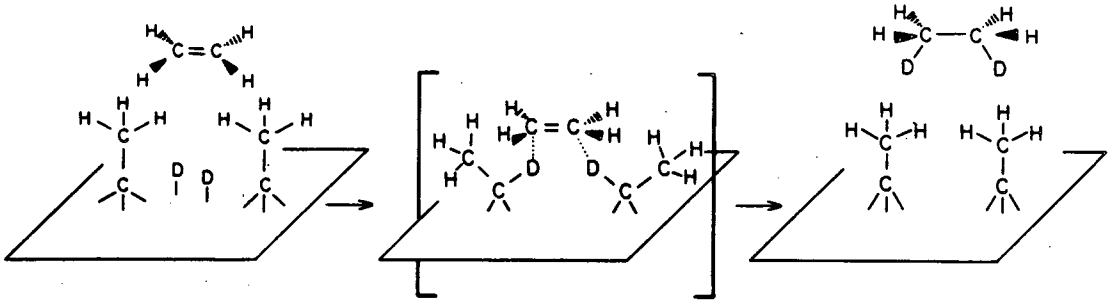

XBL 846-2494A

Figure 3.14: Proposed mechanism for the steady state catalytic hydrogenation of ethylene on Pt(111). The second panel shows schematically the proposed ethylidene intermediates derived from ethylidyne and surface deuterium.

weakly bound ethylene molecules through the α carbon of the ethylidyne species, via the formation of ethylidene ($CHCH_3$) intermediates (Figure 3.14).

In support of this scheme it has been demonstrated that hydrogen could be adsorbed on an ethylidyne saturated platinum surface when the pressure was greater than 10^{-5} Torr at temperatures between 150-320 K. The amount of hydrogen that could be adsorbed on this surface with a one atmosphere exposure ($\sim 10^{10}$ L) was about 25% the amount that could be adsorbed on a clean Pt(111) surface with a 30 L exposure.

At pressures around 10^{-5} Torr detectable quantities of hydrogen could also be adsorbed on the ethylidyne saturated surface between 150-320 K, but equivalent exposures at 10^{-6} Torr gave no detectable hydrogen adsorption. Larger coverages were obtained with higher hydrogen pressures according to the adsorption isotherm until saturation was reached. An absolute measurement of the hydrogen isotherm could not be obtained because once the hydrogen dosing is discontinued in preparation for a TPD experiment, hydrogen immediately begins to desorb from

the surface.

Two different hydrogen states were seen in the TPD depending on the adsorption temperature. The H_2 desorption peaks around 290 K (Figure 3.9b) were probably due to hydrogen desorbing from the platinum surface while the 385 K (Figure 3.9c) desorption peak was possibly related to a hydrocarbon decomposition. The presence of the 385 K peak suggests the existence of ethylidene ($CHCH_3$) on Pt(111) when higher hydrogen pressures were applied to an ethylidyne saturated surface. The peak was found on the low temperature side of the ethylidyne decomposition peak, consistent with calculations of Kang and Anderson [24] that predict ethylidene is less stable than ethylidyne at low hydrogen pressures. A high steady state concentration of ethylidene would be favored by high hydrogen pressures. However, under UHV the ethylidene $\rightleftharpoons$ ethylidyne equilibrium would be completely shifted towards the more dehydrogenated moiety. Therefore, the ethylidene decomposition product is probably ethylidyne, and within experimental error, the area and shape of the hydrogen desorption peak from ethylidene above 420 K was no different than the area and shape of a typical ethylidyne desorption spectrum (Figure 3.9).

3.6.5 The steady state catalytic hydrogenation of ethylene over platinum

These results have implications for the catalytic hydrogenation of ethylene. First, if ethylene was hydrogenated directly on the platinum surface, an activation energy of 6 Kcal/mole would probably be observed instead of 8-15 Kcal/mole as reported elsewhere [25,26,27,28,29,30]. Extrapolating the surface hydrogenation model proposed here (Table 3.3, steps (2) - (5)) to steady state conditions and moderate pressures gave a rate expression very different than that determined by Zaera and

Somorjai [7] for ethylene and hydrogen on Pt(111). Also, the ethane deuterium distribution obtained from $D_2 + C_2H_4$ experiments under UHV (Figure 3.4) was much different from that obtained for high pressure deuteration [7].

There have been observations made in the literature that support the proposed direct participation of carbonaceous deposits during the catalytic hydrogenation of ethylene on metallic surfaces. Laidler and Townsend [31] reported two activation energies for ethylene hydrogenation over Ni films (7.8 and 10 Kcal/mole) depending on whether hydrogen or ethylene was introduced into the reactor first. When hydrogen was introduced first, the fast initial rate with the lower activation energy gave way to the slower rate obtained when ethylene was introduced first, indicating that as surface hydrogen was depleted, surface metal atoms became available for the adsorption of hydrocarbon that forms stronger bonds to the surface than does hydrogen.

The possibility exists that on the Pt(111) surface, the catalytic hydrogenation still proceeds directly on the metal surface, but a larger activation energy is observed because ethylidyne hinders the approach of ethylene to the surface. Although this explanation cannot be discarded, it seems unlikely since neither ethylene nor ethane were found to desorb when attempts were made to adsorb ethylene on an ethylidyne saturated surface, even at atmospheric pressure. Another plausible explanation is that the effect of ethylidyne on the dissociation of H_2 could also be responsible for a larger activation energy of ethylene hydrogenation. The results of Section 3.6.4 show that the presence of ethylidyne leads to a greater activation energy of H_2 adsorption or dissociation. The magnitude of this increase was undetermined, but the importance of this effect may be significant.

Wieckowski *et al.* reported an activation energy of 5.9 Kcal/mole for the hydrogenation of ethylene over Pt(111) in solution where H^+ was reduced at the surface

giving surface hydrogen. They propose that ethylene is hydrogenated directly on the clean platinum surface, similar to the process of surface hydrogenation reported under UHV in Section 3.2.2 [32]. Since ethylidyne was not accumulated on the surface during these experiments, it is not proven whether or not ethylidyne affects the hydrogen or the ethylene species.

In an attempt to determine whether ethylidyne also participates in the catalytic hydrogenation of ethylene on other platinum surfaces, experiments were performed on the Pt(100) surface. Although the rates and activation energies were similar on the Pt(111) and the Pt(100) surfaces, differences were observed in the hydrogen TPD spectra obtained after reaction. The Rh(100) surfaces has been shown to form ethylidyne from ethylene under UHV and during the catalytic hydrogenation of ethylene [23]. Since the clean Rh(100) surface exhibits no reconstruction, ethylidyne can form on a surface with fourfold symmetry. The Pt(100) surface reconstructs to a hexagonal (5×20) structure, and remains in this structure after exposing the surface to ethylene and transformation to ethylidyne under UHV [13], and was also observed to do so in this laboratory. However, the reconstruction is removed by hydrogen at low temperatures [33], but it could not be verified if the reconstruction was removed during ethylene hydrogenation reactions at atmospheric pressures. No LEED pattern was observed following reaction, probably due to the large amount of carbon that accumulated on the surface during reaction. Compared to the Pt(111) surface, the Pt(100) surface accumulated 3 times more carbon and 2–3 times more hydrogen. Ethylidyne may certainly have been involved with the reaction, but it must be concluded from these results that other carbonaceous species were present on the Pt(100) surface and may have also participated in the hydrogenation of ethylene.

References

[1] H. Steininger, H. Ibach, and S. Lewald. *Surf. Sci.* **117** (1982) 685.

[2] M. Salmerón and G. A. Somorjai. *J. Phys. Chem.* **86** (1982) 341.

[3] A. M. Baro and H. Ibach. *J. Chem. Phys.* **74** (1981) 4194.

[4] J. E. Demuth. *IBM J. Res. Develop.* **22** (1978) 265.

[5] P.J. Hiett, F. Flores, P.J. Grout, N.H. March, A. Martin-Rodero, and G. Senatore. *Surface Sci.* **140** (1984) 400.

[6] L. Kesmodel, L. Dubois, and G. A. Somorjai. *J. Chem. Phys.* **70** (1979) 2180.

[7] F. Zaera and G. A. Somorjai. *J. Am. Chem. Soc.* **106** (1984) 2288.

[8] S. Davis, F. Zaera, B. Gordon, and G. A. Somorjai. *J. Catalysis* **92** (1985) 240.

[9] B.E. Koel, B.E. Bent, and G.A. Somorjai. *Surface Sci.* **146** (1984) 211.

[10] F. Zaera. PhD thesis, University of California, Berkeley, CA 94720, 1984.

[11] C.-M. Chan, R. Aris, and W.H. Weinberg. *Appl. Surface Sci.* **1** (1978) 360–387.

[12] P. Berlowitz, C. Megiris, J. Butt, and H. King. *Langmuir* **1** (1985) 206.

[13] H. Ibach. In *Vibrations in Adsorbed Layers*, page 64, Jülich, Germany, 1978.

[14] H. L. Pickering and H. C. Eckstrom. *J. Phys. Chem.* **63** (1959) 512.

[15] R. W. Roberts. *J. Phys. Chem.* **67** (1963) 2035.

[16] G. I. Jenkins and E. Rideal. *J. Chem. Soc.* (1955) 2490–2496.

[17] G. C. Bond. *Catalysis by Metals*, page 230. Academic Press, New York, 1962.

[18] J. Horiuti and K. Miyahara. *Hydrogenation of Ethylene on Metallic Catalysts.* Technical Report 13, NSRDS–NBS, 1968.

[19] W. Hasse, H.L. Gunter, and M. Henzler. *Surface Sci.* **126** (1983) 479.

[20] K. Christmann, G. Ertl, and T. Pignet. *Surface Sci.* **54** (1976) 365.

[21] N. Freyer, G. Pirug, and H.P. Bonzel. *Surface Sci.* **125** (1983) 327.

[22] D.M. Collins and W.E. Spicer. *Surface Sci.* **69** (1977) 85.

[23] Brian E. Bent. PhD thesis, University of California, Berkeley, CA 94720, 1986.

[24] D.B. Kang and A.B. Anderson. *Surface Sci.* **155** (1985) 639.

[25] A. Farkas and L. Farkas. *J. Am. Chem. Soc.* **60** (1938) 22.

[26] 0. Beeck. *Rev. Mod. Phys.* **17** (1945) 61.

[27] G. C. Bond. *Trans. Faraday Soc.* **52** (1956) 1235.

[28] V. Kazanski and V. Strunin. *Kinetics Catalysis (Engl. Transl.)* **1** (1960) 517.

[29] T. Dorling, M. Eastlake, and R. Moss. *J. Catalysis* **14** (1969) 23.

[30] J. C. Schlatter and M. Boudart. *J. Catalysis* **24** (1972) 482.

[31] K. J. Laidler and R. E. Townsend. *Trans. Faraday Soc.* **57** (1961) 1590.

[32] A. Wieckowski, S. Rosasco, G. Salaita, A. Hubbard, B. Bent, F. Zaera, D. Godbey, and G. Somorjai. *J. Am. Chem. Soc.* **107** (1985) 5910.

[33] M.A. Barteau, E.I. Ko, and R.J. Madix. *Surface Sci.* **102** (1981) 99.

Chapter 4

The Preparation and Characterization of Bimetallic Platinum–Rhenium Surfaces

4.1 Preface

Since the introduction of rhenium to the reforming catalyst in 1968 [1], many studies have been published aimed at understanding this complex system including those reported in [2–26]. Most of these studies deal with the practical catalyst as a whole, consequently the information obtained cannot separate totally the metal–metal interaction from the influence of other variables, such as the support (*e.g.* γ–alumina) and other additives (*e.g.* sulfur, chlorine, potassium).

The method used in these studies was to strip the system to the most basic components, yet still have a reforming catalyst. The rest of this thesis deals with only the metallic components of the platinum–rhenium catalyst; the purpose being to isolate the metallic components and correlate changes in chemistry and physical properties of the surface with respect to the metallic composition of the surface. To a lesser extent these studies have been concerned with changes made in surface crystallographic orientation. Studies have been performed previously in this laboratory to determine the effect of surface structure on monometallic platinum

catalysts [27,28,29]. Equipped with this background information, another variable was added to the system: rhenium.

In this chapter is reported the preparation of bimetallic surfaces of rhenium on Pt(111) and Pt(100) by vapor deposition of rhenium metal onto platinum single crystal surfaces, and of platinum metal onto Re(0001) single crystal surfaces and rhenium foils. The composition and properties of the prepared bimetallic surfaces were characterized using Auger electron spectroscopy (AES), low energy electron diffraction (LEED), and X-ray photoelectron spectroscopy (XPS).

4.2 Growth Mechanisms of Metallic Thin Films of Platinum and Rhenium

4.2.1 Rhenium Uptake on Pt(111) and Pt(100)

Rhenium uptake on Pt(111) was assessed by AES using an RFA operated in the derivative mode. A plot of the platinum 158 eV peak intensity (the platinum 150 and 158 eV peaks were unresolved on this analyzer) versus time of rhenium deposition is shown in Figure 4.1. Breaks in the rhenium uptake curve near four and eight minutes correspond to the filling of the first and second monolayers respectively. After the filling of the third monolayer, the 158 eV platinum peak was no longer resolved above the secondary electron background due to the thickness of the rhenium film. Representative spectra of some bimetallic surfaces derived from Pt(111) are shown in Figure 4.2.

The growth mechanism of rhenium on Pt(111) was found to be monolayer by monolayer at least through three monolayers. This was shown in Figure 4.1 by the presence of breaks in the Auger uptake curves of the platinum 158 eV peak at 4 and 8 minutes which is characteristic of a Frank-van der Merwe, or layer by layer

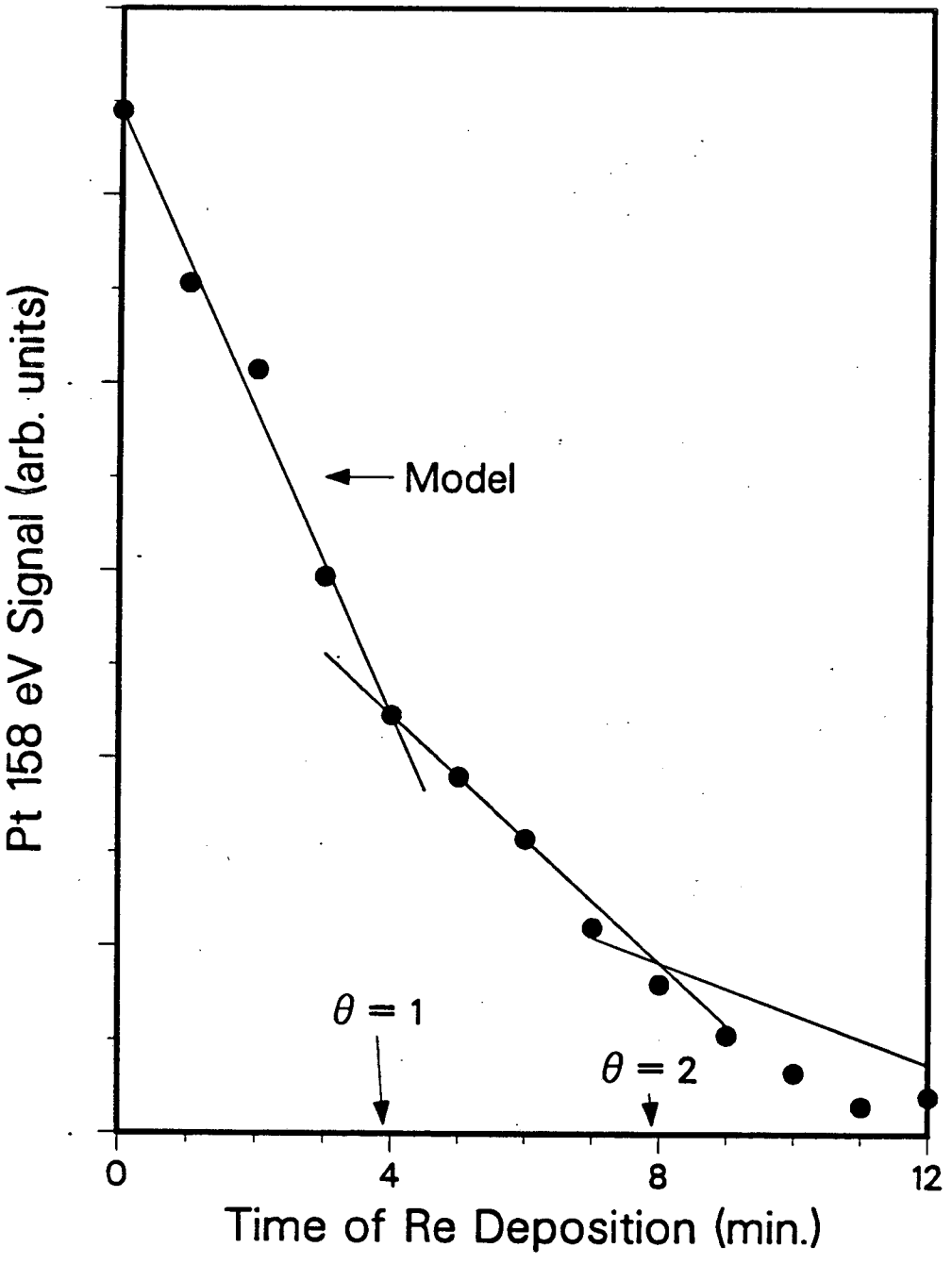

Figure 4.1: Rhenium uptake on Pt(111). Breaks near four and eight minutes correspond to the filling of the first and second monolayers of Re. The solid lines were generated by the Gallon model for layer by layer growth as discussed in Chapter 2. A similar plot was obtained for rhenium uptake on Pt(100).

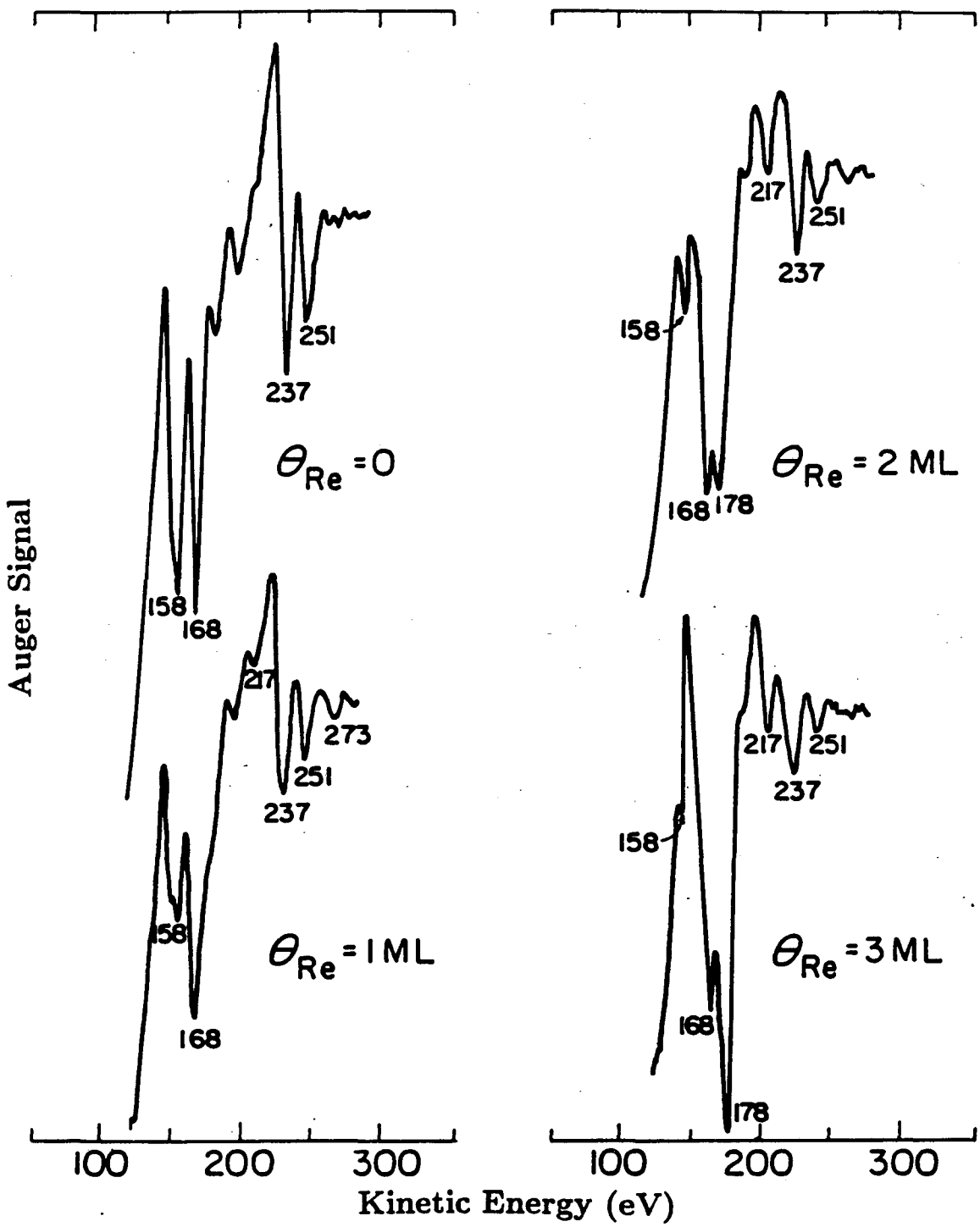

Figure 4.2: Representative Auger spectra obtained of Re on Pt(111). Shown are spectra for clean Pt, and θ_{Re} = 1, 2, and 3 monolayers on Pt(111) respectively.

growth mechanism. Adsorbate versus substrate plots gave the same information as the plot in Figure 4.1 and are not included here.

According to Equation 2.9 derived from the Gallon model [30], the intensity of the platinum 158 eV peak (I_{Pt}) should fit the Equation

$$I_{Pt} = I^{\circ}_{Pt}[1 - (1 - \alpha)\theta_{Re}]$$

for the first rhenium monolayer. The attenuation coefficient α was defined in Equation 2.7 as

$$\alpha = I^1_s / I^{\circ}_s$$

where I^1_s is the intensity of the substrate peak covered by one monolayer of adsorbate and I°_s is the intensity of the clean substrate peak. For the platinum 158 eV peak attenuated by one monolayer of rhenium metal, the attenuation coefficient α was found to be 0.41. The analysis from Equation 2.9 further leads to

$$I_{Pt} = I^{\circ}_{Pt}[\alpha(2 - \alpha) - \alpha(1 - \alpha)\theta_{Re}] \tag{4.1}$$

and

$$I_{Pt} = I^{\circ}_{Pt}[\alpha^2(3 - 2\alpha) - \alpha^2(1 - \alpha)\theta_{Re}] \tag{4.2}$$

for the filling of the second and third monolayers respectively. The above model was plotted in figure 4.1 and gives good agreement with experimental results. Further confirmation of layer by layer growth was that a well ordered (1×1) surface structure was always present during rhenium deposition on the Pt(111) crystal as shown by LEED.

The inelastic mean free path (imfp) can be estimated from these data [30,31,32]. Assuming that the atomic backscattering coefficient is the same for platinum and rhenium (they are separated by osmium and iridium in the periodic table) then

$$\alpha = \exp(-d/0.75\lambda cos\phi) \tag{4.3}$$

where λ is the imfp, the factor 0.75 comes from the acceptance angle of the retarding field analyzer [32], d is the layer spacing, and ϕ is the photoelectron takeoff angle. Using $d = 2.23$ Å for rhenium, the imfp was calculated to be 3.5 Å, which is reasonable for a 158 eV electron as can be seen from Figure 2.5.

It is important to be able to determine the coverage of an adsorbate by a single Auger spectrum. Platinum metal has a pair of Auger transitions near 158 eV, the 150 eV peak being unresolved on the analyzer used. Both platinum and rhenium metals have Auger transitions near 168 eV. As rhenium was deposited on platinum, the platinum 158 eV peak was attenuated, but the Pt + Re 168 eV peak intensity remained fairly constant up to 1.5 ML of rhenium. At larger rhenium coverages the 168 eV peak intensity increased. If the ratio of the intensities of the 158 and 168 eV peaks are plotted versus the rhenium coverage, linear behavior is observed through 2 monolayers of rhenium (Figure 4.3). The least squares line calculated from Figure 4.3 for the rhenium coverage through 2 monolayers is

$$\theta_{Re}(\pm 0.1 \text{ ML}) = (1.27 - I_{158}/I_{168})/0.56 \qquad (4.4)$$

where I_{158} and I_{168} are the intensities of the 158 eV and 168 eV Auger peaks. The coverage of rhenium was assigned after deposition using the above equation and the family of fingerprints like those shown in Figure 4.2. This method was also used by Sachtler to assign the composition of bimetallic gold–platinum surfaces [31].

Rhenium uptake was also measured on Pt(100). The uptake curves obtained were practically identical to those obtained from Pt(111), and are not included here (see Figure 4.1). The results obtained on Pt(100) indicate that a Frank-van der Merwe mechanism was also operating on this surface.

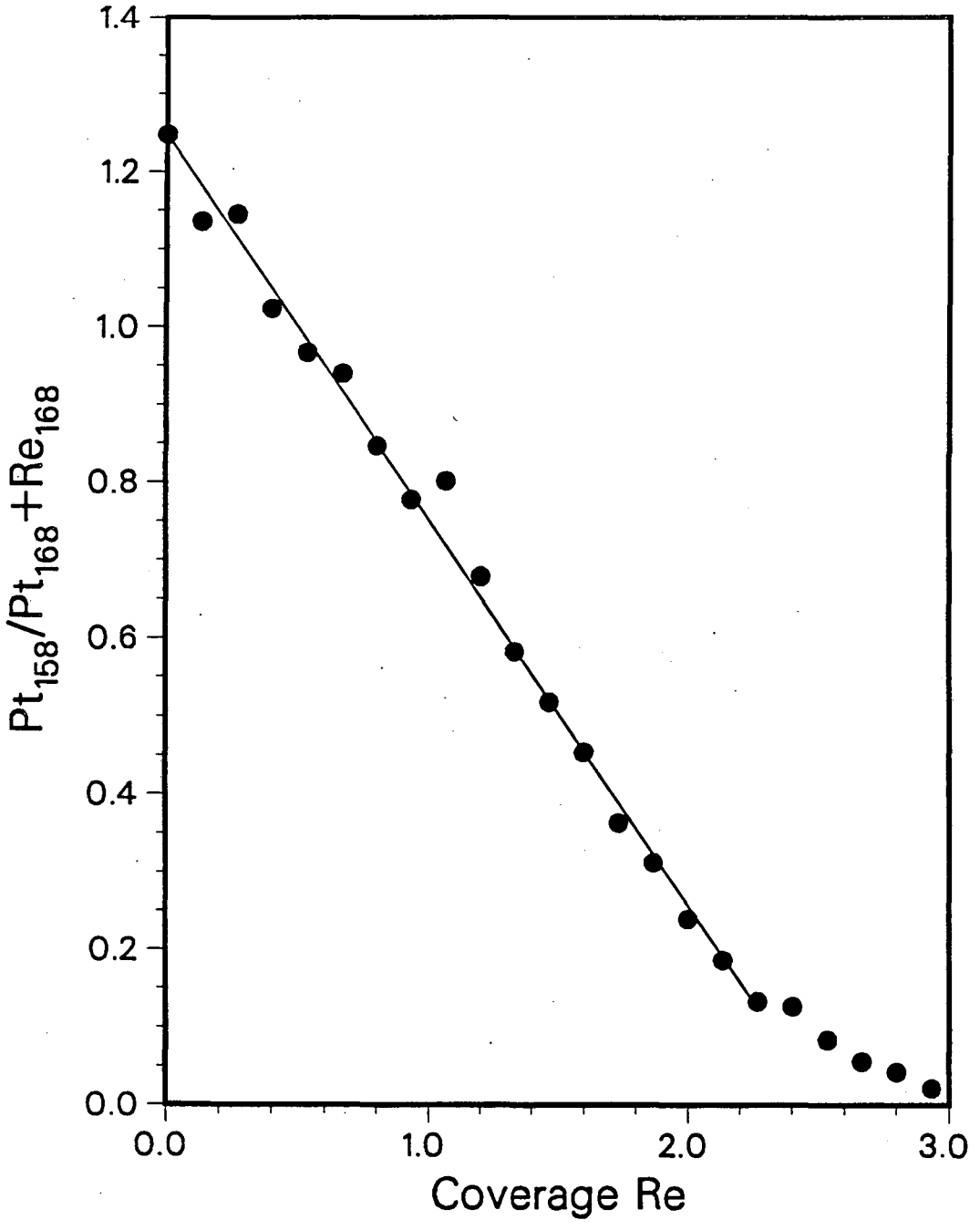

Figure 4.3: Ratio of the Auger 158 eV peak to the 168 eV peak obtained during Re uptake on Pt(111) and Pt(100).

4.2.2 Platinum uptake on Re(0001)

Platinum uptake was measured on Re(0001) using the same chamber and configuration as for the rhenium uptake on platinum crystals. The rhenium filament used on the metal deposition source was replaced with a 2 mm platinum coil composed of 0.020 inch platinum wire, as described in Chapter 2. Since the platinum deposition source operated at a much lower temperature than the rhenium source, no increase in base pressure was observed and the bimetallic surfaces generated also remained cleaner. Platinum is more inert than rhenium and this also helped in keeping the surface clean of background gases. For these reasons it was not necessary to flash the bimetallic Pt–Re(0001) or Pt–Re foil surfaces unless the preparation of alloyed surfaces were desired.

Uptake curves were obtained for platinum deposited on Re(0001) using Auger electron spectroscopy, and the plot obtained is shown in Figure 4.4. The attenuation of the rhenium 217 eV peak was measured for this system. In addition, the growth of the platinum 251 eV peak was well behaved at low platinum coverages. This is in contrast to the rhenium on platinum system where no adsorbate rhenium peak could be measured quantitatively at coverages less than 0.5 monolayers.

The behavior of the adsorbate Pt 251 eV and the substrate Re 217 eV peaks were also modeled according to Gallon [30] considering a layer by layer growth mechanism. Equations 2.8 and 2.9 were used to generate the solid lines in Figure 4.4. The model gives good agreement with the experimental data and is evidence that platinum growth on Re(0001) is layer by layer. This is in agreement with Alnot *et al.* who reported layer by layer growth of platinum on rhenium ribbon [33,34].

The attenuation coefficient of 217 eV electrons passing through one monolayer

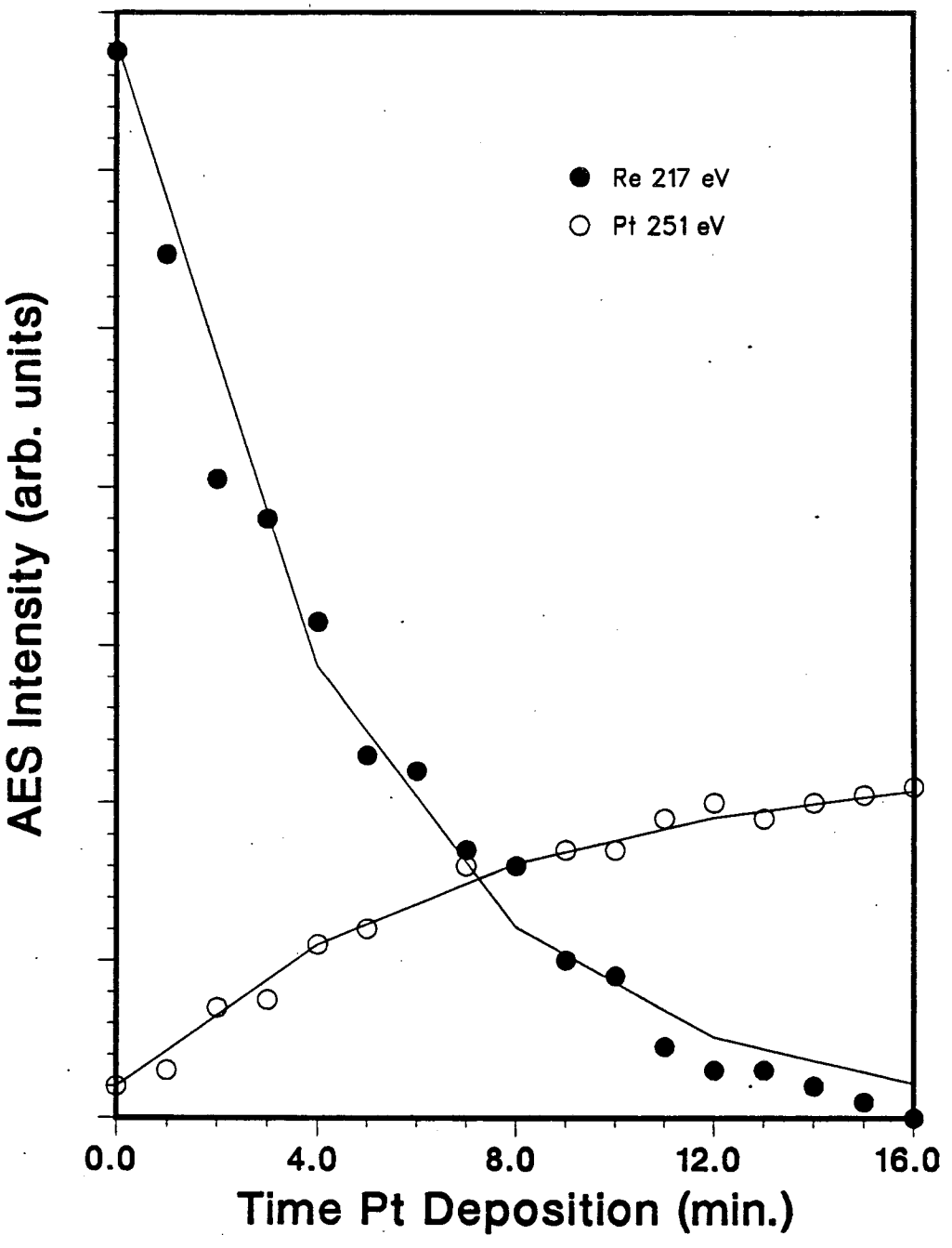

Figure 4.4: Platinum uptake on Re(0001) monitoring the adsorbate Pt 251 eV (o) and the substrate Re 217 eV peak (•). The solid lines were generated by the Gallon model for layer by layer growth.

of platinum is $\alpha = 0.42$, and is very close to the value obtained for the attenuation coefficient of 160 eV electrons through rhenium. The value corresponds to an inelastic mean free path of 3.7 Å for 217 eV electrons through platinum as calculated using Equation 4.3, and is within the range obtained for 217 eV electrons propagating through other elements as can be seen in Figure 2.5.

With the proceeding analysis complete, a set of Auger spectra were compiled that correspond to a given coverage of platinum on Re(0001). The ratio of many different peak combinations were calculated, and it was found that the ratio of the intensity of the Pt 251 eV divided by the intensity of the Pt + Re 168 eV peak versus coverage was well behaved up to at least 2 monolayers of platinum (Figure 4.5). Auger spectra obtained for platinum growing on rhenium foils also gave peak ratios that behaved similarly. The coverage of platinum on rhenium was estimated by calculating the ratio of intensities of the 251 eV and 168 eV peaks and reading the coverage from Figure 4.5. The Auger spectrum was also compared to the family of fingerprints obtained for the uptake curve of platinum on Re(0001) as was done for rhenium deposition on platinum crystals.

4.3 Properties of Bimetallic Platinum–Rhenium Films

4.3.1 Stability of metallic thin films of platinum and rhenium

The rhenium overlayer was found to be stable on platinum up to 1000 K. Above these temperatures rhenium diffused into the platinum substrate. Flashing the surface to 1100–1300 K was hot enough to obtain mixing of the platinum and rhenium metals in the interfacial region, and prolonged heating at these temperatures

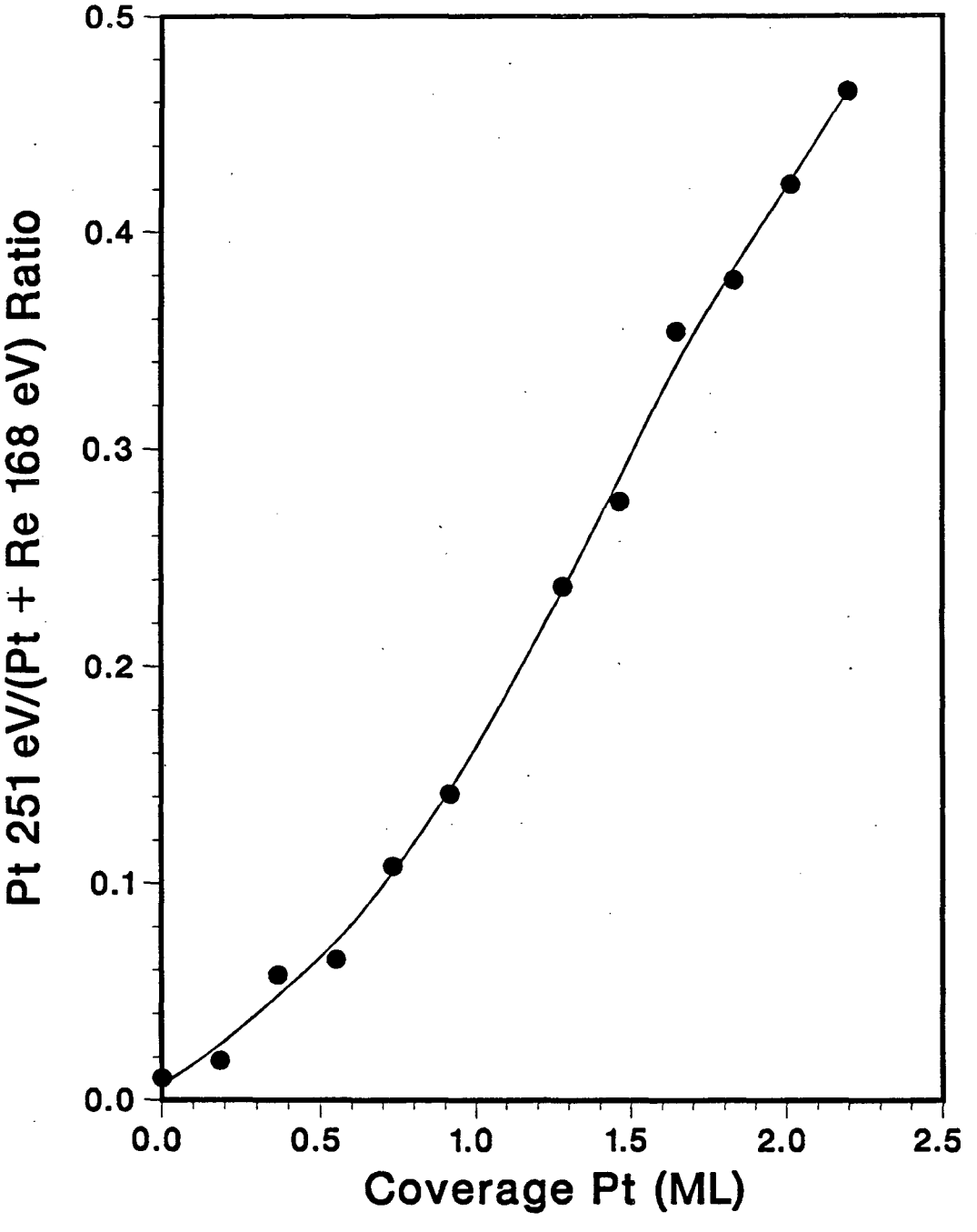

Figure 4.5: Ratio of the AES 251 eV to the 168 eV peak vs. coverage for platinum dosed Re(0001).

resulted in the eventual disappearance of rhenium into the platinum bulk. Rhenium could also be removed from the platinum surface at 300° C in the presence of 300 Torr of oxygen, probably in the form of volatile Re_2O_7.

Rhenium that was in contact with platinum metal resisted oxidation under vacuum conditions (10^{-7} Torr oxygen). However, when depositing more than one monolayer of rhenium on platinum, contamination by small amounts of oxygen from the background gases, particularly from air and water, was difficult to avoid.

There are two simple ways to remove oxygen from a rhenium surface in UHV. Heating to high temperatures ($\sim$ 2000 K) is one way, and the other is to chemisorb stoichiometric amounts of ethylene followed by flashing to 1000 K. Both methods cause bulk diffusion of the two metals, so a relatively thick rhenium film ($\sim$ 10 ML) must be deposited to insure that no platinum diffuses to the surface following annealing. For this reason it was difficult to control the surface oxygen coverage when attempting experiments at intermediate rhenium coverages such as 1 to several monolayers on platinum under vacuum conditions. Experiments performed at elevated hydrogen pressures posed no difficulties because all rhenium films were found to reduce under atmospheric hydrogen pressures at 300° C.

Platinum overlayers on rhenium were also found to be stable up to 1000 K. Above these temperatures platinum was lost from the surface by either diffusion or by thermal desorption. Thermal desorption was never checked, but it does occur to some extent according to Alnot *et al.* [34]. Platinum could mostly be removed from rhenium by heating to high temperatures, although this is an undesirable method for removing a second metal from the surface since substantial accumulation may eventually develop in the near surface region. However, in the case of platinum on rhenium, it was difficult to remove the last monolayer of platinum with heating. One monolayer of platinum on rhenium remained on the surface

for long periods of time, even at temperatures high above the diffusion threshold of the two metals. Alnot *et al.* also reported that some platinum could not be removed by heating, but they reported that 0.5 monolayers stubbornly remained on the rhenium surface [34].

The stability of a surface rhenium oxide was also tested in the presence of platinum. To remove oxygen from a rhenium surface, it was necessary to heat it in vacuum up to at least 2000 K. Experiments were performed in which oxygen was deliberately left on the rhenium surface. After dosing the rhenium surface with around 0.5 ML of platinum, the surface could be flashed free of oxygen at 400° C in vacuum. This indicates that platinum can catalyze the reduction of rhenium under UHV conditions. The catalyzed reduction of rhenium by platinum has been previously reported by investigators using temperature programmed reduction (TPR) of bimetallic supported platinum–rhenium catalysts [11,17], and the catalyzed decomposition of rhenium oxides at lower temperatures was at least partially responsible for the enhanced reduction in the presence of platinum.

The adsorbate induced surface segregation of rhenium oxides was investigated. Experiments were performed where oxygen was chemisorbed on clean Re(0001) followed by the deposition of 7 monolayers of platinum. The Re(0001) surface was dosed with oxygen until a (2×2) was observed using LEED indicating that the coverage of oxygen was $\theta_O \sim 0.25$ ML. After the deposition of platinum, the oxygen and rhenium were no longer detectable using AES. After a brief annealing of the surface to 800° C where the diffusion of platinum into rhenium is known to occur, both the rhenium and oxygen Auger signals reappeared with a decrease in the platinum Auger signal (Figure 4.6). Another brief annealing to 800 ° C resulted in an increased platinum Auger signal coupled to a decrease in the rhenium Auger signal, and disappearance of the oxygen signal. Further annealing to

800 ° C caused the platinum Auger signal to decrease as expected due to bulk diffusion of the metals. The interpretation of this effect is that rhenium oxide first segregated to the surface resulting in an increase in the rhenium and oxygen Auger signals. The increase in the platinum Auger signal observed following the first annealing resulted because the surface platinum catalyzed the reduction of the surface-segregated rhenium oxide in vacuum. The presence of oxygen apparently led to surface segregation of the rhenium oxide because the surface free energy of the oxide was less than the surface free energy of both metallic platinum and rhenium. When the oxygen desorbed, the remaining metallic rhenium diffused from the surface to the near surface region leaving platinum layers on the surface resulting in a net decrease in surface free energy.

4.3.2 XPS studies of the Re–Pt(111) system

X–ray photoelectron spectra were obtained of the Re-Pt(111) system. A reference spectrum of the clean Pt(111) 4f levels was obtained (Figure 4.7a), and all the platinum and rhenium $4f_{7/2}$ lines subsequently measured were referenced to a Pt $4f_{7/2}$ binding energy at 70.9 eV [35].

The photoelectron spectrum obtained after 10 monolayers of rhenium were deposited is shown in Figure 4.7b. Taking a value for the inelastic mean free path of 1200 eV electrons to be 18 Å from Figure 2.5, the thickness of the rhenium film was estimated by comparing the platinum XPS intensities before and after rhenium deposition. After solving Equation 4.3 with $d = 1$ ML to get α for 1200 eV electrons, Equation 4.3 can be solved for d to estimate the film thickness. The crystal was flashed periodically to 700 K during the deposition of rhenium to keep the accumulation of carbon low. X–ray photoelectron spectra obtained following deposition and flashing to 700 K gave binding energies of 71.4 and 40.4 eV for

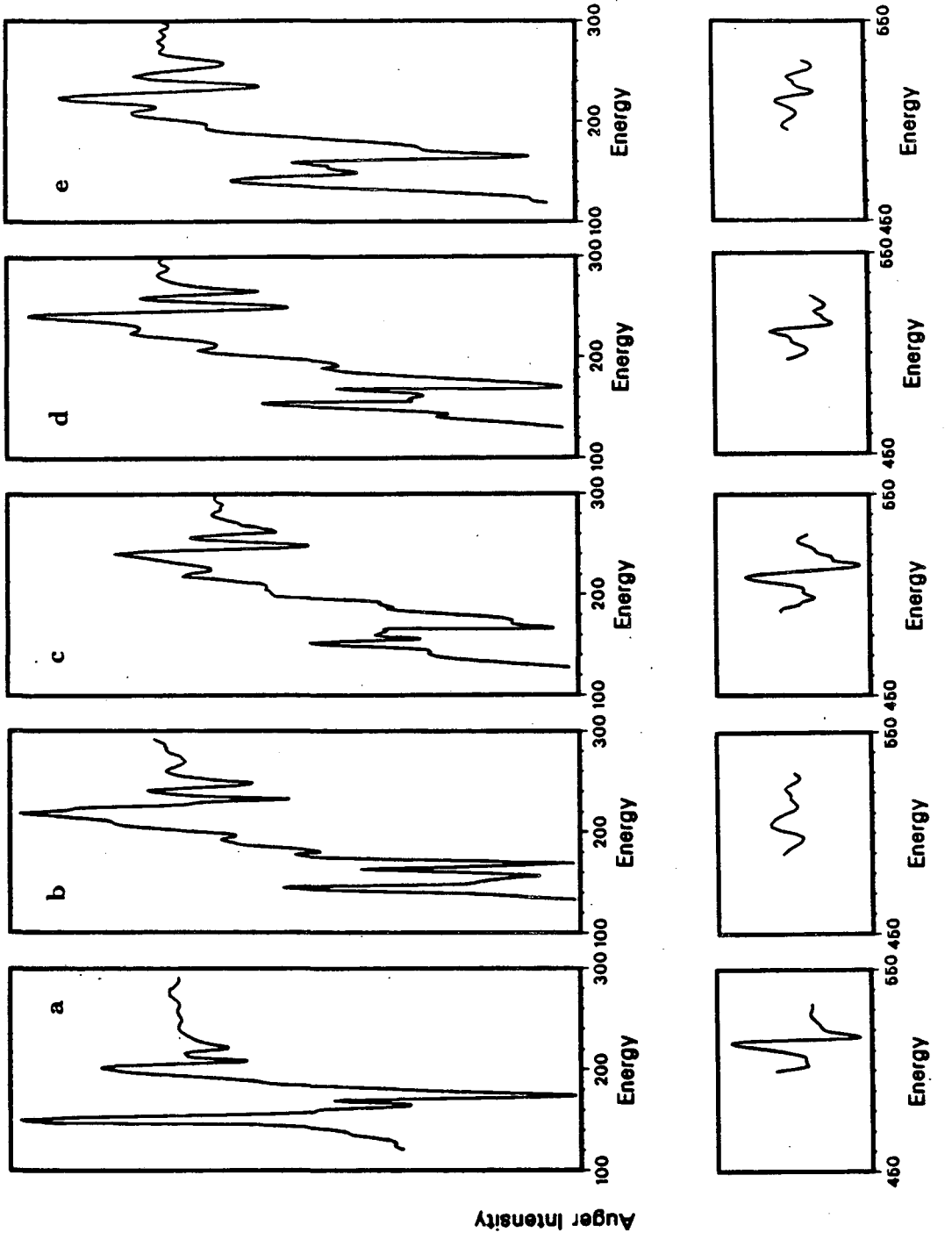

Figure 4.6: Diffusion of rhenium oxides through platinum metallic overlayers as shown by AES. The upper panels show the region 100–300 eV. Notice the behavior of the Pt 150 and 155 eV peaks. The lower panels show the oxygen region. a) Clean Re foil. b) After 10 ML Pt. c) After flashing to 800° C. d) After a second flashing to 800° C. e) After flashing to 850° C.

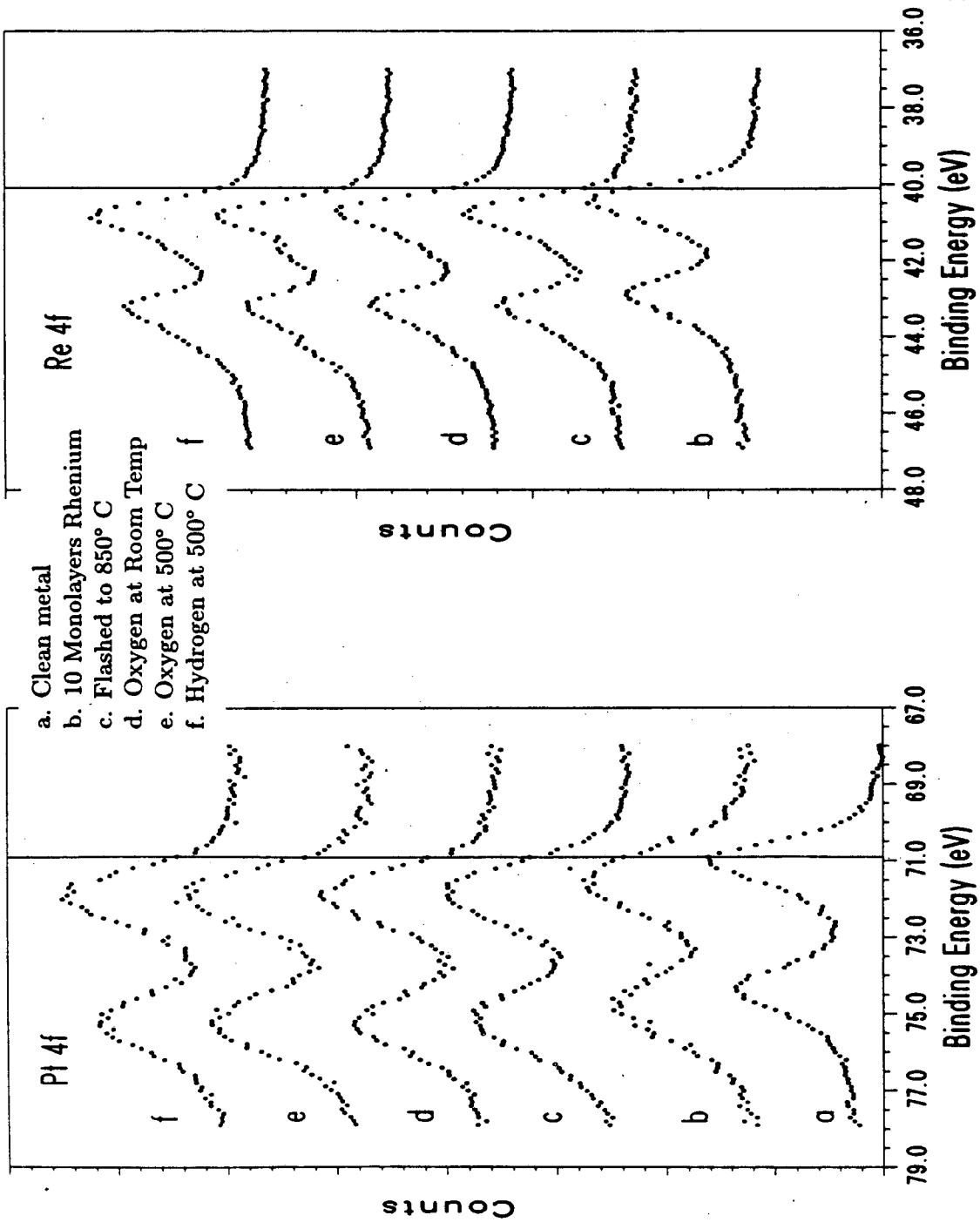

Figure 4.7: Normalized X-ray photoelectron spectra obtained from Re modified Pt(111) were recorded at room temperature. a) Clean Pt(111). b) After deposition of 10 ML of Re. c) Anneal surface from b to 1150 K. d) Surface from c treated in 2×10^{-7} Torr O_2 at room temperature. e) Surface from d heated to 800 K in 2×10^{-7} Torr O_2. f) Surface from e heated to 800 K in 1×10^{-6} Torr H_2.

the Pt and Re $4f_{7/2}$ levels respectively. This represents a shift to higher binding energy of 0.5 eV for the platinum $4f_{7/2}$ peak. The value of the binding energy for the rhenium $4f_{7/2}$ peak obtained was 0.3 eV higher than the value of 40.1 eV previously reported for clean rhenium [35]. The Pt $4f_{7/2}$ peak was also observed to widen at half maximum from 1.4 eV for clean platinum to 1.9 eV for rhenium covered platinum.

Following rhenium deposition and the above XPS measurement, the bimetallic surface was flashed to 1150 K and the results are shown in (Figure 4.7c). This caused a change in the relative intensities of the platinum and rhenium 4f lines obtained by XPS which indicates that diffusion of rhenium into the platinum bulk and/or platinum diffusion on top of the rhenium surface layers had occurred. The thickness of the rhenium layer was estimated to be about 7 monolayers following flashing to 1150 K using Equation 4.3. The binding energies obtained were 71.8 and 40.8 eV for the platinum and rhenium $4f_{7/2}$ levels respectively. This represents a total shift toward higher binding energies of 0.9 eV for platinum, and 0.4 eV for rhenium compared to the clean metals.

The annealed bimetallic surface was exposed to oxygen at room temperature for 1 hour (Figure 4.7d), and at 800 K for 10 minutes (Figure 4.7e). A shoulder was observed to grow on the rhenium $4f_{7/2}$ peak centered about 1 eV higher in binding energy than the parent peak following the oxygen treatment at 800 K. This shoulder was attenuated almost completely after treating in hydrogen at 800 K (Figure 4.7f). A summary of the XPS results is shown in Table 4.1.

Table 4.1: XPS Binding Energies in eV (±0.3 eV).

Treatment	Pt $4f_{7/2}$	Re $4f_{7/2}$
Clean Pt[a]	70.9	—
7 ML Re	71.4	40.4
Anneal to 1150 K	71.8	40.8
Oxidize 800 K	71.8	42[b]
Reduce 800 K	71.7	40.7

a. Reference [35]
b. High binding energy shoulder.

4.4 The Structure of Metallic Thin Films of Platinum and Rhenium

4.4.1 Structure of rhenium multilayers on Pt(111)

The LEED pattern generated following the deposition of any amount of rhenium on Pt(111) was always due to a (1×1) surface structure (Figure 4.8). This was the case even when 5–10 monolayers of rhenium were deposited and the platinum substrate could not be detected using AES. However, symmetry differences were observed when scanning the electron beam energy in the range of 50–200 eV. LEED spots of equivalent symmetry change intensity together when the electron beam energy is changed. Six–fold symmetry is shown by all six spots changing intensity together, while three–fold symmetry is shown by the two different sets of symmetry related spots changing intensity together as shown in Figure 4.8.

If the observed differences are caused by the formation of a different crystal structure, it is possible to distinguish between a hexagonal close-packed hcp(0001) and a face-centered cubic fcc(111) surface. The escape depth of 50–200 eV electrons is on the order of two atomic layers, so LEED experiments should show three-fold symmetry for both the ideal fcc(111) and hcp(0001) surfaces. However,

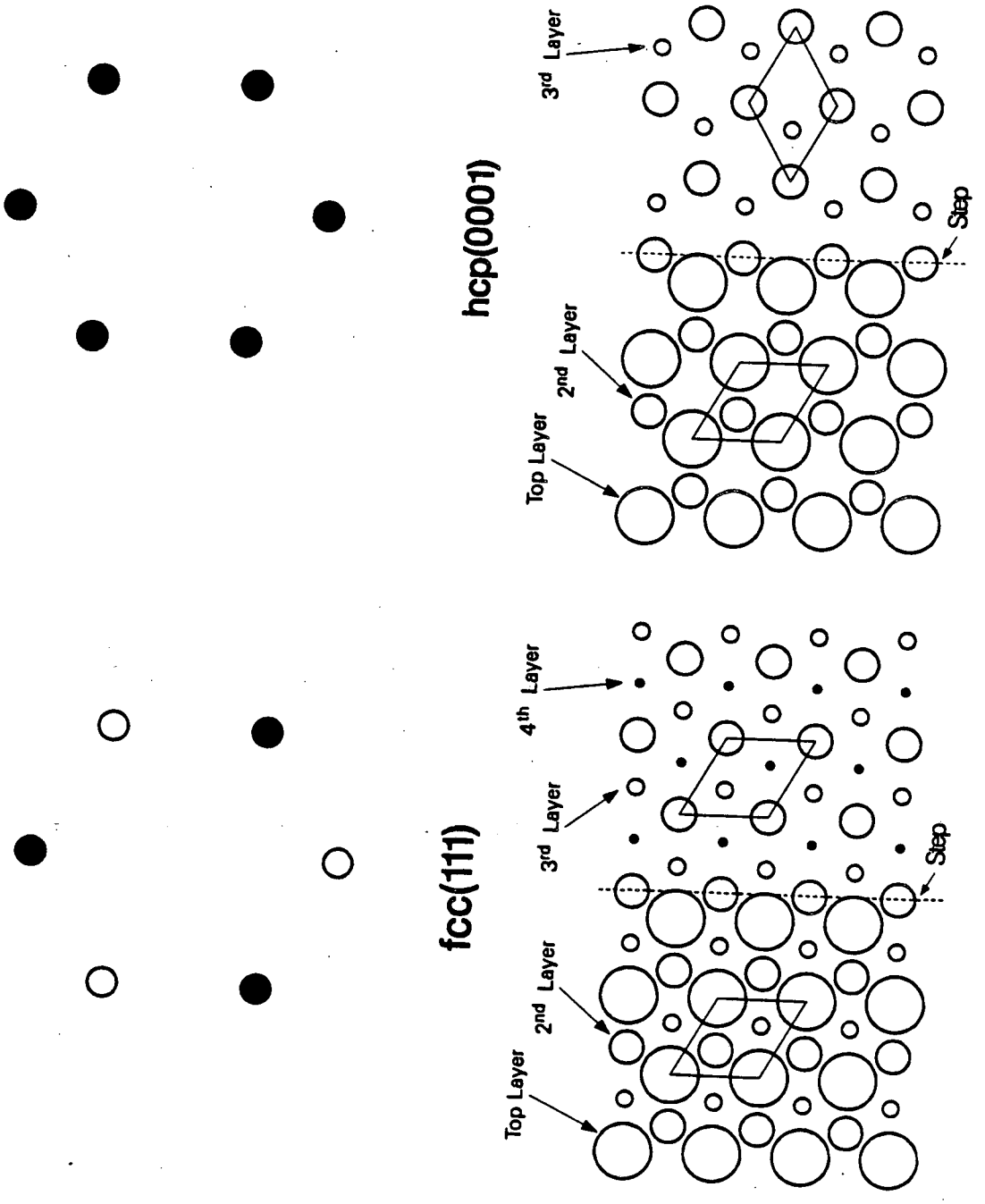

Figure 4.8: Reciprocal and real space representations of fcc(111) and hcp(0001) surfaces. For Pt(111), two equivalent sets of spots with 3-fold symmetry are indicated as solid or open spots. For Re(0001), all six spots are equivalent. Below the LEED patterns are shown schematic representations of real space surfaces with a single monatomic step for fcc(111) and hcp(0001) surfaces.

no surface is perfect and defects in the form of steps are present on the surface. If a step with the height of a single atom is considered on an fcc(111) surface, it can be seen that the surface unit cell is unchanged in moving across the step due to the *abcabc* packing of the fcc system. The LEED pattern obtained from either domain is indistinguishable, and three-fold symmetry is observed (Figure 4.8). However, the surface unit cell for the hcp(0001) surface is rotated 60° upon moving across the monatomic step due to the *ababab* packing of the hcp system. Since these two domains exist on the imperfect hcp(0001) surface, the LEED pattern is a superposition of the patterns produced by both domains, and six fold symmetry results by averaging unequal spot intensities (Figure 4.8) [36].

For the rhenium on Pt(111) system, rhenium was found to grow with an hcp structure exposing the (0001) face. This was shown by LEED because six-fold symmetry was observed when multilayers (>5 ML) of rhenium were present on the surface while three-fold symmetry was observed for clean Pt(111) [36]. These results are in agreement with those found by Zaera and Somorjai [27,37]. Intermediate structures were not analyzed, and it is not known whether rhenium fills the fcc or hcp hollow of the surface during deposition of the first and second monolayers.

4.4.2 Structure of rhenium multilayers on Pt(100)

Clean Pt(100) reconstructs to yield a (5×20) surface structure. This structure has been interpreted as an hexagonal close-packed surface layer resting on a second layer with the characteristic (1×1) square lattice (Figure 4.9a) [38,39,40]. The reconstruction can be removed by carefully leaking CO into the chamber while watching the LEED pattern change, and in this manner conversion from a (5×20) to a (1×1) surface structure was observed (Figure 4.9b). The (5×20) restructured

surface could be regenerated by flashing the crystal to 800 K which removed the adsorbed CO. The deposition of rhenium onto the Pt(100) surface also removed the (5×20) surface structure. The observed conversion to the (1×1) structure began near 0.15 ML of rhenium and was completed near 0.3 ML. The (5×20) structure was not regenerated by flashing to 900 K indicating that rhenium and not CO was responsible for the structural transformation. This phenomenon has been reported previously where copper was observed to remove the (5×20) reconstruction of Pt(100) [41].

As more rhenium was deposited on this surface, a (1×1) surface structure was continually observed, but the diffuse background intensity increased. At coverages between 0.3 and ten monolayers of rhenium, a (1×1) structure was always discernible over the diffuse background, even though no platinum could be detected using AES. Flashing the surface briefly to 1300 K caused some rhenium to diffuse into the platinum substrate. Even though AES showed no trace of the underlying platinum substrate, the LEED pattern was observed to sharpen considerably with no extra spots appearing (Figure 4.9c). The interatomic distances for pure platinum and rhenium differ by only 1% (2.77 and 2.74 Å respectively), and it was not possible to determine whether the interatomic distance obtained for the rhenium overlayer on Pt(100) was platinum- or rhenium-like. Indeed, an analysis of the spot to spot distance generated by the rhenium covered Pt(100) and the clean Pt(100) (1×1) (Figure 4.9b) showed the interatomic distance to be indistinguishable within experimental error. Since the hexagonal close-packed system does not have a surface analogous to the fcc(100) surface, it is concluded that rhenium grows face-centered cubic on Pt(100).

An additional feature observed in the rhenium covered surface was the faint lines connecting the spots (Figure 4.9c), and is evidence that strain was present

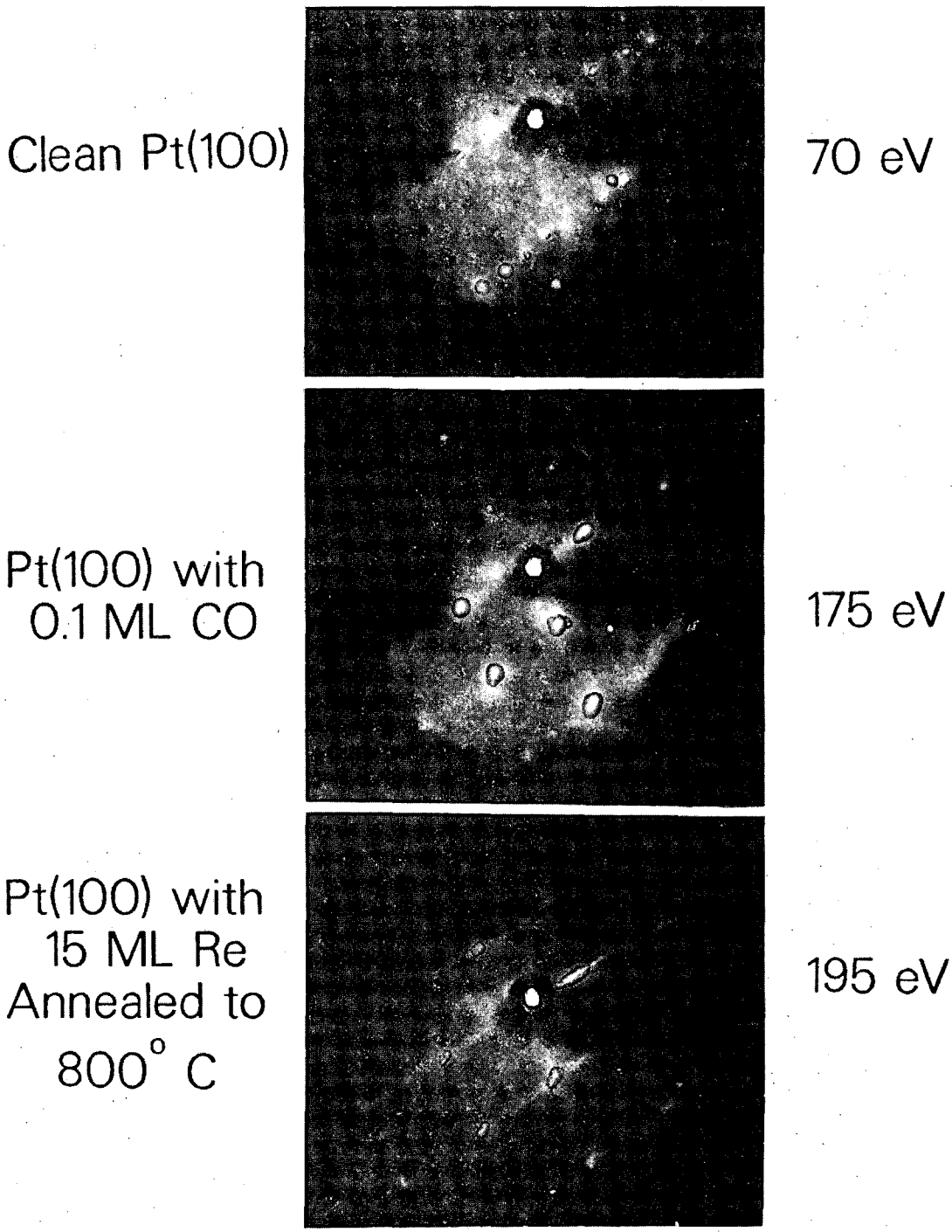

Figure 4.9: Evidence for the formation of face-centered cubic Re on Pt(100) surface. (a) Top panel. (b) Middle panel. (c) Bottom panel. XBB 866-4516

in the rhenium overlayer.

4.4.3 Platinum multilayers on Re(0001)

The LEED pattern generated by a Re(0001) surface is due to a (1×1) surface structure and displays 6 fold symmetry since rhenium is an hcp metal as discussed in Section 4.4.1. Platinum grows layer by layer on the Re(0001) surface, but the well ordered LEED pattern generated by the clean rhenium surface disappears as platinum deposition proceeds. At 15 layers of platinum the diffuse background on the LEED screen appeared bright, with little evidence of order observed.

Annealing the surface briefly to 100° C caused no change in the disorder observed. Annealing the surface briefly to 200° C did cause spots to appear although still somewhat diffuse. The symmetry that was observed appeared to be six–fold (Figure 4.8). A brief annealing to 300° C sharpened the LEED spots considerably, and the six–fold symmetry was confirmed. This surprising result indicates that platinum grows hexagonal close-packed on Re(0001) exposing the (0001) face.

4.5 Discussion

4.5.1 Stuctures and growth mechanisms

Rhenium grows ordered on platinum with an interatomic distance indistinguishable from both the pure platinum and the pure rhenium interatomic distances since they are so similar (within 1%). On Pt(111) a well ordered LEED pattern corresponding to a (1×1) surface structure was always observed. The six fold symmetry observed when 10 ML of rhenium was deposited indicates an hcp rhenium structure grows on Pt (111). For rhenium growing on Pt(100) the situation is somewhat different. Since the hcp system has no surface with a square unit cell,

rhenium is forced to grow fcc on Pt(100), and remains fcc through at least 10 ML. Strain did exist in the rhenium overlayer on Pt(100) and was evident by the lines connecting the substrate spots shown in Figure 4.9c. This strain was probably caused by the lattice mismatch between platinum and rhenium, and because the rhenium film was forced to grow in an unfavorable crystal structure. Similar behavior was observed for cobalt growing on Cu(100) by Salmerón *et al.* as they presented evidence for the formation of fcc cobalt [42].

The growth of platinum films on Re(0001) in an hexagonal close-packed film is not as easy to explain. The hexagonal close-packed and face-centered cubic systems do have a common face; the exposed atomic layer of the hcp(0001) surface has the same structure as the exposed atomic layer of the fcc(111) surface. Rhenium growing hcp on Pt(111) is not surprising since the rhenium film can grow in its natural crystal structure using the Pt(111) surface as a template. The fcc growth of rhenium on Pt(100) can also be explained as a template effect. Since rhenium can grow fcc on Pt(100) indicates that the free energy associated with the fcc crystal structure is not too much larger than the free energy of the hcp crystal structure for rhenium. An inspection of the phase diagram for the rhenium-platinum system (Figure 1.3) cannot explain this, however. The phase diagram shows that on the platinum rich side an fcc solid solution exists and an hcp solid solution exists on the rhenium rich side. From 40–60 % rhenium, both of the above phases exist. However, AES showed that the upper three layers were devoid of platinum while LEED showed the existence of fcc rhenium layers. Apparently a template effect is strong enough to support fcc rhenium for many monolayers.

With platinum deposition on Re(0001) a different picture emerges. Platinum grows disordered on this surface as shown by the loss of the LEED pattern during platinum deposition, even though AES showed that it grows layer by layer. If

the temperature was not high enough to support surface diffusion, then at room temperature a layer by layer growth mechanism might not be expected, as was observed experimentally. Annealing the surface to 300° C was high enough to attain the ordered hcp surface structure, but not high enough to cause bulk diffusion, which required temperatures in excess of 700° C. Therefore the growth of hcp platinum on Re(0001) is indicative of long range order because the difference between the fcc structure and the hcp structure as viewed through their basal planes is not manifest until the third layer is examined. The rhenium metal substrate was apparently able to perturb the platinum overlayer and cause it to form an hcp structure through at least 10–15 monolayers.

Comments are also in order regarding the growth mechanism observed for rhenium on platinum. Sachtler *et al.* observed that gold grows layer by layer on platinum substrates, but that platinum forms three dimensional crystallites on gold substrates [31]. This is reasonable because the surface free energy of gold is lower than that of platinum as calculated by the method of Tyson and Miller (1.48 and 2.46 J/m^2 for Au and Pt respectively) [43]. Using the above surface free energy argument, platinum should grow layer by layer on rhenium, but rhenium should form three dimensional crystallites on platinum (3.61 J/m^2 was calculated for the surface free energy of rhenium from reference [43]). Since rhenium also grows layer by layer on platinum, there must be forces operating of sufficient strength to overcome the differences in the surface free energies of the two components. An explanation invoking a lattice mismatch is not a good one because the difference in nearest neighbor distance of platinum and rhenium is small at 1% (2.77 Å and 2.74 Å for Pt and Re respectively). A more plausible explanation invokes the formation of relatively strong Pt–Re bonds and a surface alloy.

4.5.2 Alloy formation in bimetallic Pt–Re surfaces

The formation of a surface alloy is also supported by XPS results. Following deposition of a 10 ML film of rhenium on Pt(111), the binding energy for the platinum $4f_{7/2}$ line was found to increase relative to clean platinum. The magnitude of this shift in the presence of epitaxial rhenium was 0.5 eV for the platinum $4f_{7/2}$ peak and is similar to the shift reported in the literature for supported and unsupported alloyed systems [10,18,33,34].

It is somewhat surprising that a 0.5 eV shift was observed for the platinum substrate in the presence of *epitaxial* rhenium overlayers. Although the XPS signal generated by the platinum layer in contact with a rhenium layer might be expected to experience such a shift, the bulk unperturbed platinum underneath this layer should dominate the XPS signal resulting in no observed shift. Frequent checks against a gold foil attached to the back side of the manipulator revealed that the energy calibration of the spectrometer was not drifting. A possible cause of the platinum shift was in the preparation of the epitaxial surface. The rhenium–platinum surface was flashed at intervals to 700 K for the epitaxial system before making the XPS measurement, but this temperature is too low to cause a significant bulk diffusion of rhenium into platinum. However, it is probable that this temperature was high enough to cause surface diffusion, so the mixing of platinum and rhenium in the interfacial region may have caused an enhancement with respect to the bulk platinum signal of the interfacial platinum signal under the 20–30 Å rhenium overlayer. The broadening of the Pt $4f_{7/2}$ peak may also have been caused by this alloying effect, and the broadness of the signal observed may have been caused by the contribution from a mixture of many $PtRe_x$ species, including a contribution from the underlying bulk platinum substrate.

After annealing the bimetallic surface to higher temperatures (1150 K), a further increase in binding energy of the 4f levels of both platinum and rhenium was observed. The binding energy increase for platinum and rhenium was 0.9 and 0.5 eV respectively compared to the clean metals. Similar results were obtained by Alnot *et al.* who evaporated platinum on rhenium ribbon [34]. They reported a Pt $4f_{7/2}$ binding energy of 71.6 eV at low coverages (<0.5 ML) which decreased to 71.1 eV at three monolayers of platinum. They also report that annealing a thick platinum deposit ($\sim$ 70 ML) on rhenium ribbon to 1400 K gave binding energy shifts to higher binding energies of 1 and 0.6 eV for the platinum and rhenium $4f_{7/2}$ peaks respectively (relative to the clean metals), with an increase in the full width at half maximum (fwhm) for the platinum peak of 0.3 eV. The increase in width of the Pt $4f_{7/2}$ peak observed in this study was 0.5 eV when 10 layers of rhenium were deposited on Pt(111). The shift to higher binding energy of the $4f_{7/2}$ peaks for both platinum and rhenium was also observed for SiO_2 supported Pt–Re catalysts by Biloen *et al.* [18].

4.5.3 Oxidation and reduction of bimetallic surfaces

The oxidation and reduction of rhenium in an alloyed platinum–rhenium surface under vacuum conditions was also examined using XPS. The bimetallic alloyed surface could be partially oxidized only at elevated temperatures ($\geq$ 800 K). It is possible that longer exposure to 3×10^{-7} Torr of oxygen would oxidize the underlying bulk rhenium more completely. However, results obtained by Zaera indicate that higher pressures of oxygen are needed to cause a complete shift in the peak position of the Re $4f_{7/2}$ peak. Comparison to Zaera's results suggest that after high temperature oxidation of the alloyed surface, the shoulder observed at higher binding energies was due to an oxidized rhenium species. The peak position of this

shoulder was located between the peak positions determined for ReO (Re^{2+}) and ReO_2 (Re^{4+}) as compared to the chemical shifts observed towards higher binding energies relative to rhenium metal of $\sim$ 1 and 2 eV respectively for ReO and ReO_2 [27].

Platinum has been observed previously to catalyze the reduction of rhenium, and the catalyzed reduction of rhenium by platinum reported from TPR studies has been attributed to migration over the support by either hydrated rhenium oxides to platinum reduction centers, or of activated hydrogen [11,17]. Hydrogen is activated with dissociation on platinum metal, and the hydrogen atoms produced can then spillover onto the support with migration to the rhenium oxide particles which are then reduced [44]. Although the migration of hydrogen under high pressure conditions may be important, it was shown that platinum catalyzes the desorption of oxygen from rhenium in vacuum. This means that platinum catalyzes the decomposition of rhenium oxides to metal and O_2

$$ReO_x \xrightarrow{Pt} Re + \frac{x}{2}O_2$$

and under industrial conditions would probably result in the sticking together and alloying of the Pt and Re species to form the nucleus of a bimetallic particle.

4.6 Summary

A moderately strong interaction between platinum and rhenium metals has been shown to exist, and is supported by the results presented in this chapter. Rhenium grows ordered and layer by layer on Pt(111) and Pt(100), and even forms an fcc structure on Pt(100). Platinum grows layer by layer on the Re(0001) surface forming a hexagonal close-packed structure. A surface alloy was observed to form

between the two metals at 700 K and is shown by the broadening of the Pt $4f_{7/2}$ peak in the presence of rhenium, and by the chemical shifts observed for the Re and Pt $4f_{7/2}$ peaks following vapor deposition of rhenium onto Pt(111). The presence of platinum on a rhenium surface facilitates the decomposition of rhenium oxides and subsequent desorption of oxygen under UHV at temperatures much lower than would be possible from clean rhenium.

References

[1] H. E. Kluksdahl. *U. S. Patent 3,415,737* (1968) .

[2] A. N. Webb. *J. Catalysis* **39** (1975) 485.

[3] M. F. L. Johnson and V. M. LeRoy. *J. Catalysis* **35** (1974) 434.

[4] H.C. Yao and M. Shelef. *J. Catalysis* **44** (1976) 392.

[5] L. Wang and W.K. Hall. *J. Catalysis* **82** (1983) 177.

[6] E.S. Shapiro, V.I. Avaev, G.V. Autoshin, M.A. Ryashentseva, and K.M. Minachev. *J. Catalysis* **55** (1978) 402.

[7] M.F.L. Johnson. *J. Catalysis* **39** (1975) 487.

[8] J.B. Peri. *J. Catalysis* **52** (1978) 144.

[9] H. Charcosett, R. Frety, G Leclercq, E. Mendes, M. Primet, and L. Tournayan. *J. Catalysis* **56** (1979) 468.

[10] M. Alnot, A. Cassuto, R. Ducros, J.J.Ehrhardt, and B. Weber. *Surface Sci.* **114** (1982) L48.

[11] B.H. Isaacs and E.E. Petersen. *J. Catalysis* **77** (1982) 43.

[12] J.M. Parera, C.A. Querini J.N. Beltramini, E.E. Martinelli, E.J. Churin, P.E. Aloe, and N.S. Figoli. *J. Catalysis* **99** (1986) 39.

[13] C. Betizeau, G. Leclercq, R. Maurel, C. Bolivar, H. Charcosset, R. Fretty, and L. Tourayan. *J. Catalysis* **45** (1976) 179.

[14] J.H. Onuferko, D.R. Short, and M.J. Kelley. *Appl. of Surface Sci.* **19** (1984) 227.

[15] D.R. Short, S.M. Khalid, J.R.Katzer, and M.J. Kelley. *J. Catalysis* **72** (1981) 288.

[16] R.J. Bertolacinni and R.J. Pellet. *Catalyst Deactivation*, pages 73–77. Elsevier, Amsterdam, The Netherlands, 1980.

[17] R.L. Mieville. *J. Catalysis* **87** (1984) 437.

[18] P. Biloen, J.N. Helle, H. Verbeek, F.M. Dautzenberg, and W.M.H. Sachtler. *J. Catalysis* **63** (1980) 112.

[19] J. Margitfalvi, S. Gőbölös, E. Kwayzer, M. Hegedüs, F. Nagy, and L. Koltai. *React. Kinet. Catal. Lett.* **24** (1984) 315.

[20] V. Eskinazi. *Applied Catalysis* **4** (1982) 37.

[21] R.W. Coughlin, A. Hasan, and K. Kawakami. *J. Catalysis* **88** (1984) 163.

[22] V.K. Shum, J.B. Butt, and W.M.H. Sachtler. *J. Catalysis* **99** (1986) 126.

[23] V.K. Shum, J.B. Butt, and W.M.H. Sachtler. *J. Catalysis* **96** (1985) 371.

[24] M.A. Pacheco and E.E. Petersen. *J. Catalysis* **96** (1985) 507.

[25] C.R. Apestequía and J. Barbier. *J. Catalysis* **78** (1982) 352.

[26] J. Barbier, H. Charcosset, G. dePeriera, and J. Riviere. *Applied Catalysis* **1** (1981) 71.

[27] F. Zaera. PhD thesis, University of California, Berkeley, CA 94720, 1984.

[28] W.D. Gillespie. PhD thesis, University of California, Berkeley, CA 94720, 1980.

[29] S.M. Davis. PhD thesis, University of California, Berkeley, CA 94720, 1981.

[30] T.E. Gallon. *Surface Sci.* **17** (1969) 486.

[31] J.W.A. Sachtler, M.A. Van Hove, J.P. Biberian, and G.A. Somorjai. *Surface Sci.* **110** (1981) 19.

[32] M.P. Seah. *Surface Sci.* **32** (1972) 703.

[33] M. Alnot, V. Gorodetskii, A. Cassuto, and J.J. Ehrhardt. *Surface Sci.* **162** (1985) 886.

[34] M. Alnot, A. Cassuto, J.J. Ehrhardt A. Slavin, and B. Weber. *Appl. of Surface Sci.* **10** (1982) 85.

[35] C.D. Wagner, W.M. Riggs, L.E. Davis, J.F. Moulder, and G.E. Muilenberg (editor). *Handbook of X-Ray Photoelectron Spectroscopy.* Perkin-Elmer Corporation, 1979.

[36] H.L. Davis and D.M. Zehner. *Bull. Am. Phys. Soc.* **24** (1979) 468.

[37] F. Zaera and G.A. Somorjai. *Surface Sci.* **154** (1985) 303.

[38] M.A. Van Hove, R.J. Koestner, P.C. Stair, J.P. Biberian, L.L. Kesmodel, I. Barton, and G.A. Somorjai. *Surface Sci.* **103** (1981) 189.

[39] D.G. Fedak and N.A. Gjostein. *Surface Sci.* **8** (1967) 77.

[40] P.W. Palmberg and T.N. Rhodin. *J. Chem. Phys.* **49** (1968) 134.

[41] C.J. Barnes, M. Lindroos, and M. Pessa. *Surface Sci.* **152/153** (1985) 260.

[42] L. González, R. Miranda, M. Salmerón, J.A. Vergés, and F. Ynduráin. *Phys. Rev. B* **24** (1981) 3245.

[43] W.R. Tyson and W.A. Miller. *Surface Sci.* **62** (1977) 267.

[44] R. Lamartine and R. Perrin. *Spillover of Adsorbed Species*, page 251. Elsevier Science Publishers, Amsterdam, The Netherlands, 1983.

Chapter 5

The Adsorption and Desorption of Small Molecules on Bimetallic Platinum–Rhenium Surfaces

5.1 Preface

The preparation and characterization of bimetallic platinum–rhenium surfaces were described in the previous Chapter. The systems studied include both platinum films deposited on a rhenium substrate and rhenium films deposited on a platinum substrate. In this Chapter the adsorption and desorption of some small molecules (H_2, CO, NO, and N_2) from these bimetallic surfaces will be discussed.

The behavior of chemisorption systems on the bimetallic Pt–Re surface are important for a number of reasons. Titration techniques using small molecules (mainly H_2, O_2, and CO) are routinely used for the determination of metallic surface areas and dispersions on supported metallic catalysts. Materials used as supports, such as alumina and silica [1] do not reversibly adsorb these gases, so titration with them is a technique thought to reliably measure the metallic surface areas. The existence of spillover onto the support might add a small degree of uncertainty to the measurements [1,2], but for monometallic catalysts, hydrogen and CO titration reliably and reproducibly gives information on metallic surface

areas.

When a second metal is introduced, titration techniques become more complicated and less reproducible [3]. One problem is that platinum and rhenium have different hydrogen chemisorption capacities, about 1 H atom per Pt surface atom, and 0.4 H atoms per Re surface atom as determined by chemisorption techniques [4,5]. When these two metals are codeposited on a support, measurements of the metallic surface area using hydrogen and CO chemisorption sometimes indicate false results such as a metallic dispersion in excess of 100% [6]. The reason for this is that the chemisorption of hydrogen and CO on bimetallic Pt–Re surfaces is not a linear function of the metallic surface composition. Evidence suggesting the existence of an electronic effect between platinum and rhenium is presented in this Chapter. A result of this electronic interaction is an enhanced adsorption capacity for CO and hydrogen on bimetallic surfaces.

Understanding the behavior of the bimetallic surface toward hydrogen is important for another reason. Several investigators have implicated hydrogen as a key in the enhanced activity maintenance demonstrated by platinum–rhenium catalysts compared to monometallic platinum catalysts. For example, Barbier *et al.* found that hydrogen adsorption is enhanced on a Pt/Al_2O_3 catalyst when rhenium had been codeposited [6], and Margitfalvi *et al.* reported that the presence of rhenium increases the hydrogen available for hydrodepolymerization reactions, which are important for removing deactivating carbonaceous deposits [7]. Pacheco and Petersen report that the presence of both rhenium and sulfur changes the hydrogen pressure dependence for fouling reactions on the bimetallic Pt–Re catalyst [8,9].

The behavior of the bimetallic surface towards other small molecules can also give useful information. The main object of the chemisorption experiments was to find a suitable titrant that would give an independent determination of the

surface composition of bimetallic surfaces–a measurement that would compliment Auger measurements as described in Section 4.2. Carbon monoxide (CO) played this role for determination of the surface composition in gold/platinum and copper/platinum surfaces [10,11,12]. Nitric oxide (NO) and dinitrogen (N_2) were also examined. Unfortunately, none of these molecules could be used as titrants, but their behavior on bimetallic Pt–Re surfaces is interesting and is the subject of this Chapter.

5.2 Hydrogen

5.2.1 Hydrogen TPD from the Re–Pt(111) System

Hydrogen adsorption with temperature programmed desorption was studied on the Re–Pt(111) system. Representative spectra for a low hydrogen exposure, 0.02 Langmuirs (L) are shown in Figure 5.1. A high temperature shoulder was observed on the clean Pt(111) spectrum near 480 K after a 0.02 L hydrogen dose, probably due to hydrogen desorbing from defect sites on the platinum surface (Figure 5.1a). At 0.19 ML of rhenium, the high temperature shoulder disappeared, and was also absent at higher rhenium coverages. The hydrogen desorption area did not change with the disappearance of this shoulder, rather the area was found to incorporate into the main peak at rhenium coverages less than one monolayer. The disappearance of the high temperature shoulder suggests that the first adsorbing rhenium atoms populate platinum defect sites that are responsible for the 480 K desorption feature on clean Pt(111). Rhenium was deposited at room temperature so sufficient energy was probably available for the surface diffusion of rhenium atoms.

To compare the behavior of the different bimetallic surfaces towards hydrogen

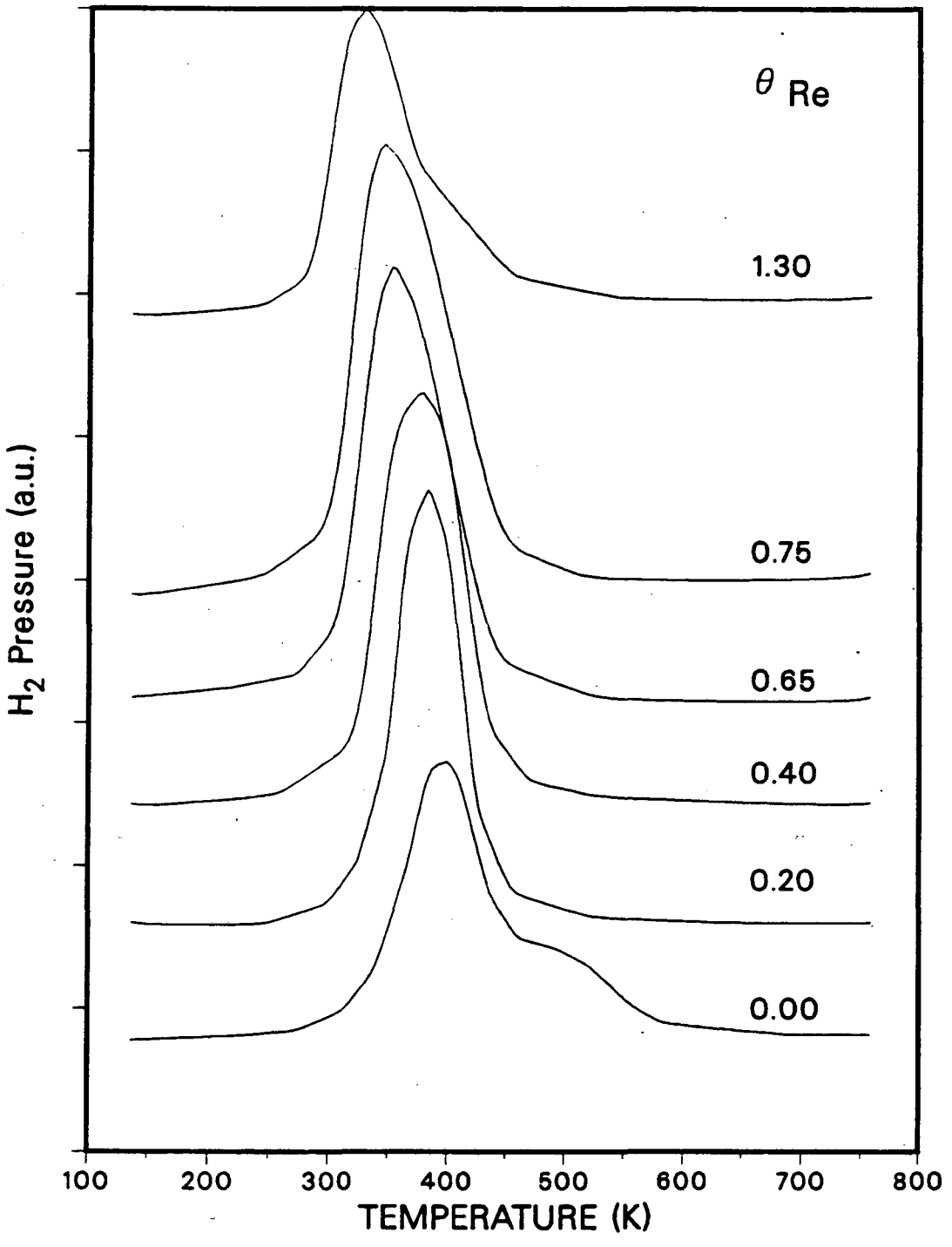

Figure 5.1: Hydrogen temperature programmed desorption spectra from Re modified Pt(111). The H_2 exposure was 0.02 L at an adsorption temperature of 150 K; the heating rate was 30 K/sec. In monolayers, θ_{Re} = (a) 0 (b) 0.19 (c) 0.37 (d) 0.66 (e) 0.77 (f) 1.3.

Table 5.1: Hydrogen Desorption Parameters for Rhenium Modified Pt(111).

θ_{Re}	T^{o}_{max} [a]	H_2 Area[b]	E^{c}_{des1}	E^{c}_{des2}
0	410	1.0	19.0	4.3
0.19	398	1.2	17.5	4.4
0.37	392	1.1	16.5	4.8
0.66	370	0.9	11.5	5.0
0.77	370	0.7	7.0	1.6
1.3	336	0.5	7.5	—
∞[d]	461	—	—	—

a. Extrapolated to 0 exposure of H_2, ± 5 K.
b. Maximum relative H_2 desorption area, compared to clean Pt(111).
c. Activation energy of desorption in Kcal/mole ± 2 Kcal/mole.
d. Re(0001)

adsorption and desorption, the position of T_{max} extrapolated to zero coverage of hydrogen was determined (T^{o}_{max}). The extrapolation was meaningful because the position of T_{max} decreased linearly with increasing hydrogen exposure at low exposures (Figure 5.2). T^{o}_{max} from H_2 TPD obtained from a clean Re(0001) surface was found to be higher than from clean Pt(111) (460 and 410 K respectively). For bimetallic surfaces, the position of T^{o}_{max} versus θ_{Re} was found to be decreasing through at least 1.3 ML of rhenium (Table 5.1). This is in agreement with previous TPD results reported for Re(0001) [13,14], and for thick rhenium overlayers deposited on Pt(111) [15,16]. The results show that submonolayer coverages of rhenium on Pt(111) desorb H_2 at lower temperatures than either Re(0001) or Pt(111). Complex LEED patterns were not observed since a monolayer of rhenium on Pt(111) produced a (1×1) overlayer as discussed in the previous Chapter. Evidence for a high temperature "rhenium–like" hydrogen desorption feature first appeared at coverages greater than one rhenium monolayer as shown in Figure 5.1.

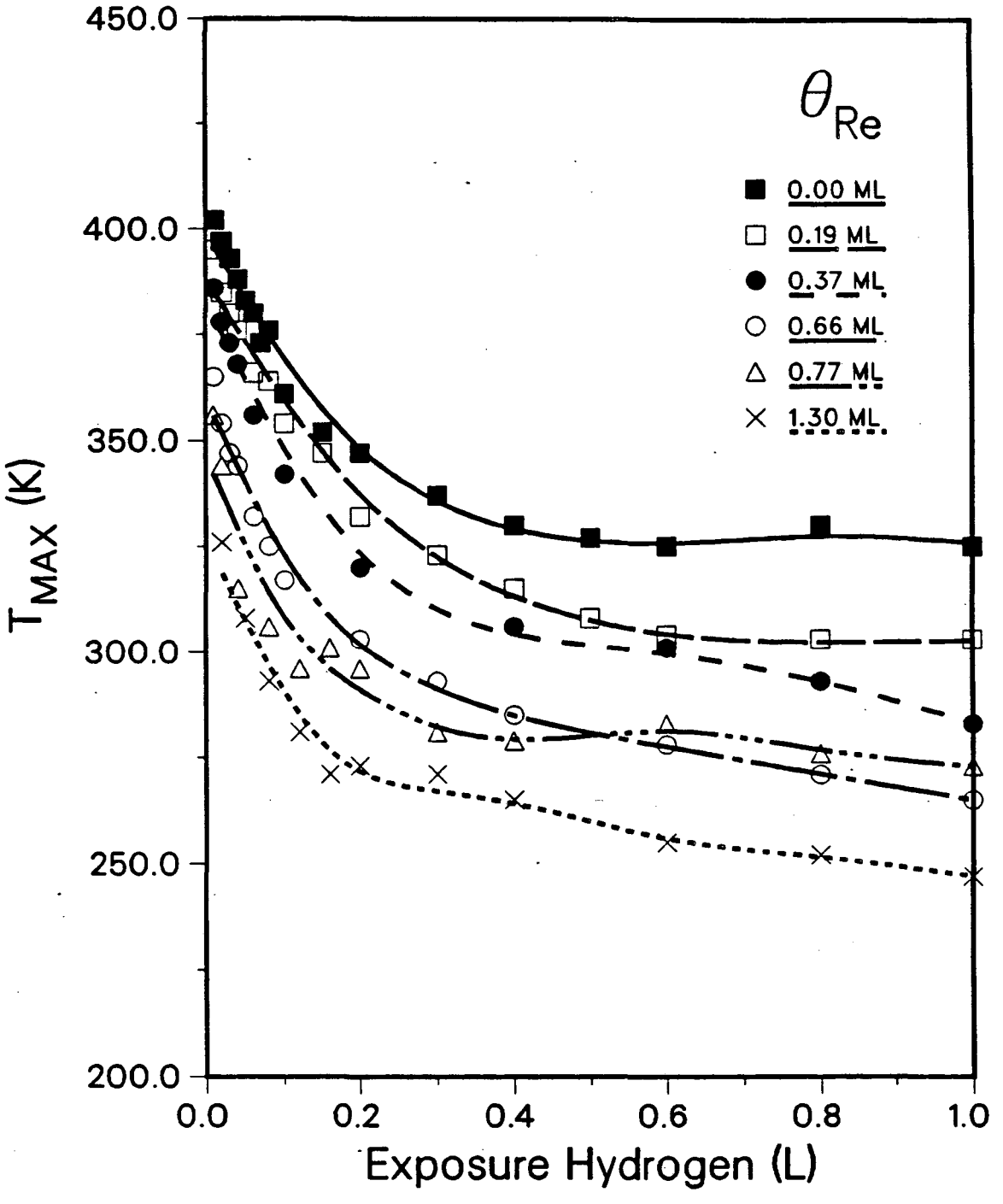

Figure 5.2: Temperature of the desorption maximum (T_{max}) from H_2 TPD of Re modified Pt(111) as a function of H_2 exposure and Re coverage. H_2 was adsorbed at 150 K; the heating rate was 30 K/sec.

A bimetallic surface with a rhenium coverage of $\theta_{Re} \sim 1.3$ ML produced a shoulder on the high temperature side of the main peak.

Interpretation of results obtained at coverages higher than $\theta_{Re} = 1$ ML were complicated by the difficulty in keeping the bimetallic *epitaxial* surfaces free of oxygen. Oxygen can be removed from rhenium films on a platinum substrate through chemisorption of ethylene followed by flashing, but the flashing temperature needed for this procedure is high enough to cause significant diffusion of the two metals into each other.

With a linear crystal heating rate and high pumping speed, the desorption peak area is proportional to the hydrogen coverage for TPD [17]. At low hydrogen exposures, the hydrogen peak areas were equivalent for all rhenium coverages studied, but at higher hydrogen exposures the hydrogen uptake curves diverged for different rhenium coverages (Figure 5.3). With saturation hydrogen exposures, the surface containing 0.19 ML of rhenium bound the most hydrogen, 20% more than the clean platinum surface, and the surface with 0.37 ML of rhenium bound 10% more hydrogen than the clean platinum surface. The surface containing 1.3 ML of rhenium bound about half as much hydrogen as clean Pt(111). These results are summarized in Table 5.1 and Figure 5.4.

5.2.2 Activation energy calculations for H_2 desorbing from bimetallic surfaces

Assuming a second order desorption, the activation energy of desorption (E^a_{des}) can be calculated for the desorption of hydrogen from bimetallic platinum–rhenium surfaces using the experimental data and the method of Redhead [17,18]. Using Equation 2.15, a plot of $\ln(n_o T^2_{max})$ versus $1/T_{max}$ should give a straight line with a slope of E^a_{des}/R, where E^a_{des} is the activation energy of desorption, R is

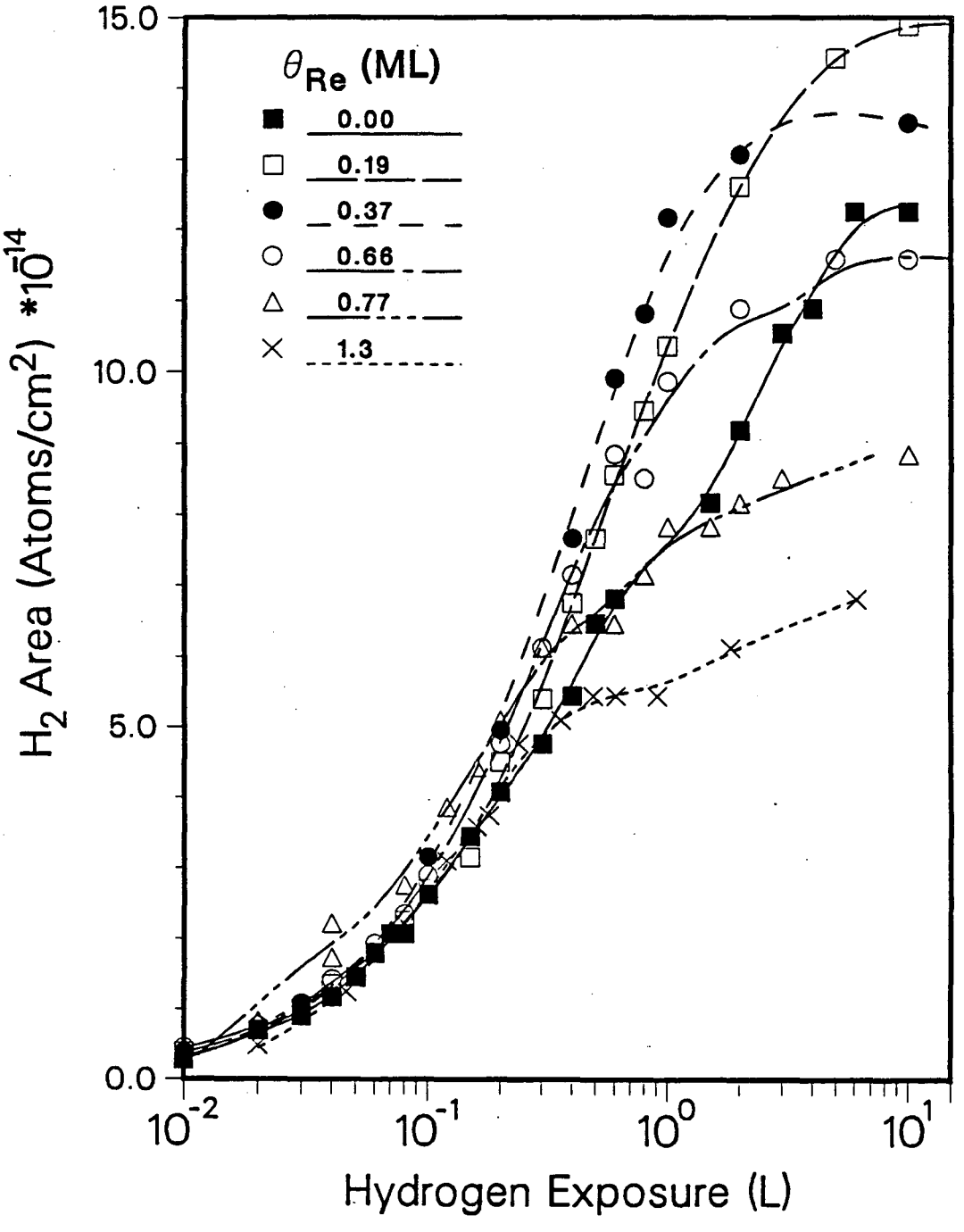

Figure 5.3: H_2 desorption area vs. hydrogen exposure for TPD from Re–Pt(111) surfaces. T_{ads} = 150 K. The heating rate was 30 K/sec.

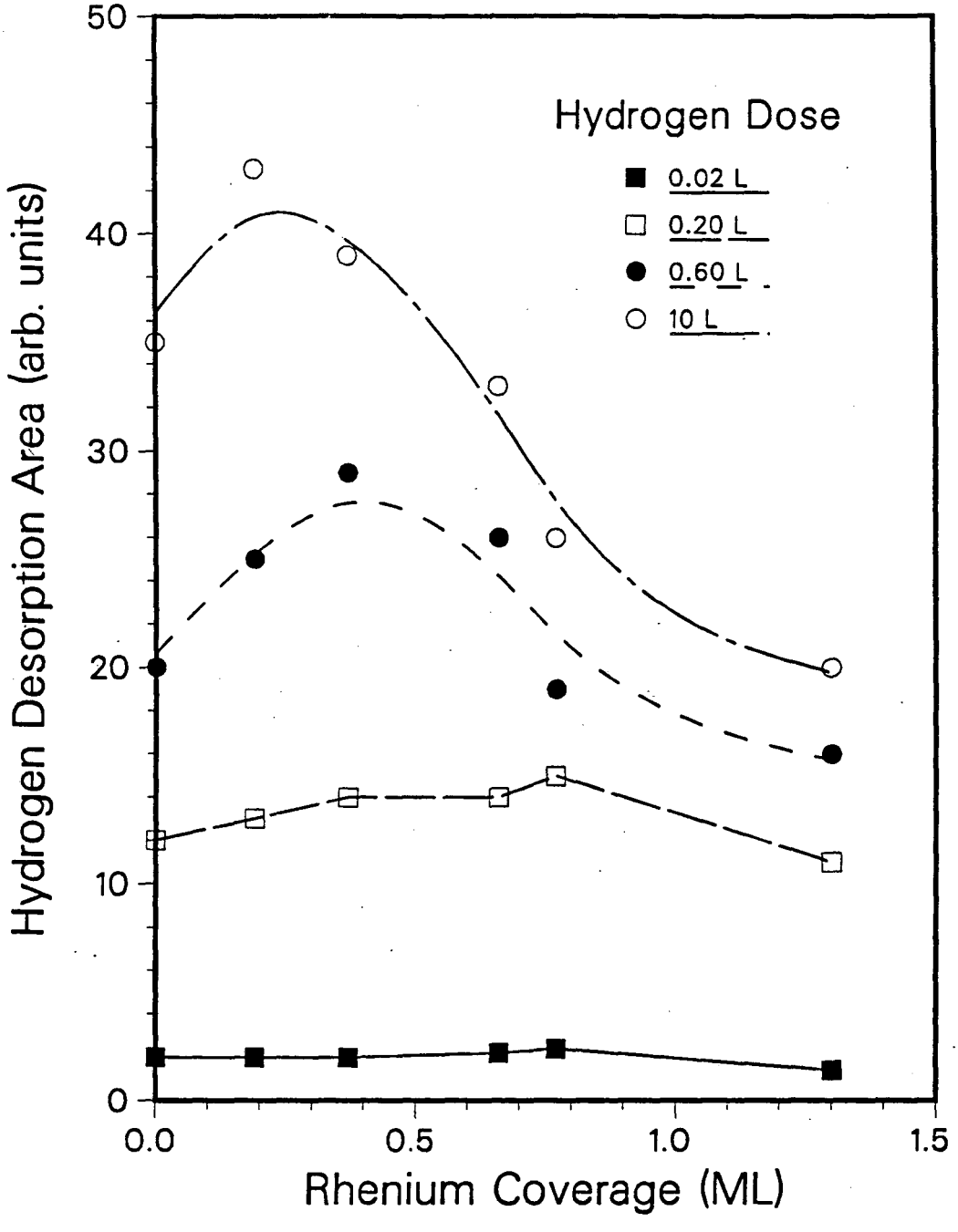

Figure 5.4: Relative maximum H_2 TPD desorption area as a function of θ_{Re}.

the gas constant, T_{max} is the temperature of the desorption maximum, and n_o is the number of hydrogen atoms on the surface before desorption. The value of n_o was estimated by comparing the area of the desorption peak obtained to the area obtained for a saturated clean Pt(111) surface. The clean Pt(111) surface was assumed to adsorb one H atom per Pt atom at saturation, or 1.5×10^{15} H atoms/cm^2. TPD traces for hydrogen from clean Pt(111) are shown in Figure 5.5 and the corresponding activation energy plot obtained is shown in Figure 5.6.

Plots similar to the one shown in Figure 5.5 were obtained for hydrogen desorption from the other bimetallic surfaces used. The main difference between the plots was that the temperature maxima shifted to lower temperatures with increasing rhenium coverage for a given hydrogen dose. Activation energy plots were also similar for the bimetallic surfaces (Figure 5.6); the difference here was that the slopes of the curves at low hydrogen doses were different as tabulated in Table 5.1. Two regions on the activation energy plots exist (Figure 5.6). With a hydrogen dose of less than 0.06 L (region 1), E^a_{des} was 19±2 Kcal/mole for clean Pt(111). With a higher hydrogen dose, *i.e.* 0.06 to 0.3 L (region 2), E^a_{des} was 4.3 Kcal/mole for clean Pt(111). For low hydrogen exposures (region 1), it can be seen that the activation energy of desorption decreases with increasing rhenium coverage for all the surfaces tested. The activation energies are unchanged in region 2 within experimental error for bimetallic surfaces with $\theta_{Re} \leq 0.66$ ML.

5.3 Carbon Monoxide

The study of carbon monoxide is of keen interest because it had been used successfully as a titrant for other bimetallic surfaces in this laboratory. Yeates and Sachtler used CO to titrate platinum sites on platinum–copper and platinum–gold bimetallic surfaces [10,11,12]. CO was an excellent titrant for these bimetallics be-

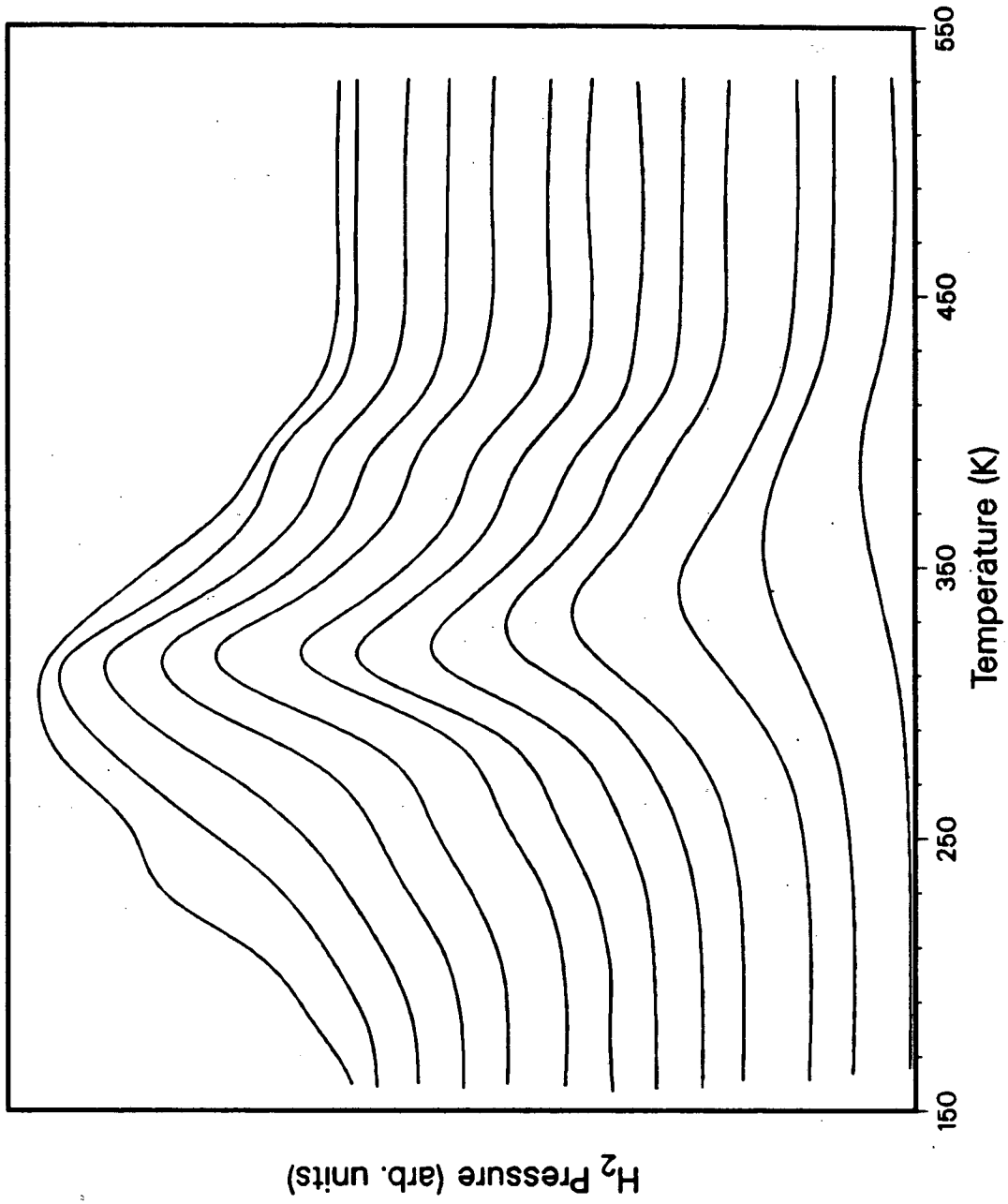

Figure 5.5: Hydrogen temperature programmed desorption (TPD) spectra from clean Pt(111). The temperature of adsorption was 150 K with a heating rate of 30 K/sec. The plots shown are for hydrogen doses of 0.1, 0.3, 0.5, 0.7, 0.9, 1.2, 1.6, 2.0, 2.8, 4.0, 6.0, 10, and 60 Langmuirs.

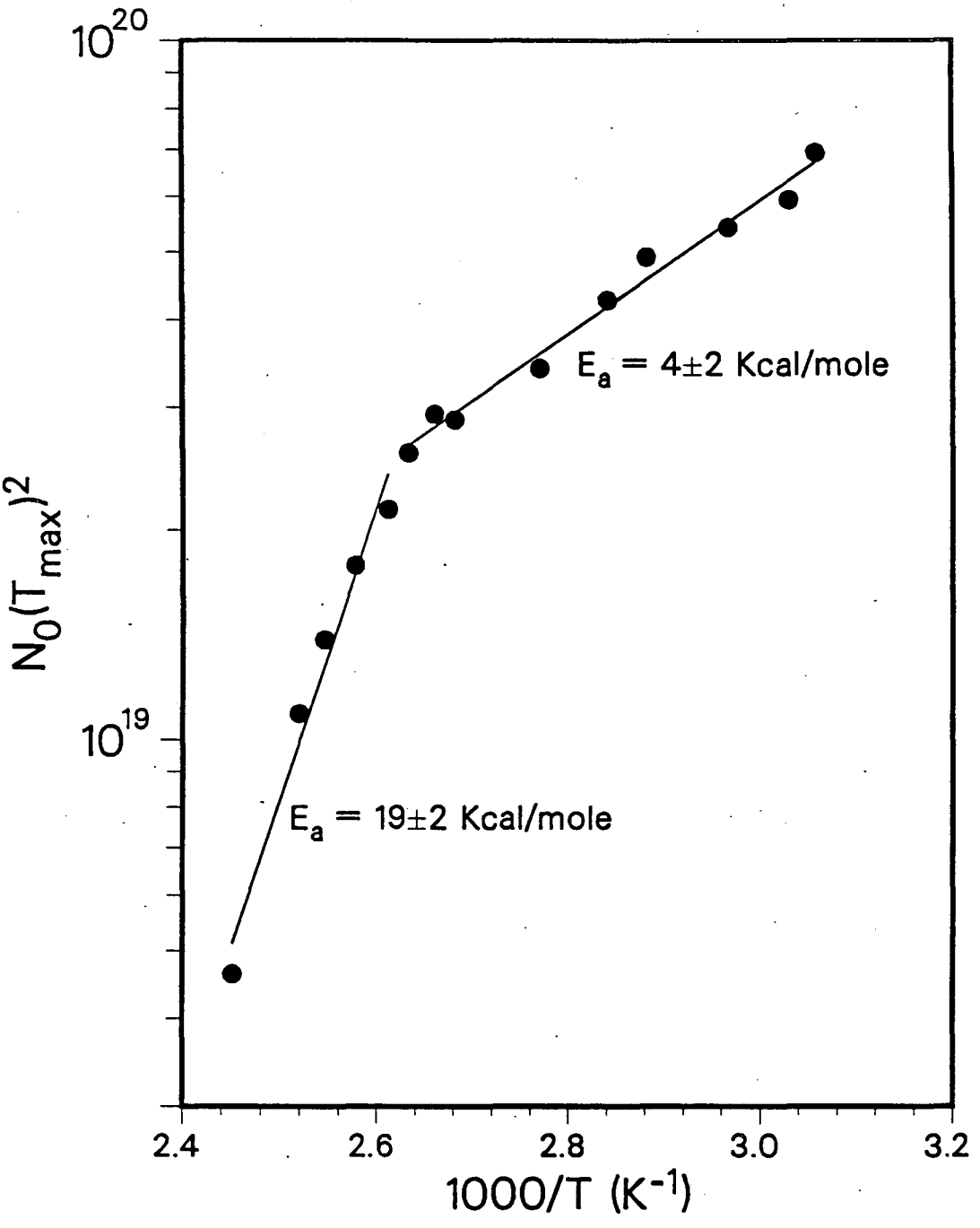

Figure 5.6: Activation energy plot for H_2 desorption from Pt(111). The experimental conditions are the same as for Figure 5.5.

cause it does not adsorb on gold or copper. Carbon monoxide does adsorb on rhenium as well as on platinum, but it was anticipated that the adsorption/desorption behavior would be sufficiently different on the two metals so that separate quantitation of platinum and rhenium sites would be possible.

5.3.1 CO TPD from 0 to 0.55 ML of rhenium on Pt(111)

Temperature programmed desorption studies of carbon monoxide from the Pt(111) and the Re(0001) surfaces are well represented in the literature. The desorption of CO from Pt(111) results in a single peak and is known to occur by first order kinetics with respect to CO coverage [19,20,21,22,23]. The activation energy of desorption (E^a_{des}) is reported to be 26-30 Kcal/mole. The position of T_{max} shifts to a lower temperature with coverage for CO because E^a_{des} is coverage dependent and decreases with increasing CO coverage; this is perhaps due to lateral interactions on the Pt(111) surface.

The desorption of CO from the Re(0001) surface is somewhat different. A single peak is obtained at low CO coverages with the addition of a second lower temperature peak at higher coverages resulting in 2 α peaks in the temperature range 350–500 K [24]. The 2 α peaks were not clearly resolved for these experiments from Re(0001) or thick rhenium overlayers on Pt(111) because of the position of the mass spectrometer in relation to the surface; instead a broad peak was observed. The position of T_{max} for CO on Re(0001) does not shift with coverage, only the ratio of intensities of the two different α desorption states changes. This indicates first order desorption kinetics for CO on Re(0001) with E^a_{des} independent of coverage [13,14,25,24]. Some CO dissociation also occurs on Re(0001) and this results in a high temperature (800 K) β peak. Housley *et al.* reported E^a_{des} for the α peaks of 24 and 27 Kcal/mole, and 50 Kcal/mole for the β peak [24].

Table 5.2: CO desorption parameters from bimetallic Re–Pt(111) surfaces.

θ_{Re}	$T_{max}\pm$ 5 K	Area†	$E^a_{des}\pm$ 0.5 (Kcal/mole)†
0.0	467	1.0	27.1
0.3	470	1.4	27.2
0.55	457	1.2	26.5

† Relative to CO desorption from clean Pt(111).

TPD experiments were performed on bimetallic surfaces of Re–Pt(111) with coverages of $\theta_{Re} \sim 0$, 0.3, and 0.55 ML. Spectra obtained for several different CO doses, *i.e.* 0.01, 0.1, and 0.6 L, on these bimetallic surfaces are shown in Figure 5.7. At 0.01 L of CO, the desorption from clean Pt(111) is fairly broad and centered near 520 K. There are actually two unresolved peaks, as can be seen by comparing the desorption from the other two surfaces. The high temperature feature is probably due to desorption from defect sites on the surface and from the edge of the crystal [21]. The attenuation of the high temperature shoulder with an increase in the intensity of the main peak when rhenium was evaporated onto the surface is indicative of preferential adsorption, or migration following desorption, of rhenium onto defect sites on the platinum surface. This was also observed for hydrogen TPD from Pt–Re surfaces.

With a 0.1 L dose of CO as shown in Figure 5.7b, the presence of the main desorption peak is apparent for the three coverages of rhenium studied. Additional desorption features were never introduced by the deposition of rhenium on Pt(111) as was also the case for hydrogen TPD. Activation energies were calculated from these spectra using Equation 2.13, and the values calculated were 27.1, 27.2, and 26.5 Kcal/mole for $\theta_{Re} = 0$, 0.3, and 0.55 ML. The results are summarized in Table 5.2, and show that the position of T_{max} for CO is not very different for these

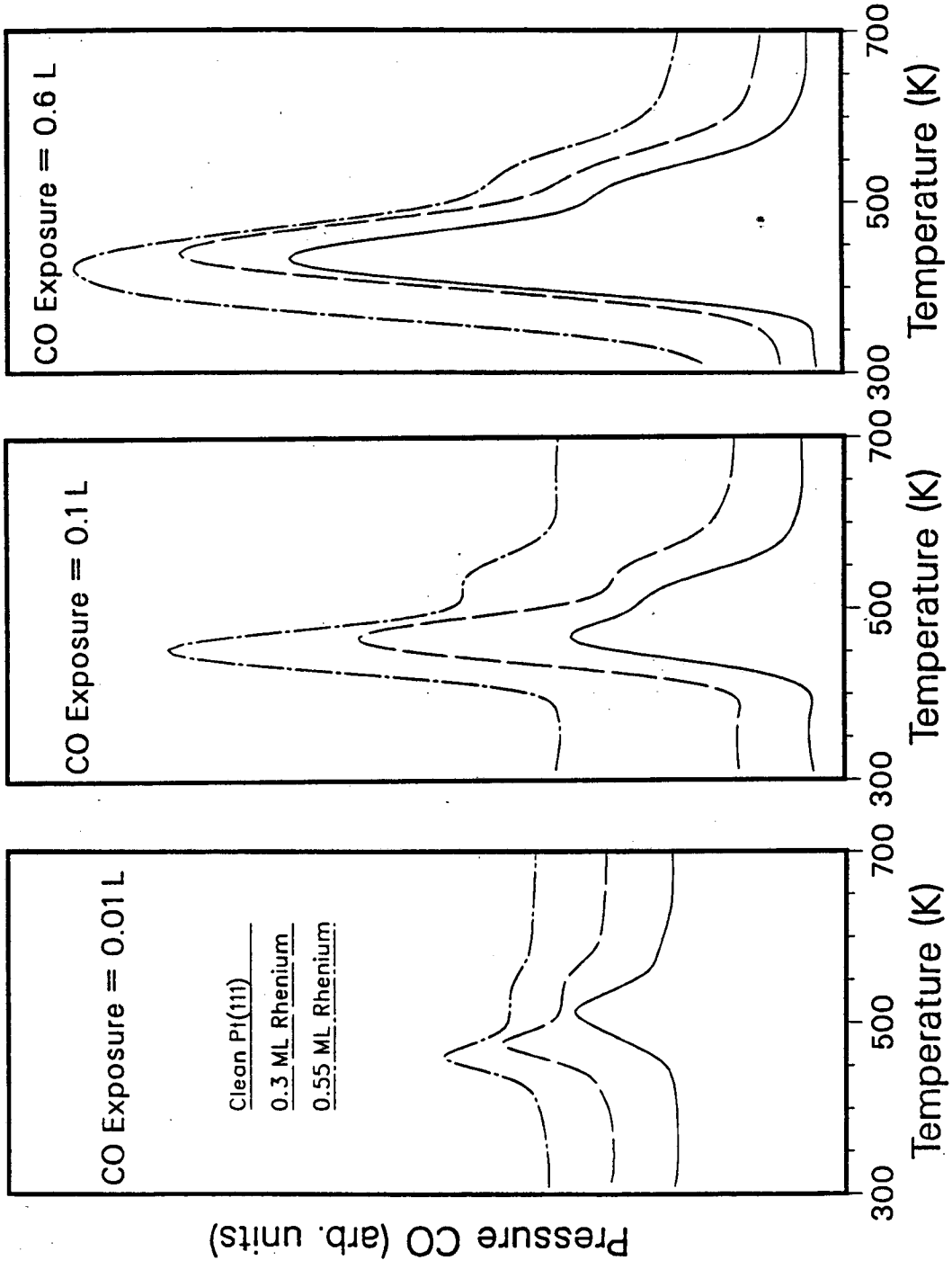

Figure 5.7: CO TPD from bimetallic Re–Pt(111) surfaces. The adsorption temperature was 300 K; the heating rate was 30 K/sec. CO exposure in Langmuirs was: a) 0.01. b) 0.1. c) 0.6.

three surfaces. TPD spectra for a higher dose of 0.6 L CO is shown in Figure 5.7c. The similarity in desorption behavior displayed by the three bimetallic surfaces is also apparent here.

The position of the desorption maximum versus the CO dose is shown in Figure 5.8. At low CO coverages, the position of T_{max} for clean platinum is high around 520 K, but this reflects desorption from platinum defect sites. Otherwise, the position of T_{max} was observed within a band 10 K wide.

The desorption area versus CO dose is shown in Figure 5.9. As in the case with hydrogen on bimetallic surfaces, surfaces exposing both platinum and rhenium atoms adsorbed more CO than did clean Pt(111) or thick rhenium films. At CO saturation the θ_{Re} = 0.3 ML surface bound 40% more CO than clean Pt(111). The θ_{Re} = 0.55 ML surface bound 20% more CO than did clean Pt(111).

5.3.2 CO TPD from 0.8 to 3 ML of rhenium on Pt(111)

Experiments were also performed on platinum surfaces with higher rhenium coverages at saturation exposures of CO (36 L). The results of these experiments are shown in Figure 5.10 and in Table 5.3. It can be seen that rhenium–covered Pt(111) does not bind as much CO as does clean platinum. With rhenium coverages of 0.8 ML, 3 ML, and 3 ML oxidized, the surfaces bound less CO: 25%, 50%, and 75% less respectively. The relative saturation CO desorption area vs. rhenium coverage is shown for all the surfaces studied in Figure 5.11. Only the 3 ML epitaxial rhenium surface displayed evidence for dissociative chemisorption, as shown by the peak near 730 K in Figure 5.10c.

The position of T_{max} for these surfaces reflects the surface composition in that the surface displays both platinum-like and rhenium-like behavior. This means that clean Pt(111) gives a single desorption peak around 440 K while the two

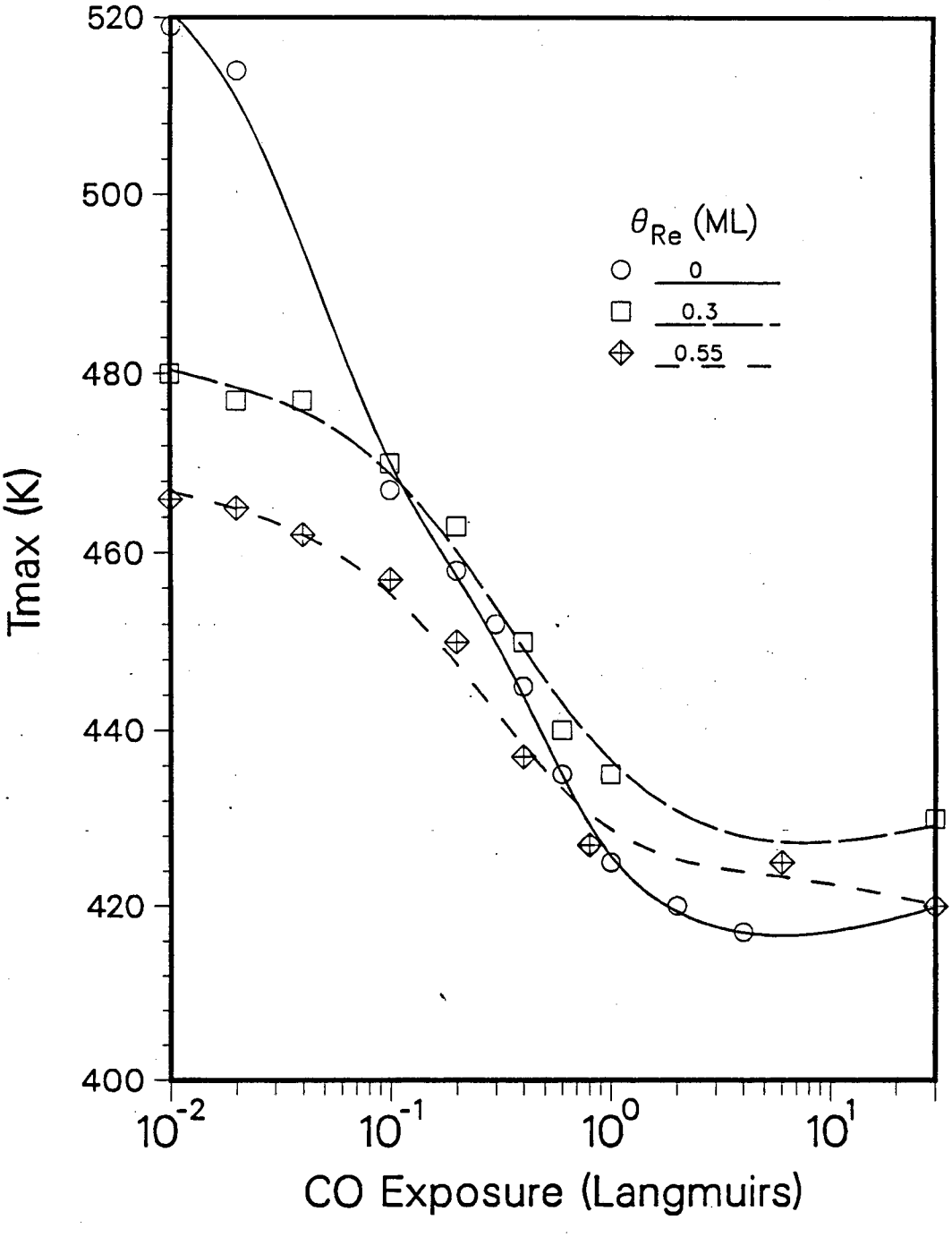

Figure 5.8: Position of the desorption maximum (T_{max}) vs. CO exposure for three bimetallic Re–Pt(111) surfaces. The adsorption temperature was 300 K, and the heating rate was 30 K/sec.

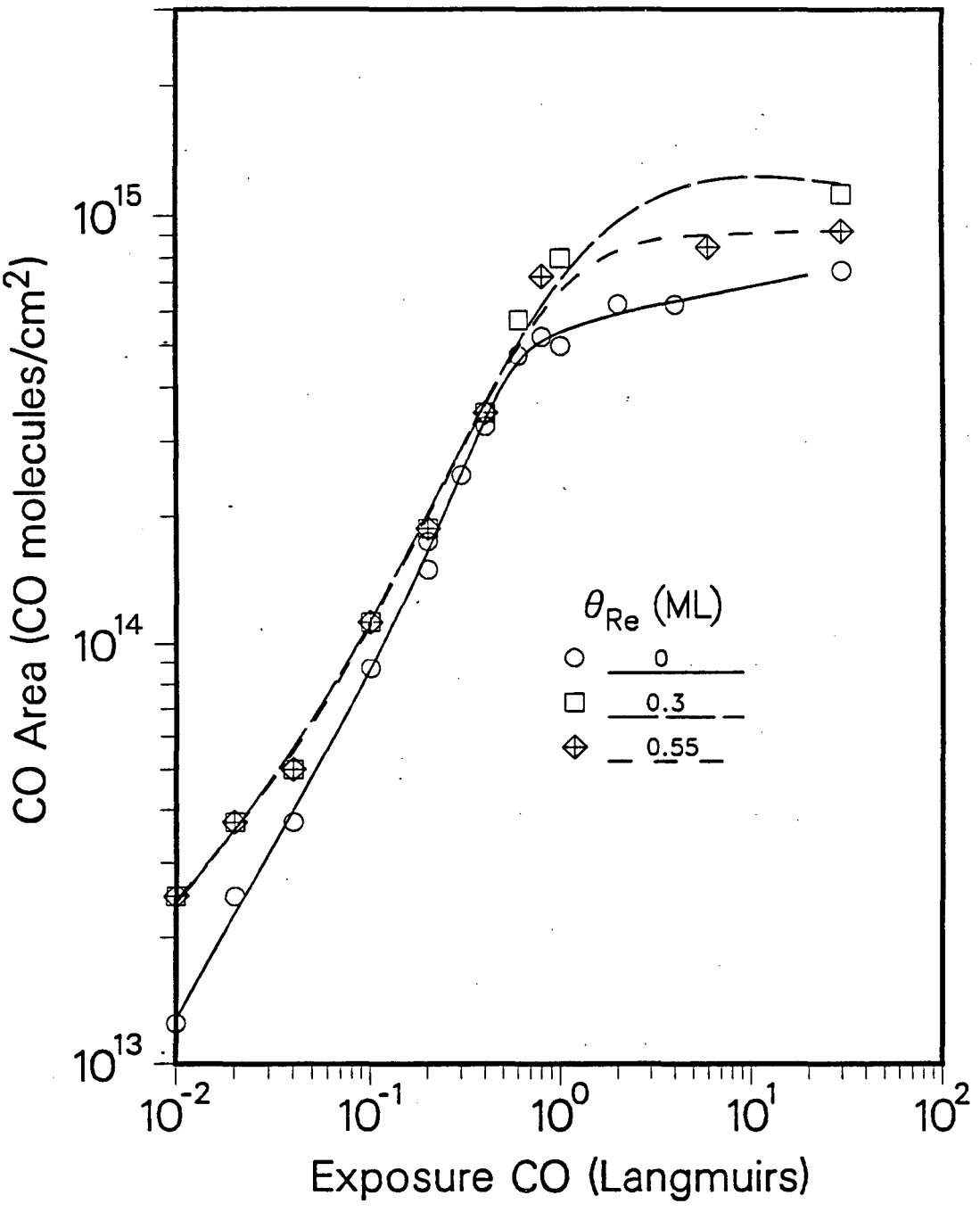

Figure 5.9: CO desorption area vs. exposure for bimetallic Re–Pt(111) surfaces. Adsorption temperature was 300 K; the heating rate was 30 K/sec.

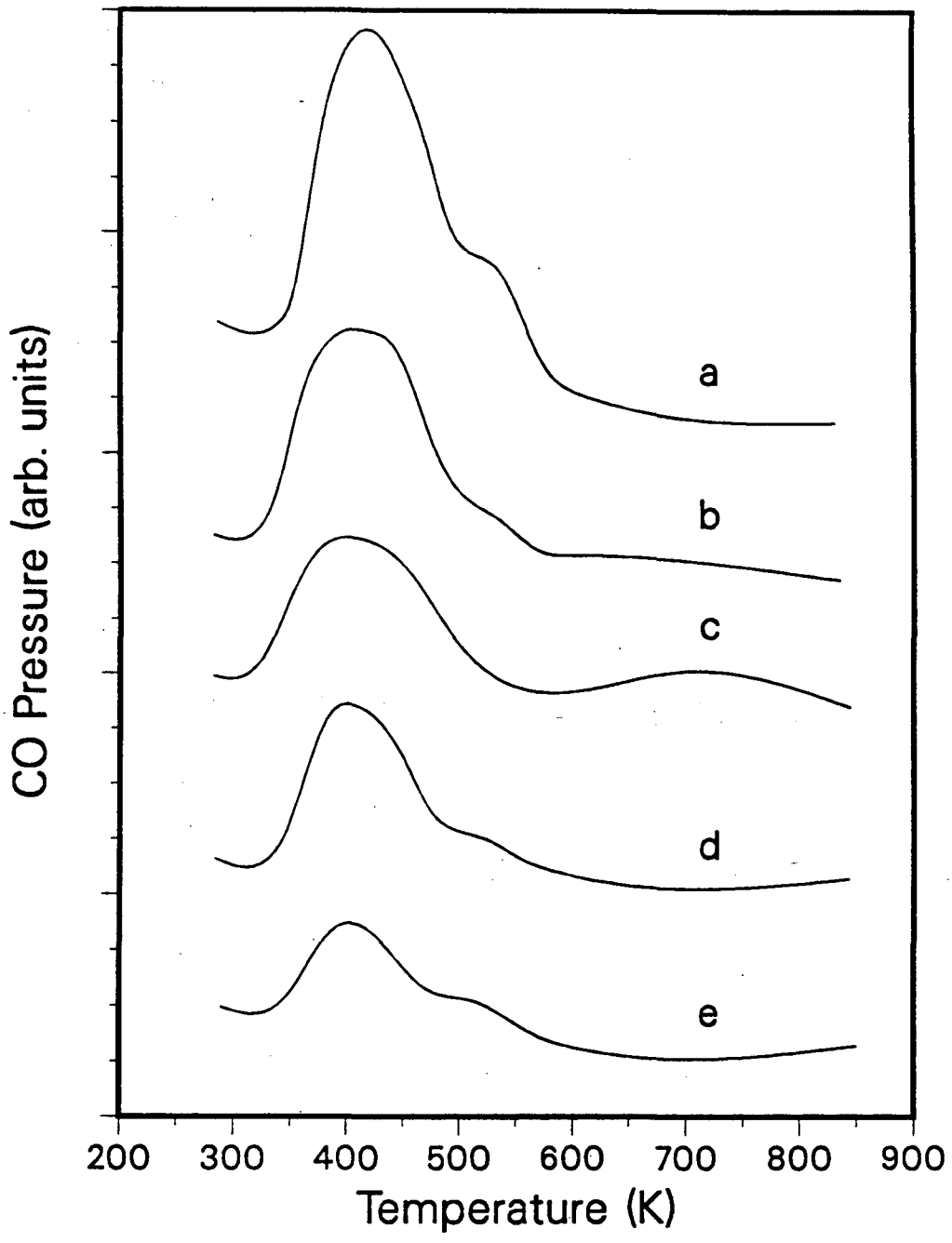

Figure 5.10: CO TPD spectra obtained from bimetallic Re–Pt(111) surfaces at higher rhenium coverages. Adsorption temperature was 300 K; the heating rate was 30 K/sec. The CO exposure was 36 L on the following surfaces: a) Clean Pt(111). b) 0.8 ML Re. c) 3 ML epitaxial Re. d) 3 ML Re annealed to 1150 K. e) 3 ML Re oxidized at 800 K with 100 L O_2.

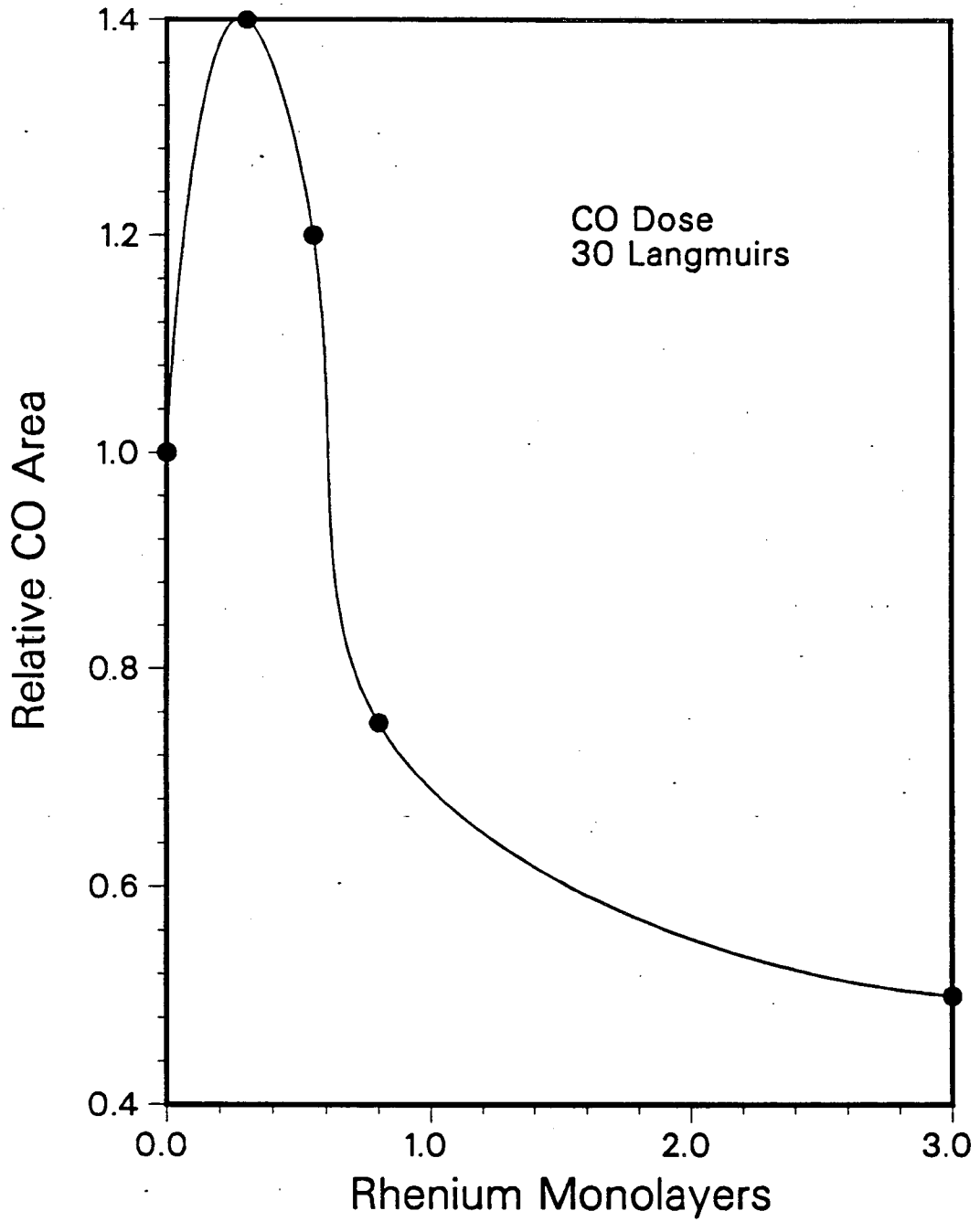

Figure 5.11: Maximum CO desorption area vs. rhenium coverage for Re–Pt(111) surfaces.

Table 5.3: CO TPD parameters from rhenium–covered Pt(111). The results shown here are from Figure 5.10.

Label from Figure 5.10	θ_{Re} (ML)	T_{max} (K)	Relative desorption area
(a)	0	425	1
(b)	0.8	390–430	0.75
(c)	3 epitaxial	385–410	0.5
(d)	3 alloyed	405	0.5
(e)	3 oxidized	400	0.25

desorption peaks as observed by Ducros *et al.* [13,14,24,25] gave a single broad peak between 385 and 410 K. These results are summarized in Table 5.3.

5.4 Other Molecules on the Re–Pt(111) Surface

5.4.1 Dinitrogen–N_2

Dinitrogen adsorption has been previously examined on platinum catalysts [26], and was found to adsorb on Pt(111) and rhenium–covered ($\theta_{Re} > 3$ ML) Pt(111) surfaces at low temperatures. The desorption temperatures found during TPD were around 160 K, and are characteristic of physisorption on these surfaces. No differences were observed between platinum and rhenium–covered platinum, even when exposed to 10^3 langmuirs of nitrogen. This adsorbate showed no promise as a potential titrant, so no other rhenium coverages were examined.

5.4.2 Nitric oxide–NO

The desorption of NO and its decomposition products from Pt(111) after room temperature and low temperature adsorption have been previously reported [27-29]. Gland *et al.* reported substantial decomposition of NO to form N_2 and O_2 [28], but decomposition on the (111) surface was later shown not to occur by Gorte

et al. [29]. The decomposition reaction is very sensitive to surface structure; it occurs readily on Pt(100) and Pt(110), and defects on the surface of Gland's crystal was probably the reason he observed NO decomposition on Pt(111). The Pt(111) surface in this study was found to desorb substantial quantities of N_2 indicating the presence of defect sites. According to Gorte *et al.*, very high annealing temperatures (1600 K) are required to eliminate NO decomposition on Pt(111) [29], and our samples were annealed only to 1400 K following argon ion sputtering. There was probably also a contribution from the edges of the crystal which expose many other crystallographic faces.

The adsorption of NO is reported to be dissociative on Re(0001) at room temperature [13,14,30]. The only molecule that was observed to desorb from this surface was N_2 that resulted from NO decomposition. Oxygen remained on the surface.

The results of the NO TPD experiments are shown in Figure 5.12 and Table 5.4. The desorption of NO and N_2 from clean Pt(111) is shown in Figure 5.12a. The N_2 desorption peak obtained from clean Pt(111) was near 470 K and was in agreement with results obtained by Gland *et al.* [28].

The results of NO TPD experiments from 1.5 ML rhenium on Pt(111) are shown in Figure 5.12b and in Table 5.4. When 1.5 monolayers of rhenium were added to the surface, the NO desorption peak was attenuated only by one half, indicating that a single layer of rhenium on Pt(111) can associatively adsorb NO. T_{max} of the N_2 peak decreased to 435 K in the presence of 1.5 ML of rhenium.

Although the chemistry of NO on the bimetallic surface appears to be quite interesting, it was obvious NO was not a suitable titrant since it doesn't decompose completely on a monolayer of rhenium on Pt(111). Apparently 2 monolayers are required before complete decomposition is observed. For this reason these studies

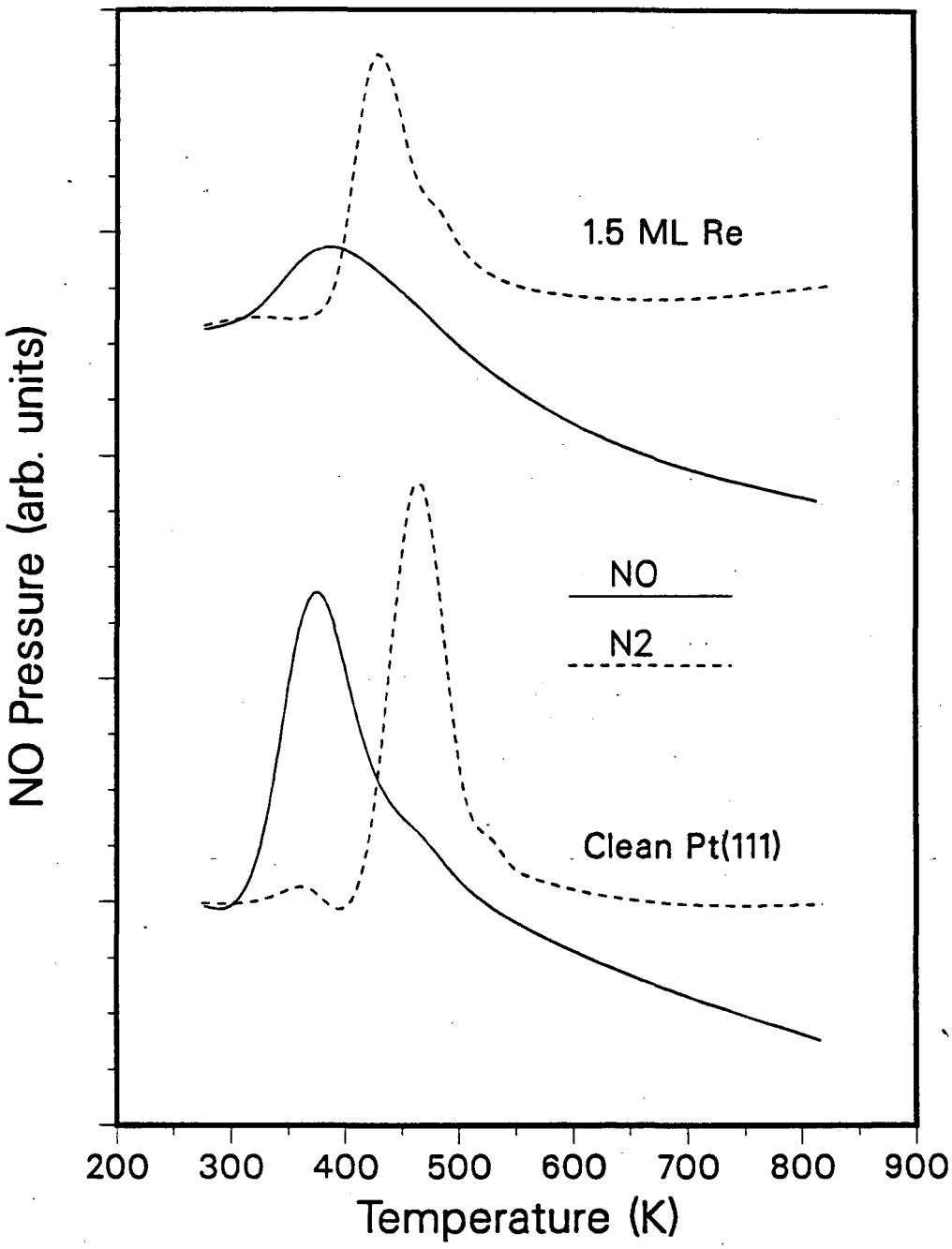

Figure 5.12: NO and N_2 TPD after room temperature adsorption on Pt(111), and on 1.5 ML Re on Pt(111). The heating rate was 30 K/sec and the NO exposure was 1.5 L. a) Desorption from Pt(111). b) Desorption from 1.5 ML Re on Pt(111).

Table 5.4: Desorption parameters of NO and N_2 TPD following NO adsorption on Pt(111) and on 1.5 ML Re on Pt(111). The results are from Figure 5.12.

	NO		N_2	
θ_{Re}	T_{max} (K)	Relative area	T_{max} (K)	Relative area
0	380	1.0	470	1.0
1.5	385	0.5	435	0.7

were not continued.

5.5 Discussion

5.5.1 The position of the hydrogen desorption maximum

The addition of rhenium to a Pt(111) surface was found to effect the adsorption and desorption of hydrogen. T_{max} extrapolated to zero hydrogen coverage was found to decrease with increasing rhenium at least for rhenium coverages less than or equal to 1.3 ML. T_{max} for the H_2 desorption peak from a Re(0001) surface or from multilayers of rhenium on Pt(111) was about 50 K higher than it was from clean Pt(111). This shows that T_{max} shifts in the direction opposite of what would be expected if the bimetallic surface behaved as a simple combination of the two metals making up the surface. The shifting to lower temperatures of the hydrogen T_{max} when the first monolayer of rhenium was added to the surface is probably the result of a chemical interaction that changes the electronic structure of the surface.

Multiple desorption peaks were never observed as might be expected due to the introduction of defects by depositing rhenium metal onto the platinum surface. Kinks and defects in the surface of clean platinum single crystals are known to be sites of higher temperature hydrogen desorption states [31, page 288]. An explanation for the absence of a high temperature shoulder for submonolayer rhe-

nium coverages is as follows. Stepped and kinked platinum surfaces are known to desorb hydrogen at higher temperatures than the flat terraces [31,32]. This was also shown by the disappearance of the high temperature shoulder with the introduction of rhenium on the platinum surface. On the other hand, structural defects were not found to yield high temperature shoulders on stepped and kinked rhenium surfaces with terraces in the (0001) orientation [13]. Rhenium defects were not found to add hydrogen desorption features to clean rhenium surfaces as mentioned above, and apparently not to a Pt(111) surface either. Additional hydrogen desorption peaks were also not observed for gold–platinum films nor for copper on Ru(0001) [33,34].

A few interesting new studies have been reported regarding the behavior of metallic monolayers on other metals. Apparently the band structure of a single monolayer of a metallic adsorbate does not resemble the bulk metal band structure in many systems. Pan *et al.* showed that 1 monolayer of platinum on niobium did not chemisorb CO even though both metals alone do so readily [35].

Surface contamination could possibly alter the behavior of the surface and must be considered. Every effort was made to minimize surface contamination; however, traces of carbon and oxygen were sometimes found on the surface after operating the rhenium source. Impurities might change the position of T_{max} in two ways: 1) surface impurities may cause different desorption kinetics through an electronic effect; 2) if hydrogen is unable to occupy some parts of the surface due to the presence of the impurities, then the density of hydrogen would be higher than it should be for a given hydrogen dose. Hydrogen follows second order desorption kinetics and a higher hydrogen density would result in a lower T_{max} for a given hydrogen dose. This possibility can be excluded since T°_{max} was determined by extrapolation to zero hydrogen coverage, in which case all surfaces should converge

to the same temperature at zero hydrogen coverage. It also seems unlikely that trace carbon and oxygen impurities would cause such a large temperature shift when the surface impurity level is dominated by the presence of relatively large amounts of rhenium. In addition, carbon and oxygen impurities are likely to block sites [16,36] rather than result in an increased hydrogen adsorption capacity as was observed.

5.5.2 The hydrogen desorption area

The hydrogen desorption area was a function of the metallic composition of the surface as can be seen in Figures 5.3 and 5.4. At a high coverage of rhenium (θ_{Re} = 1.3 ML) the surface was found to adsorb about half as much hydrogen as the clean Pt(111) surface at hydrogen saturation (Figure 5.4). This is in agreement with results obtained for supported catalysts by Carter *et al.* [4] and Kubrika [5]. The hydrogen dosing was done at 150 K, so any effects related to changes in the *adsorption* activation energy with surface composition must be considered. These effects were probably not important under these conditions since saturating the surface at 400 K followed by cooling to 150 K with continued hydrogen dosing were found to give similar results.

At low coverages of rhenium it was found that some bimetallic surfaces held more hydrogen than a clean Pt(111) surface at hydrogen saturation (Figure 5.4). The maximum hydrogen area obtained was from a bimetallic surface with θ_{Re} = 0.19 ML, and this surface held 20% more hydrogen at saturation than did clean Pt(111) (Figure 5.4). One possible explanation for this is an increase in surface roughness. If the prepared bimetallic surface was not flashed to high enough temperatures to smooth out the surface, then the addition of rhenium to the surface should increase the surface area somewhat. This possibility was not fully explored

because during TPD experiments, surfaces were never heated to temperatures high enough to cause bulk diffusion of the metals. Experiments were also not performed on alloyed Pt–Re surfaces. Another explanation is that an electronic interaction between platinum and rhenium results in a metallic surface that can hold more hydrogen. The maximum in hydrogen adsorption area was also observed at hydrogen doses less than saturation, and this indicates that the sticking probability of hydrogen (or probability of H_2 dissociation) is highest on bimetallic surfaces (Figure 5.4). Although one must extrapolate results obtained in UHV to high pressures with great care, it is possible that the enhanced hydrogenolysis activity displayed by the bimetallic surface described in Chapter 6 was due to an enhanced hydrogen binding of the surface. This phenomenon has also been described for supported platinum–rhenium catalysts by Barbier [6] and Margitfalvi [7].

5.5.3 The activation energy of hydrogen desorption

The activation energy of hydrogen desorption was found to decrease from the clean Pt(111) value when rhenium was added to the surface. This phenomenon was also described by Shimizu *et al.* for hydrogen adsorption on Cu/Ru(0001) surfaces [34]. Similar to the Re/Pt(111) case described here, they found T_{max} to shift with copper coverage, with no additional peaks or shoulders appearing due to copper or mixed copper-ruthenium sites. At 50% of a copper monolayer, they found a 50% decrease in hydrogen area. A decrease in E^a_{des} was reported for copper coverages above $\theta_{Cu} = 0.1$ monolayers.

A change in E^a_{des} such as observed for the platinum–rhenium system can have profound implications for hydrocarbon catalysis. If the activation energy of adsorption is assumed constant, then a decrease in E^a_{des} means a decrease in the heat of adsorption(ΔH_{ads}), and consequently a decrease in the metal hydrogen bond

strength. Figure 5.13 illustrates this point. As stated,

$$\Delta H_{ads} = 2D_{M-H} - D_{H-H} \tag{5.1}$$

where

$$E^a_{des} = \Delta H_{ads} + E^a_{ads} \tag{5.2}$$

Although this only translates to a difference in D_{M-H} between monometallic platinum and a $\theta_{Re} \sim 0.37$ ML on Pt(111) of 1 to 2 Kcal/mole (a supported industrial Pt/Re catalyst probably exposes about 50% of each metal on the surface), coupling this effect to an increased hydrogen availability may lead to a substantial effect on the enhancement of activity maintenance displayed by the bimetallic catalyst. This change in behavior towards hydrogen for the bimetallic surface compared to the monometallic platinum surface may partially explain the difference in fouling kinetics with respect to hydrogen pressure observed by Pacheco and Petersen for the supported Pt/Al_2O_3 and the $PtRe/Al_2O_3$ catalysts [8].

5.5.4 Energetics of CO desorption from Re–Pt(111)

Assuming that CO follows first order desorption kinetics and that the T_{max} shift to lower temperatures with increasing CO coverage is a result of a decreasing E^a_{des} with CO coverage, it can be seen that on all surfaces tested where $\theta_{Re} < 1$, E^a_{des} is coverage dependent (Figure 5.8). This indicates platinum–like behavior even at $\theta_{Re} = 0.55$ ML. Since rhenium does not show a shift of T_{max} with coverage, the shift in T_{max} vs. CO coverage should eventually decrease and disappear as more rhenium is evaporated onto the surface. Evidence was observed that this was occurring since at a one Langmuir dose of CO the slopes of the curves are apparently less steep at the higher rhenium coverages shown in Figure 5.8.

The position of T_{max} is not sufficiently different on the two metals, and this

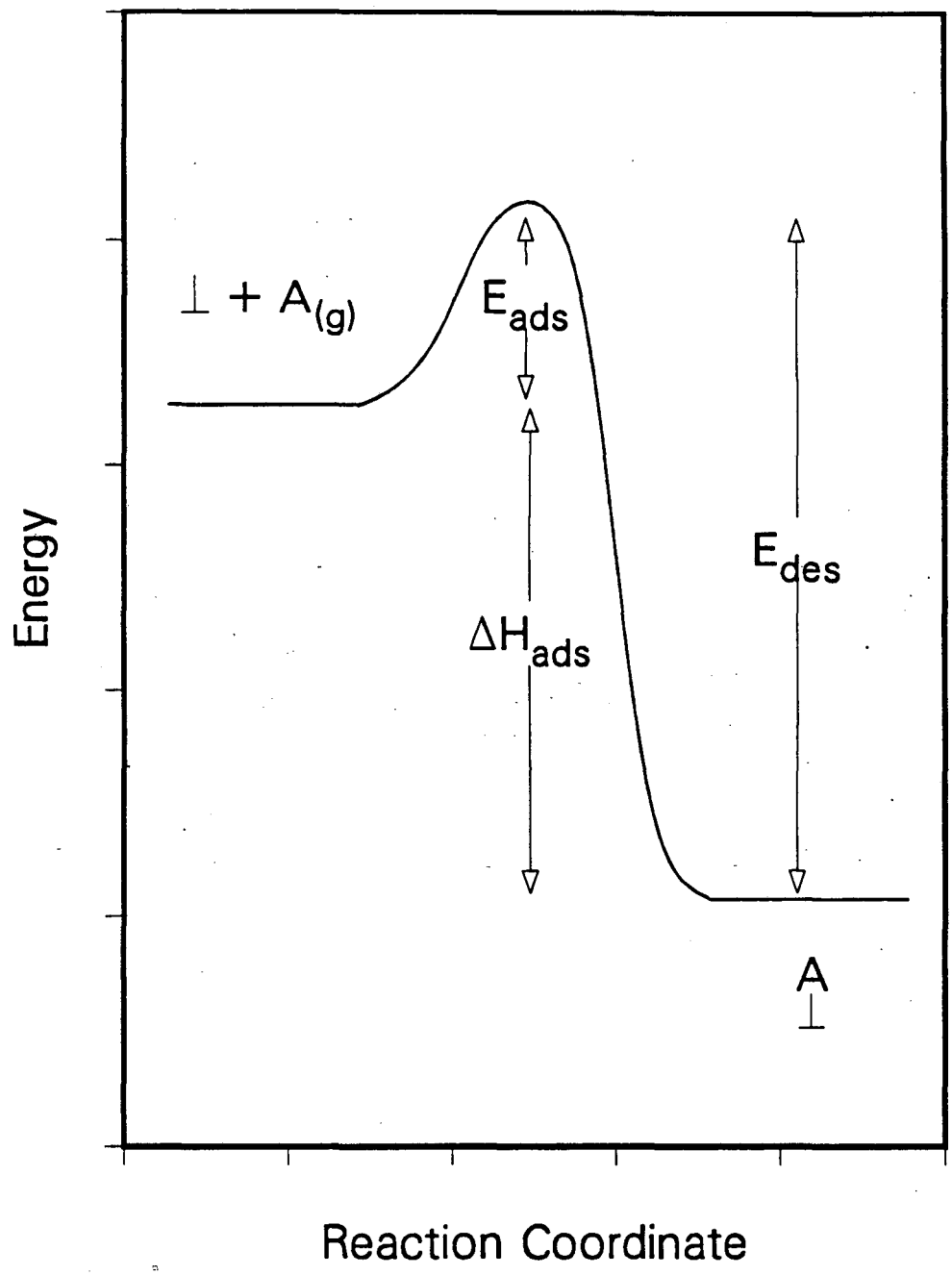

Figure 5.13: Energy vs. reaction coordinate for an adsorption/desorption process.

translates to a heat of adsorption which is nearly the same on clean Pt(111) and the two low rhenium coverage surfaces. This means that the platinum and rhenium sites exposed on the surface cannot be distinguished quantitatively using CO TPD. As will be seen in Chapter 6, the interesting chemistry is within the first rhenium monolayer on platinum; but unfortunately CO is not a reasonable titrant for these surfaces.

5.5.5 CO adsorption capacity on Re–Pt(111) surfaces

The room temperature adsorption capacity for CO on clean Pt(111) is about double that of a clean Re(0001) surface. The saturation coverage on Pt(111) was reported to be 7.5×10^{14} molecules/cm^2 by Ertl *et al.* [21], and 4×10^{14} molecules/cm^2 on Re(0001) [13,24]. A comparison of the CO adsorption on clean Pt(111) compared to CO adsorption on 3 ML of rhenium on Pt(111) show that these results are in agreement with the previously reported results (Table 5.3).

At low rhenium coverages a 40% increase in CO capacity was observed (Table 5.2 and Figure 5.11). This increased capacity for adsorbate binding was also observed for hydrogen at low rhenium coverages (Figure 5.4). Two possible explanations can be invoked to explain the 40% increase in CO chemisorption of the $\theta_{Re} = 0.3$ ML surface: an electronic interaction at the surface or the presence of surface roughness. At low rhenium coverages the surface is expected to be somewhat rough compared to a well annealed surface. The problem with this explanation is that the increase in roughness is accomplished with rhenium metal. A Re(0001) surface binds about half as much CO as does Pt(111), and work done by Housley *et al.* showed that the stepped Re[14(0001)×(10$\bar{1}$1)] surface has the same capacity for the molecular CO state as did the Re(0001) surface [24]. Since CO was also not observed to dissociate on a roughened $\theta_{Re} = 0.3$ ML surface, it

must be concluded that low coordinated rhenium cannot do the job. An electronic effect is the most likely explanation. In support of this, it was found that at room temperature a 0.7 ML coverage of CO was obtained in the presence of rhenium. The compression structure observed on Pt(111) ($\theta_{CO} \sim 0.7$) is formed only when the platinum surface is cooled to liquid nitrogen temperatures [21]. Both factors could contribute, but if an increase in surface roughness was a factor, it was because rhenium is capable of adsorbing more CO through an electronic effect since it was in contact with an underlying platinum substrate.

Except for the increase in CO binding at low rhenium coverages, the binding capacity of CO decreased as expected on rhenium covered Pt(111) (Table 5.3 and Figures 5.10 and 5.11). At higher rhenium coverages ($\theta_{Re} \geq 0.8$ ML), the behavior towards CO can be explained through the separate contributions of rhenium and platinum. Only a surface composed of 3 ML of *epitaxial* rhenium was observed to dissociate CO (Figure 5.10c). When the surface was annealed to 700° C, it was no longer observed to dissociate CO. This is in agreement with results obtained by Housley *et al.* [24] where CO was not found to dissociate on a flat Re(0001) surface.

Oxidizing the 3 ML rhenium surface apparently had no effect other than site blocking as the CO desorption area from the oxidized surface was one half the desorption area obtained from 3 ML of rhenium on Pt(111). T_{max} was the same on these two surfaces (Table 5.3 and Figure 5.10).

References

[1] D. Bianchi, G.E.E. Gardes, G.M. Pajonk, and S.J. Teichner. *J. Catalysis* 38 (1975) 135.

[2] R. Lamartine and R. Perrin. *Spillover of Adsorbed Species*, page 251. Elsevier Science Publishers, Amsterdam, The Netherlands, 1983.

[3] C. Bolivar, H. Charcosset, R. Fretty, M. Primet, L.Tournayan, C. Betizeau, G. Leclercq, and R. Maurel. *J. Catalysis* **45** (1976) 163.

[4] J.L. Carter, G.B. Vicker, W. Weissman, W.S. Kmak, and J.H. Sinfelt. *Applied Catalysis* **3** (1982) 327.

[5] H. Kubricka. *J. Catalysis* **12** (1968) 223.

[6] J. Barbier, H. Charcosset, G. dePeriera, and J. Riviere. *Applied Catalysis* **1** (1981) 71.

[7] J. Margitfalvi, S. Gőbölös, E. Kwayzer, M. Hegedüs, F. Nagy, and L. Koltai. *React. Kinet. Catal. Lett.* **24** (1984) 315.

[8] M.A. Pacheco and E.E. Petersen. *J. Catalysis* **96** (1985) 499.

[9] M.A. Pacheco and E.E. Petersen. *J. Catalysis* **96** (1985) 507.

[10] J.W.A. Sachtler and G.A. Somorjai. *J. Catalysis* **81** (1983) 77.

[11] R.C. Yeates. PhD thesis, University of California, Berkeley, CA 94720, 1985.

[12] R.C. Yeates and G.A. Somorjai. *Surface Sci.* **134** (1983) 729.

[13] R. Ducros, M. Alnot, J.J. Ehrhardt, M. Housley, and G. Piquard. *Surface Sci.* **94** (1980) 154.

[14] R. Ducros, M. Housley, G. Piquard, and M. Alnot. *Surface Sci.* **109** (1981) 235.

[15] F. Zaera and G.A. Somorjai. *Surface Sci.* **154** (1985) 303.

[16] F. Zaera. PhD thesis, University of California, Berkeley, CA 94720, 1984.

[17] P.A. Redhead. *Vacuum* **12** (1962) 203.

[18] K. Christmann, G. Ertl, and T. Pignet. *Surface Sci.* **54** (1976) 365.

[19] D.M. Collins and W.E. Spicer. *Surface Sci.* **69** (1977) 85.

[20] R.W. McCabe and L.D. Schmidt. *Surface Sci.* **65** (1977) 189.

[21] G. Ertl, M. Neumann, and K.M. Streit. *Surface Sci.* **64** (1977) 393.

[22] H. Steininger, S. Lehwald, and H. Ibach. *Surface Sci.* **123** (1982) 264.

[23] H. Hopster and H. Ibach. *Surface Sci.* **77** (1978) 109.

[24] M. Housley, R. Ducros, G. Piquard, and A. Cassuto. *Surface Sci.* **68** (1977) 277.

[25] S. Tatarenko, R. Ducros, and M. Alnot. *Surface Sci.* **126** (1983) 422.

[26] R. van Hardeveld and A. van Montfoort. *Surface Sci.* **4** (1966) 396.

[27] H. Ibach and S. Lehwald. *Surface Sci.* **76** (1978) 1.

[28] J.L. Gland and B.A. Sexton. *Surface Sci.* **94** (1980) 355.

[29] R.J. Gorte, L.D. Schmidt, and J.L. Gland. *Surface Sci.* **109** (1981) 367.

[30] S. Tatarenko, M. Alnot, and R. Ducros. *Surface Sci.* **163** (1985) 249.

[31] Gabor A. Somorjai. *Chemistry in Two Dimensions.* Cornell University Press, Ithaca, New York 14850, 1981.

[32] K. Christmann and G. Ertl. *Surface Sci.* **60** (1976) 365.

[33] J.J. Stephan, V. Ponec, and W.M.H. Sachtler. *Surface Sci.* **47** (1975) 403.

[34] H. Shimizu, K. Christmann, and G. Ertl. *J. Catalysis* **61** (1980) 412.

[35] Xiao-he Pan, M.W. Ruckman, and M. Strongin. *Phys. Rev. B* **35** (1987) 3734.

[36] S.M. Davis. PhD thesis, University of California, Berkeley, CA 94720, 1981.

Chapter 6

Hydrocarbon Conversion on Bimetallic Platinum–Rhenium Surfaces

6.1 Preface

In this chapter the role of surface composition towards the catalytic activity of platinum and platinum–rhenium bimetallic surfaces will be discussed. The preparation of bimetallic surfaces was described in Chapter 4, and here it will be shown how the activity and selectivity of hydrocarbon reactions is under the control of the surface metallic composition. It was found under some circumstances that the nature of the carbonaceous overlayers differed depending on surface composition, and the likelihood that the behavior towards hydrogen of a bimetallic surface as described in Chapter 5 is in some way responsible, will be discussed.

The molecules that were studied and that are reported in this Chapter are: ethane (C_2H_6), butane (C_4H_{10}), normal hexane (C_6H_{14}), cyclohexane (c-C_6H_{12}), and methylcyclopentane (MCP).

6.2 Ethane Hydrogenolysis

The hydrogenolysis of ethane has been studied over many metals [1,2,3], and was used in this study because of the wide differences in activity displayed by platinum and rhenium towards ethane hydrogenolysis. The reaction is

$$C_2H_6 + H_2 \rightarrow 2CH_4 \tag{6.1}$$

Sinfelt reports that rhenium is 5-6 orders of magnitude more active that platinum towards this reaction when both metals are supported on silica (SiO_2). Table 6.1 shows the kinetic parameters for some metals previously studied and summarized by Sinfelt [2]. The rate law for Table 6.1 is

$$r = kP^n_{C_2H_6}P^m_{H_2} \tag{6.2}$$

where r and k are the rate and rate constant, respectively. The rate constant k is tabulated at a set of standard pressures of 0.030 and 0.20 atmospheres of C_2H_6 and H_2, respectively, and is given by

$$r_o = r'_o \exp(-E/RT) \tag{6.3}$$

where r'_o represents the preexponential factor and E the apparent activation energy.

6.2.1 Re–Pt(111): Activity vs. Re coverage

The activity of the ethane hydrogenolysis reaction was examined as a function of the rhenium surface composition, and the results are shown in Figure 6.1. The reaction conditions were: P_{H_2} = 100 Torr; $P_{C_2H_6}$ = 10 Torr; and T = 300° C.

The initial rate of reaction on clean Pt(111) was 5×10^{-3} CH_4 molecules/Pt atom-sec. Reactions involving C–C bond breaking are usually structure sensitive,

Table 6.1: Summary of kinetic parameters for ethane hydrogenolysis over SiO_2 supported metals.

	Reaction Orders					
Metal	Temp. range °C	n[a]	m[b]	Temp. °C[c]	E[d]	r_o'[e]
Fe	239-376	0.6	+0.5	270	–	–
Co	219-259	1.0	-0.8	219	30	3.0×10^{25}
Ni	177-219	1.0	-2.4	177	40.6	4.9×10^{31}
Cu	288-330	1.0	-0.4	330	21.4	4.5×10^{20}
Ru	177-210	0.8	-1.3	188	32	1.3×10^{28}
Rh	190-224	0.8	-2.2	214	42	5.8×10^{31}
Pd	343-377	0.9	-2.5	354	58	3.7×10^{33}
Re	229-265	0.5	+0.3	250	31	1.8×10^{26}
Os	125-161	0.6	-1.2	152	35	7.0×10^{30}
Ir	177-210	0.7	-1.6	210	36	5.2×10^{28}
Pt	344-385	0.9	-2.5	357	54	5.9×10^{31}

a. Order with respect to ethane.
b. Order with respect to hydrogen.
c. Temperature at which the reaction orders were determined.
d. Apparent activation energy, kcal/mole.
e. Pre-exponential factor, molecules/sec/cm^2,
in the equation $r_o = r_o' \exp(-E/RT)$.

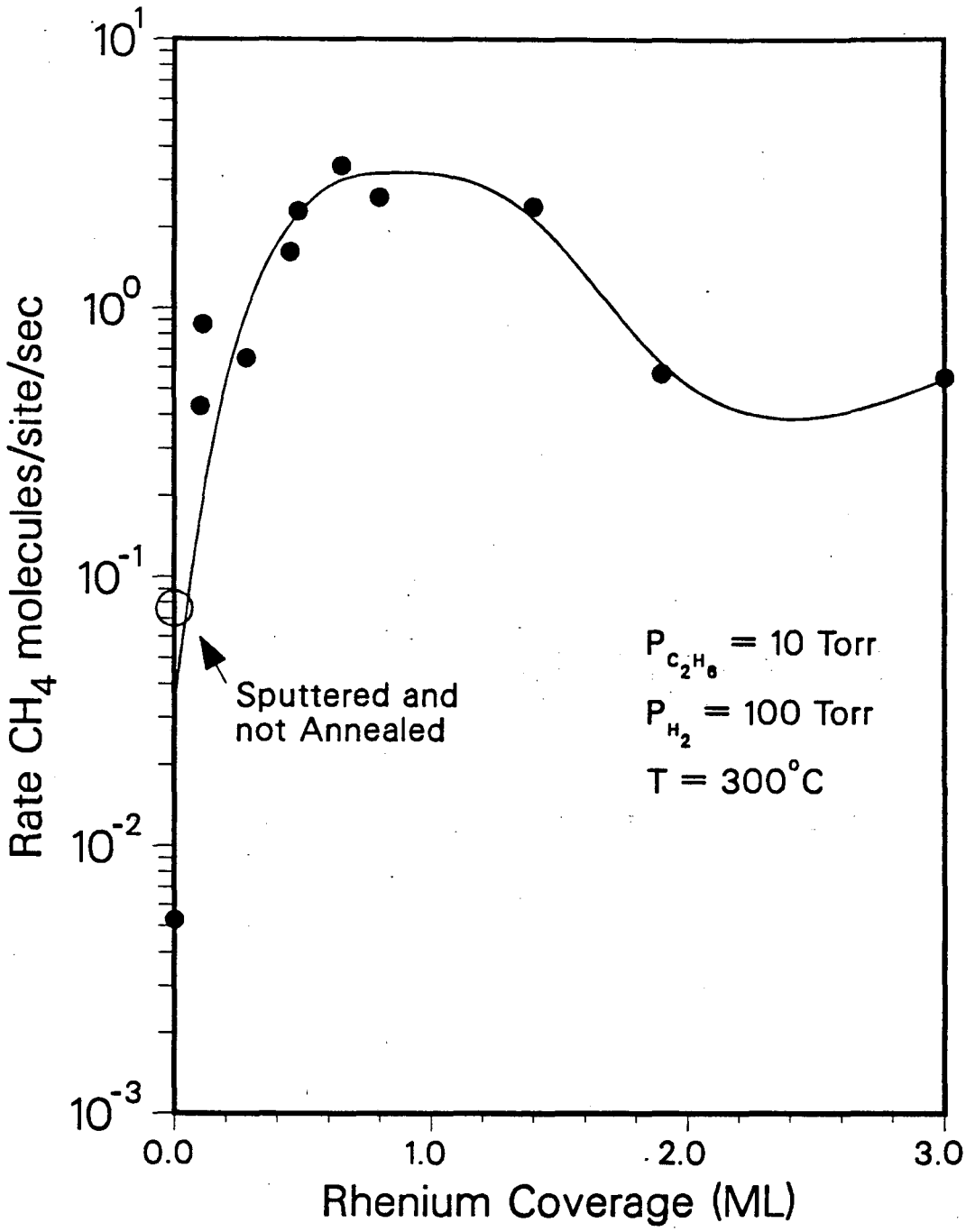

Figure 6.1: Ethane hydrogenolysis activity vs. rhenium coverage on Pt(111).

and the rate of reaction was increased over an order of magnitude to 7×10^{-2} by roughening the surface with argon ion sputtering at room temperature and no annealing. With a large rhenium coverage, $\theta_{Re} > 2$ ML, the rate of methane formation was 0.5 CH_4 molecules/site-sec.

With the addition of a small amount of rhenium to Pt(111), the activity was dramatically increased compared to clean Pt(111). Even with a rhenium coverage of between 0.1 to 0.2 monolayers, the initial rate was two orders of magnitude higher than that of clean Pt(111), and gave an activity equivalent to multilayers of rhenium on Pt(111). At even slightly higher rhenium coverages, between 0.6 and 1 monolayer of rhenium, it was observed that a maximum rate of formation of methane was obtained.

6.2.2 Re(0001) and Pt–Re(0001): Activity vs. Pt coverage

The activity of a Re(0001) surface and bimetallic surfaces derived from Re(0001) were examined. The temperature dependence for ethane hydrogenolysis on clean Re(0001) was measured between 300 and 350°C, and the results are shown in Figure 6.2. An activation energy of 18 ± 1 Kcal/mole was obtained between these temperatures with hydrogen and ethane partial pressures of 100 and 10 Torr, respectively.

The initial rates obtained over platinum dosed Re(0001) surfaces are shown in Figure 6.3. In this case the less active platinum metal was deposited on the more active rhenium. The conditions used were the same as those described for Figure 6.1: 300° C, 10 Torr C_2H_6, and 100 Torr H_2.

The rate of methane formation was 0.55 CH_4 molecules/site-sec and very close to the initial rates observed for multilayers of rhenium on Pt(111) ($\theta_{Re} \geq 2$ ML). Again the activity could be increased by roughening the surface with argon ion

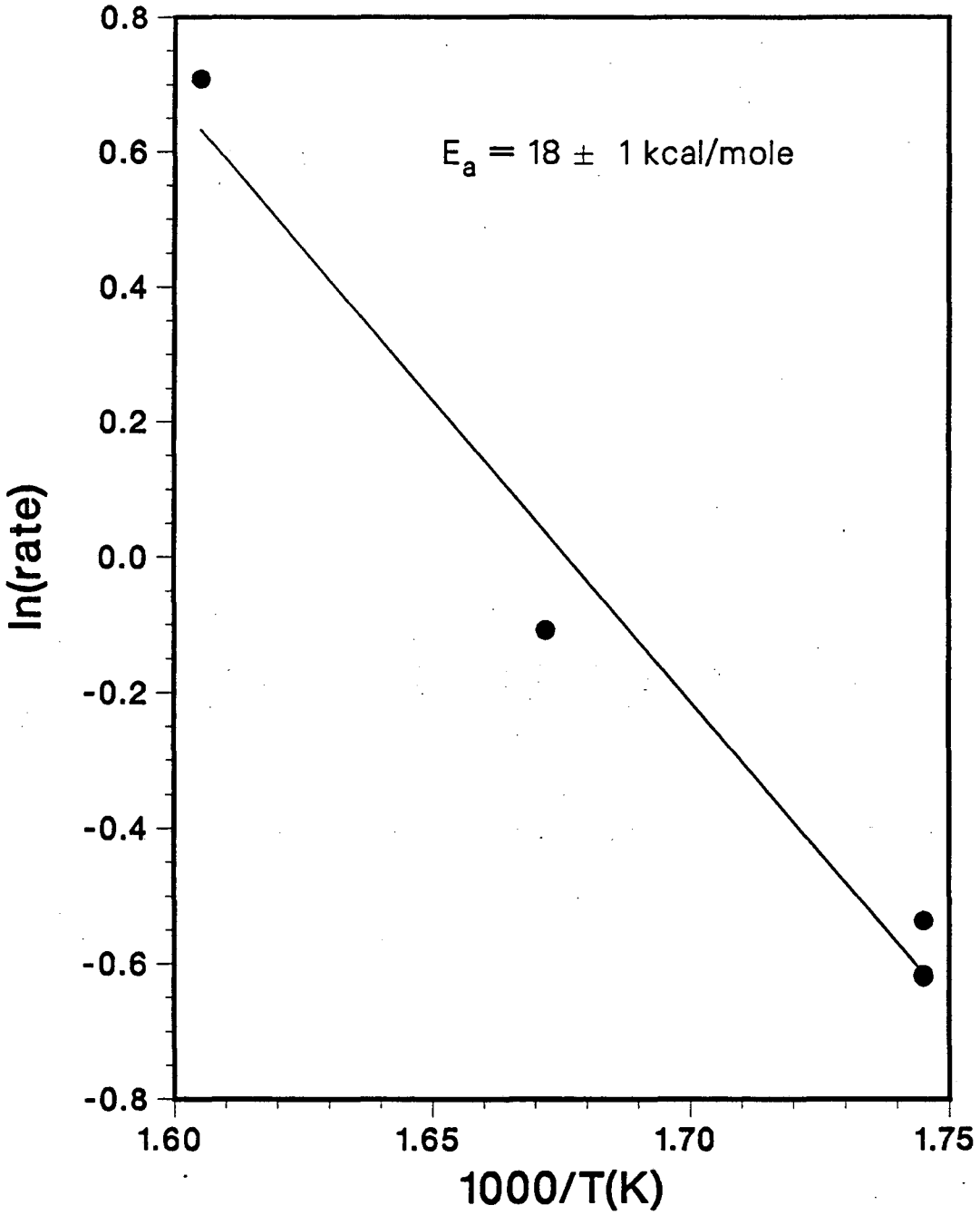

Figure 6.2: Activation energy plot for C_2H_6 hydrogenolysis on Re(0001). The reaction conditions were: $P_{C_2H_6}$ = 10 Torr, P_{H_2} = 100 Torr, and the temperature ranged from 300 to 350° C.

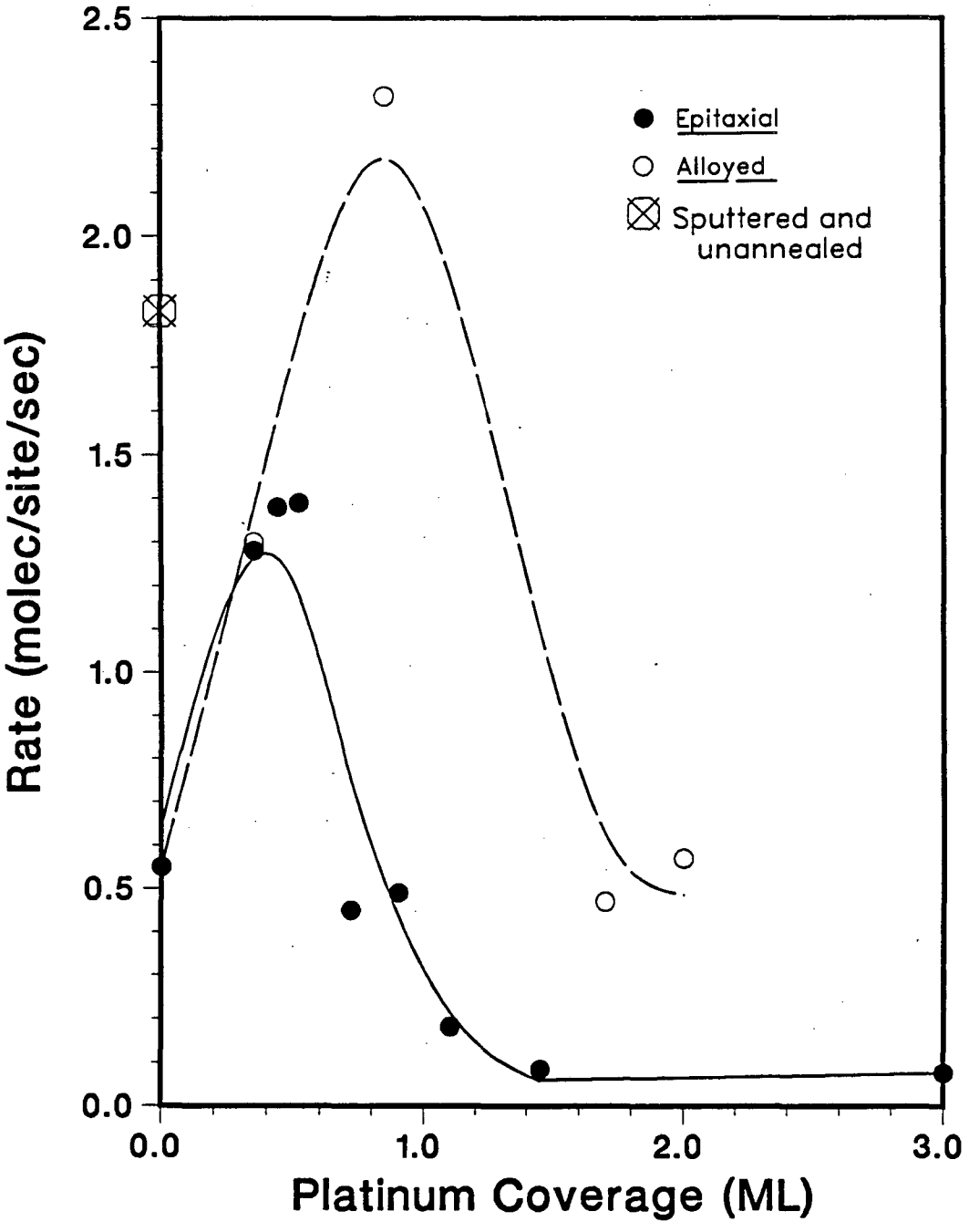

Figure 6.3: Ethane hydrogenolysis activity vs. platinum coverage on Re(0001). The reaction conditions were: $P_{C_2H_6} = 10$ Torr, $P_{H_2} = 100$ Torr, and T = 300° C.

sputtering at room temperature and no annealing. On the roughened Re(0001) surface the activity was higher by a factor of 3.5 over the annealed Re(0001) surface.

With the addition of platinum to the surface, an enhancement was obtained in the hydrogenolysis rate, reaching a maximum rate of methane formation about 3 times greater than that obtained on clean Re(0001) between 0.3 to 0.5 ML platinum. Even at a platinum coverage of $\theta_{Pt} \sim 1$ ML, the surface had an activity equivalent to the clean Re(0001) surface. The activity of the surface was not observed to be less than that of clean Re(0001) until a second monolayer of platinum was introduced. When the platinum coverage exceeded 1.5 ML, a background rate of near 0.07 molecules/site-sec was observed, which was equivalent to the rate observed on a roughened Pt(111) surface.

For the Pt–Re(0001) system, experiments were also performed on alloyed surfaces, *i.e.* bimetallic surfaces heated above the bulk diffusion threshold which was 700°C. To generate this surface, an epitaxial surface was flashed briefly to 850°C. The coverages reported were determined by using AES; the spectra obtained for alloyed surfaces always resembled spectra obtained for epitaxial surfaces although the number of substrate atoms that diffused to the surface was unknown. The platinum coverage measured after alloying was also less than the coverage observed of the generating epitaxial surface as was expected.

Rates obtained on alloyed surfaces were in general higher than on the corresponding epitaxial surfaces. In fact, an alloyed surface composed of 0.9 ML of platinum gave a rate almost five times higher than clean Re(0001), and was also higher than the rate obtained on a roughened clean Re(0001) surface. An alloyed surface with a surface composition of $\theta_{Pt} \sim 2$ ML was as active as clean Re(0001).

6.2.3 Pt–Re: The state of the surface following ethane hydrogenolysis reactions

Post reaction surface characterization following ethane hydrogenolysis reactions included: Auger analysis; H_2 TPD to estimate the quantity of hydrogen bound to the surface and carbonaceous deposits; exposure to saturation levels of carbon monoxide ($\sim$ 36 L) followed by CO TPD to estimate the number of bare metal sites remaining exposed; and followed by a second Auger analysis.

The state of the surface following C_2H_6 hydrogenolysis reactions on Re–Pt(111)

The amount of carbon remaining on the surface after reaction was determined by AES for the Re–Pt(111) system, and was found to be independent of the rhenium coverage. The value obtained was $\theta_C \sim 1.5 \pm 0.3$ ML.

Hydrogen TPD performed released hydrogen from the carbonaceous deposits on the surface, and the amount observed to desorb was also fairly independent of the surface rhenium coverage. The TPD area obtained for post reaction characterization was compared to the TPD area obtained when hydrogen was adsorbed at 150 K on a clean Pt(111) surface at saturation, and assuming that $\theta_H = 1$ under these circumstances. A value of $\theta_H \sim 0.9 \pm 0.2$ following ethane hydrogenolysis reactions was obtained for all the surfaces tested. This amount of hydrogen is about 10 times more hydrogen than a clean Pt(111) surface can adsorb at room temperature, and this demonstrates that most of the hydrogen is bound to carbonaceous surface deposits. The above results indicate that the H/C ratio of the carbonaceous deposits obtained under these conditions was H/C $\sim$ 0.6.

For the Re–Pt(111) system, it was found that the desorption area of CO was smaller following 36 L of exposure after ethane hydrogenolysis reactions were per-

formed at higher rhenium coverages. On Pt(111) following reaction, there remained 30-40% bare platinum sites compared to clean Pt(111). About half the CO desorption area was obtained on three monolayers of rhenium compared to platinum, but since clean Re(0001) adsorbs about half as much CO as does clean Pt(111) (see Chapter 5 and reference [4]), the conclusion reached is that there is no difference in remaining bare metal surface area following ethane hydrogenolysis of Re–Pt(111) with respect to the metallic composition of the surface.

The state of the surface following C_2H_6 hydrogenolysis reactions on Pt–Re(0001)

The same sequence of post reaction characterization techniques was performed for the Pt–Re(0001) system, and similar results were obtained regarding carbon deposition and hydrogen desorption following C_2H_6 hydrogenolysis reactions. However, it had been observed that when several monolayers of rhenium were deposited onto Pt(111), it was easier to remove carbon from the surface following ethane hydrogenolysis reactions. For this reason, the following comparisons were made when studying the Pt–Re(0001) system towards ethane hydrogenolysis. The amount of carbon left on the surface following reaction (θ_{C1}), and the carbon still remaining following TPD of hydrogen and CO (θ_{C2}), were determined using AES as it was for the Re–Pt(111) system. Some carbon was observed to leave the surface during TPD since $\theta_{C2} < \theta_{C1}$. The ratio θ_{C2}/θ_{C1} then gives the fraction of irreversibly adsorbed carbon which was found to be highest on thick platinum overlayers. The results obtained are shown in Figure 6.4.

When the rhenium surface was covered with less than one monolayer of platinum, better than 80% of the carbon desorbed during TPD. With platinum films 1-4 monolayers thick, only between 10-40% of the carbon was found to desorb.

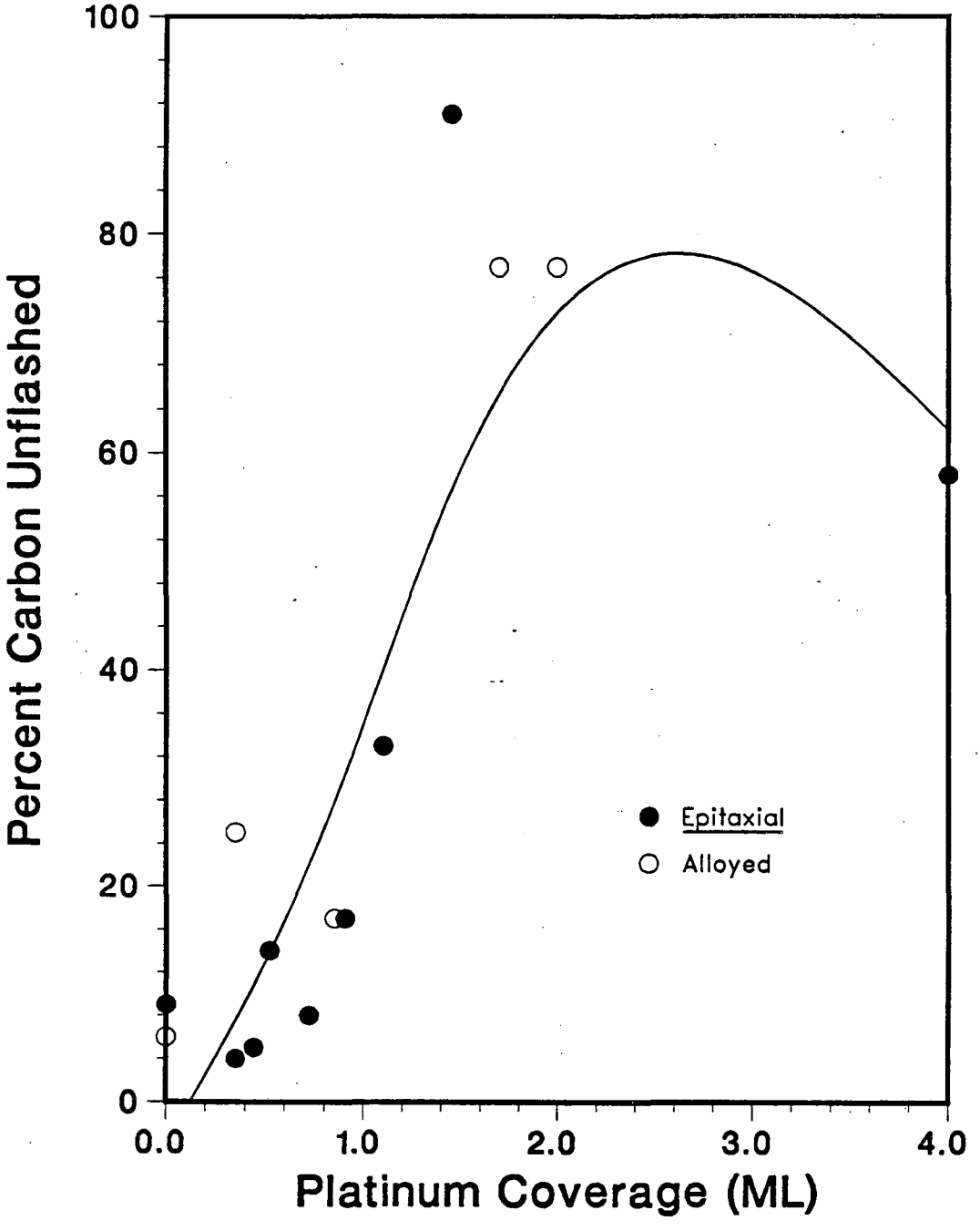

Figure 6.4: Irreversibly adsorbed carbon vs. platinum coverage on Re(0001). The reaction conditions were the same as in Figure 6.3.

These results were similar whether or not the surface was alloyed.

An attempt was made to determine the identity of the desorbing species. Neither C_2H_6 nor CH_4 were observed to desorb, which probably means that carbon desorbed as oxygenated species such as CO or CO_2. This is plausible since oxygen was found associated with the surface following reactions, and probably came from the adsorption of H_2O on the surface during pump down of the high pressure cell before its opening. The oxygen also disappeared from the surface following the TPD characterization steps.

6.2.4 Hydrogen pressure dependence

The hydrogen pressure dependence for the ethane hydrogenolysis reaction was previously reported by Sinfelt to be very different over the two metals (see Table 6.1 and reference [2]). This indicates that a different reaction mechanism operates over the two surfaces, and experiments were performed to observe how the reaction mechanism might be influenced by the metallic composition of a bimetallic surface.

The reaction conditions used for these experiments were: T = 350° C; $P_{C_2H_6}$ = 5 Torr; and $P_{H_2} = 500 - 1000$ Torr. The initial rates and the hydrogen partial pressure dependence of this reaction on three different surfaces are shown in Figure 6.5. The rate law for this reaction was described previously and was shown in Equation 6.2. For clean Pt(111), the value for the hydrogen pressure dependence (m) obtained was -2.0 ± 0.2. When the surface was covered with 2 ML of rhenium, m was found to be -0.7 ± 0.1.

The bimetallic surface that was tested had a rhenium coverage of 0.2 ML. This surface was chosen because it exposed 80% platinum yet it was as active as 2 ML of rhenium on Pt(111) (Figure 6.1). The hydrogen pressure dependence obtained from this surface was similar to that obtained from Pt(111), $m = -1.8 \pm 0.2$.

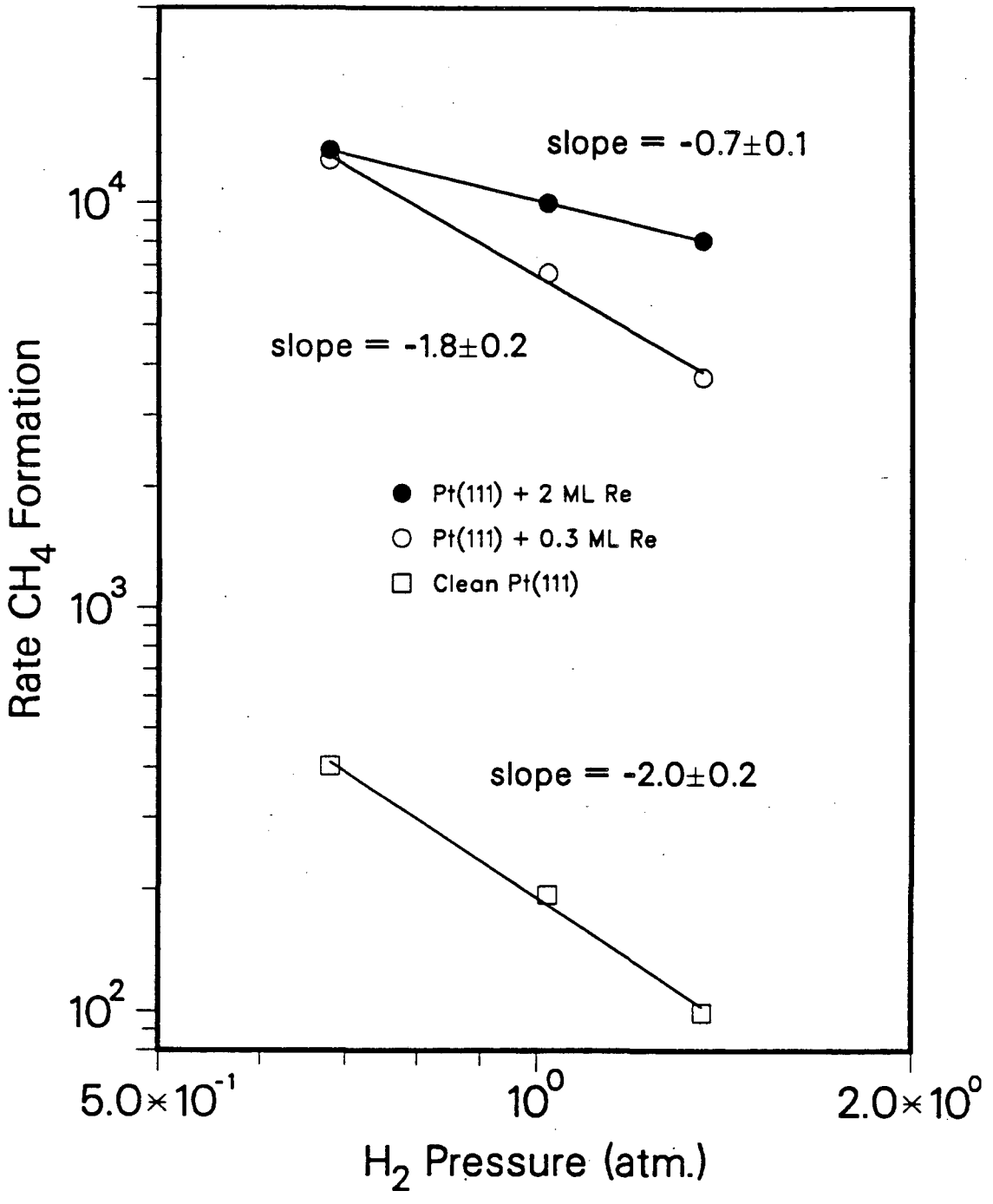

Figure 6.5: Hydrogen pressure dependence for ethane hydrogenolysis on Re–Pt(111). The reaction conditions were: $P_{C_2H_6}$ = 5 Torr, P_{H_2} = 500 – 1000 Torr, T = 350° C.

6.3 Re–Pt(111): Butane Conversion

The conversion of normal butane (C_4H_{10}) was studied over bimetallic Re–Pt(111) surfaces. In addition to hydrogenolysis reactions, butane can undergo bond shift to form isobutane. The reactions of n–butane are:

$$C_4H_{10} + H_2 \rightarrow C_3H_8 + CH_4$$

$$C_4H_{10} + H_2 \rightarrow 2C_2H_6$$

$$n\text{–}C_4H_{10} \rightarrow i\text{–}C_4H_{10}$$

The conversion of butane over platinum catalysts is discussed by Sinfelt [2], and over platinum, rhenium, and platinum–rhenium catalysts by Betizeau *et al.* [5]. The data of Betizeau *et al.* is particularly interesting since they examined the behavior of platinum–rhenium catalysts over the entire composition range of platinum and rhenium, similar to experiments used in this study. Butane conversion was also studied by Wong *et al.* for a series of Rh–Pt/silica bimetallic catalysts [6].

6.3.1 Re–Pt(111): Butane hydrogenolysis

The reaction conditions used in the butane studies were: $P_{C_4H_{10}} = 10$ Torr, $P_{H_2} = 100$ Torr, and T = 300° C. The initial rates of formation of hydrogenolysis products generated from n–butane accounted for 75% of the initial activity of the clean Pt(111) surface. Hydrogenolysis rates accounted for over 90% of the initial activity with 2 monolayers of rhenium on the surface. Where the initial rate of methane formation was maximum at a coverage of $\theta_{Re} \sim 0.7$ ML, hydrogenolysis accounted for 99% of the total activity. The hydrogenolysis results are shown in Figure 6.6.

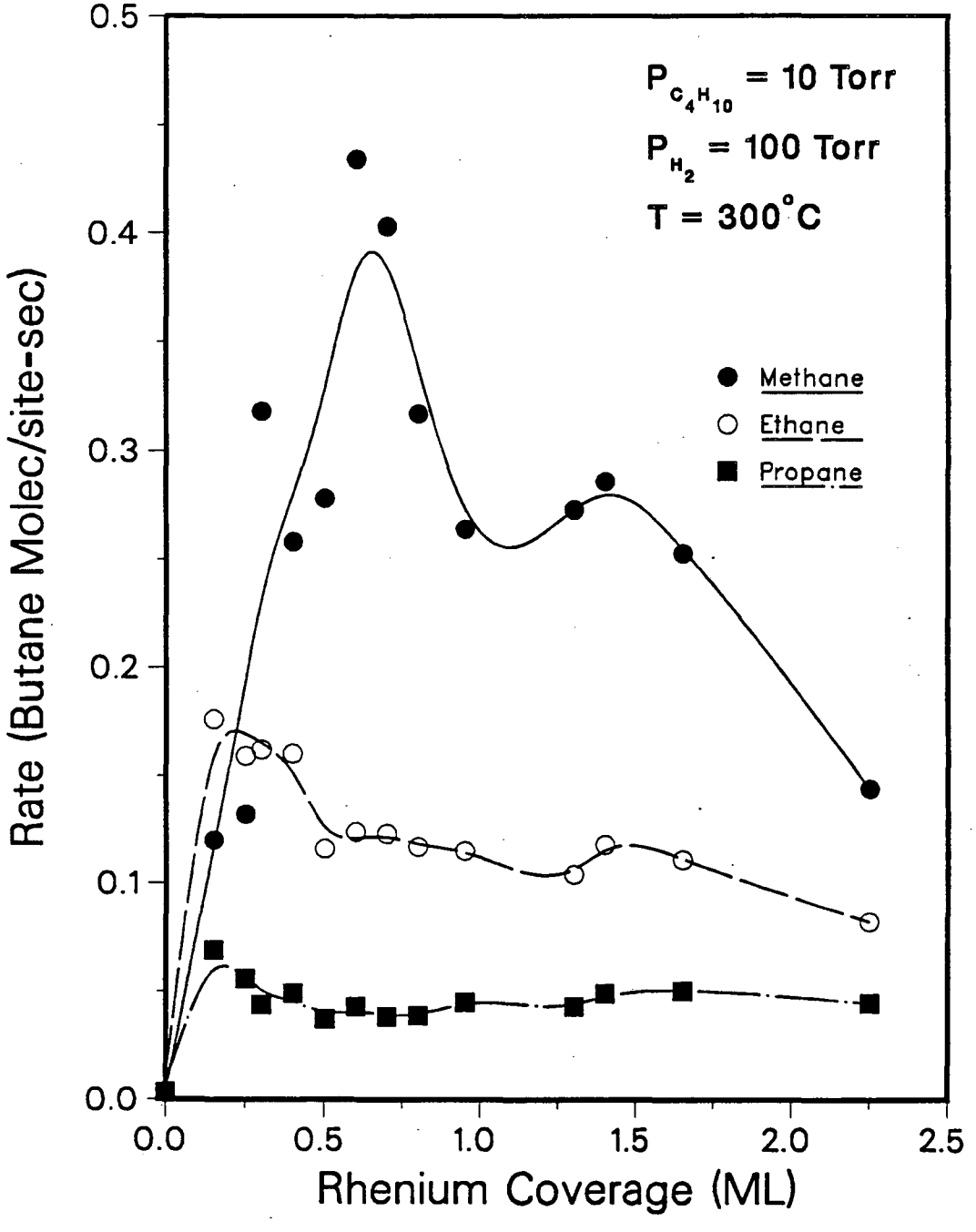

Figure 6.6: Hydrogenolysis of butane vs. rhenium coverage over Re–Pt(111) surfaces. The reaction conditions were: $P_{C_4H_{10}}$ = 10 Torr, P_{H_2} = 100 Torr, T = 300° C.

The initial rate of formation of methane from clean Pt(111) was similar when both ethane and butane were used as reactants. However, the methane formation rate was 2 to 3 times higher from ethane than from butane for any coverage of rhenium.

Rate maxima for all the hydrogenolysis products were observed within the first monolayer of rhenium from butane. Similar to ethane, the rate of maximum initial activity was at $\theta_{Re} \sim 0.7$ ML. The first data points obtained at a rhenium coverage $\theta_{Re} \sim 0.15$ ML gave maximum initial rates for ethane and propane formation. The ratio of the maximum rates divided by the clean Pt(111) initial rates shown in Figure 6.6 for methane, ethane, and propane were 125, 50, and 20 respectively.

The fission parameter (M_f) has been introduced to classify hydrogenolysis selectivities of hydrocarbons, and is defined below [7]:

$$M_f = [C_1]^{-1} \sum_{i=2}^{n-1} (n-i)[C_i] \tag{6.4}$$

where $[C_i]$ is the total concentration of all the hydrocarbon isomers containing i carbon atoms, $[C_1]$ is the concentration of CH_4, and n is the number of carbon atoms in the reactant hydrocarbon, which is 4 for butane. Selective hydrogenolysis of the terminal C–C bond results in a fission parameter of $M_f = 1$, whereas purely statistical cracking results in a fission parameter of $M_f = 10$. When multiple hydrogenolysis is important, the fission parameter is $M_f \ll 1$. For the butane system, Equation 6.4 becomes:

$$M_f = [C_1]^{-1}(2[C_2] + [C_3])$$

In Figure 6.7, M_f is plotted vs. rhenium coverage. M_f was found to be 2 for clean Pt(111), and this shows that clean Pt(111) tends towards terminal C–C bond breaking of n–butane. As rhenium is added to the surface, multiple

hydrogenolysis increases dramatically as indicated by the decrease in M_f. The surface with a rhenium coverage of $\theta_{Re} \sim 0.2$ ML displays a value of $M_f = 1$, and the surface which displayed a maximum rate of CH_4 formation showed a minimum M_f of ~ 0.2. With rhenium coverages in excess of 0.7 monolayers, the value of M_f increased some, and was near 0.6 for a rhenium coverage of $\theta_{Re} \sim 2$ ML.

6.3.2 Re–Pt(111): Butane isomerization

The isomerization rate of n–butane to isobutane was $(2.9\pm0.1)\times10^{-3}$ molecules/site-sec for Pt(111) and was found to increase only slightly with the addition of rhenium to the surface. At 2 ML of rhenium, the rate of formation of isobutane was 4.5×10^{-3} molecules/site-sec, only about a 50% rate increase over the rate obtained on clean Pt(111). These results are shown in Figure 6.8, and within experimental error, the rates obtained over all the surfaces are not substantially different.

6.3.3 Re–Pt(111): The state of the surface following butane reactions

Characterization of the surface following butane reactions was performed as described in Section 6.2.3. As was observed for ethane reactions, the results were also independent of rhenium coverage for butane conversion. The post reaction carbon coverage was determined using AES to be $\theta_C \sim 1.8 \pm 0.4$ ML. The hydrogen area obtained was 50% higher than was obtained from ethane, and the hydrogen content of the surface and the adsorbed carbonaceous layers was estimated to be $\theta_H \sim 1.4 \pm 0.4$ ML. This gives a hydrogen to carbon ratio of H/C ~ 0.8 for the carbonaceous overlayers derived from butane. The fraction of bare surface left following reaction as determined using CO titration was 40% and independent of rhenium coverage.

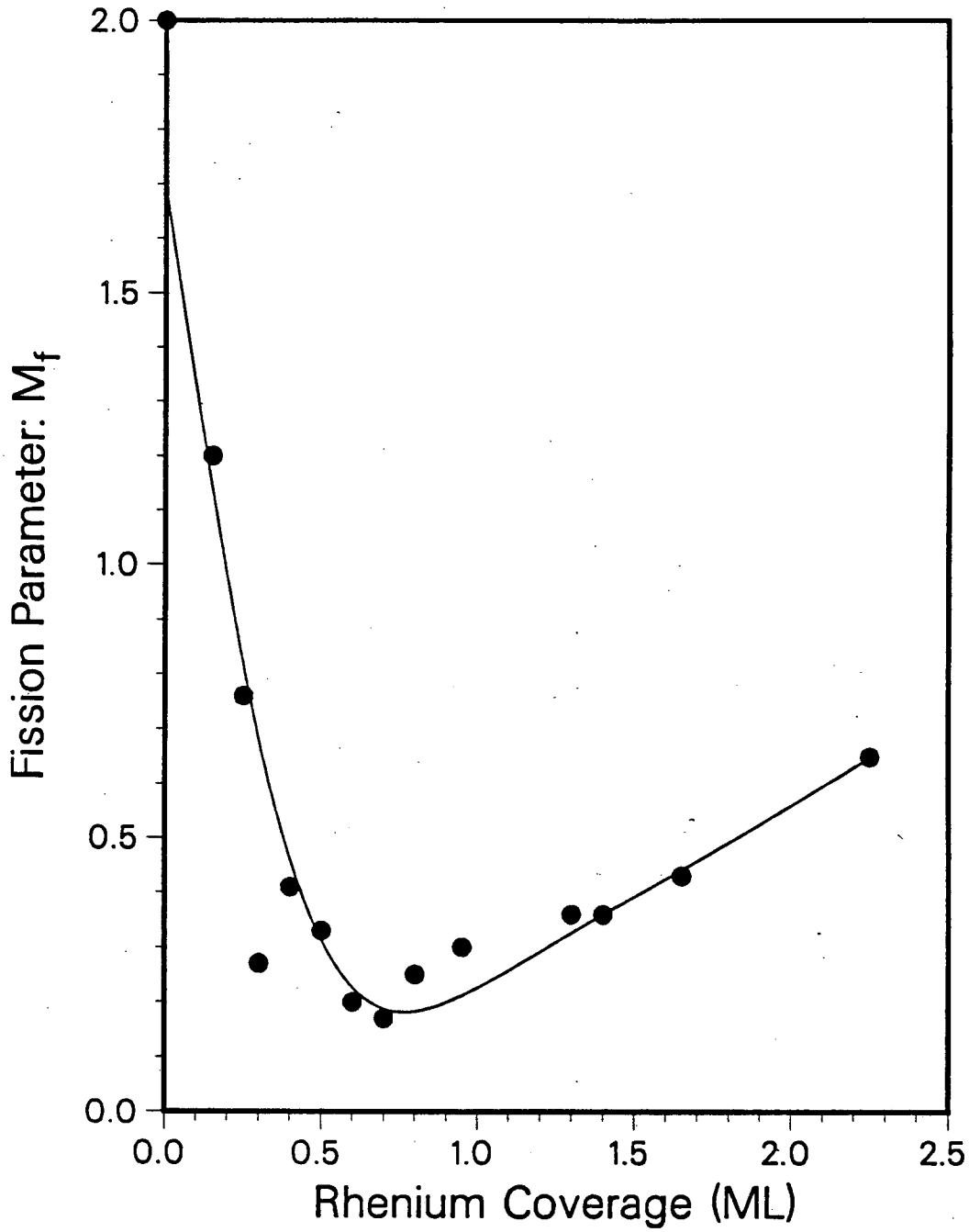

Figure 6.7: Fission parameter vs. rhenium coverage for butane hydrogenolysis over Re–Pt(111) surfaces. The reaction conditions are the same as for Figure 6.6.

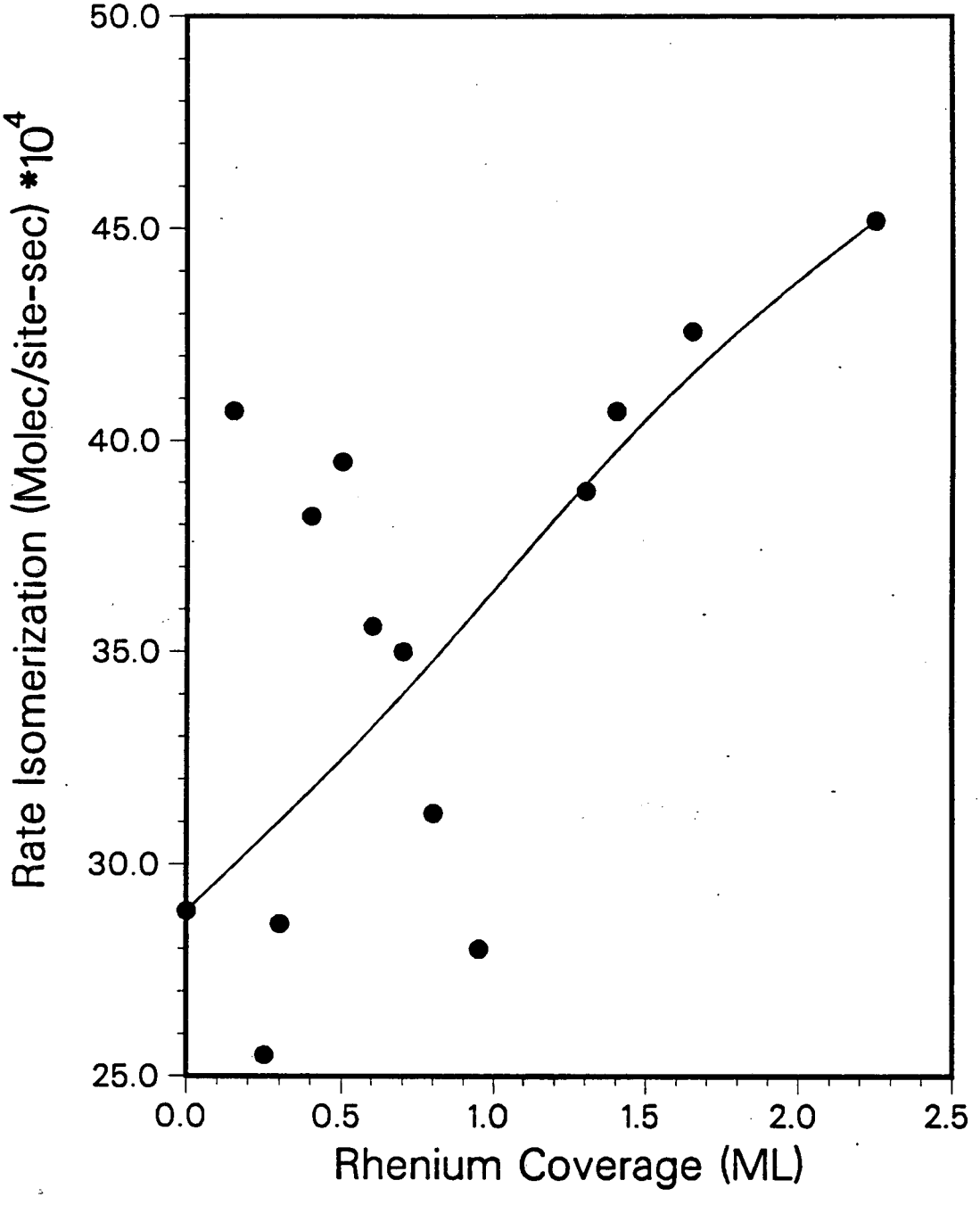

Figure 6.8: Rate of n–butane isomerization vs. rhenium coverage over Re–Pt(111) surfaces. The reaction conditions are the same as for Figure 6.6.

6.4 Re–Pt(111): n–hexane Conversion

The conversion of normal hexane has been studied extensively on both supported and unsupported catalysts [8,9,10,11,12]. There are two other classes of reactions which this molecule can sustain in addition to cracking and bond shift: cyclization and aromatization. In fact, it is the smallest molecule that can undergo the full spectrum of reforming reactions. The formation of five and six membered rings is facile over platinum based catalysts, and cyclohexane (c-C_6H_{12}) and methylcyclopentane (MCP) can be formed from n–hexane (C_6H_{14}). Once cyclohexane is formed, dehydrogenation may follow resulting in the formation of cyclohexene and benzene. The isomerization of n–C_4H_{10} to iso–C_4H_{10} was via a bond shift mechanism, but an additional isomerization path is available to molecules that can undergo cyclization. Once methylcyclopentane is formed, immediate scission of the ring may follow resulting in the formation of 2- and 3-methylpentanes. The reactions of n-C_6H_{14} are shown below.

Reactions of n–hexane

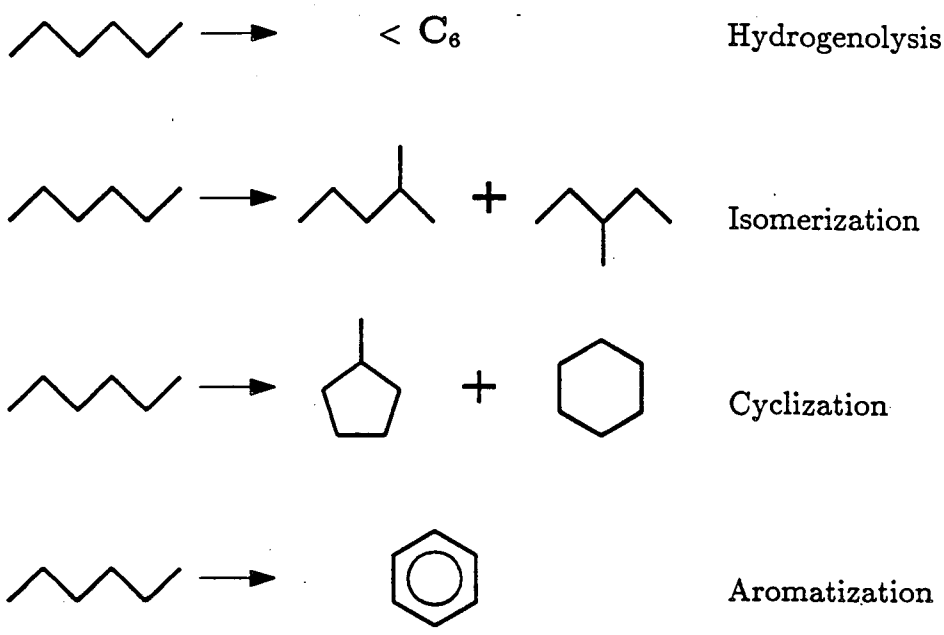

For the series of hydrocarbons containing six carbon atoms, the octane rating of the molecules increase in the order

$$n-\text{hexane} < 2-\text{and } 3-\text{methylpentane} < \text{cyclohexane and MCP} < \text{benzene}$$

It is the purpose of catalytic reforming to generate molecules of higher octane.

6.4.1 Re–Pt(111): Hexane hydrogenolysis

The conversion of hexane was performed under the following conditions: 20 Torr C_6H_{14}, 200 Torr H_2, and T = 300° C. The hydrogenolysis activity of n–hexane over the bimetallic Re–Pt(111) surface was examined as a function of rhenium coverage, and the results are shown in Figure 6.9 along with activity data for the other reforming reactions. The activity is defined as the initial rate of formation of the products. The hydrogenolysis activity was found to increase with the addition

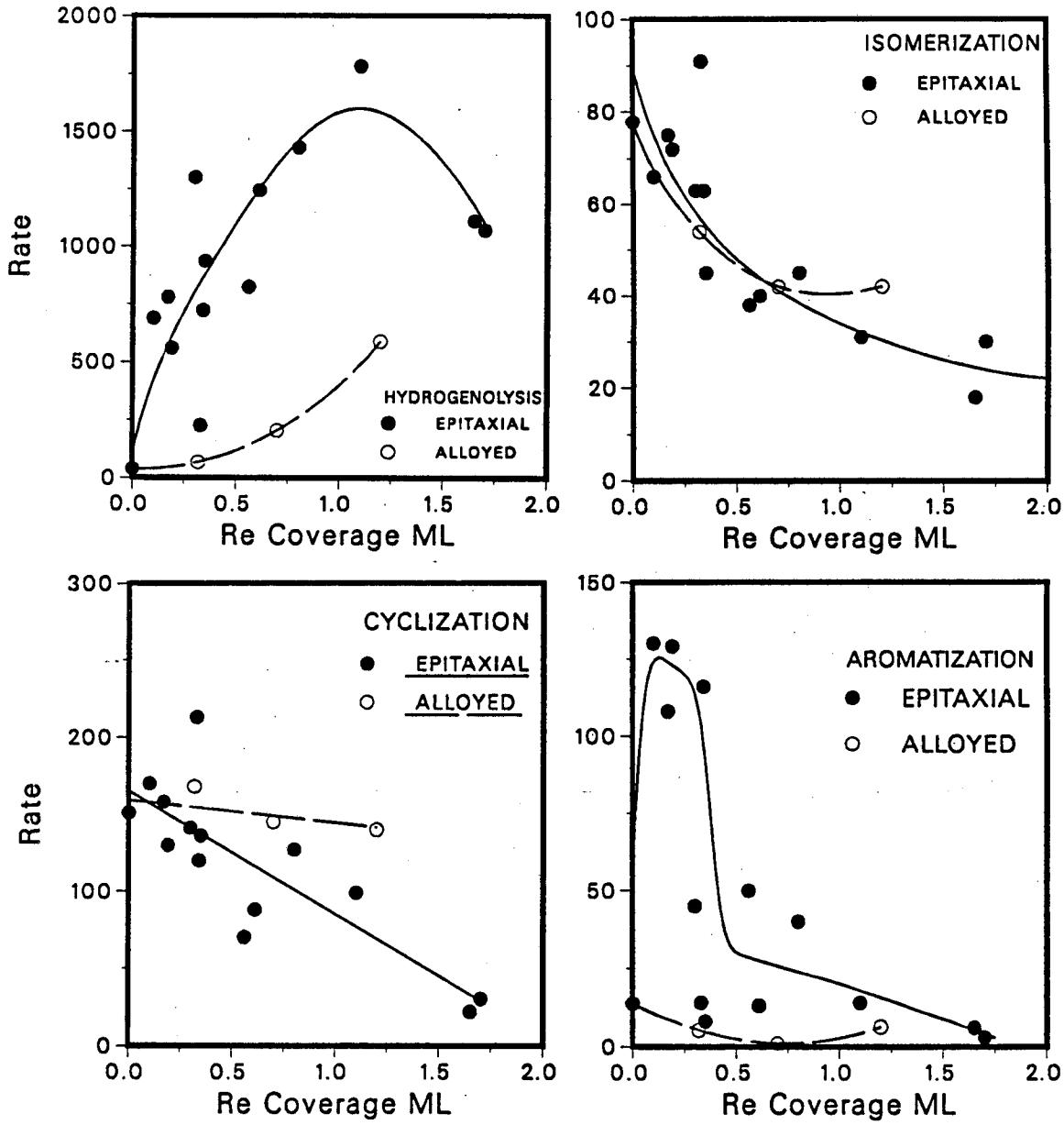

Figure 6.9: Activity of the Re–Pt(111) surface for n–hexane conversion. Shown here are the activities for hydrogenolysis, isomerization, cyclization, and aromatization. The reaction conditions were: $P_{C_6H_{14}}$ = 20 Torr, P_{H_2} = 200 Torr, T = 300° C. Rates in counts/min.

Table 6.2: Rate maxima vs. rhenium coverage for hydrogenolysis products from n–hexane over Re–Pt(111) surfaces.

Molecule	θ^a_{Re}(max)	Rate^b	$R^c_{Pt(111)}$
CH_4	1.1	300	6.4
C_2H_6	0.8	62	1.3
C_3H_8	0.8	37	2.1
C_4H_{10}	0.6	26	0.9
C_5H_{12}	0.4	25	0.8

a. Rhenium coverage (ML) where rate is maximum ± 0.2 ML.
b. Maximum rate observed: HC molecules/site-sec$\times 10^3$.
c. Clean Pt(111) rate: HC molecules/site-sec$\times 10^3$.

of rhenium, and a maximum rate was observed near one monolayer of epitaxially deposited rhenium. Alloyed rhenium overlayers displayed a less dramatic increase in hydrogenolysis with increasing rhenium coverage and this was probably due to an atomically smoother surface. Rate maxima were observed for all hydrogenolysis products and the rhenium coverage at which the rate maximum was obtained was smallest when the hydrocarbon was largest, *i.e.* for pentane. Table 6.2 shows the maximum rate of each hydrogenolysis product and the rhenium coverage where the maximum was observed. The rates obtained on clean Pt(111) is also shown.

The selectivity of a species is defined as the amount of the species produced divided by the total products produced. The selectivity data of products produced from n–hexane is shown in Figure 6.10. Clean Pt(111) produces $\sim$ 50% cracked products, but with just 10% of a monolayer of rhenium added to the surface, the selectivity towards hydrogenolysis approaches 90-95%. The fission parameter was

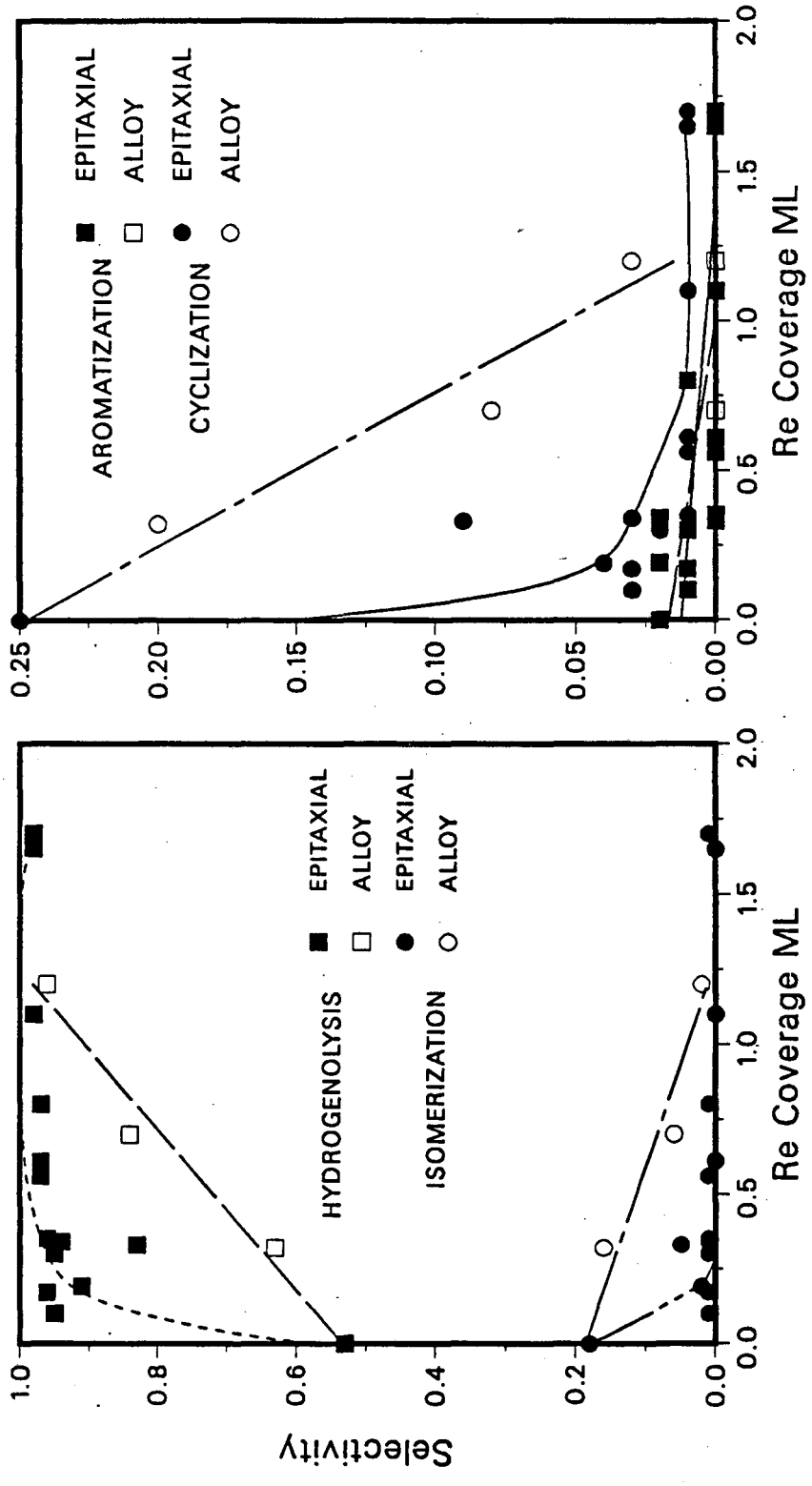

Figure 6.10: Selectivity of the Re–Pt(111) surface during n–hexane conversion. The reaction conditions are the same as for Figure 6.9.

also calculated for n–hexane from Equation 6.4 with $n = 6$. The results are shown in Figure 6.11.

6.4.2 Re–Pt(111): Hexane reforming

The activity of the rhenium–Pt(111) system for isomerization, cyclization, and aromatization is shown in Figure 6.9. The isomerization activity drops with increasing rhenium coverage and the behavior was quite similar whether or not the surface was alloyed. The cyclization activity also drops with increasing rhenium coverage; however, at low rhenium coverages ($\theta_{Re} <$ 0.4 ML) the activity obtained was close to the clean platinum activity. In contrast to isomerization, an alloyed Re–Pt(111) was as active for cyclization as clean Pt(111) up to rhenium coverages of $\theta_{Re} \sim$ 1 ML. Interesting behavior was observed for the aromatization of n–hexane. An enhancement in the rate of benzene formation was observed at rhenium coverages near 0.25 ML, where a five fold increase in benzene formation was observed on surfaces with a rhenium coverage of $\theta_{Re} = 0.2$ ML compared to clean Pt(111). Surfaces with a rhenium coverage of $\theta_{Re} >$ 1.5 ML did not make much benzene, and a smaller activity was observed that was 2-4 times less than the clean Pt(111) activity.

An inspection of Figure 6.10 shows that the selectivity of the Re–Pt(111) surface is dominated by hydrogenolysis, especially for epitaxial rhenium. Alloyed surfaces showed a definite increase in hydrogenolysis selectivity with increasing rhenium coverage, although the increase was not so steep with respect to increasing rhenium coverage as they were for epitaxial surfaces. Perhaps this was due to the difference in the degree of roughness between the alloyed and the epitaxial surfaces.

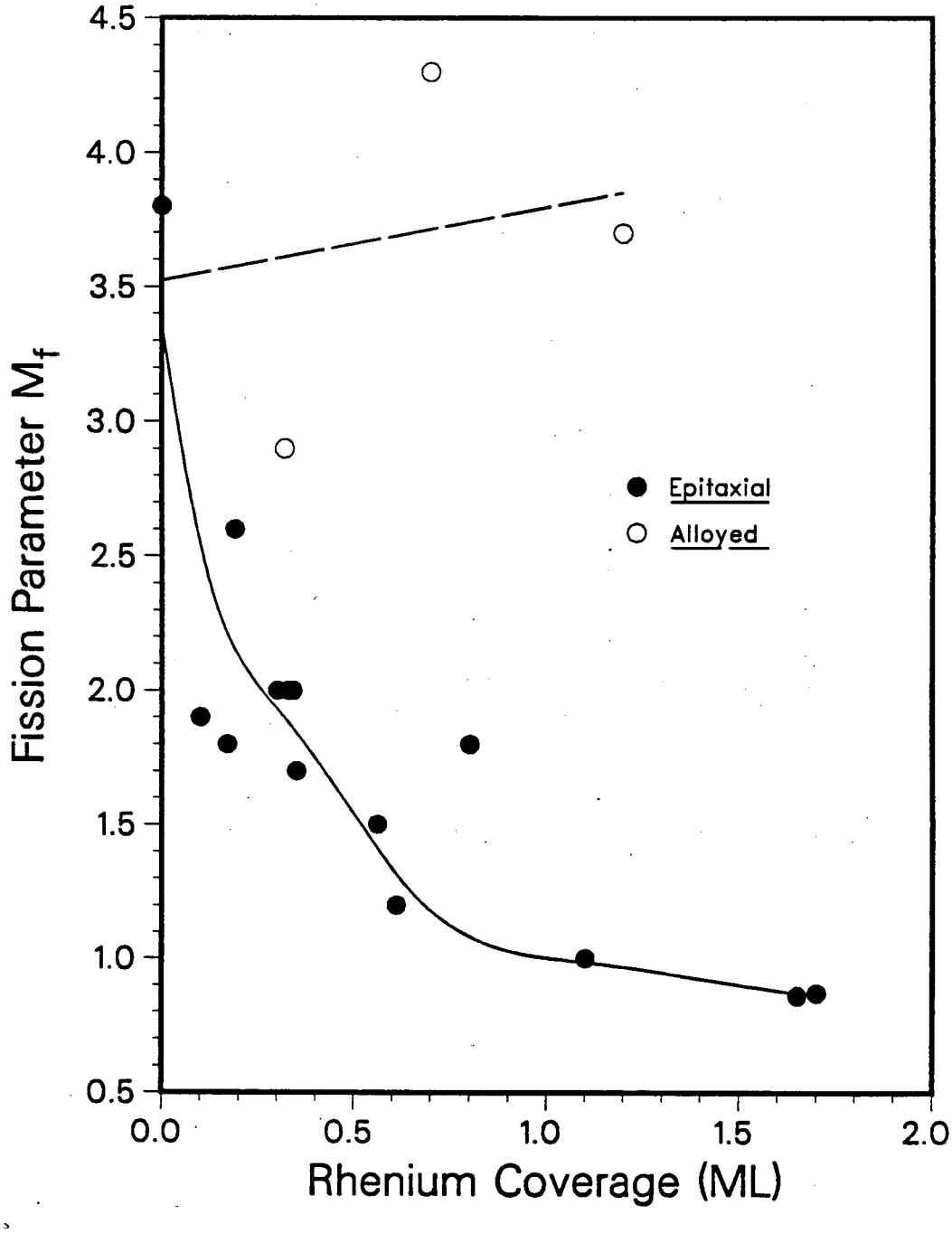

Figure 6.11: Fission parameter vs. rhenium coverage for n– hexane hydrogenolysis over Re–Pt(111) surfaces. The reaction conditions are the same as for Figure 6.9.

Table 6.3: Carbonaceous deposits from n–hexane on Re–Pt(111).

Coverage	Carbon monolayers ± 0.5 ML
$0 \leq \theta_{Re} < 0.7$	2
$\theta_{Re} > 0.7$	1
Alloys $\theta_{Re} > 0.3$	1

6.4.3 Re–Pt(111): The state of the surface following hexane reactions

Post reaction surface characterization was performed as described in Section 6.2.3 following n–hexane reactions. Differences were observed from n–hexane in the amount of carbon left on the surface following a two hour reaction with respect to the rhenium coverage in contrast to the results obtained for C_2H_6 and C_4H_{10} conversion. When the exposed surface had a rhenium coverage greater than two thirds of a monolayer, the amount of carbon left on the surface was about half as much as was left on surfaces exposing more platinum. However, one third of a rhenium monolayer seemed to be enough to keep the surface carbon coverage below 2 monolayers when the surface was alloyed. These results are summarized in Table 6.3.

The hydrogen desorption areas that were obtained from these surfaces were measured, as well as the remaining bare metal sites determined by CO titration. The results were not qualitatively different than those obtained from n–butane regarding the hydrogen content of the surface carbonaceous deposit and the fraction of uncovered metal sites.

6.4.4 n–hexane reactions on Pt(111)

A set of n–hexane reactions were performed over Pt(111) at 5 Torr C_6H_{14} and 760 Torr H_2 at 350°C. The rates obtained in n–hexane molecules/Pt atom-sec were for hydrogenolysis, isomerization, cyclization, and aromatization: 0.026, 0.033, 0.028, and 7.8×10^{-3} respectively. These results will be further discussed in Section 6.7 in conjunction with surface deactivation by carbonaceous deposits.

6.5 Pt–Re Foil: Cyclohexane Conversion

Discussed in the previous sections was the hydrogenolysis of C_2H_6, C_4H_{10}, and C_6H_{14}, as well as isomerization reactions of C_4H_{10} and C_6H_{14}. Platinum is known to be an extremely effective dehydrogenation catalyst, and some investigators have suggested that the role of rhenium is to moderate the deep dehydrogenation characteristic of platinum [13,14,15]. In order to investigate the dehydrogenation activity of well characterized Pt–Re catalysts, the conversion of cyclohexane was examined.

6.5.1 Cyclohexane hydrogenolysis

The reaction conditions used for cyclohexane were: 20 Torr c-hexane, 200 Torr of H_2, and T = 300° C. The hydrogenolysis activity of a rhenium foil was higher when platinum was added to the surface. The hydrogenolysis activity of this system towards cyclohexane is shown in Figure 6.12 where the rates of formation of CH_4, C_2H_6, and C_3H_8 are shown vs. platinum coverage. A maximum rate of formation of CH_4 was observed near 0.2 monolayers of platinum. The rates of formation of C_2H_6 and C_3H_8 were also observed to maximize, although these

maxima were broader with respect to platinum coverage. The hydrogenolysis activity was also nearly an order of magnitude less from cyclohexane than the hydrogenolysis activity observed from n–hexane.

6.5.2 Cyclohexane aromatization

The formation of benzene (C_6H_6) from cyclohexane was the most abundant product obtained from all the surfaces tested. The initial rate of formation of benzene was one to two orders of magnitude higher than the initial rate of formation of methane over a clean rhenium foil, and on a rhenium foil covered with a monolayer of platinum, the rate of formation of benzene compared to methane was four to five orders of magnitude higher. A plot of the initial aromatization rates versus platinum coverage is shown in Figure 6.13. The rate of formation of benzene was maximum around one monolayer of platinum.

6.5.3 Deactivation behavior of cyclohexane on a Pt–Re foil

The formation of aromatics is quite important for the generation of high octane fuels from a naphtha feedstock. The industrial Pt–Re catalyst after sulfidation is reported to behave very much like a monometallic platinum catalyst except for the deactivation behavior [13,16]. For this reason, the deactivation behavior was examined for cyclohexane on Pt–Re foils. Following an initial reaction of around 2 hours, the high pressure cell was evacuated and subsequently repressurized with a fresh reaction mixture. The product accumulation was then monitored under identical reaction conditions. This process was sometimes repeated an additional time. Product accumulation curves for restart studies over surfaces with two different platinum coverages are shown in Figure 6.14.

The activities for the initial run for both these surfaces were similar. It had

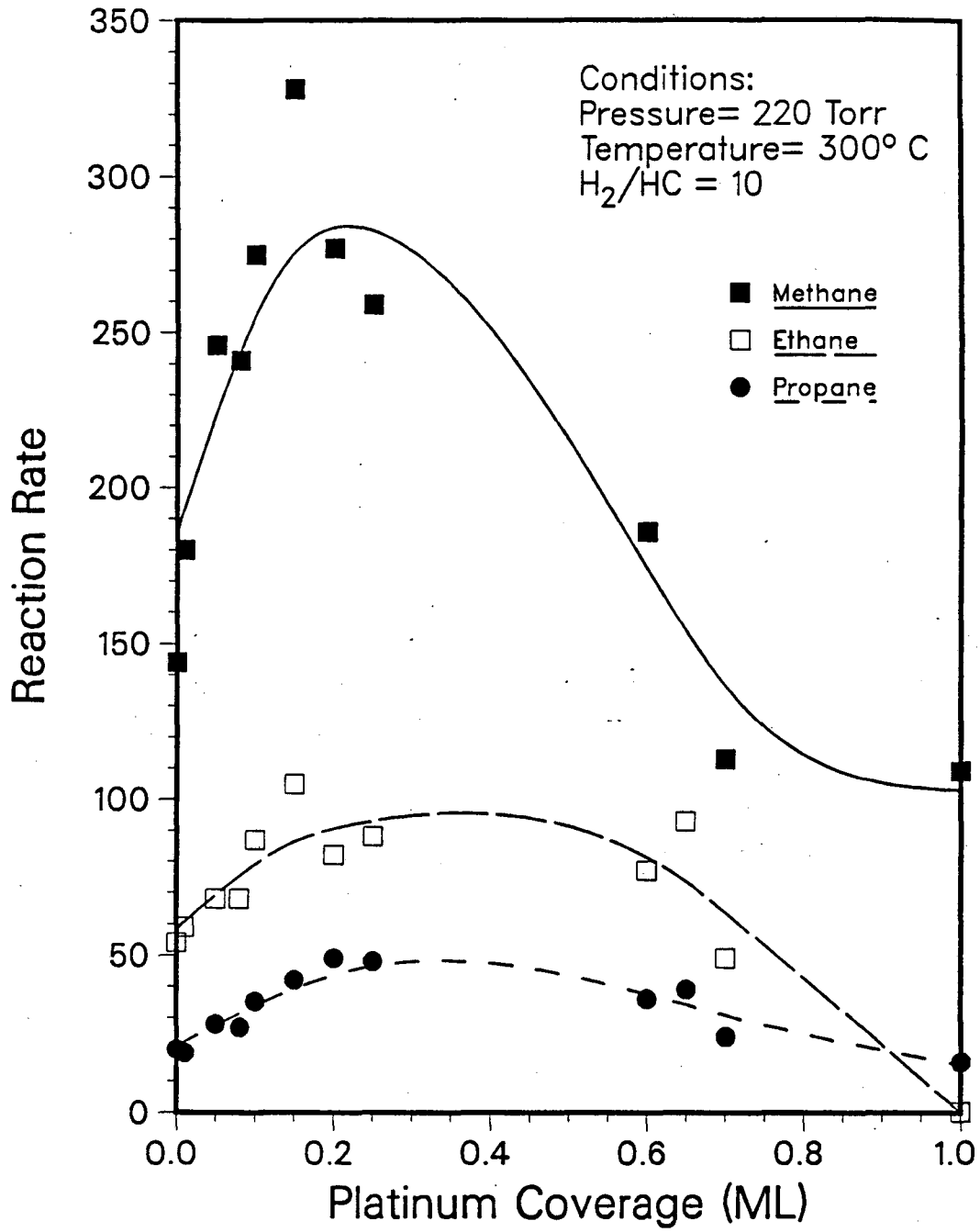

Figure 6.12: Cyclohexane hydrogenolysis vs. platinum coverage for a Pt–Re foil. The reaction conditions were: $P_{c-C_6H_{12}}$ = 20 Torr, P_{H_2} = 200 Torr, and T = 300° C. Rates in counts/min.

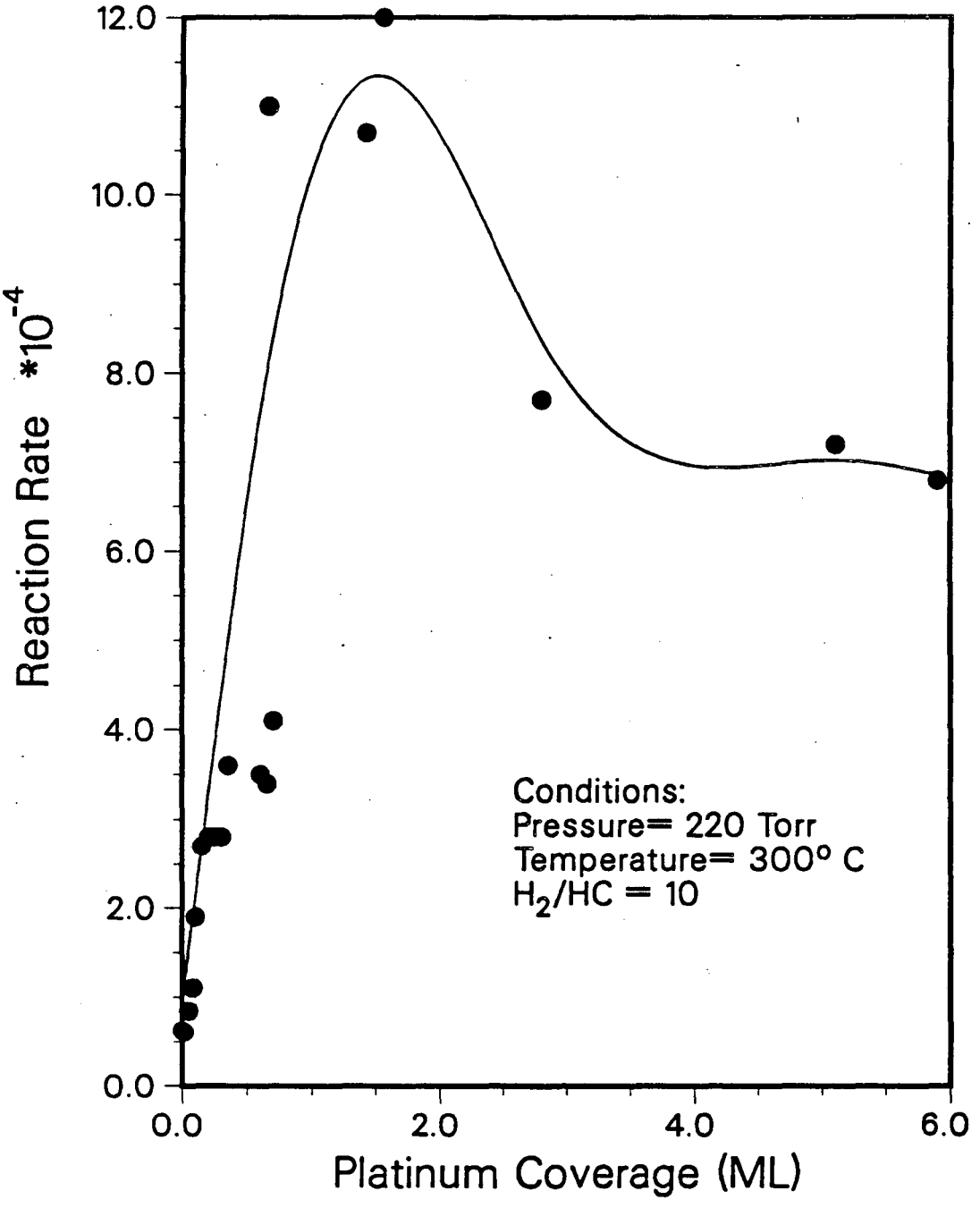

Figure 6.13: Cyclohexane aromatization rate vs. platinum coverage for a Pt–Re foil. The reaction conditions are the same as for Figure 6.12. Rates in counts/min.

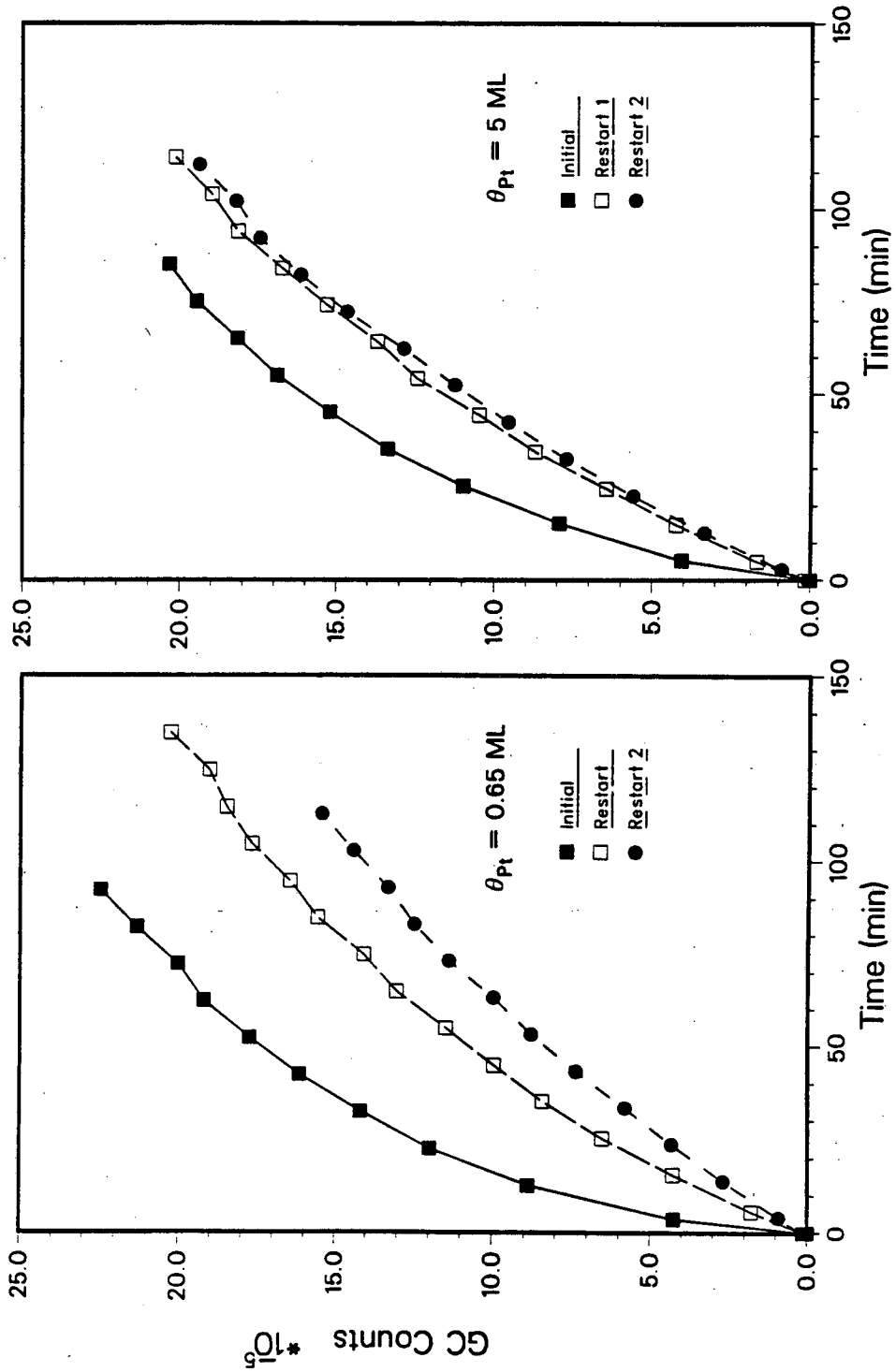

Figure 6.14: Product accumulation of benzene from cyclohexane for Pt–Re foils. The left panel shows results for a surface composed of θ_{Pt} = 0.65 ML; the right panel shows results for a surface with a thick 5 ML platinum film. The reaction conditions are the same as for Figure 6.12. Rates in counts/min.

been previously observed that clean rhenium foil continually deactivates with time for the cyclohexane reaction. What is meant by continuous deactivation is as follows: Three consecutive cyclohexane runs are performed. The initial aromatization rate of the second run (first *restart* run) was less than the initial rate of the first run (performed over a clean surface) over all surfaces tested; this was the *initial* deactivation observed over all surfaces. If the initial rate of the third run (second restart run) is significantly less than the initial rate of the first restart run, then *continuous* deactivation was observed over that surface. Continuous deactivation was observed over the surface with a platinum coverage of $\theta_{Pt} \sim$ 0.65 ML illustrated in Figure 6.14. It appears that when rhenium was exposed on the surface, continuous surface deactivation was observed. When five monolayers of platinum were present completely covering the rhenium substrate, initial deactivation was still observed but continuous deactivation was not. In fact, the second restart reaction gave a product accumulation curve that almost traced over the product accumulation curve of the first restart reaction. This indicates that following an initial accumulation of deactivating species on the surface, the surface became passivated towards further deactivation when only platinum was exposed on the surface. On one occasion a thick platinum film on the rhenium foil was exposed to the reaction mixture for the first restart reaction overnight (14 hours) under reaction conditions. Equilibrium had been obtained by morning of the reaction mixture. Following evacuation and repressurization with a fresh reaction mixture, the second restart reaction performed gave an accumulation curve that retraced the initial part of the first restart accumulation curve, indicating that following the rapid initial deactivation, deactivation was very slow.

The conversion of cyclohexane to benzene on the surfaces whose rates are displayed in Figure 6.13 are shown in Figure 6.15 for the initial reaction of cy-

clohexane, and for the second restart reaction, both measured at 60 minutes of reaction time. The initial conversion plot shows a maximum (Figure 6.15) which reflects the maximum in initial rates observed in Figure 6.13. Restart conversions show a similar trend in this plot (Figure 6.15), and an increase in conversion with increasing platinum coverage was observed until a plateau was reached above one monolayer of platinum. The deactivation is shown by the ratio obtained between the two curves of Figure 6.15 and this ratio is plotted in Figure 6.16. Here it can be seen that about 55% of the rhenium surface is deactivated when no platinum is present, and that the amount of deactivation decreased to around 25% when 6 ML of platinum had been deposited on the surface.

The deactivation of the surface is further illustrated in Figure 6.17. This Figure shows that the second restart rate was always less than the first restart rate when rhenium was exposed on the surface indicating a continuous deactivation of the surface; when no surface rhenium was exposed these two rates were very close indicating a very slow continuous deactivation over platinum for the aromatization of cyclohexane.

6.6 Re–Pt(111): Methylcyclopentane Conversion

The conversion of methylcyclopentane (MCP) was performed under the following conditions: 5 Torr MCP, 760 Torr of H_2, and at 350°C. Higher hydrogen pressures were necessary because the co-elution of some olefin (probably methylcyclopentene) was observed with the methylpentanes. The high hydrogen pressures employed shifted the equilibrium towards the saturated parent compound, and therefore minimized the distortion of the observed 3- to 2-methylpentane ratio. The changing 3- to 2-methylpentane ratio with time previously reported for

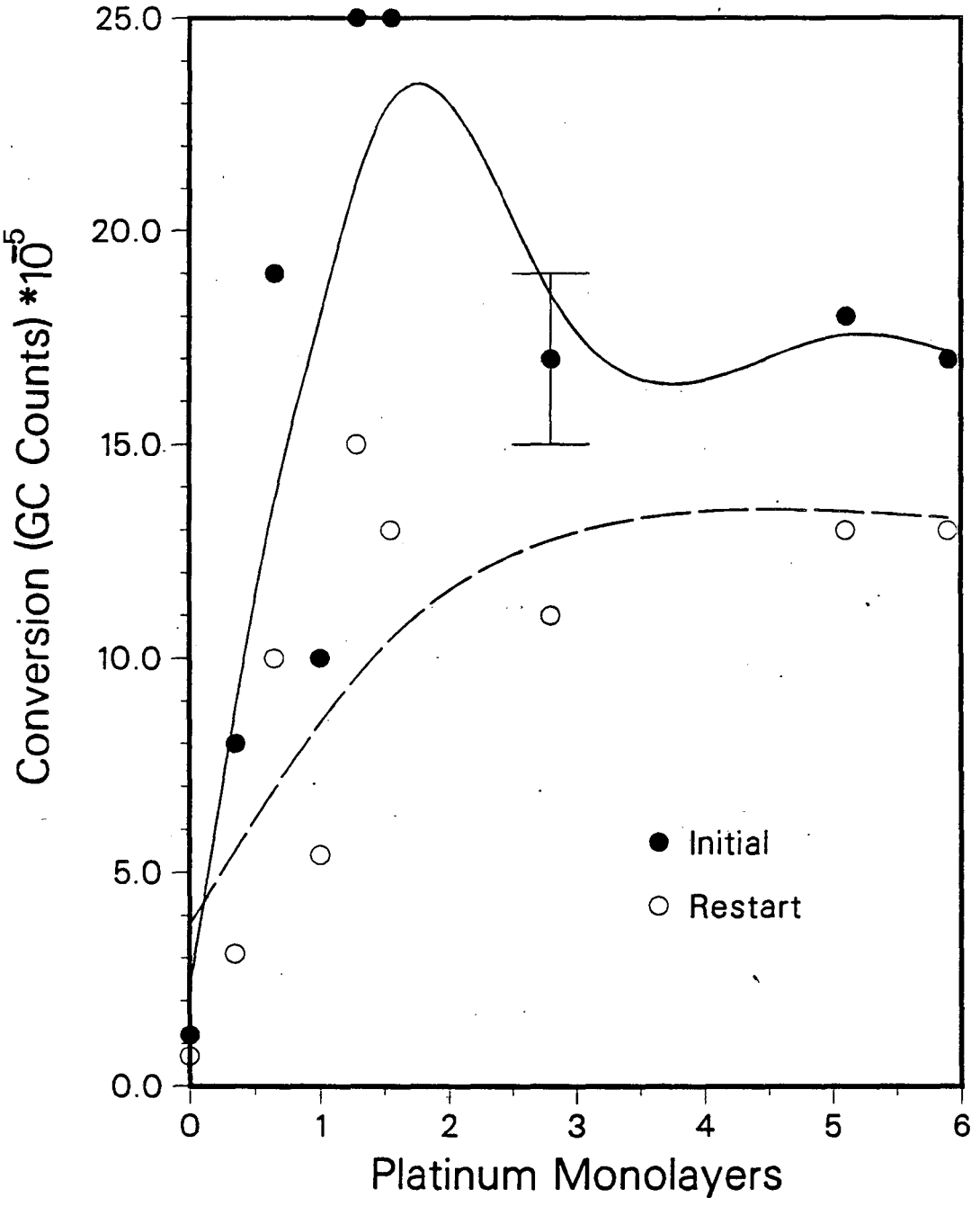

Figure 6.15: Total conversion of cyclohexane to benzene vs. platinum coverage over Pt–Re foils obtained at 60 minutes of reaction time. The reaction conditions are the same as for Figure 6.12.

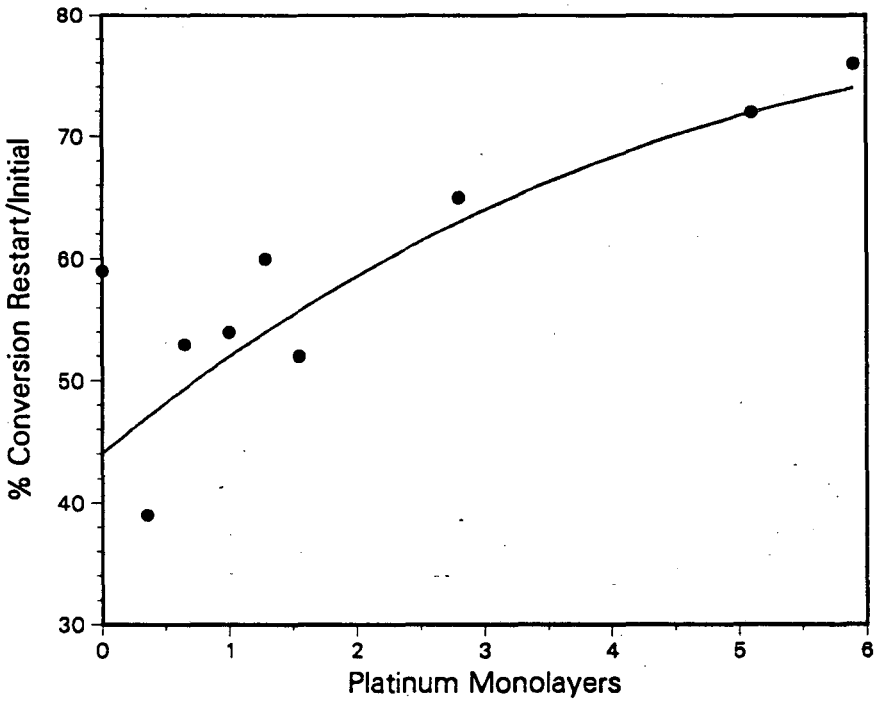

Figure 6.16: Ratio of the curves of Figure 6.15 give the restart/initial conversion at 60 minutes of reaction time vs. platinum coverage.

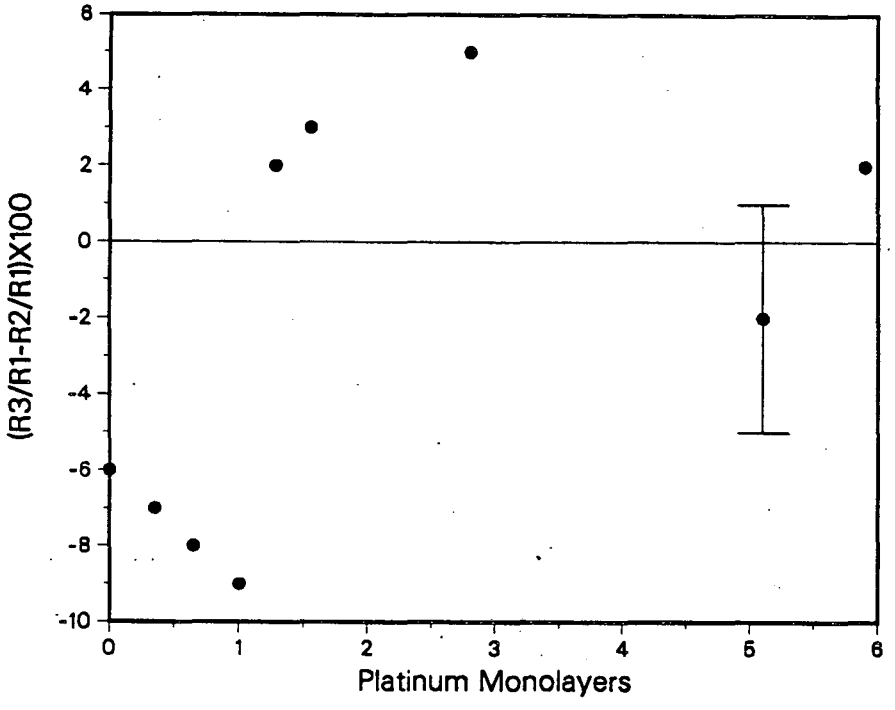

Figure 6.17: Deactivation of Pt–Re foil surfaces vs. platinum coverage for the aromatization of cyclohexane. The ordinate axis reflects the difference in the two restart reactions for a given platinum coverage. A negative value indicates that continuous deactivation of the surface is operating, while a value of 0 indicates that no continuous deactivation is occurring.

both n–hexane and MCP conversion was probably due to the co-elution of this olefin [10,12]. The reactions of MCP are shown below.

Reactions of Methylcyclopentane

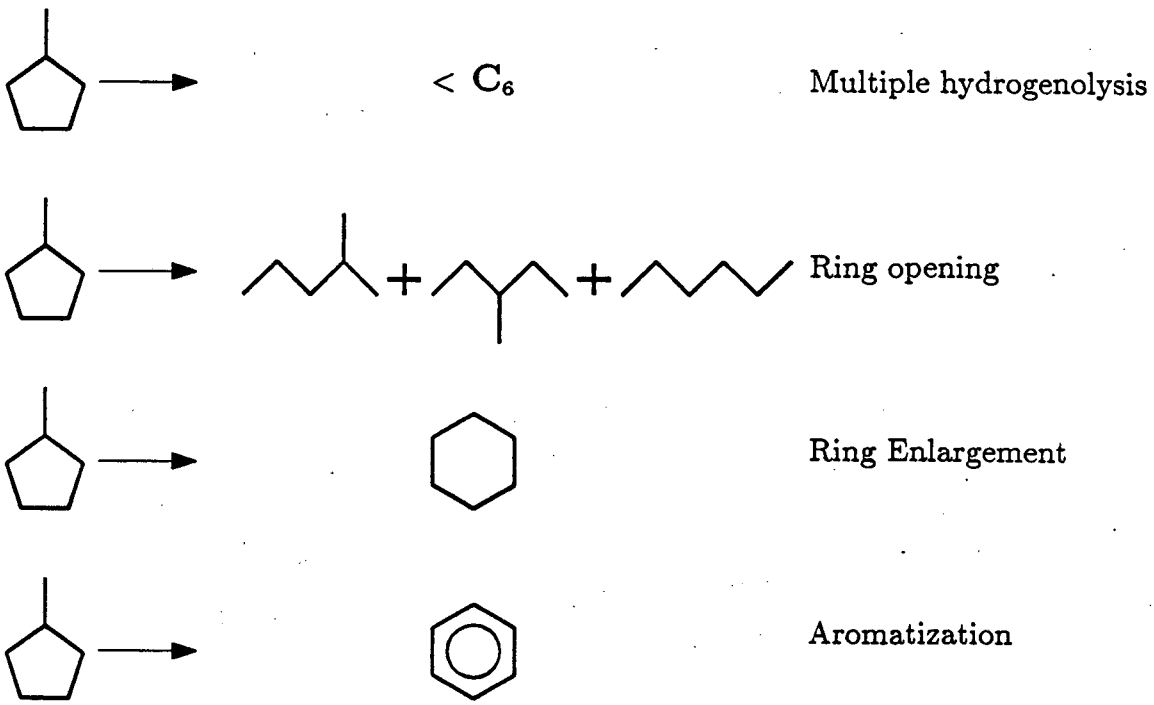

Hydrogenolysis of MCP refers to multiple cracking and desorption of hydrocarbons smaller than six carbon atoms, while ring opening refers to the rupture of a single C–C bond and desorption of n–hexane, 2–, or 3–methylpentane (2–, 3–MP).

Under the reaction conditions used, the hydrogenolysis and ring opening reactions were important, but not the ring enlargement or aromatization reactions. The ring enlargement mechanism is reported to be mainly an acid catalyzed function [14,17,18], and is perhaps the reason that formation of C_6 rings occurs only to a limited extent on unsupported metal catalysts from C_5 rings.

MCP reactions were performed over three metallic surfaces: clean Pt(111), 0.15 ML of rhenium on Pt(111), and 0.4 ML of rhenium on Pt(111). The hydrogenolysis and ring opening rates are shown in Table 6.4, and the selectivity

Table 6.4: Initial reaction rates for multiple hydrogenolysis and ring opening of MCP over Re–Pt(111). The reaction conditions were: P_{MCP} = 5 Torr, P_{H_2} = 760 Torr, T = 350° C. The rates are given in MCP molecules/site-sec$\times 10^4$.

θ_{Re} (ML)	$\Sigma < C_6$	n-Hex + 2MP + 3MP
0	61	1915
0.15	384	1425
0.4	938	925

results are shown in Table 6.5. With the addition of rhenium to Pt(111), the hydrogenolysis rates were always observed to increase relative to clean Pt(111). In fact, an increase in the rate of production of all hydrogenolysis products was observed to increase when rhenium was added to the surface. This includes the rate of production of pentane, isopentane, and cyclopentane. However, the rate of formation of ring opening products, n–hexane, 2–MP, and 3–MP, was always found to decrease when rhenium was added to the surface. Technically, ring opening is a hydrogenolysis reaction, but apparently the ring opening products do not desorb readily from rhenium, rather multiple hydrogenolysis reactions prevail on these surfaces. It was found that the rate of ring-opening was almost proportional to the area of surface platinum exposed. The relative rates of hydrogenolysis and ring opening are summarized in the first panel of Figure 6.18, and the distribution of products formed during these experiments are tabulated in Table 6.6.

Table 6.5: Ring opening selectivities for MCP over three Re–Pt(111) surfaces.

θ_{Re} (ML)	$\frac{\text{3-MP}}{\text{n-hex}}$	$\frac{\text{2-MP}}{\text{3-MP}}$
0	4.5	2.3
0.15	3.4	2.5
0.4	n.d.	2.7

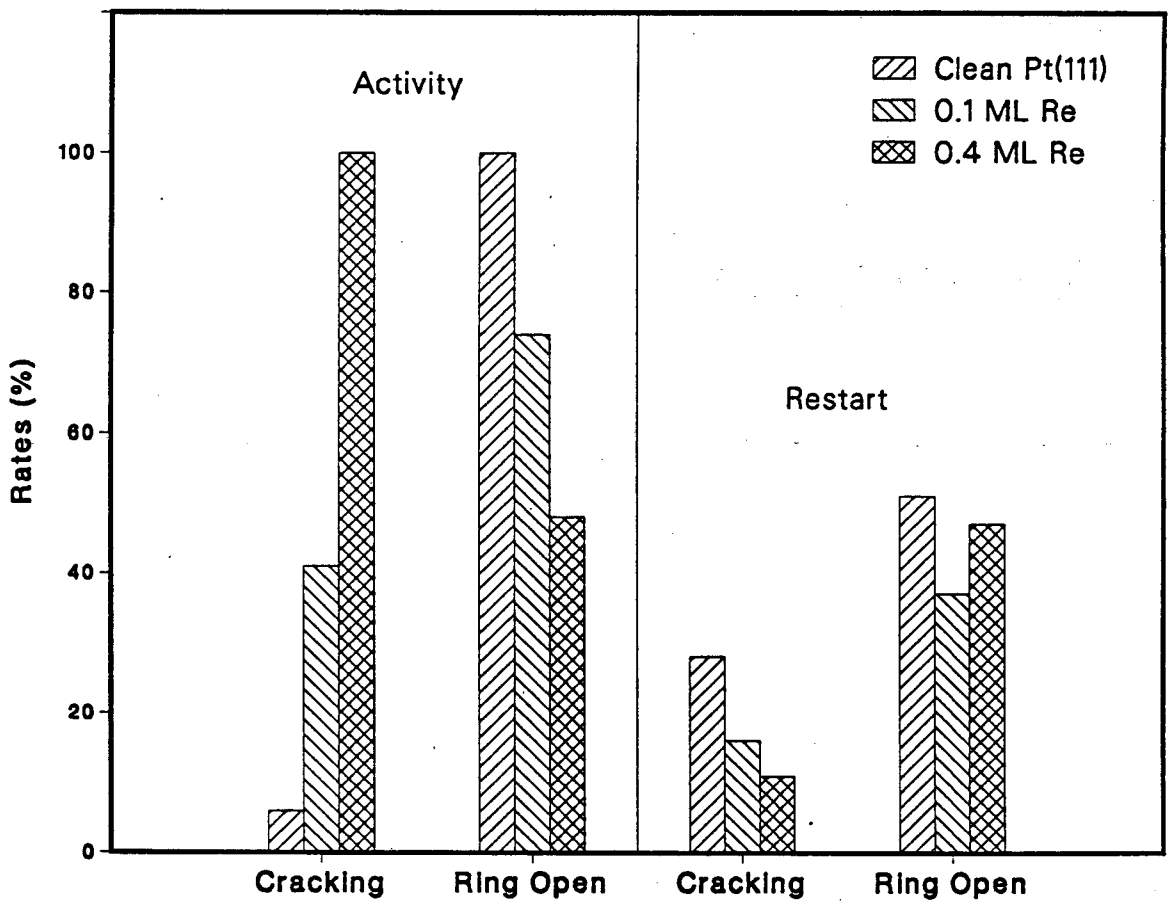

Figure 6.18: Relative rates of hydrogenolysis and ring opening from MCP over Re–Pt(111) surfaces. The left panel shows the rates relative to the most active surface. The right panel shows the restart rates relative to the initial rates shown in the left panel. The reaction conditions were: P_{MCP} = 5 Torr, P_{H_2} = 760 Torr, T = 350° C.

Table 6.6: The production of hydrocarbons from MCP and n–hexane after 2 hours reaction time on Pt(111), 0.15 ML Re–Pt(111), and 0.40 ML Re–Pt(111). The conditions were 5 Torr hydrocarbon, 760 Torr H_2, and T = 350° C.

	θ_{Re}: MCP			n–hexane
HC	0	0.15	0.4	$\theta_{Re} = 0$
C1	1584	23110	98770	4102
C2	1764	–	–	2623
C3	3976	9008	14880	1420
*i*C4	3007	10150	17220	1257
C4	1199	5588	8760	6292
CP	809	2270	2611	728
*i*C5	1486	26140	27530	502
C5	1248	11060	7474	9656
CH	433	266	–	2632
C6	19050	13850	4022	–
MCP	–	–	–	32375
3MP	97040	45450	21690	21220
2MP	214600	120600	60440	37780

The entries are in counts, and can be converted to turnovers (molecules/Metal atom) by multiplying with 2.5×10^{-3} per carbon number in the product molecule. Cn indicates linear hydrocarbon with n carbon atoms, *i*Cn indicates iso-Cn, CP = cyclopentane, CH = cyclohexane.

6.7 Surface Deactivation by Hydrocarbons

The major advantage of utilizing the platinum–rhenium catalyst over a monometallic platinum catalyst is the enhanced activity maintenance exhibited by the bimetallic catalyst. This section is divided into two parts: the self-deactivation of MCP over Pt(111) and bimetallic Re–Pt(111) surfaces, and the differences in deactivation activity displayed by several hydrocarbons over Pt(111). The object of this study was to work up some protocol by which to measure the deactivation of the reforming catalyst as a function of the metallic composition of the surface.

6.7.1 Re–Pt(111): Self-deactivation of MCP

The discussion of the MCP conversion experiments are also divided into two parts; the first part, already having been discussed in Section 6.6, was concerned with the initial activities of Pt(111) and bimetallic Re–Pt(111) surfaces. Now the deactivation of these surfaces using restart reactions as described in Section 6.5.3 for cyclohexane experiments are discussed.

Restart reactions were performed using MCP following the initial reactions of Section 6.6. The results obtained are shown in the restart (right) panel of Figure 6.18. Here the bars have a slightly different meaning than the bars in the first panel. The ratio of the restart rates to the initial rates are shown by each bar. The right panel in Figure 6.18 shows that the ratio of the restart/initial rates of hydrogenolysis are smaller with a larger surface rhenium coverage. The bimetallic surfaces always displayed a higher activity towards hydrogenolysis than did clean Pt(111); however, the bimetallic surface deactivated towards hydrogenolysis activity more quickly than the monometallic Pt(111) surface.

The behavior of the surfaces towards ring opening was different. It has already

been observed that ring opening behaves more like an isomerization reaction since the desorption rate of ring opening products is smaller when platinum is covered with rhenium compared to monometallic platinum. Restart reactions showed that the deactivation of the surface toward ring opening was relatively insensitive to the surface rhenium coverage, where restart activities observed were always 40-50% of the initial activity on the same surface.

6.7.2 Pt(111): Deactivation by hydrocarbons

Three molecules were examined in these experiments, and the ability of each molecule to deactivate the Pt(111) surface towards the conversion of each of the reactants examined. The molecules used were MCP, n–hexane, and cyclohexane. The results of these experiments are shown in Figure 6.19, where each bar represents an initial restart rate obtained after a reaction was performed using the "poison". The restart rate is compared to an initial rate obtained on a clean "unpoisoned" Pt(111) surface of the same reactant molecule.

Methylcyclopentane reactions were performed on a Pt(111) surface following deactivation by an MCP or a cyclohexane reaction. It can be seen that MCP was more effective in deactivating the surface towards MCP reactions than was c-hexane. Normal hexane reactions were deactivated by MCP and n–hexane. In this case, n–hexane deactivated hydrogenolysis and isomerization reactions more effectively, but MCP still deactivated the surface more effectively towards aromatization. Finally, cyclohexane reactions were deactivated by MCP and c-hexane reactions. MCP deactivated the surface most effectively for the dehydrogenation of c-hexane.

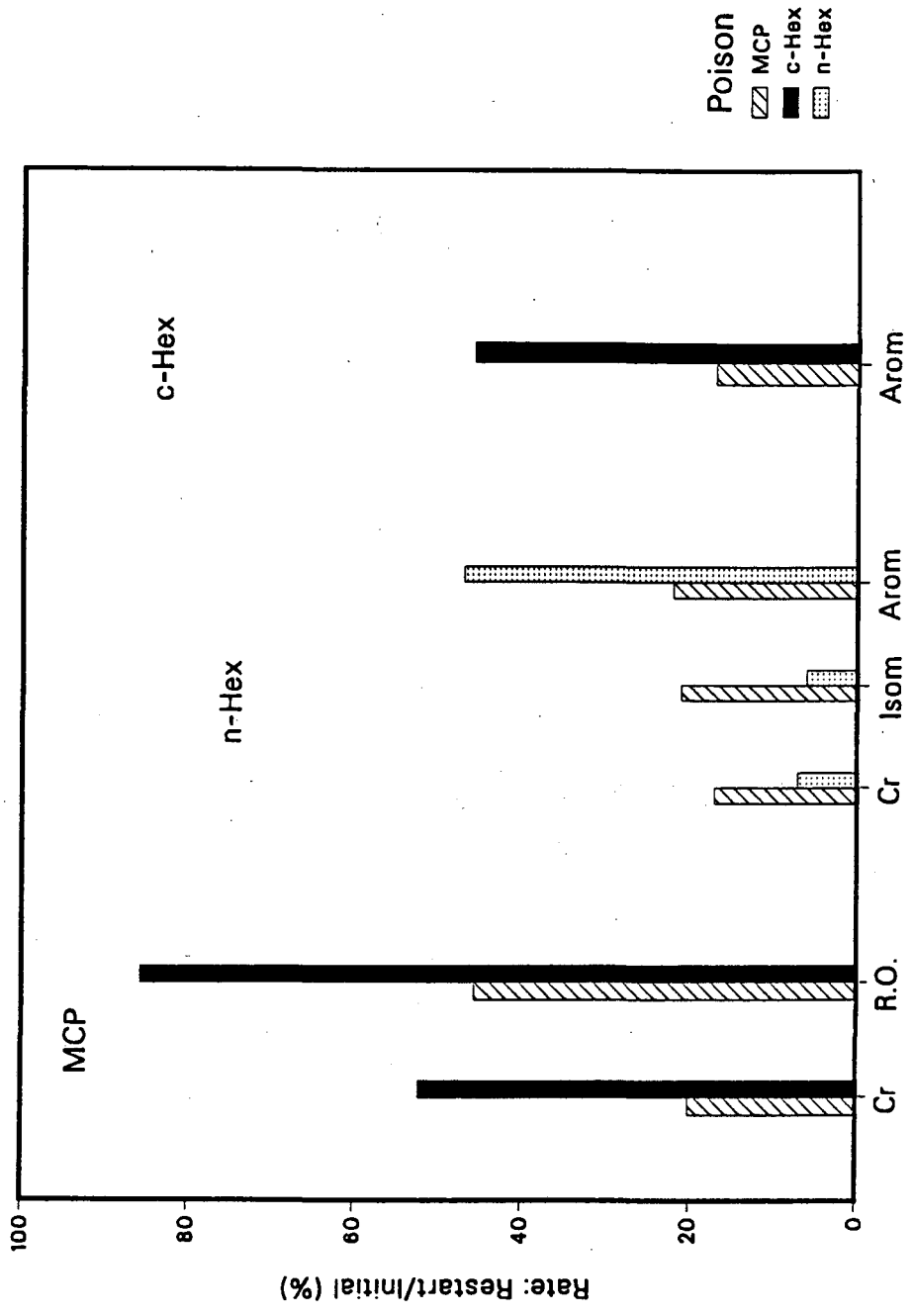

Figure 6.19: Deactivation of Pt(111) surfaces by MCP, n–hexane, and cyclohexane. Each bar in this figure represents a ratio of restart/initial rates when a surface was first deactivated by a particular hydrocarbon that is represented by the shading of the bar. The initial rate was obtained over an initially clean Pt(111) surface. The reaction conditions were: $P_{HC} = 5$ Torr, $P_{H_2} = 760$ Torr, and T = 350° C.

6.8 Discussion: I. The Conversion of Hydrocarbons

The bimetallic platinum–rhenium catalyst has been used heavily in petroleum refineries since its introduction in 1968 by Chevron [19]. Even though it has been studied extensively for almost 20 years, the role played by rhenium in making the bimetallic a better catalyst than the monometallic platinum catalyst is not well understood. Although it is fairly well accepted that the metals are alloyed in the working reforming catalyst [13,20], there are still those who favor an independent mode of operation of each metal; *i.e.* that the catalyst can operate as well with separate independently supported unalloyed platinum and rhenium particles [21,22]. In this Chapter has been described the behavior of hydrocarbon systems where the composition of the metallic Pt–Re surfaces are known with a good deal of certainty. For this reason correlations between the behavior of the catalyst and *surface* composition can be made. In the following discussion the importance of the metallic interaction between platinum and rhenium as it pertains to the conversion of hydrocarbons is analyzed.

6.8.1 Ethane and butane hydrogenolysis

Hydrogenolysis was found to be an important reaction pathway on all the surfaces examined and for all the hydrocarbons tested with the exception of cyclohexane. Cyclohexane did not crack at an appreciable rate over a platinum covered rhenium foil, and when platinum was absent from the rhenium surface, aromatization still dominated since the production rate of benzene was an order of magnitude higher than the production rate of methane. In all cases examined, it was found that hydrogenolysis was highest on a mixed platinum–rhenium ensemble. The magni-

Table 6.7: Hydrogenolysis enhancement of platinum–rhenium surfaces for several hydrocarbons.

System/Molecule	$\theta_{ads}(max)^a$	$\frac{R_{max}}{R(\theta=0)}{}^b$	$\frac{R(\theta=\infty)^c}{R(\theta=0)}$
Re–Pt(111)/Ethane	0.7	10^3	10^2
Re–Pt(111)/n–butane	0.6	150	50
Re–Pt(111)/n–hexane	1	35	20
Pt–Re(0001)/Ethane	0.4	3–5	<1
Pt–Re foil/Cyclohexane	0.3	2	<1

a. Adsorbate coverage where hydrogenolysis rate was maximum.
b. Rates ratio between most active surface and uncovered substrate.
c. Rates ratio between covered substrate (> 2 ML) to clean substrate.

tude of the increase in hydrogenolysis over the most active surface compared to the least active surface (platinum) was highest for the smallest molecule tested, C_2H_6. The larger the molecule, the less pronounced was the increase in cracking; but the increase was always substantial. A summary of the hydrogenolysis reactions is shown in Table 6.7, and bell shaped curves of hydrogenolysis activity vs. adsorbate coverage are indicated for each system since the value in the second to last column of Table 6.7 was always less than 1 and larger than the value in the last column.

The earliest experiments performed to explore catalytic activity vs. surface metallic composition was done using ethane. The reason this system was chosen was because of the large difference in activity towards hydrogenolysis displayed between platinum and rhenium as reported by Sinfelt and coworkers [2,3,23]. The

experiments shown in Figure 6.1 demonstrate a large difference in activity also exists over single crystal catalysts. These experiments showed a difference in activity between the clean metal surfaces of only 2 orders of magnitude in contrast to Sinfelt's paper which reports a 5-6 orders of magnitude difference between platinum and rhenium.. The reason for this discrepancy is possibly due to the differences in dispersion between the supported catalysts investigated by Sinfelt and the single crystal catalysts used here.

The C_2H_6 hydrogenolysis activity of platinum was low under the conditions used. However, when rhenium was added to the surface the hydrogenolysis activity increased, and near one third of a monolayer of rhenium, the activity was close to the activity of a Re(0001) surface (Figure 6.1). A surface with a rhenium coverage between $0.3 < \theta_{Re} < 1$ monolayers displayed an activity greater than a Re(0001) surface, and a maximum rate of CH_4 formation was obtained near 2/3 of a monolayer. One obvious explanation for the higher rates observed on a mixed Pt–Re ensemble is an alloying effect, which will be discussed. However, another possibility is that the reaction is structure sensitive, and less coordinated rhenium atoms exposed on the surface may be more active to account for the higher activity. This explanation is plausible because C_2H_6 hydrogenolysis is structure sensitive over platinum because a roughened surface was about 10 times more active than a well annealed Pt(111) surface as shown in Figure 6.1.

A Re(0001) surface roughened in a similar way also displayed a higher C_2H_6 hydrogenolysis activity by a factor of four over the well annealed surface (Figure 6.3). To prove that a synergistic effect due to alloying was responsible for the hydrogenolysis enhancement of a mixed ensemble, experiments were performed on the rhenium basal plane (the Re(0001) surface) and bimetallic platinum–rhenium surfaces derived from this surface. When the less active platinum metal is added

to a rhenium surface, the activity should drop unless an alloying or electronic effect is operative. The results from these experiments are shown in Figure 6.3 and provide clear proof that an electronic perturbation is experienced between the two metals when they are in intimate contact. For the Pt–Re(0001) system a maximum rate of methane formation was observed close to one third of a platinum monolayer. A surface with between two thirds and one monolayer of platinum had an activity quite close to the clean Re(0001) activity. This interesting result demonstrates that a single monolayer of platinum can make a good cracking catalyst when perturbed by an underlying rhenium substrate. When bimetallic surfaces were annealed to 1150 K to form an alloy, an even larger enhancement was observed in C_2H_6 hydrogenolysis. For this situation it can be argued that more rhenium atoms are exposed on the surface than determined by AES because several metallic layers are sampled by this technique. When platinum diffuses underneath the surface layer, rhenium atoms left exposed on the surface sitting on top of platinum atoms are very active for C_2H_6 hydrogenolysis. In fact, the two surfaces that gave the highest C_2H_6 hydrogenolysis activity were the 2/3 of a rhenium monolayer deposited on Pt(111) and the one monolayer of platinum on Re(0001) annealed surface. Finally, it was shown that 2 monolayers of rhenium on Pt(111) behaved like a bulk rhenium surface since the rate of CH_4 formation on clean Re(0001) and on 2 ML of rhenium on Pt(111) were quite close. This indicates that the perturbation of a rhenium adsorbate by platinum is mostly attenuated at the second rhenium monolayer.

As studies progressed on the platinum–rhenium system, it became apparent that catalytic hydrogenolysis was more sensitive to the presence of trace amounts of platinum on rhenium or of rhenium on platinum than Auger electron spectroscopy. Auger measurements are accurate to within 0.1 ML of metal adsorbate,

and trace amounts of adsorbate could sometimes be undetected using AES yet cause an unexpectedly high hydrogenolysis rate. Sometimes after initiating a controlled catalytic reaction on an assumed clean substrate (platinum or rhenium), it became apparent that the surfaces had not been cleaned thoroughly enough, and the reaction would have to be aborted for further cleaning of the substrate. Argon ion sputtering was usually performed for at least two hours at room temperature to insure that all of the adsorbate metal was removed.

Butane experiments were subsequently performed to see how the hydrogenolysis and bond shift isomerization were under the control of the surface metallic composition for a larger molecule. The isomerization of n–butane to isobutane hardly depended at all on the composition of the surface. Changes observed over the composition range of $0 \leq \theta_{Re} < 2$ ML on a Pt(111) substrate showed an increase in isomerization rate of less than 2 times that of the most active surface (rhenium) to the least active surface (platinum). Although the activity of both of these metals is not significantly different for bond shift isomerization reactions, the fact that rhenium is more active can be explained if the cracking and bond shift surface intermediates are closely related as suggested by Anderson and Avery [24], and found by Gault and Garin from experiments using C_5 hydrocarbons [25].

The initial hydrogenolysis activity of butane versus rhenium coverage on a Pt(111) substrate is shown in Figure 6.6, and it was found that the rates of all the hydrogenolysis products increased when rhenium was added to the surface. At less than 0.2 ML of rhenium, the rate of production of ethane and propane was maximum, and here the rate of production of propane was almost the same as the rate of methane production. It is typical of hydrocarbons on platinum to experience a single cracking event per sojourn on the surface [7] since multiple hydrogenolysis is not a property of platinum as it is for rhenium. At very low

rhenium coverages on this surface ($\theta_{Re} < 0.2$ ML), platinum–like cracking selectivity was observed even though hydrogenolysis proceeded at a higher rate. As the rhenium coverage was increased, multiple hydrogenolysis was higher as the surface assumed more rhenium like behavior. Similar results were reported by Betizeau *et al.* for cyclopentane hydrogenolysis where little multiple cracking was observed for an alumina supported Pt–Re catalyst with less than 25% rhenium [5].

In further support of platinum–like hydrogenolysis selectivity at low rhenium coverages on Pt(111), it was found that the fission parameter decreased in a continuous manner with increasing rhenium coverage up to 0.7 ML. At a rhenium coverage of $\theta_{Re} \sim 0.2$ ML, the fission parameter was still above 1 which is expected for platinum catalysts, but the downward trend with increasing rhenium coverage may indicate a smooth transition to rhenium–like behavior. The hydrogenolysis activity of a clean Pt(111) surface and a bimetallic surface with a low rhenium coverage are not equivalent; the activity of the surface with a rhenium coverage of $\theta_{Re} \sim 0.15$ ML was at least an order of magnitude higher than the clean Pt(111) surface. Since the fission parameter did not behave like a step function when the hydrogenolysis activity increased by an order of magnitude, it must be concluded that the platinum moiety exerted substantial influence over the cracking selectivity of the catalyst even though the rhenium moiety apparently dominated the cracking activity. Otherwise, if the hydrogenolysis activity of the platinum atoms on the bimetallic surface were not increased considerably in the presence of rhenium, then the specific activity of the rhenium atoms will have had to increase by two orders of magnitude compared to clean Pt(111). An increase this large was observed for C_2H_6 hydrogenolysis, but the activity for butane conversion was about an order of magnitude less than towards ethane conversion for similar surfaces.

The single crystal bimetallic catalysts used here showed similar trends in hydrocarbon conversion as over alumina supported catalysts, indicating that they can be used effectively to model supported bimetallic catalysts. Betizeau *et al.* performed butane hydrogenolysis experiments over alumina supported platinum–rhenium catalysts of varying rhenium composition [5], and also found a maximum activity over mixed bimetallic ensembles. They obtained a maximum rate at 80% rhenium, which is in qualitative agreement with the results obtained here.

6.8.2 Proposed surface site model for hydrocarbon hydrogenolysis

Maximum rates of hydrogenolysis were observed near two thirds of a monolayer of rhenium for both ethane and butane. These results then suggest that a surface site such as Re_2Pt is best for hydrogenolysis. It has been suggested that rhenium can form multiple metal-carbon bonds better than platinum, and that these multiply adsorbed species are precursors to hydrogenolysis [16]. According to Shum *et al.*, the chance of obtaining a multiply adsorbed carbonaceous species increases in the order

$$\text{Pt ensemble} < \text{mixed ensemble} < \text{Re ensemble}$$

The Pt ensemble forms multiple chemisorption bonds too weakly to result in substantial cracking, and Re ensembles forms multiple chemisorption bonds so strong that product desorption becomes rate limiting. The mixed ensemble forms chemisorption bonds strong enough so that cracking occurs, but not so strong that the cracked products have difficulty desorbing [16]. If this is the case, it remains to be determined how a maximum of these sites can be formed. At what coverage of rhenium on Pt(111) would a maximum number of three fold sites with a stoichiometry of Re_2Pt be found?

The answer to this question may depend on the way rhenium overlayers grow on Pt(111). The following situations have been considered: rhenium adsorbs in a random fashion on Pt(111), and rhenium adsorbs and nucleates in islands around platinum defect sites. Figure 6.20 shows the results of calculations performed when rhenium adsorbs randomly, nucleates around 1% defect sites, or nucleates around 0.1% defect sites. Random growth can also be considered as nucleation around 100% defect sites. The calculations were performed by computer considering a large Pt(111) surface. After substituting rhenium atoms for platinum atoms according to the growth mechanism under consideration, each three fold site in the lattice was examined and the number of each Pt_xRe_{3-x} site was counted. As can be seen in Figure 6.20, all of these mechanisms give a maximum surface density of Re_2Pt sites at a rhenium coverage of $\theta_{Re} = 2/3$ ML. The validity of this model is consistent with the maximum in hydrogenolysis activity observed near a rhenium coverage on Pt(111) of $\theta_{Re} \sim 2/3$ ML from both ethane and butane. Why the bimetallic site is better for hydrogenolysis is perhaps also related to the behavior of the bimetallic surfaces towards hydrogen as discussed in Chapter 5.

6.8.3 Electronic model for enhanced hydrocarbon hydrogenolysis

An electronic effect may also be responsible for the enhancement observed in hydrogenolysis on mixed Pt–Re ensembles. The part of the periodic Table encompassing platinum and rhenium includes Re, Os, Ir, and Pt. According to the simple rigid band model for metal alloys, a Pt–Re alloy composed of 1/3 rhenium has an electronic structure identical to iridium, and an alloy with 2/3 rhenium has an electronic structure identical to osmium. Betizeau *et al.* performed butane hydrogenolysis experiments over these four metals to check this idea, and they

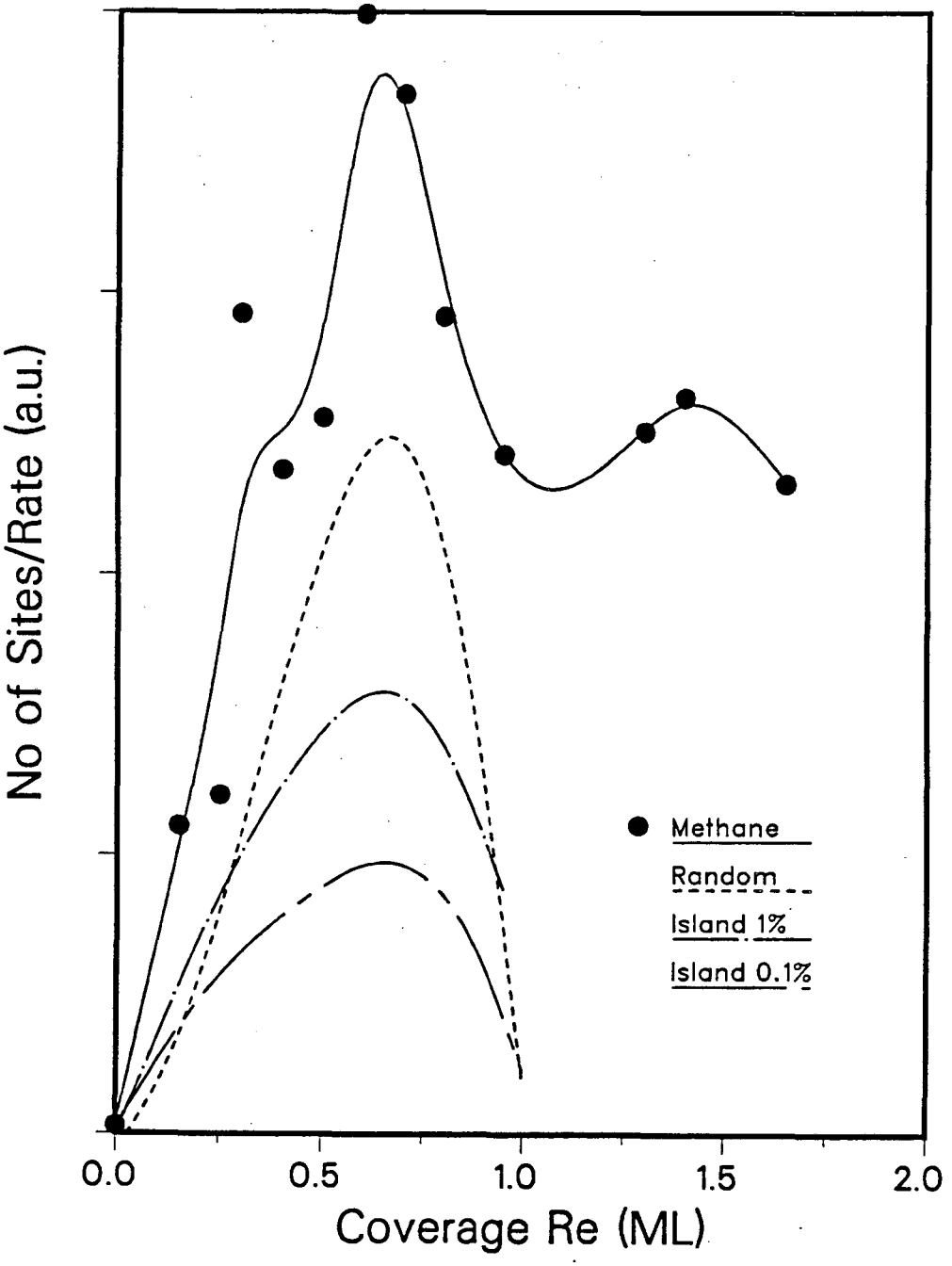

Figure 6.20: Model for the formation of three–fold Re_2Pt sites vs. rhenium coverage on Pt(111). The three situations considered were: a random rhenium growth mode, and islands growing around 1% and 0.1% defect sites. The rate of methane formation from butane vs. rhenium coverage is shown for comparison.

obtained reactivities for these alumina supported metals that increased in the following order [5] : Pt < Re < Ir < Os. Now suppose that the band structure of the surface can be treated independently of the bulk metal. Then the surfaces composed of rhenium on Pt(111) with coverages of θ_{Re} = 0, 1/3, 2/3, and 1 ML should behave like surfaces of pure Pt, Ir, Os, and Re respectively. Ethane and butane hydrogenolysis activities obtained on the following surfaces increase in the order: $(\theta_{Re} = 0) < (\theta_{Re} = 2.5) < (\theta_{Re} = 1/3) < (\theta_{Re} = 2/3)$. The results shown in Figure 6.6 agree qualitatively with the results of Betizeau *et al.*, and the rigid band model seems to explain the order of activities of the bimetallic surfaces for ethane and butane hydrogenolysis.

Other investigators have attempted to correlate *d* orbital occupancy with the cracking of hydrocarbons. Kubricka examined the hydrogenolysis of several hydrocarbons over Ru, Re, Pt, Pd, and Tc [26]. He suggested that hydrogenolysis correlated with the number of unpaired *d* electrons which is reported to be 1 for rhenium and 0.6 for platinum. This explanation cannot take into account maximum rates observed on bimetallic surfaces, even with electron transfer occurring from rhenium to platinum as suggested by Bolivar and Biloen [13,27], unless the promotion of electrons into *s* and *p* bands occurs upon alloying.

Sinfelt noticed that hydrogenolysis of ethane correlated well with the percent *d*-character of the metallic bond as described by Pauling in his resonating valence bond theory of metals [2,28]. Ethane hydrogenolysis shows the same trend in reactivity on the 5*d* metals, *i.e.* Pt $\ll$ Re < Ir $\ll$ Os, as the percent *d* character of the metallic bonds. The C_2H_6 hydrogenolysis activities reported for rhenium and iridium were very close at 205° C. If the mixing of rhenium and platinum result in surfaces that behave like the metals found between them as described by the rigid band model, then the hydrogenolysis results suggest that the Re–Pt(111)

bimetallic surface with a rhenium coverage of $\theta_{Re} = 2/3$ ML has a percentage of d-character in the surface metallic bonds similar to osmium. It would be useful to see if ultra-violet photoelectron studies of these surfaces would provide support for this idea.

6.8.4 Hydrogen pressure dependence for C_2H_6 hydrogenolysis on Re–Pt(111)

To explain the hydrogen pressure dependence results shown in Figure 6.5, a summary of the kinetic mechanism proposed by Sinfelt for C_2H_6 hydrogenolysis is presented [2].

$$
\begin{array}{lrcl}
(1) & C_2H_{6\ (g)} & \overset{K_1}{\rightleftharpoons} & C_2H_{5\ (ads)} + H_{\ (ads)} \\
(2) & C_2H_{5\ (ads)} + H_{\ (ads)} & \overset{K_2}{\rightleftharpoons} & C_2H_{x\ (ads)} + aH_{2\ (g)} \\
(3) & C_2H_{x\ (ads)} + H_{2\ (g)} & \overset{k_3}{\rightarrow} & CH_{y\ (ads)} + CH_{z\ (ads)} \quad \text{(RDS)} \\
(4) & CH_{y\ (ads)} + H_{2\ (g)} & \rightarrow & CH_{4\ (g)}
\end{array}
$$

The symbol a is equal to $(6 - x)/2$. The first two steps are rapid so that an effective equilibrium is maintained for the surface coverage of C_2H_5 and C_2H_x. Let θ_H and θ_x represent the fraction of the surface covered by H and C_2H_x, respectively. Combining the first two equilibrium steps and using simple Langmuir kinetics, an expression can be written for the coverage of C_2H_x, and θ_x is given by

$$\theta_x = \frac{KP_E/P_H^a}{1 + KP_E/P_H^a} \tag{6.5}$$

where P_E and P_H are the partial pressures of C_2H_6 and H_2 respectively, and K is the combined equilibrium constant for steps 1 and 2. Over a moderate range of pressures, the approximation can be made

$$\theta_x = \left(\frac{KP_E}{P_H^a}\right)^n \tag{6.6}$$

Now, the overall rate is given by the rate determining step or

$$r = k_3\theta_x P_{H_2} \tag{6.7}$$

Substituting for θ_x from Equation 6.6 gives an expression for the rate law

$$r = kP_{\mathrm{E}}^{n} P_{\mathrm{H}}^{(1-na)} \tag{6.8}$$

Knowing the ethane pressure dependence, the value of a can be chosen and the hydrogen pressure dependence calculated. The value of a can, of course, be chosen to get agreement with experiment. With these kinetics, values of a were found to be 1 and 3 for rhenium and platinum respectively, which corresponds to a value of x in C_2H_x of 4 and 0 for the two metals.

Sinfelt discussed 11 metals in his article, and the only two to show positive hydrogen pressure dependencies were Fe and Re (see Table 6.1). A problem exists in the analysis for Fe because no deuterium exchange seems to occur on ethane. If equilibrium exists between C_2H_6 and surface C_2H_x species, deuterated ethanes would have to be formed [29]. Although deuterium exchange on C_2H_6 has not been reported for rhenium, it is possible that rhenium also does not exchange deuterium during ethane hydrogenolysis. If it is true that iron and rhenium do not exchange deuterium, then one way to explain the positive hydrogen pressure dependence is that equilibrium is not attained for $\theta_{C_2H_x}$ (steps (1) and (2)) because the C–C bond is broken as soon as the surface intermediate is produced (step (3)). If the rehydrogenation of the C_1 fragments is rate limiting (step (4)), then the lack of deuterium exchange on C_2H_6 and the positive order in hydrogen pressure observed for hydrogenolysis is explained.

A modification of Sinfelt's mechanism was published more recently [3]. The difference is that step (3) becomes

$$C_2H_{x(\mathrm{ads})} \rightarrow C_1 \text{ fragments} \tag{6.9}$$

so that the hydrogen pressure no longer appears in the RDS with this modification.

Then Equation 6.8 becomes

$$r = kP_E^n P_H^{-na} \tag{6.10}$$

The above described mechanism can be used to explain the results shown in Figure 6.5. Clean Pt(111) showed a strongly negative hydrogen pressure dependence of –2, while 2 monolayers of rhenium displayed a less negative hydrogen pressure dependence of –0.7 for ethane hydrogenolysis. The results obtained differ from Sinfelt's due to the different conditions employed. In these experiments temperatures of 350°C were used in comparison to Sinfelt's 200°C. Sinfelt's pressure regime was also different: $P_{C_2H_6}$ = 23 Torr and $P_{H_2} \sim 150$ Torr compared to $P_{C_2H_6}$ = 5 Torr and $P_{H_2} \sim 760$ Torr used in these experiments.

Rhenium and platinum surfaces clearly showed different hydrogen pressure dependencies, but what about a bimetallic Pt–Re surface? The addition of 0.3 monolayers of rhenium to Pt(111) increased the activity over an order of magnitude to near the activity displayed by clean rhenium but the hydrogen pressure dependence on this surface was a surprising –1.8. If the rigid band model adequately describes the formation of this surface alloy, then the hydrogen pressure dependence should behave similar to iridium for a surface with this rhenium coverage. Sinfelt reports for Re, Ir, and Pt hydrogen pressure dependencies of +0.3, -1.6, and -2.5, respectively. Qualitatively, it can be seen that the values obtained for Pt(111) surfaces with rhenium coverages of 2, 0.3, and 0 ML had hydrogen pressure dependencies that decrease in the same order, *i.e.* –0.7, –1.8, –2, and the rigid band model seems to account for the observed results. On the other hand, the hydrogen pressure dependence was equivalent over clean Pt(111) and a surface with a rhenium coverage of $\theta_{Re} \sim 0.3$ ML within experimental error. The activity of the latter surface was nearly two orders of magnitude greater than the activity of the clean Pt(111) surface. Apparently rhenium dominated the activity

of this surface while the hydrogen pressure dependence was under the control of platinum. Based on the comparison of the hydrogen pressure dependencies of the three surfaces shown in Figure 6.5, it appears that the reaction mechanism occurring on the bimetallic surface more closely resembles the mechanism occurring on the clean Pt(111) surface.

Another explanation for the large hydrogenolysis activity but a high negative hydrogen pressure dependence obtained on the surface with a rhenium coverage of $\theta_{Re} \sim 0.3$ ML is as follows. In Chapter 5 it was shown that a bimetallic Pt–Re surface with a rhenium coverage of $\theta_{Re} \sim 0.3$ ML could adsorb more hydrogen with a slightly smaller hydrogen–metal bond strength than clean Pt(111). If it is true that the breaking of the C–C bond is facile on rhenium but the rehydrogenation of C_1 fragments is rate determining, then perhaps the presence of platinum on the surface enhances the hydrogenation of the C_1 fragments to the extent that rehydrogenation is no longer rate limiting. This is certainly possible if the surface has a larger hydrogen reservoir and it can exchange hydrogen more easily. So the decrease in activity expected by diluting the active rhenium with the relatively inactive platinum is offset by the greater surface hydrogen made available by the presence of the less active platinum.

6.8.5 Hexane hydrogenolysis

What can be said about the hydrogenolysis of n–hexane has already been summed up in the discussion of butane, so there is no reason to discuss n–hexane in great detail. One additional fact that has yet to be considered is the difference in hydrogenolysis behavior between epitaxial and alloyed Re–Pt(111) surfaces. The selectivity towards hydrogenolysis products appears not to change much with increasing rhenium coverages when the surface is alloyed, even though the activity at

1 ML of rhenium is an order of magnitude higher than clean Pt(111) (Figure 6.11). This effect may be due to a lack of surface roughness, but a well annealed rhenium foil had a fission parameter of $M_f = 1$, similar to the epitaxial $\theta_{Re} = 1.7$ ML surface. Although a foil is the wrong surface to compare and a Re(0001) surface would be more appropriate, n–hexane experiments were not performed on Re(0001) surfaces. However, it would not be unexpected to see platinum moderate the hydrogenolysis selectivity of Re(0001). Here again is an example of the hydrogenolysis activity being dominated by rhenium while the selectivity appears to be under the control of platinum.

6.8.6 Methylcyclopentane hydrogenolysis

The hydrogenolysis of MCP is treated here separately because the ring–opening of this five membered cyclic hydrocarbon behaves differently than the hydrogenolysis reactions already discussed. This molecule has received a lot of attention in the past over many metals: platinum [18,30,31,32,33,34,35,36], iridium [37], nickel [38], and rhodium [39]. Over low dispersed platinum this molecule opens via a selective ring opening mechanism with the formation predominantly of 2– and 3–methylpentane. Highly dispersed platinum displays a non-selective mechanism where the ring has a equal chance of opening between any of the C–C bonds forming n–hexane, 2–methylpentane, and 3–methylpentane in a ratio of 2:2:1. Zaera *et al.* reported that MCP ring opening on single crystal surfaces was similar to low dispersed catalysts and occurred via a selective mechanism [18].

Experiments performed on clean Pt(111) showed an activity in agreement with results of Zaera *et al.* [18]. In addition, the ratio of ring opening products formed on all surfaces tested, including bimetallic Re–Pt(111) surfaces, was consistent with a selective ring opening mechanism. It was found that the rate of desorption

of the C_6 products decreased from MCP (Figure 6.18) with increasing rhenium coverage on the Pt(111) surface. Isomerization activity also decreased from n–hexane conversion over the same surfaces (Figure 6.9). The formation of a C_5 cyclic surface intermediate is thought to be the precursors for isomerization from n–hexane on platinum based catalysts under these conditions. The decrease in isomerization is probably due to a decrease in the desorption of ring opening products because the formation of MCP from n–hexane did not decrease very much with the addition of moderate amounts of rhenium to the Pt(111) surface.

The ring opening of MCP is a hydrogenolysis reaction, so the decrease in ring opening activity from MCP with the addition of 0.15 ML of rhenium to Pt(111) is an intriguing result. At low rhenium coverages it had been previously found that a single cracking event was always enhanced relative to clean Pt(111). For example, a surface with a rhenium coverage of $\theta_{Re} = 0.15$ ML displayed an increase in formation of pentane from n–hexane and of propane from butane. Why then does the formation of 2– and 3–MP from methylcyclopentane decrease?

It has been observed that the formation of ring opening products is the favored reaction on platinum. Since platinum is a better dehydrogenation catalyst and also forms ring opening products at a higher rate than rhenium, then perhaps the initiation of dehydrogenation results in an increase of strain experienced by the C_5 cyclic species that causes it to rupture. The remaining surface species is more easily hydrogenated than the cracking precursors of paraffins. The pressure dependence of cracking reactions is more highly negative on platinum than it is for the ring opening of MCP, and it already has been discussed how rhenium can form multiple carbon–metal bonds better than platinum. The result is that the cracking of a "π" intermediate occurs more readily on platinum than on rhenium, and leaves a lightly dehydrogenated surface species following ring opening that is

as likely to be hydrogenated and desorb as methylpentane species than they are to undergo further dehydrogenation and cracking. Obviously the easy cracking of the ring occurs on the Re surface as well because hydrogenolysis products were observed to increase when rhenium was added to the surface. The difference with rhenium compared to platinum is that formation of multiple carbon–metal bonds is more facile on a rhenium surface, and surface intermediates on rhenium rapidly form multiple metal–carbon bonds. These species quickly undergo demethylation so that the ring opening products are not observed to readily desorb. This scheme is supported by Table 6.6 where it can be seen that an order of magnitude increase in the formation of methane, pentane, and isopentane was observed between clean Pt(111) and a bimetallic surface with a rhenium coverage of $\theta_{Re} \sim 0.15$ ML. This is compared to only a three-fold increase for all the other cracking products between these same two surfaces. If adsorption on rhenium is initiated through a single C atom, this would explain the similar increase for both CH_4 and C_5 products simultaneously. In addition, an observed increase in the isopentane/pentane ratio from 1.2 for clean Pt(111) to 2.4 for a surface with a rhenium coverage of $\theta_{Re} \sim$ 0.15 ML indicates that this reaction prefers initiation at the carbon atom furthest from the 3° carbon atom, perhaps due to steric reasons. The following illustration shows how this mechanism might operate.

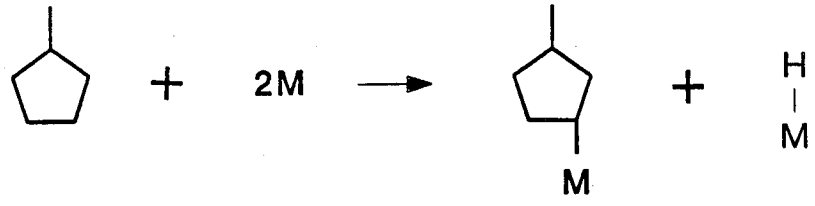

On Pt

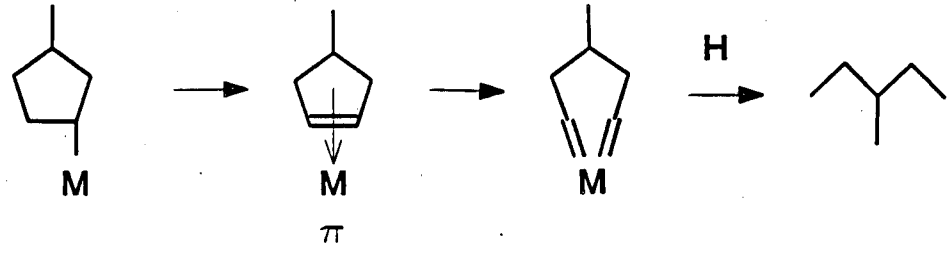

On Re

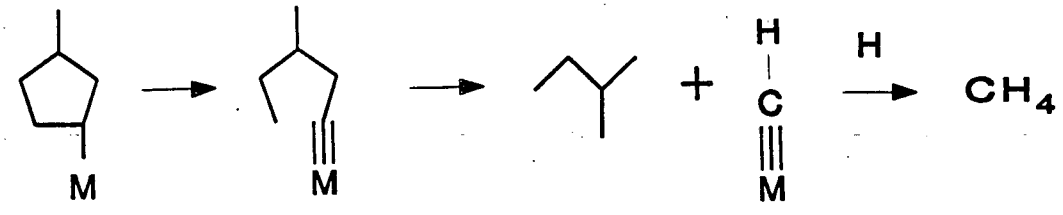

The evidence obtained from MCP conversion on platinum and bimetallic Re–Pt surfaces shows that ring opening behaves like an isomerization reaction and not a hydrogenolysis reaction since a "π" cracking intermediate may be associated with a ring opening precursor.

6.8.7 Reforming

In the previous section was discussed how the ring opening of MCP behaves more like an isomerization reaction than a hydrogenolysis reaction. The inability of rhenium to desorb ring opening products explains the decrease in isomerization

of n–hexane when rhenium is added to the surface even though the cyclization activity did not decrease at low coverages of rhenium (see Figure 6.9).

Perhaps the most exciting result obtained from n–hexane was the increase in benzene formation obtained at rhenium coverages near $\theta_{Re} \sim 0.25$ ML. At these low rhenium coverages, it was also observed that cyclization activity was maintained with respect to clean platinum. This suggests that the desorption of the product benzene may be a limiting factor in n–hexane aromatization. To check this idea, the dehydrogenation activity of cyclohexane was examined since cyclohexane may be an intermediate in the n–hexane aromatization. The results are shown in Figure 6.13, and suggest that product deactivation is a valid possibility since a maximum rate of benzene production was observed. The maximum was observed at a platinum coverage of $\theta_{Pt} \sim 1$ ML, so one conclusion that may be drawn is that platinum atoms with rhenium ligands are the best sites for producing and desorbing benzene since one full monolayer of platinum would experience a perturbation caused by the rhenium substrate lying directly under it. An improved selectivity of Pt–Re catalysts towards aromatization is a well known phenomenon [40,41,42], and our results indicate that a ligand effect is an important reason why this is true. In Chapter 5 it was shown that the bond strength between the metal surface and hydrogen was less for a bimetallic surface, and it would be interesting to see if a moderation of bonding towards some hydrocarbon species such as benzene would also be observed on bimetallic surfaces compared to monometallic platinum surfaces.

6.8.8 Summary

Before the discussion turns to the deactivation of surfaces by hydrocarbons, it might be helpful to present a summary of what has been learned concerning the

conversion of hydrocarbons over well characterized Pt–Re bimetallic surfaces.

A bimetallic platinum–rhenium surface is more active towards hydrogenolysis than either clean rhenium or clean platinum surfaces are, except in the case of MCP ring opening which behaves like an isomerization reaction. The cracking of hydrocarbons is an undesired effect, but can be controlled through the use of sulfur pretreatments as discussed extensively in the literature [13,14,40,41,42,43]. A study of the sulfided Re–Pt(111) system is now underway in this laboratory.

The isomerization of hydrocarbons is inhibited by the addition of rhenium to a platinum surface, and in the case of n–hexane this is due to the inability of rhenium to desorb ring opening products. Hydrogenolysis activities were highest on a bimetallic surface, but if cracking and isomerization intermediates for a bond shift isomerization are related as has been suggested, then perhaps the addition of sulfur can change the selectivity away from hydrogenolysis towards isomerization [24,44,45,46].

The most important effect that has been observed is the enhancement in aromatization behavior from n–hexane over a 0.25 ML rhenium on Pt(111) surface, and is due to the increased desorption rate of the product benzene. Betizeau *et al.* found an enhancement in deuterium exchange on benzene for mixed ensembles [5], and one of the reasons for the exchange enhancement is the more facile desorption of benzene from the bimetallic surface as was also concluded for the cyclohexane aromatization studies. It will be interesting to see how the addition of sulfur to the system will change aromatization behavior. Is the system dominated by a geometric effect as suggested by Shum and Carter [16,40] or is an electronic effect important with the addition of sulfur needed to moderate the cracking activity, as our results suggest?

6.9 Discussion: II. Deactivation of Metallic Surfaces

6.9.1 The contribution of rhenium

Once the excess hydrogenolysis activity is eliminated in a bimetallic Pt–Re catalyst, usually through presulfiding, the resulting bimetallic catalyst has an activity and selectivity very similar to a monometallic platinum catalyst. However, the difference between the monometallic and the bimetallic catalysts is that the deactivation of the catalyst after presulfiding is much slower on the bimetallic catalyst than on the monometallic catalyst. Many models have been proposed for the enhanced activity maintenance displayed by the Pt–Re catalyst. Past proposals found in the literature include: 1) the addition of rhenium increases the amount of hydrogen available on both the metal and the support [47,48]; 2) the action of rhenium actively destroys coke precursors [13,14] and can do so even when the metals are not intimately mixed [15,22]; 3) the action of rhenium is to keep certain sites free of deactivating deposits and can help remove deposits when they form [41,42,49]. Probably the most popular model is due to Sachtler, *i.e.* that Re–S species break up big multiplets of platinum, and by doing so the rearrangement of surface carbon deposits to irreversibly adsorbed deactivating surface deposits is hindered [13,40,50]. Pacheco and Petersen suggest that the activation energy of fouling reactions is smallest on large ensembles, and by breaking up these large ensembles it becomes energetically more expensive for deactivating deposits to form thereby slowing the deactivation of the surface dramatically [20,43].

Using surface science techniques it should be possible to answer some of these questions. In Chapter 5 evidence was presented that showed a Pt(111) surface with a rhenium coverage of $\theta_{Re} \sim 0.2$ ML held more hydrogen than a clean Pt(111) sur-

face, and with a slightly lower bonding energy. Under the high vacuum conditions employed, this hydrogen would be the so-called strongly bound hydrogen in terms of Nacheff *et al.* [51], and could be related to moderating the surface against excessive dehydrogenation and the buildup of coking deposits. In addition, higher amounts of surface hydrogen would be expected to prevent the decomposition of surface hydrocarbon species, and to help rehydrogenate and remove potential coking intermediates. In Chapter 3 it was shown that high surface coverages of hydrogen inhibited the decomposition of propylidyne on Pt(111).

The question concerning the role of sulfur in this process is an important one, and it has just begun to be addressed in our laboratory. Some preliminary work has been performed in the absence of sulfur to try to determine the most effective species for deactivating surface sites, and the effect of rhenium on preventing the deactivation. Figure 6.18 shows that the more rhenium present on the surface during MCP reactions, the smaller was the percentage of the restart rate towards hydrogenolysis. It was still observed that a surface with mixed Pt–Re ensembles always had a higher cracking activity than a platinum surface, but the ratio of the restart/initial reaction rates was smallest on these surfaces. This suggests that hydrogenolysis reactions are related to fouling reactions, at least for the fouling of hydrogenolysis sites.

The fouling activity of hydrogenolysis sites was related to the metallic surface composition; however, the ring opening restart/initial activity did not change much with respect to the surface rhenium coverage. This implies that multiple hydrogenolysis and ring opening reactions are catalyzed preferentially on rhenium and Pt–Re sites for hydrogenolysis, and on platinum sites for ring opening. Since ring opening reactions proceeded at a rate proportional to the exposed platinum atoms indicates also that a small ensemble of platinum atoms is required for this

reaction. This rules out the possibility that the role of rhenium is to destroy deactivating naphthenes, particularly MCP as suggested by Bertolacinni and Pellet [22]. If MCP is good at deactivating platinum surfaces, and results obtained show that it fouls Pt(111) better than n–hexane and cyclohexane, then it is more likely that species left on the surface following ring opening are responsible for deactivating the surface. In fact, it is desirable for making the highest octane reformate to leave these naphthenes intact so that they can undergo ring enlargement on acid sites followed by aromatization on metallic sites.

6.9.2 The contribution of hydrocarbons

To examine the fouling of a metallic surface by hydrocarbons, the cyclohexane system was first examined. Rhenium metal has a cyclohexane aromatization activity almost 20 times less than platinum, and Figure 6.14 shows product accumulation curves for cyclohexane aromatization on surfaces exposing both platinum and rhenium atoms, and on a surface exposing only platinum atoms. Both surfaces had similar initial activity, and this indicates that exposed platinum atoms have a higher specific activity when they have rhenium ligands compared to platinum atoms having no rhenium ligands. There was a large difference toward deactivation, however. Both surfaces showed initial deactivation because the first restart reaction yielded less benzene and smaller initial rates in both cases. However; the second restart reaction showed that no further deactivation had occurred on the thick platinum film while the Pt–Re surface showed a continuous deactivation. The bimetallic surface was more active than the platinum surface towards hydrogenolysis, so the implication is that the cracking is related to the deactivation of aromatization activity for this system. Perhaps cracking intermediates formed on the bimetallic surface spill out onto active aromatization sites deactivating them

with time. Figure 6.19 shows that nearly 50% of the intial activity of cyclohexane aromatization was recovered during a restart reaction. Perhaps the carbonaceous deposit formed from cyclohexane leaves a lot of open space and good access for cyclohexane molecules to approach the platinum surface. However, when excessive hydrogenolysis occurs, the cracking precursors spilled onto the surface arrange either in a more dense packing or in a configuration that is somehow unfavorable to transferring hydrogen atoms between adsorbed intermediates and the surface.

When MCP was used to deactivate a clean platinum surface before a subsequent cyclohexane reaction, it was found that the restart aromatization activity was only 20% of the initial clean platinum activity. An inspection of Table 6.6 and Figure 6.12 reveals that MCP cracks much more readily than does cyclohexane on clean platinum. It is clear from Figure 6.19 that MCP more effectively deactivates cyclohexane aromatization than does cyclohexane itself, and perhaps the reason is due to the readiness of MCP to undergo hydrogenolysis and ring opening, where the dehydrogenated intermediates sometimes do not come off and polymerize into deactivating deposits.

The deactivation of MCP reactions are also shown in Figure 6.19. In this case MCP deactivated the surface towards hydrogenolysis and ring opening of MCP far more effectively than did cyclohexane. The high restart value of ring opening when the surface was deactivated with cyclohexane (80-90% of clean surface rate) indicates as previously suggested, that carbonaceous deposits formed from cyclohexane leave a lot of open space or ready access to the surface of reacting hydrocarbons. Ring opening is apparently a less demanding reaction than is aromatization from c-hexane, perhaps for steric reasons since only 1 or 2 carbon atoms need bond to the surface for ring opening of MCP compared to 6 carbon atoms needed for the aromatization of c-hexane.

The deactivation of n–hexane reactions is also shown in Figure 6.19. The greater ability of n–hexane to deactivate hydrogenolysis and isomerization reactions compared to MCP is easily understood in terms of the greater hydrogenolysis reactivity of n–hexane (see Table 6.6). However, MCP was the more effective poison for the aromatization reaction. Apparently when n–hexane deactivates the surface towards hydrogenolysis and isomerization, it does so by breaking up large ensembles while still leaving a substantial number of platinum atoms available for aromatization.

In summary, it has been found that MCP is the most effective hydrocarbon in deactivating Pt(111) compared to cyclohexane and n–hexane in agreement with results previously reported in references [22,52]. The deactivation results are also in agreement with the concept of selective poisoning proposed by Barbier *et al.* for Al_2O_3 supported platinum [53].

References

[1] J.H. Sinfelt and W.F. Taylor. *Trans. Faraday Soc.* **64** (1968) 3086.

[2] J.H. Sinfelt. *Catalysis Reviews* **3** (1970) 175.

[3] J.H. Sinfelt. *J. Catalysis* **27** (1977) 468.

[4] R. Ducros, M. Alnot, J.J. Ehrhardt, M. Housley, and G. Piquard. *Surface Sci.* **94** (1980) 154.

[5] C. Betizeau, G. Leclercq, R. Maurel, C. Bolivar, H. Charcosset, R. Fretty, and L. Tourayan. *J. Catalysis* **45** (1976) 179.

[6] T.C. Wong, L.C. Chang, G.L. Haller, J.A. Oliver, N.R. Scaife, and C. Kemball. *J. Catalysis* **87** (1984) 389.

[7] V. Ponec and W.M.H. Sachtler. *Proc. 5th Intern. Congr. Catal.* (1972) 645.

[8] S.M. Davis and G.A. Somorjai. *The Chemical Physics of Solid Surfaces and Heterogeneous Catalysis*, page 217. Volume 4, Elsevier Science Publishers, Amsterdam, The Netherlands, 1982.

[9] V. Ponec. *Proc. 5th Intern. Congr. Catal.* (1972) 365.

[10] F. Zaera. PhD thesis, University of California, Berkeley, CA 94720, 1984.

[11] R.C. Yeates. PhD thesis, University of California, Berkeley, CA 94720, 1985.

[12] S.M. Davis. PhD thesis, University of California, Berkeley, CA 94720, 1981.

[13] P. Biloen, J.N. Helle, H. Verbeek, F.M. Dautzenberg, and W.M.H. Sachtler. *J. Catalysis* **63** (1980) 112.

[14] J.M. Parera, C.A. Querini J.N. Beltramini, E.E. Martinelli, E.J. Churin, P.E. Aloe, and N.S. Figoli. *J. Catalysis* **99** (1986) 39.

[15] R. Burch and A.J. Mitchell. *Applied Catalysis* **6** (1983) 121.

[16] V.K. Shum, J.B. Butt, and W.M.H. Sachtler. *J. Catalysis* **96** (1985) 371.

[17] G.A. Mills, H. Heinemann, T.H. Milliken, and A.G. Oblad. *Ind. Eng. Chem.* **45** (1953) 134.

[18] F. Zaera, D. Godbey, and G.A. Somorjai. *J. Catalysis* **101** (1986) 73.

[19] H. E. Kluksdahl. *U. S. Patent 3,415,737* (1968) .

[20] M.A. Pacheco and E.E. Petersen. *J. Catalysis* **96** (1985) 499.

[21] J.B. Peri. *J. Catalysis* **52** (1978) 144.

[22] R.J. Bertolacinni and R.J. Pellet. *Catalyst Deactivation*, pages 73–77. Elsevier, Amsterdam, The Netherlands, 1980.

[23] D.J.C. Yates and J.H. Sinfelt. *J. Catalysis* **14** (1969) 182.

[24] J.R. Anderson and N.R. Avery. *J. Catalysis* **7** (1967) 315.

[25] F. Garin and F.G. Gault. *J. Am. Chem. Soc.* **97** (1975) 4466.

[26] H. Kubricka. *J. Catalysis* **12** (1968) 223.

[27] C. Bolivar, H. Charcosset, R. Fretty, M. Primet, L.Tournayan, C. Betizeau, G. Leclercq, and R. Maurel. *J. Catalysis* **45** (1976) 163.

[28] L. Pauling. *Proc. Roy. Soc. London* **A196** (1949) 343.

[29] J.R. Anderson and C. Kemball. *Proc. Roy. Soc. London* **A223** (1954) 361.

[30] G. Maire, C. Corolleur, D. Juttard, and F.G. Gault. *J. Catalysis* **21** (1971) 250.

[31] R. Kramer and H. Zuegg. *J. Catalysis* **80** (1983) 446.

[32] R. Kramer and H. Zuegg. *J. Catalysis* **85** (1984) 530.

[33] F. Garin, O. Zahrra, C. Crouzet, J.L. Schmitt, and G. Maire. *Surface Sci.* **106** (1981) 466.

[34] J.R. Anderson and Y. Shimoyama. *Proc. 5th Intern. Congr. Catal.* (1972) 695.

[35] J. Dartiques, A. Chambellan, S. Corolleur, F. Gault, A. Revouprez, B. Moraweck, P. Bosch-Giral, and G. Dalmai-Imelick. *J. de Chimie* **10** (1979) 591.

[36] Z. Paál and P. Tétényi. *J. Catalysis* **29** (1973) 176.

[37] J.G. van Sender, E.H. van Broekhoven, C.T. Wreesman, and V. Ponec. *J. Catalysis* **87** (1984) 468.

[38] F. Schepers, E. van Broekhoven, and V. Ponec. *J. Catalysis* **96** (1985) 82.

[39] G. Del Angel, B. Coq, R. Dutartre, and F. Figueras. *J. Catalysis* **87** (1984) 27.

[40] J.L. Carter, G.B. Vicker, W. Weissman, W.S. Kmak, and J.H. Sinfelt. *Applied Catalysis* **3** (1982) 327.

[41] R.W. Coughlin, K. Kawakami, and A. Hasan. *J. Catalysis* **88** (1984) 150.

[42] R.W. Coughlin, A. Hasan, and K. Kawakami. *J. Catalysis* **88** (1984) 163.

[43] M.A. Pacheco and E.E. Petersen. *J. Catalysis* **96** (1985) 507.

[44] V. Ponec. *Advances in Catalysis* **32** (1983) 149.

[45] F. Gault. *Advances in Catalysis* **30** (1981) 1.

[46] G. Maire, G. Plouidy, J.C. Prudhomme, and F.J. Gault. *J. Catalysis* 4 (1965) 556.

[47] J. Barbier, H. Charcosset, G. dePeriera, and J. Riviere. *Applied Catalysis* **1** (1981) 71.

[48] J. Margitfalvi, S. Gőbölös, E. Kwayzer, M. Hegedüs, F. Nagy, and L. Koltai. *React. Kinet. Catal. Lett.* **24** (1984) 315.

[49] C.R. Apestequía and J. Barbier. *J. Catalysis* **78** (1982) 352.

[50] V.K. Shum, J.B. Butt, and W.M.H. Sachtler. *J. Catalysis* **99** (1986) 126.

[51] M.S. Nacheff, L.S. Kraus, M. Ichikawa, B.M. Hoffman, J.B. Butt, and W.M.H. Sachtler. *J. Catalysis* **106** (1987) 263.

[52] B.J. Cooper and D.L. Trimm. *Catalyst Deactivation*, page 63. Elsevier, Amsterdam, The Netherlands, 1980.

[53] J. Barbier, P. Marecot, N. Martin, L. Elassal, and R. Maurel. *Catalyst Deactivation*, page 53. Elsevier, Amsterdam, The Netherlands, 1980.

LAWRENCE BERKELEY LABORATORY
TECHNICAL INFORMATION DEPARTMENT
UNIVERSITY OF CALIFORNIA
BERKELEY, CALIFORNIA 94720